VALIDATED PREDICTION OF PRESSURANT GAS REQUIREMENTS IN CRYOGENIC RUN TANKS AT SUBCRITICAL AND SUPERCRITICAL PRESSURES

By

Laurence de Quay

A Dissertation
Submitted to the Faculty of
Mississippi State University
in Partial Fulfillment of the Requirements
for the Degree of Doctor of Philosophy
in Mechanical Engineering
in the Department of Mechanical Engineering

Mississippi State, Mississippi

December 2009

ProQuest LLC
789 East Eisenhower Parkway
P.O. Box 1346
Ann Arbor, MI 48106-1346

VALIDATED PREDICTION OF PRESSURANT GAS REQUIREMENTS IN CRYOGENIC RUN TANKS AT SUBCRITICAL AND SUPERCRITICAL PRESSURES

By

Laurence de Quay

Approved:

B. Keith Hodge
Professor of Mechanical Engineering
(Director of Dissertation)

George A. Adebiyi
Professor of Mechanical Engineering
(Committee Member)

Rogelio Luck
Professor of Mechanical Engineering
and Graduate Coordinator
(Committee Member)

Pedro Mago
Associate Professor of Mechanical
Engineering
(Committee Member)

Steven R. Daniewicz
Professor of Mechanical Engineering
Interim Head of the Department of
Mechanical Engineering

Sarah A. Rajala
Dean of the College of Engineering

Name: Laurence de Quay

Date of Degree: December 11, 2009

Institution: Mississippi State University

Major Field: Mechanical Engineering

Major Professor: Dr. B. Keith Hodge

Title of Study: VALIDATED PREDICTION OF PRESSURANT GAS REQUIREMENTS IN CRYOGENIC RUN TANKS AT SUBCRITICAL AND SUPERCRITICAL PRESSURES

Pages in Study: 200

Candidate for Degree of Doctor of Philosophy

The development, testing, and use of liquid propellant and hybrid rocket propulsion systems for spacecraft and their launch vehicles routinely involves the use of cryogenic propellants. These propellants provide high energy densities that enable high propulsive efficiency and high engine thrust to vehicle weight ratios. However, use of cryogenic propellants also introduces technical problems not associated with other types of propellants.

One of the major technical problems is the phenomenon of propellant tank pressurant and ullage gas collapse. This collapse is mainly caused by heat transfer from most of the ullage gas to tank walls and interfacing propellant, which are both at temperatures well below those of this gas. Pressurant gas is supplied into cryogenic propellant tanks in order to initially pressurize these tanks and then to maintain required pressures as propellant is expelled from these tanks. The cryogenic propellants expelled from the tanks feed rocket engine assemblies, subassemblies, and components at required interface pressures and mass flow rates.

The net effect of pressurant and ullage gas collapse is increased total mass and mass flow rate requirements of pressurant gases. For flight vehicles this leads to significant and undesirable weight penalties. For rocket engine component and subassembly ground test facilities this results in high construction and operational cost impacts.

Accurate predictions of pressurant gas mass transfer and flow rate requirements are essential to the proper design of systems used to supply these gases to cryogenic propellant tanks. While much work has been done in the past for predicting these gas requirements at low subcritical tank pressures, very little has been done at supercritical tank pressure conditions and there are selected cases where errors of analytical predictions are high.

The objectives of this study are to develop a new generalized and improved computer program to determine pressurant gas requirements at both subcritical and supercritical tank pressure conditions, and then evaluate and validate the consistent accuracy of this program over a wide range of conditions by comparison of program results to empirical data.

DEDICATION

This work is dedicated to my parents, Emily and Rutger, to my daughters, Rachel, Emily, and Sarah, to my Godparents, Helen and Cas, and to my special friends, Ed, Ernie, Jim, Keith, and Robert. These people helped me through "dark journeys of my soul" or gave me the inspiration and desire to complete this work; probably much more than they realize. I hope that my work serves as an indelible inspiration to them.

Finally, I must acknowledge and dedicate this work to the Almighty Creator, Father, Son, and Holy Spirit, who make all things possible and have given me more than I can say with mere words.

ACKNOWLEDGEMENTS

I wish to acknowledge a number of people who made this dissertation possible.

My sincere gratitude goes to Dr. B. Keith Hodge for his patience, guidance, and support as director of this dissertation. He has provided me with the enabling knowledge and skills through prior consultations and coursework.

I also wish to acknowledge the current and former members of my graduate committee, Drs. George A. Adebiyi, Louay Chamra, Rogelio Luck, Pedro Mago, and Robert P. Taylor. All supported me in one way or another at various critical times. This support came in the form of formal coursework, informal technical discussions and interchanges, and simple acts of kindness and encouragement.

There are many other individuals who have provided me the career opportunities and furthered my educational growth and development which have also made this dissertation possible. My key benefactors and career mentors who have my sincere gratitude are Ms. Florence Kailiwai-Barnett, Mr. Douglas McLaughlin, and Mr. Patrick Mooney.

Finally, this section would not be complete without acknowledging teachers from my youth who set or kept me on the "right track," inspired my love of learning, and supported me in my educational growth and development. These people, who have my unending gratitude, are Ms. Jacqueline Kitt, Mr. Richard McManus, Mr. Robert Neubert, and Mr. Arthur Walters.

TABLE OF CONTENTS

LIST OF TABLES

LIST OF FIGURES

NOMENCLATURE

A or A_z	Area of horizontal plane bounded by tank wall at elevation or vertical position z in the tank
A_d	Total area of holes, slots, perforations, or other openings in diffuser where pressurant gas enters the tank ullage
$A_{l,w,K}$	Area of tank wall in contact with cryogenic propellant segment K
A_s	Area of (horizontal plane) interface between cryogenic propellant and ullage gas
$A_{w,J}$	Area of tank wall in contact with ullage gas segment J
b	Minor axis for ellipsoid inner wall contour of top and bottom heads on tank (if tank is spherical or heads are hemispheres this dimension equals inside diameter of tank shell or equator)
b_1	Coefficient for forced convection component of ullage-gas-to-tank-wall heat transfer coefficient
b_2	Reynolds number exponent for forced convection component of ullage-gas-to-tank-wall heat transfer coefficient
b_3	Prandtl number exponent for forced convection component of ullage-gas-to-tank-wall heat transfer coefficient
c	Specific heat
c_1	Coefficient for general natural convection heat transfer correlation
c_4	Exponent for general natural convection heat transfer correlation
c_7	Grashof number coefficient for wall incline

c_{7a}	Grashof number coefficient for wall incline of inclined vertical walls
c_{7b}	Grashof number coefficient for wall incline based on horizontal walls
c_p	Specific heat at constant pressure
c_v	Specific heat at constant volume
d_1	Coefficient for forced convection component of ullage-gas-to-cryogenic-propellant interface heat transfer coefficient
d_2	Reynolds number exponent for forced convection component of ullage-gas-to-cryogenic-propellant interface heat transfer coefficient
d_3	Prandtl number exponent for forced convection component of ullage-gas-to-cryogenic-propellant interface heat transfer coefficient
D	Mass diffusion coefficient (for one of two gas species in a binary gas mixture)
D_0	Mass diffusion coefficient at reference pressure and temperature
EK_{gJ}	Equivalent forced convection component of total convective coefficient for heat transfer across upper boundary of ullage gas segment J
EK_{gJ-1}	Equivalent forced convection component of total convective coefficient for heat transfer across lower boundary of ullage gas segment J
g_c	Gravimetric constant; 32.174 ft-lb_m/lb_f-sec^2
Gr	Grashof number
Gr_L	Grashof number for natural convection heat transfer along wall of equivalent length L
h	Convective heat transfer coefficient
$h_{c,J}$	Natural convection component of heat transfer coefficient $h_{w,J}$

h_{fl}	Convective heat transfer coefficient (cryogenic propellant or ullage gas)
h_{la}	Equivalent convective heat transfer coefficient for upper boundary of uppermost cryogenic propellant segment in contact with ullage gas
$h_{l,w,K}$	Convective heat transfer coefficient for crogenic-propellant-to-tank-wall heat transfer for cryogenic propellant segment K
h_L	Convective heat transfer coefficient along wall of equivalent length L
h_o	Overall forced convection heat transfer coefficient for ullage gas region at boundary layer adjacent to tank walls
$h_{o,J}$	Forced convection component of heat transfer coefficient $h_{w,J}$
h_s	Convective heat transfer coefficient for boundary layer on ullage gas side of the ullage-gas-to-cryogenic-propellant interface
h_{sc}	Natural convection component of heat transfer coefficient h_s
h_{so}	Forced convection component of heat transfer coefficient h_s
$h_{w,J}$	Convective heat transfer coefficient for ullage-gas-to-tank-wall heat transfer for ullage gas segment J
H	Coefficient for forced mixing component of mass transfer of cryogenic propellant species in ullage gas region
i	For the main computer model, time step number in the main computer program or, for the transient tank wall heat conduction part of the model, incremental increase in tank wall segment thickness when traversing from inner to outer wall surfaces of tank
i_J	Specific enthalpy of ullage gas segment J
i_{lK}	Specific enthalpy of cryogenic propellant segment K
i_{ntm}	Number of local time steps across global time step $\Delta\tau$

i_{PG}	Specific enthalpy of pressurant gas entering tank ullage
$jpass$	Tracking integer in main computer program to set one of three cases for each time step (explained in detail in Chapter IV)
J	Ullage gas segment index number
$J_{O,max}$	Total number of ullage gas segments at end of prior time step
k	Thermal conductivity
$k_{l,sat}$	Thermal conductivity of cryogenic propellant species in saturated liquid state at pressure of lowermost ullage gas segment
$\left(\frac{k^*}{\Delta z}\right)_{J-1,J}$	Equivalent convective heat transfer coefficient for lower boundary of ullage gas segment J
$\left(\frac{k^*}{\Delta z}\right)_{J,J+1}$	Equivalent convective heat transfer coefficient for upper boundary of ullage gas segment J
$\left(\frac{k^*}{\Delta z}\right)_{K-1,K}$	Equivalent convective heat transfer coefficient for upper boundary of cryogenic propellant segment K
$\left(\frac{k^*}{\Delta z}\right)_{K,K+1}$	Equivalent convective heat transfer coefficient for lower boundary of cryogenic propellant segment K
K	Cryogenic propellant segment index number
K_{max}	Total number of cryogenic propellant segments; also index number of lowermost (bulk) cryogenic propellant segment
$K_{O,max}$	Total number of cryogenic propellant segments at end of prior time step

L	Characteristic or equivalent wall length for convective heat transfer correlations
L_4	Characteristic or equivalent wall length of inclined vertical wall in contact with ullage gas
L_T	Vertical height of tank cylindrical section (equals zero if tank is a sphere or oblate spheroid)
m	Fluid (segment) mass
m_{PGT}	Total cumulative mass of pressurant gas transferred into tank ullage
$\dot{m}_l$	Mass flow rate of cryogenic propellant out of bottom of tank
$\dot{m}_{PG}$	Mass flow rate of pressurant gas into tank ullage
$\dot{m}_{PG,J}$	Mass flow rate of pressurant gas into ullage gas segment J
$\hat{m}$	Mass fraction of a fluid species in gas mixture
n	Index number to track number of sequential local time steps across global time step $\Delta\tau$
n_{seg}	Total number of finite element tank wall segments from inner to outer wall surfaces of tank for numerical finite-difference modeling of transient tank wall heat conduction
Nu	Nusselt number
Nu_F	Nusselt number for forced convection heat transfer
$Nu_{F,O}$	Nusselt number for forced convection heat transfer associated with ullage gas boundary layer at ullage-gas-to-cryogenic-propellant interface
$Nu_{F,w}$	Nusselt number for forced convection heat transfer along tank wall
Nu_L	Nusselt number for natural convection heat transfer along wall of equivalent or characteristic length L

Nu_T	Nusselt number for total combined forced and natural convection heat transfer
P	Pressure
P_0	Reference fluid pressure (generally 14.7 psia or 0.1013 MPa)
P_{Crit}	Critical pressure of cryogenic propellant species
Pr	Prandtl number
r	Radial distance of inner tank wall from vertical tank centerline at a given tank elevation
r_{60}	Radial distance of inner tank wall from vertical tank centerline at tank elevation where incline angle of tank wall is 60^o off-vertical
r_a	Outside radius of pressurant gas inlet diffuser (based on standard vertical cylindrical shape of diffuser)
r_i	Radial distance of inner tank wall from vertical tank centerline at elevation of ullage-gas-to-cryogenic-propellant interface
r_m	Reference radial distance of inner boundary of finite-element tank wall segment m [see Figure 3.6 and Equation (3-81)]
r_m^*	Reference radial distance of mid-span radial distance between inner and outer boundary of finite-element tank wall segment m [see Figure 3.6 and Equation (3-80)]
R	Inside radius of tank equator or cylindrical section
Ra	Rayleigh number (product of Grashof and Prandtl numbers)
Ra_L	Rayleigh number for fluid natural convection heat transfer along wall of equivalent or characteristic length L
Ra^*	Modified Rayleigh number
Ra_L^*	Modified Rayleigh number for fluid natural convection heat transfer along wall of equivalent or characteristic length L

t	Tank wall thickness
T	Temperature
T_0	Reference temperature (typically 525 to 540 R)
T_{Crit}	Critical temperature of cryogenic propellant species
T_{fl}	Temperature of fluid (cryogenic propellant or ullage gas) segment outside the thermal boundary layer adjacent to tank wall
$T_{l,w,K}$	Temperature of inner tank wall surface in contact with cryogenic propellant segment K
$T_{l,Sat}$	Saturation temperature of cryogenic propellant at given ullage gas pressure
T_w	Temperature of inner tank wall surface
$T_{w,J}$	Temperature of inner tank wall surface in contact with ullage gas segment J
u	Specific internal energy
V	Volume
V_{Ull}	Total volume of tank ullage
z	Vertical position (depth) below $z = 0$ reference (refer to Figure 3.2)
$z_{1,JOLD}$	Vertical dimension defined and illustrated in Figures 3.8 and 3.9
$z_{1,KOLD}$	Vertical dimension defined and illustrated in Figures 3.8 and 3.9
$z_{2,JOLD}$	Vertical dimension defined and illustrated in Figures 3.8 and 3.9
$z_{2,KOLD}$	Vertical dimension defined and illustrated in Figures 3.8 and 3.9
z_d	Vertical position of lowest point on pressurant gas inlet diffuser (see Figure 3.2)

z_{dc}	Vertical position of mid-elevation where pressurant gas enters the tank ullage (see Figure 3.2)
z_{ds}	One half of vertical distance covering all locations where pressurant gas enters the tank ullage (see Figure 3.2)
z_i	Vertical position of ullage-gas-to-cryogenic-propellant interface
z_{min}	Vertical position of intersection between tank wall and outside diameter of (standard vertical cylinder) diffuser (see Figure 3.2)
z_{ull}	Vertical position of ullage-gas-to-cryogenic-propellant interface (see Figure 3.2; same as z_i)
z_w	Vertical position of tank wall location being evaluated for heat transfer
α	Thermal diffusivity
β	Bulk compression modulus
β_s	Exponential decay parameter for forced convection heat transfer coefficient at ullage-gas-to-cryogenic-propellant interface
$\beta_{s,a}$	Ullage-gas-to-cryogenic-propellant interface forced convective heat transfer coefficient parameter defined by Equation (3-52) and used in Equation (3-51)
$\beta_{s,max}$	Ullage-gas-to-cryogenic-propellant interface forced convective heat transfer coefficient parameter defined by Equation (3-53) and used in Equation (3-51)
β_w	Exponential decay parameter for forced convection component of ullage-gas-to-tank-wall heat transfer coefficient
$\beta_{w,a}$	Ullage-gas-to-tank-wall forced convective heat transfer coefficient parameter defined by Equation (3-44) and used in Equation (3-43)
$\beta_{w,max}$	Ullage-gas-to-tank-wall forced convective heat transfer coefficient parameter defined by Equation (3-45) and used in Equation (3-43)

Δr_m	Radial distance between inner and outer boundaries of finite-element tank wall segment m
$\Delta r_m'$	Distance between reference radial distances r_{m+1}^* and r_m^*
$\Delta\tau$	Time interval of current (global) time step under evaluation
$\Delta\tau_n$	Time interval of each local time step across the global time step under evaluation
μ	Absolute viscosity
ν	Kinematic viscosity
ρ	Density
θ	Off-vertical incline angle of tank wall
τ	Time at start of current time step or end of prior time step
ψ	Parameter defined by Equations (3-34) and (3-59)

Subscripts:

a	Property for propellant species in binary gas mixture [Except for Nusselt number correlation in Equation (3-57)]
b	Property for pressurant gas species in binary gas mixture [Except for Nusselt number correlation in Equation (3-57)]
Btm	Parameter evaluated for bottom of fluid (cryogenic propellant or ullage gas) segment
J	Ullage gas segment index number or upper boundary of ullage gas segment with index number J
$J-1$	Lower boundary of ullage gas segment with index number J
$Je0$	Interface between cryogenic propellant and ullage gas

$JOLD$ or J_{OLD}	Ullage gas segment index number at end of prior time step or beginning of current time step
K or lK	Cryogenic propellant segment index number or lower boundary of cryogenic propellant segment with index number K
$K-1$ or $lK-1$	Upper boundary of cryogenic propellant segment with index number K
$KOLD$ or K_{OLD}	Cryogenic propellant segment index number at end of prior time step or beginning of current time step
L	Parameter evaluated with characteristic or equivalent length of L for wall surface where heat transfer between fluid and wall occurs
L_4	Parameter evaluated with characteristic or equivalent length of L_4 for wall surface where heat transfer between ullage gas and wall occurs
m	Index number of tank wall segment, finite element, for modeling transient heat conduction with non-uniform temperature profile in tank wall
Mid	Parameter evaluated for elevation midway between top and bottom of fluid (cryogenic propellant or ullage gas) segment
Top	Parameter evaluated for top of fluid (cryogenic propellant or ullage gas) segment
w	Tank wall material
w,m	Tank wall segment m material property or inner boundary of tank wall segment m
$w,m-1$	Tank wall segment $m-1$ material property
$w,m+1$	Tank wall segment $m+1$ material property or outer boundary of tank wall segment m

Superscripts:

$\langle \tau \rangle$	Value of parameter, variable, or property corresponding to start of current time step or end of prior time step
$\langle \tau + \Delta\tau \rangle$	Value of parameter, variable, or property corresponding to end of current time step
$\langle \tau + n(\Delta\tau_n) \rangle$	Value of parameter, variable, or property corresponding to end of current local time step number n where multiple local time steps span across global time step $\Delta\tau$

CHAPTER I

INTRODUCTION

Following initial developmental work in the 1920's and 1930's by Robert H. Goddard, liquid propellant rockets have been further developed and utilized extensively for military missile, earth-to-orbit launch system, and space propulsion-system applications. The vast majority of larger high thrust (greater than 10,000 pound) liquid propellant rockets utilize one or more cryogenic liquid propellants because of the high combustion-energy-to-mass ratio or high combustion-energy-to-volume ratio provided with these types of propellants.

The 80-year history of liquid propellant rockets has been a series of continuous improvements in propulsive efficiency, increased thrust levels, significant increases in thrust-to-weight ratios, and an expanding variety of engine cycles.

Initiatives starting in the late 1980's have placed the emphasis on reduction of costs with improved reliability and safety in the manufacture, ground testing, and operation of all rocket propulsion systems. Further development initiatives starting in the middle 1990's have included renewed interest in liquid-oxidizer-solid-fuel (hybrid) rocket motors and liquid propellant rocket engines with oxidizer-rich, staged-combustion power cycles or unchoked low differential pressure propellant injectors.

All liquid propellant and hybrid rocket engines require one or more pressurized propellant tanks in which propellant is expelled from tanks to supply one or more rocket engines. As shown in Figure 1.1, some liquid propellant rockets utilize high pressure propellant tanks that directly feed fuel, oxidizer, or both directly into the main injector of the rocket engine combustion chamber. The majority of liquid propellant rocket engines utilize pumps, usually driven by gas turbines to provide the high pumping power requirements. These enable lower propellant tank pressures and, thus, allows for thinner tank walls which significantly reduces flight vehicle weight. A simplified schematic of a pump fed liquid propulsion system, which employs one of the basic power cycles, is shown in Figure 1.2. In this system, turbopumps boost the pressures of propellants supplied from the propellant tanks such that these propellants can be injected into the rocket engine's main combustion chamber denoted in Figure 1.2. Figures 1.1 and 1.2 are both obtained from Sutton (1992), and a more detailed discussion about liquid propellant rockets is also provided in this reference.

Background

A key and critical component for design concept evaluation, development, flight certification, and subsequent use of rocket propulsion systems is the ground testing of rocket engine assemblies, subassemblies, and components as well as integrated rocket stages and major segments of the flight vehicle. The ground testing of individual rocket engine components and subassemblies during the early stages of development has been given increased attention and importance due to the aforementioned cost reduction and reliability and safety enhancement initiatives started in the late 1980's. Additionally,

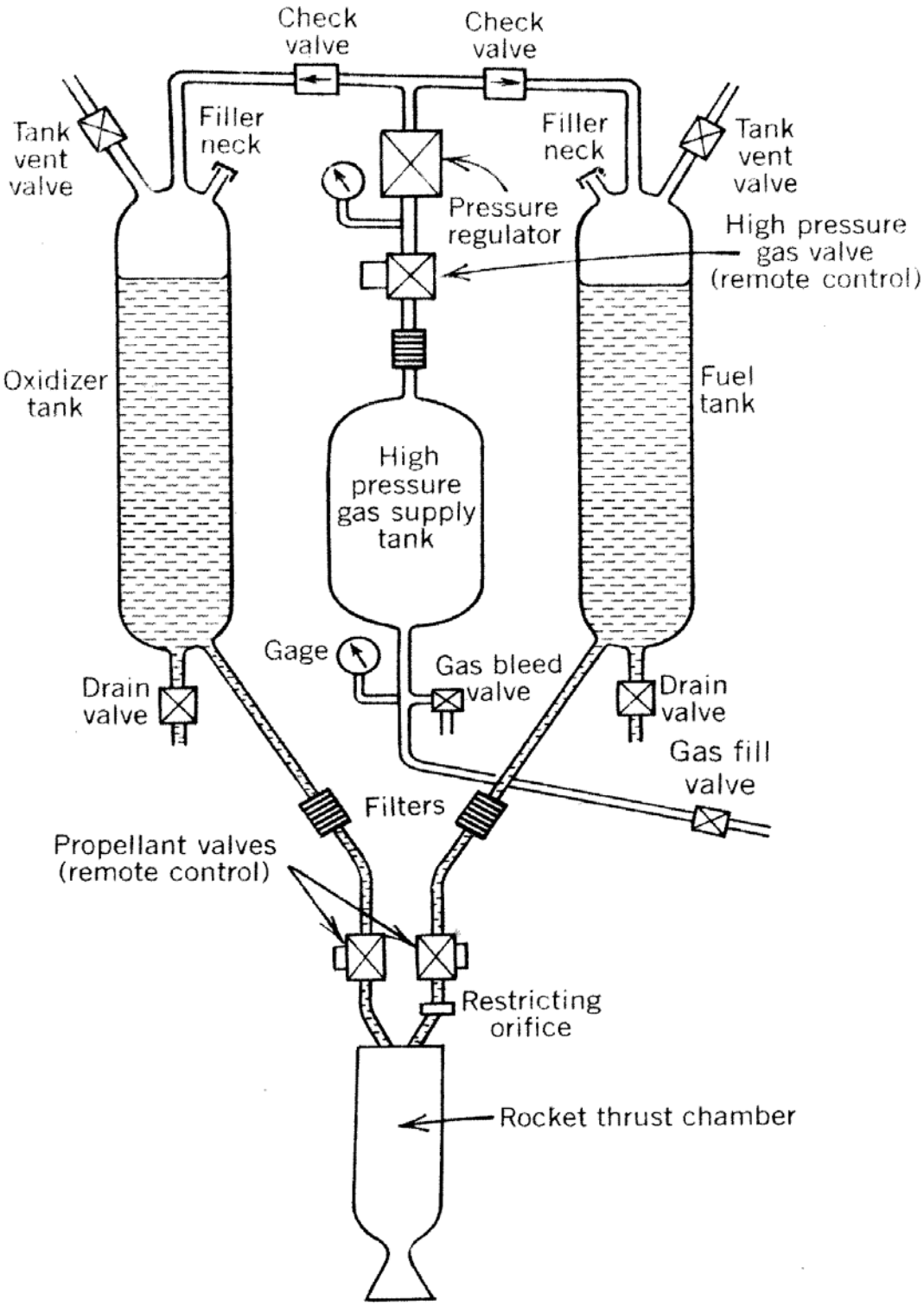

Figure 1.1 Simplified Schematic of a Direct Pressure Fed Liquid Rocket Propulsion System

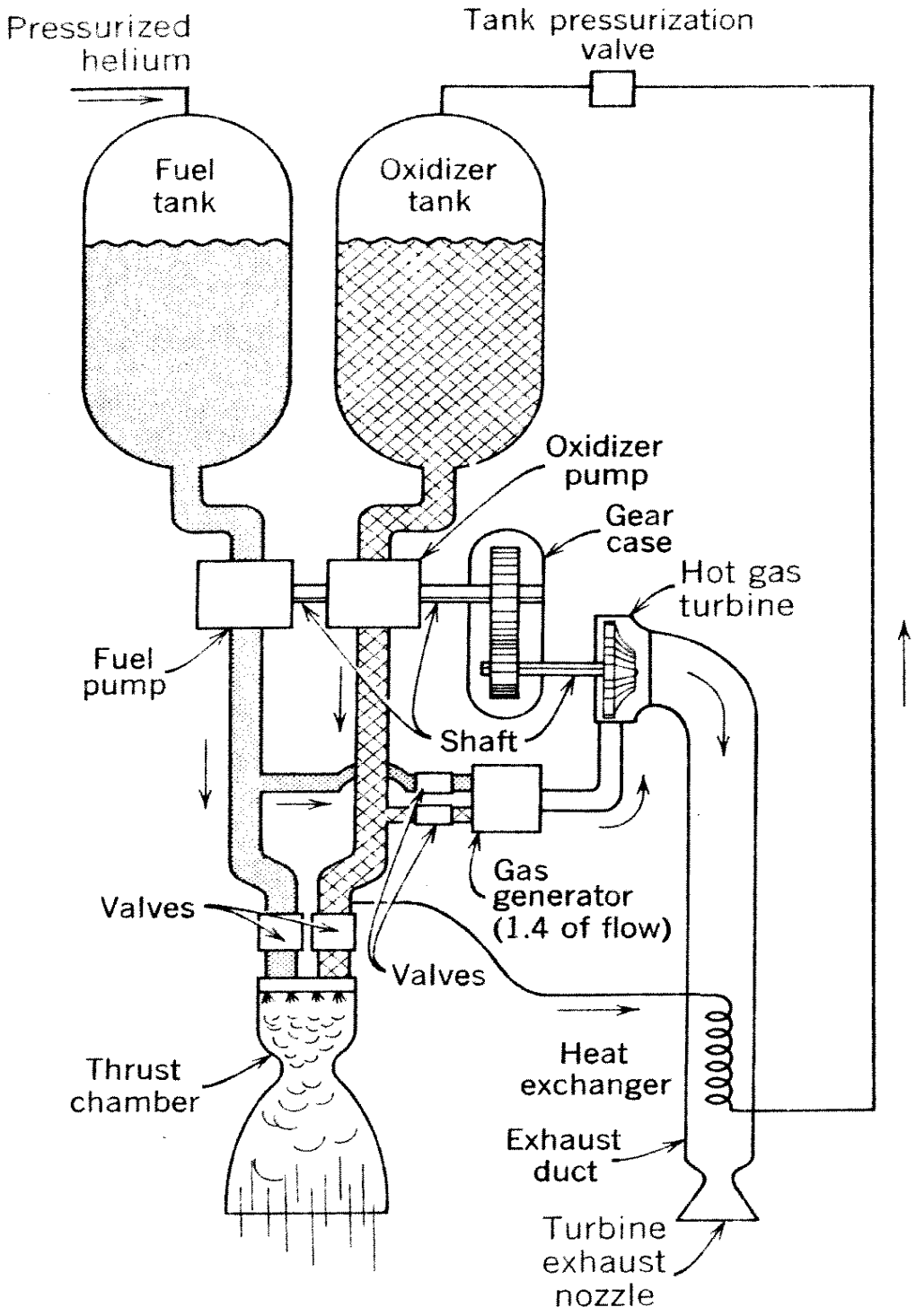

Figure 1.2 Simplified Schematic of a Typical Pump Fed Liquid Rocket Propulsion System (Gas Generator Cycle, Single Turbine Driving Both Pumps)

increased complexity and higher propulsion system pressures associated with a number of recent liquid propellant rockets to increase propulsive efficiency has emphasized the importance of rocket engine component and subassembly ground testing.

For the majority of high-thrust liquid propellant rocket engines and hybrid rocket motors, where one or more pressurized cryogenic propellants are used, a high fidelity and performance ground testing facility is essential. This facility normally operates one to three low- and high-pressure cryogenic propellant feed (run) systems that supply propellants to rocket engine assembly, subassembly, or component test articles at required interface pressures and mass flow rates. For the cases where rocket engine subassemblies and components, such as turbopumps and combustion devices, are ground tested, one or more of the test facility cryogenic propellant run systems operates at high subcritical or supercritical pressures. In all cases, the ground testing facility is required to simulate the remaining propulsion system or flight vehicle by providing required propellant pressures, mass flows, and temperatures at main fluid interfaces of the component being tested.

Cryogenic Propellant Feed System

Figure 1.3 shows a simplified schematic of a ground test facility cryogenic propellant feed system, which supplies propellant to a typical interface on a test article.

Cryogenic Run Tank

The main component of the cryogenic propellant feed (or run) system is the cryogenic propellant run tank. This component serves as the system reservoir where

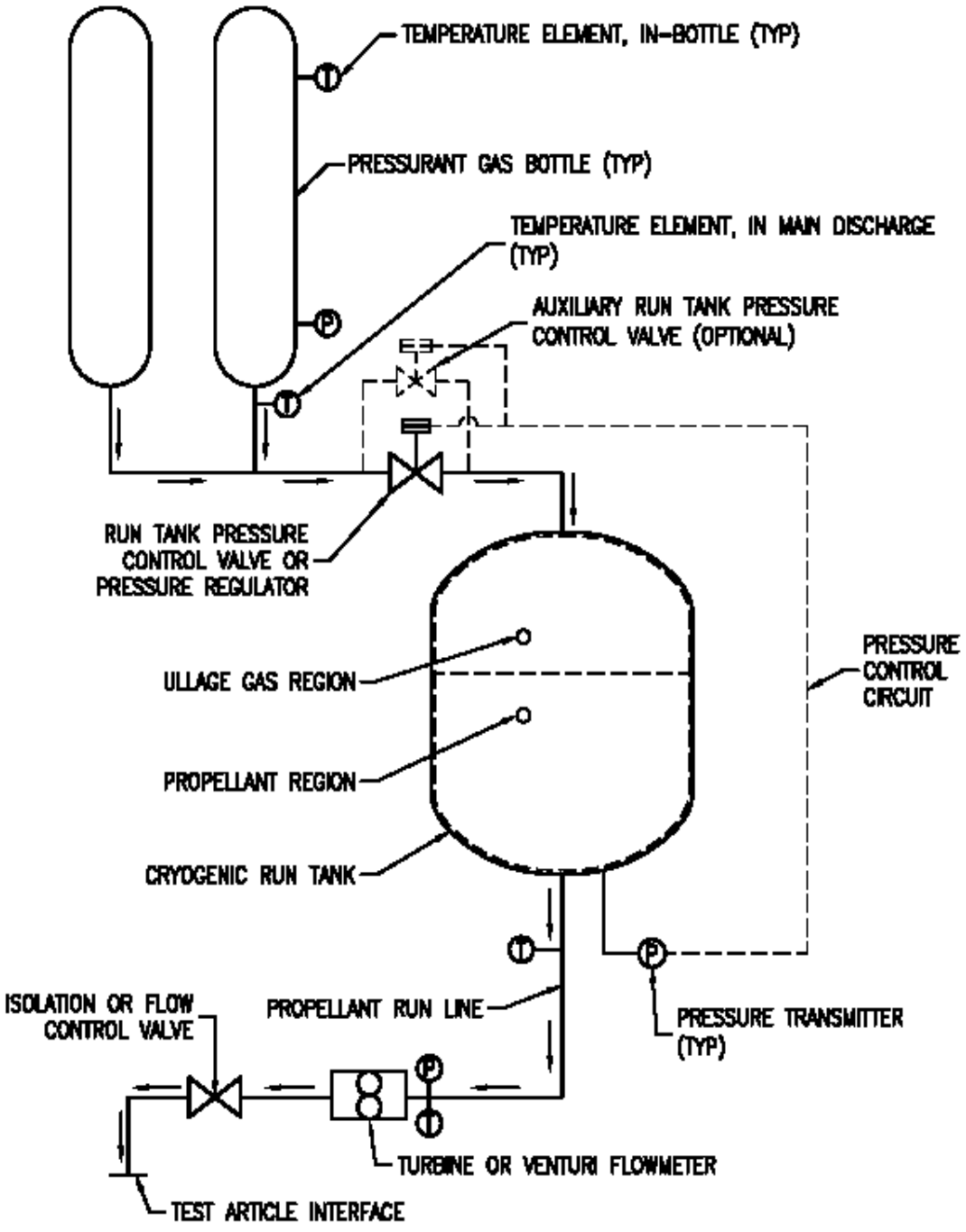

Figure 1.3 Simplified Schematic of a Cryogenic Propellant Feed System

liquid or cold supercritical cryogenic propellant; typically liquid oxygen, liquid hydrogen, or liquid methane; is expelled under pressure at the main discharge nozzle. (Critical pressures for hydrogen, nitrogen, and oxygen are 187.5-psia, 493.0-psia, and 731.2-psia, respectively.) This propellant is conveyed via a cryogenic propellant run system, comprised of series of lines that generally includes valves, filtration device, and flow meter(s), to one or more of the test article interfaces. The cryogenic run tank main discharge nozzle is located at or near the lowest point of the tank such that nearly all propellant can be expelled from the tank.

Referring to Figure 1.3, the internal volume of the cryogenic run tank is comprised of two regions, the propellant region and the ullage gas region.

Pressurant gas needs to be supplied into the ullage gas region as the volume or internal pressure of this region increases. This pressurant gas is normally supplied by one of two methods. In one method, called the autogenous tank pressurant gas supply method, a portion of the liquid or supercritical cryogen exiting the main discharge of the run tank is vaporized or heated by a heat exchanger and is then routed into the tank ullage region at one or more entry points near the top of the tank. For the other method, called the external pressurant gas supply method, pressurant gas is supplied into the tank ullage externally from one or more gas bottles or other sources. To reduce the required mass flow rate of pressurant gas for run tank pressurization and pressurized propellant expulsion, the gas may be heated to elevated temperatures by flow through a heat exchanger prior to entry into the run tank ullage gas region.

For cryogenic propellant run systems used on ground testing facilities, the external pressurant gas supply method is generally employed. Pressurized gas bottles, as

shown in Figure 1.3, provide this gas via a series of pipelines and components to the cryogenic run tank ullage. This method of supplying pressurant gas is generally employed for ground testing facilities for one or more of the following reasons:

1.) High subcritical and supercritical tank pressures would require an excessively large portion of expelled propellant to maintain required tank pressures as density decreases (or specific volume increases) of vaporized or heated propellant are one to three orders of magnitude smaller than those for low to moderate subcritical propellant pressure conditions.

2.) Propellant flow rates are often very high, on the order of 10 to 1000 pounds mass per second (lb_m/sec), and would, therefore, require extremely high heat transfer rates and impractical heat exchanger devices to sufficiently vaporize or heat cryogenic propellant to be used as pressurant gas.

3.) Since oxygen propellant becomes hazardous at elevated pressures and at near ambient or elevated temperatures, nitrogen gas is generally the pressurant gas of choice for oxygen propellant run systems ground testing facilities.

4.) The greatly increased weight of pressurant gas supply bottles, pipelines, and components is not a concern for ground testing facilities.

Pressurant Gas Subsystem

The pressurant gas subsystem supplies all or most of the additional gas needed in the run tank ullage for maintaining required cryogenic run tank pressures as propellant is expelled from the tank. The pressurant gas subsystem is depicted as the gas bottles and

pipelines with associated components between these bottles and the cryogenic run tank ullage gas region in Figure 1.3. The external pressurant gas supply method is modeled in this study because:

1.) It is the method most commonly used on all rocket engine ground testing facilities.

2.) It is generally the most practical and economic method when the cryogenic run tank is operating at high subcritical or supercritical pressures.

The proper sizing and design of the pressurant gas subsystem to provide the needed flow rates of pressurant gas into the run tank ullage for all operating conditions is very critical for both flight vehicles and ground testing facilities. An undersized subsystem results in system or flight vehicle mission failure as the propellant mass flow rate out of the tank cannot be maintained for the required time durations. Conversely, an oversized pressurant gas subsystem results in significant construction and operational cost impacts with no beneficial returns. For flight vehicles, the severe penalty of added weight also exists with an oversized pressurant gas subsystem.

Heat and Mass Transfer Processes in the Cryogenic Run Tank

Unique heat and mass transfer processes occur in cryogenic propellant tanks. For tanks where the fluid propellant is not a cryogen, the pressurant gas, ullage gas, propellant, and tank walls are generally at or near the same temperature. Therefore, negligible heat transfer occurs across ullage gas and propellant region boundaries and mass transfer is limited (negligible evaporation of liquid propellant into ullage gas or

negligible amounts of ullage gas dissolving into the propellant). In these cases, thermodynamic equations of state and well known, easily determined fluid properties can be used with conservation of mass equations to calculate required mass and flow rates of pressurant gas.

However, cryogenic run tanks (and flight vehicle propellant tanks) have propellant regions and tank walls that are generally tens to hundreds of degrees R colder than most of the ullage and the pressurant gases that enter the ullage gas regions. This results in significant rates of heat transfer from the ullage gas region to both tank walls and the cryogenic propellant. Subsequently this heat transfer reduces the temperatures of the ullage gas region, thereby causing its mean density to increase (as compared to the ideal condition where negligible heat transfer takes place). This increase in mean ullage gas density is known as ullage gas collapse and has the net effect of increasing the mass flow rate and total mass accumulation of pressurant gas entering the cryogenic run tank ullage.

Additional factors associated with cryogenic propellant run tank (and flight vehicle propellant tank) pressurization and propellant expulsion processes add complexity and increase the level of difficulty in accurately predicting pressurant gas requirements using analytical methods. These factors include:

1.) Non-uniformity of ullage gas region temperature,

2.) Ullage gas region temperature distribution having a large dependence on entry conditions of the incoming pressurant gas,

3.) Non-uniform temperature distribution within the tank walls,

4.) Temperature dependent thermal properties of the metallic tank wall materials.

5.) Mass transfer between the cryogenic propellant and ullage gas regions.

In order to properly determine pressurant gas reservoir (gas bottle) storage capacity and mass flow rate capacity of pressurant gas pipelines, the heat and mass transfer processes previously described must be 1.) sufficiently understood and modeled through reliable correlations or 2.) accounted for with empirically obtained correction factors/coefficients. For the latter case, the parameters and operating conditions of the cryogenic propellant run tank being evaluated should be within the ranges of parameters and operating conditions that were used for obtaining the correction factors/coefficients.

Accurately Predicting Pressurant Gas Requirements

The ability to accurately predict mass transfer and flow rate requirements, at least with acceptable performance and safety margins, during the initial design process and prior to large financial and labor resource expenditures to construct a ground testing facility or manufacturer flight vehicle hardware is critically important. Analytical tools, computation methods, or computer programs are needed to determine requirements with sufficient levels of accuracy such that the subsystems that supply pressurant gases to propellant tanks are properly designed and sized.

For cases where storage bottles supply pressurant gas to cryogenic propellant tanks, the total accumulated mass transfer of this gas to the tank ullage has a direct effect on the volume and pressure ratings of these bottles. The maximum required flow rates of pressurant gas and the available differential pressures between bottles and tank ullage,

directly affect the sizes of pipelines, valves, and other components in the pressurant gas supply subsystem. For typical rocket engine component ground testing facilities the costs of this hardware is on the order of tens of millions of dollars. Additionally, most of these hardware items are specially engineered and manufactured (not stocked or readily available), which translates to one- to two-year lead times to acquire these items.

Not only are construction costs of ground testing facilities and system weights of flight systems impacted significantly, but the prediction of pressurant gas requirements also has major effects on recurring costs to operate ground testing facilities. Under-predicted requirements result in unsuccessful completion of operational test objectives. Over-predicted requirements result in added labor and commodity costs to re-pressurize pressurant gas supply bottles between tests. The associated cost impacts can range from thousands to hundreds of thousands of dollars per test. With typical rocket engine test programs requiring a series of multiple tests and the operation of one to three separate cryogenic propellant run (feed) systems for each test, the associated cost impacts can be quite significant.

Another operational issue is the virtually certain occurrence of changed operating conditions for the cryogenic propellant run systems in a ground testing facility as a test program progresses. These changed operating conditions can be a benefit when interface pressures or mass flow rates decrease, but will almost certainly be a severe detriment when either or both of these increase.

An additional design and operational performance issue that can arise is the requirement for "pressurization on the fly" where mass flow rates of pressurant gas into a cryogenic run tank can increase by one or two orders of magnitude. Under this

requirement, cryogenic propellant expulsion mass flow rates out of a tank increase usually by a factor of three to 20 while the cryogenic run tank pressure simultaneously increases by a factor of two to six. "Pressurization on the fly" is normally an undesirable, but sometimes unavoidable, requirement because it introduces high levels of uncertainty in addition to significant increases in pressurant gas mass flow rate requirements. The need to apply "pressurization on the fly" is usually the result of throttle range limitations for control valves in the cryogenic propellant run lines from run tank to test article interface(s) coupled with selected test program requirements. These selected requirements generally include dwell time at very low propellant mass flow rate(s) and interface pressure(s) followed by controlled ramp up to much higher flow rates and pressures.

The final consideration regarding operational issues returns to cost and schedule constraints, which are omnipresent for virtually every facility construction project and test program. These constraints generally preclude the ability to perform an extensive series of functional and "cold flow" tests for ground testing facility cryogenic propellant run systems where the full range of system flow conditions are validated prior to testing rocket engine assemblies, subassemblies, and components. The sheer difficulty and expense of performing this series of tests on ground testing facility cryogenic propellant run systems to support each subsequent rocket engine test program would entail use of resources beyond constraints of existing and all foreseeable future test programs. Therefore, the ability to analytically determine run tank pressurant gas requirements in a highly reliable and accurate manner becomes a critical component in assuring that a

ground test facility is able to meet all test objectives of each particular test program slated to utilize that facility.

The typical design approaches used in the development of new technologies or in proving and validating performance of newly designed systems and hardware are usually not practical nor reliable for determining cryogenic run tank pressurant gas requirements. Empirical data for cryogenic propellant run tanks operating at low to moderate subcritical pressures show that collapse factor values vary significantly and are not scalable [Clark (1968); Epstein, Georgius, and Anderson (1965), Nein and Head (1962), and Thompson and Nein (1965)]. For example, the effects of heat transfer between ullage gas and propellant have been found to have minor and sometimes negligible effects in large tanks, but had significant effects in smaller tanks [Nein and Head (1962); Epstein (1965), and Epstein, Georgius, and Anderson (1965)].

Limitations of Prior Work

A large variety of analytical computation methods and tools have been developed since the late 1950's to predict mass flow rate and total mass transfer of pressurant gas into a cryogenic propellant feed (run) tanks. Beginning in the early 1960's when very large cryogenic propellant tanks were being developed and constructed for new and larger spacecraft launch vehicles, computer modeling programs have been developed and used to analytically compute pressurant gas requirements. Some program modeling tools have provided analytical results that have good-to-excellent agreements with empirical results for a wide variety of experimental and in-service conditions. Tank volumes of 25 gallons to hundreds of thousands of gallons were analyzed and studied. For some prior

studies, a limited variety of pressurant gas inlet diffuser geometries were also evaluated for their effects on cryogenic propellant run tank pressurant gas requirements.

However, at the time of development of the higher fidelity and more complex computer programs, main-frame computer systems were required and these programs were generally restricted to entities and organizations with large financial resources. Other more simple computation methods were also developed to enable prediction of cryogenic propellant tank collapse factors without using main-frame computer systems.

With the subsequent developments in personal computers, high-fidelity collapse computer programs developed in the early 1960's have been modified and enhanced. However, work in the development and use of personal computer based programs has been limited and the main focus has been placed on use of the simpler models with enhancements based on new knowledge in the areas of heat transfer, effects of different propellant and pressurant gas species combinations, effects of internal hardware in the propellant tank, and effects of different tank geometric shapes. A typical example of this work is reported in Van Dresar (1995) where the semi-empirical curve fit models presented in Epstein (1965) and in Epstein and Anderson (1968) were enhanced and improved.

Even with the great advancements made to personal computers, virtually all of the computer modeling programs used and developed in the 1960's and early 1970's have been applied only to cases where cryogenic propellant tank pressures are well below the critical pressure of the propellant in the tank. Although ground testing facilities with high supercritical pressure cryogenic propellant feed (run) systems were constructed and put into operation as early as the middle 1970's for testing of rocket engine turbopumps and

combustion devices, very little analytical work is found in the literature regarding pressurant gas requirements for cryogenic tanks operating at higher pressures. Typical tank operating pressures for these ground testing facilities range from 2000 psig to 8500 psig and the ullage gas collapse phenomenon with its associated problems have occurred at these higher tank pressures.

Empirical data for determining pressurant gas requirements in cryogenic propellant tanks at supercritical pressures are virtually non-existent in literature prior to the early 1990's, and data since that time are still limited to a few sources.

In addition to the limited number of analysis tools and computer programs that have been developed for cryogenic propellant tanks operating at supercritical pressures, there are other important attributes that are not contained in any single analytical tool or program. These attributes include:

1.) Newer and more accurate natural convection heat transfer coefficient and Nusselt number correlations for all intra-tank heat transfer processes,

2.) Inclusion of forced convection effects due to incoming pressurant gas velocities and properties in conjunction with the natural convection effects,

3.) Accurate modeling of vertical temperature non-uniformities and gradients known to exist within the cryogenic propellant, ullage gas, and tank walls during tank pressurization and pressurized propellant expulsion processes,

4.) Ability to model non-uniform temperature distribution through the thickness of tank walls while accounting for temperature dependence of tank wall material thermal properties, important for thick-walled tanks used in supercritical pressure applications,

5.) Capability of modeling mass transfer processes between cryogenic propellant and ullage gas,

6.) Ability to model pressurant gas mass transfer within the ullage gas for cases where pressurant gas and cryogenic propellant are different species,

7.) Computational methods that address the lack of phase change and distinct interface between cryogenic propellant and ullage gas regions at supercritical tank pressures.

Objectives of the Study

The main objectives of this study are the development and validation of a high fidelity model to accurately predict pressurant gas requirements and associated collapse factors for cryogenic propellant run tank pressurization and pressurized propellant expulsion processes. This model is in the form of a Visual FORTRAN based computer program having the all but one of the attributes listed in the "Limitations of Prior Work" section earlier in this chapter [Modeling mass transfer across the ullage-gas-to-cryogenic-propellant interface is not provided in the computer model.] Furthermore, this program is designed to handle the run tank geometries (radially symmetric tanks about a vertical axial centerline) used on ground testing facilities and for many flight vehicles.

The new computer program also incorporates interactive program libraries and subroutines that provide highly accurate fluid and tank wall material properties. These are described in further detail in Chapter III.

In addition to the development of a new high-fidelity computer model, validation of this model is also provided by comparing its output results with data obtained from

actual operational tests of ground testing facilities. The major focus of this study is directed toward cryogenic propellant run tanks operating at high supercritical pressures where most of the empirical data are obtained from the high-pressure liquid oxygen and liquid hydrogen run systems on the E-1 test stand at NASA/SSC (National Aeronautics and Space Administration Stennis Space Center) in Hancock County, Mississippi.

Computer model predicted pressurant gas requirements are compared with those obtained empirically. Uncertainties and associated errors in model and empirical results are also evaluated and presented. Adjustments to the computer model, usually by revisions to heat and mass transfer correlation constants, to reduce errors to be within acceptable limits are made and described as necessary.

Justification and Usefulness of the Study

As discussed in previous sections of this chapter, the ability to accurately determine (or predict) cryogenic propellant run tank pressurant gas mass transfer and flow rate requirements early in the initial design is essential to proper sizing of pressurant gas subsystems. This capability is also critical for flight vehicle liquid cryogen propellant tanks and their pressurant gas supply subsystems, usually operated at low subcritical pressures, where weight reduction is critically important.

The ability to accurately predict pressurant gas requirements is equally or even more critical for ground testing facilities that operate cryogenic propellant run systems at near critical and supercritical pressures where previously-developed analytical tools and methods are not usable or may not provide sufficiently accurate results as these were developed only for low subcritical tank pressure applications. Other cryogenic propellant

run feed systems that include tanks operating at low subcritical pressures can also benefit in cases where simplifying assumptions used for previously-developed analytical tools and models may be invalid and can potentially propagate into unacceptable errors.

The availability and proper use of a high-fidelity collapse factor computer program developed as part of this study enables not only more optimal designs of cryogenic propellant run systems and selected design features of the run tanks in these systems, it also enables an accurate and comprehensive parametric evaluation of the widely varying operating conditions that are routinely invoked during test programs. These capabilities translate into the construction and operation of cryogenic propellant run (feed) systems with pressurant gas supply subsystems having required capacities and performance characteristics within facility project or rocket engine test program schedule and budgetary constraints.

Scope and Limitations of Study

The resulting computer program developed under this study is applicable to nearly all processes where cryogenic propellant run tanks are pressurized from near atmospheric or low subcritical pressure to elevated pressure followed by pressurized expulsion of cryogenic propellant from the main (bottom) discharge nozzle of these tanks. This program can be used for both subcritical and supercritical tank pressures. There are, however, a number of limitations and limiting assumptions associated with this study that apply to the proper use and understanding of the program. The specific

limitations and limiting assumptions associated with the program developed under this study are as follows:

1.) The cryogenic propellant run tank must have radial symmetry about a vertically-oriented axial centerline,

2.) The tank must be either a sphere, oblate spheroid, or cylinder with top and bottom end hemisphere or ellipsoid heads,

3.) The tank must have a uniform wall thickness,

4.) The cryogenic propellant must always be expelled from a bottom main discharge nozzle in the tank such that no ullage gas is expelled from this nozzle,

5.) Pressurant gas must always enter the ullage gas region in the tank,

6.) A horizontal virtual interface subdivides the internal volume of the tank into two regions, the cryogenic propellant region and the ullage gas region,

7.) There are no tank or internal fluid motions or fluid flow conditions inside the tank that significantly disturbs the horizontal plane interface between cryogenic propellant and ullage gas,

8.) Initial conditions in the cryogenic propellant run tank prior to initial tank pressurization without propellant expulsion are determined by the user selected initial tank pressure and the following applied conditions:

   a) uniform pressure throughout ullage gas region,

   b) initial pressure less than one half of the critical pressure of the propellant species,

   c) propellant is in saturated liquid state,

d) ullage gas is initially the same species as propellant in the saturated vapor state,

e) tank walls at uniform temperature (saturation temperature of propellant),

9.) All external wall surfaces of the cryogenic run tank are modeled as being adiabatic, considered to be a valid assumption for ground testing facilities that generally have vacuum jacketed tanks and for flight vehicles with well insulated tanks,

10.) The subdivision of the ullage gas region and the upper section of the cryogenic propellant region into finite vertically-stacked-horizontal-lumped-mass segments provides an acceptable approximation of the vertical temperature distribution in these regions (Each segment being treated as having homogeneous fluid properties and the set limits for segment heights in the model are assumed to assure accurate modeling of vertical temperature distribution in cryogenic propellant and ullage gas regions),

11.) No mass transfer occurs across the ullage-gas-to-cryogenic-propellant interface,

12.) Although the model includes limit checks for user input time intervals, tank bottom pressures, and propellant mass flow rates, the program is based on linear changes in these parameters and all fluid properties across each time interval.

Summary and Plan of Presentation

The effects of intra-tank heat and mass transfer processes unique to cryogenic fluid tanks and how these relate to pressurant gas subsystem requirements are explained in generic terms in the previous sections of this chapter. Additionally, the various design and operating parameters and conditions having effects on pressurant gas requirements and an overview of analytical methods used for predicting these requirements have also been described. Finally, the generic computer model attributes necessary for consistently accurate predictions of pressurant gas mass transfer and flow rate requirements are presented. These attributes, not incorporated into any single previously developed computer models, are incorporated into the new model developed under this study.

The remaining chapters of this study present the following:

1.) Further details of prior work and studies related to this study or deemed to be of significance to this study,

2.) Presentation of computer program algorithms developed and utilized for the new computer model,

3.) Descriptions and illustrations showing how algorithms are assembled and sequentially utilized in modules, routines, and subroutines of the model,

4.) Presentation of cryogenic propellant run tank pressurant gas mass transfer results obtained from the model,

5.) Comparison of new computer program pressurant gas mass transfer and other parametric results with empirical results including the evaluation and presentation of the effects of uncertainties and associated errors,

6.) Summary of the above items with conclusions including recommendations for future work.

CHAPTER II

LITERATURE REVIEW

A great deal of work has been performed regarding ullage gas collapse in cryogenic propellant tanks and the analytical predictions and empirical measurements of pressurant gas mass transfer and flow rate requirements.

This chapter presents a general overview and summary of the prior work and studies. The chapter is subdivided into two main sections. The first section presents empirically obtained data from the studies and the last section presents an overview of analytical correlations and techniques, computation routines, and modeling programs used for predictions of pressurant gas mass transfer and flow rate requirements.

Collapse Factor

An important parameter, "Collapse Factor," has been defined and used in much of the literature as a measure of performance for the process in which a pressurant gas is transferred into the ullage of a cryogenic propellant tank in order to maintain and control pressures in the tank.

"Collapse Factor" is defined as the ratio of actual-to-ideal pressurant gas requirements for both tank pressurization and pressurized propellant expulsion from a cryogenic propellant run tank. There are two types of collapse factor that are defined as

performance metrics when designing, analyzing, or evaluating pressurant gas subsystems used for cryogenic run tanks. These are "Instantaneous Collapse Factor" and "Cumulative Collapse Factor." Instantaneous collapse factor is defined as the ratio of pressurant gas mass flow rate into a cryogenic propellant run tank under actual conditions to the mass flow rate under ideal conditions. Cumulative collapse factor is defined as the total mass of pressurant gas transferred into the cryogenic propellant tank under actual conditions divided by the total mass of this gas transferred under ideal conditions. For both types of collapse factors, the ideal conditions are based on and derived under the following assumptions:

1.) Negligible heat transfer at ullage gas and propellant region boundaries,

2.) Propellant and ullage gas occupy two distinct regions in the tank,

3.) Propellant region and ullage gas region are each at uniform temperatures,

4.) Pressurant gas that enters the ullage gas region is uniformly mixed with ullage gas in this region,

5.) Mass transfer across the interface between the propellant and the ullage gas is negligible,

6.) The ullage gas region has a uniform mixture ratio of gases if more than one species of gas is present in the region.

Actual conditions take into account all heat and mass transfer processes that occur across the propellant and ullage gas region boundaries and that occur within each of these regions. For low-to-moderate subcritical pressure cryogenic propellant run systems, actual conditions can be obtained empirically from existing systems. This has often been done in studies to check the results of analytical methods and computer programs used

for prediction of collapse factors. For run systems operating at near critical and supercritical pressures there are very little data that have been compared to predicted collapse factors.

Empirical Collapse Factor Data

Since the late 1950's, a wide variety of collapse factor data have been obtained. Table 2.1 presents a sampling of empirically-obtained collapse factors for tank pressurization and pressurized tank expulsion of liquid oxygen (LOX), liquid methane (LCH_4), and liquid nitrogen (LN). Table 2.2 reviews empirical collapse factor data from tank pressurization and pressurized tank expulsion of liquid hydrogen (LH) and slush hydrogen (SLH) propellants. In both Tables 2.1 and 2.2, other data are presented in addition to collapse factors to provide an indication of the variety and range of propellant tank and interfacing system conditions associated with the range of collapse factor values. These data include the reference citation and test run numbers, if available, associated with each of the empirical collapse factors. Unless noted otherwise, all empirical collapse factors in Tables 2.1 and 2.2 are cumulative collapse factors at the end of tank expulsion where single values are listed. Where a range of collapse factor values is presented, this range defines the minimum and maximum cumulative collapse factors between the start of propellant expulsion from the tank and the end of this expulsion process, unless noted otherwise on the tables.

In seven of the cited references in Tables 2.1 and 2.2, the actual pressurant gas requirements are presented, but collapse factors and ideal pressurant gas requirements are not provided by these references. These references are Barber (1966),

Table 2.1 Selected Empirical Collapse Factor Data for Non-Hydrogen Propellant Tanks

					Propellant Expulsion				Pressurant Gas			
Reference Citation	Test Run #	Tank Volume (gallons)	Tank Shape	Prop.	Mass Flow Rate (lb/sec)	Vol. Flow Rate (gpm)	Time (sec)	Tank Press. (psia)	Species	Inlet Temp. (deg R)	Notes	Empirical Collapse Factor
Barber (1966)	None	25	Cylindrical	LN	10.0 - 14.0	88.9 - 124.3	16	172.3 - 300.4	He	523 - 530	(1)	1.540
Barber (1966)	None	25	Cylindrical	LN	10.0 - 14.0	88.9 - 124.3	16	155.2 - 321.6	Steam/He	1938 - 2029	(1), (2)	1.510
DeWitt and McIntire (1974)	36	489.5	Sphere	LCH_4	3.62	61.5	389.2	49.3	He	407		1.769
DeWitt and McIntire (1974)	41	489.5	Sphere	LCH_4	3.625	61.5	390.3	49.5	He	407		2.431
DeWitt and McIntire (1974)	40	489.5	Sphere	LCH_4	2.332	39.5	598.5	49.5	He	596		2.423
DeWitt and McIntire (1974)	6	489.5	Sphere	LCH_4	2.244	38.1	632.8	49.5	GCH_4	407		2.352
DeWitt and McIntire (1974)	11	489.5	Sphere	LCH_4	6.137	104.6	233.5	49.2	GCH_4	608		2.550
DeWitt and McIntire (1974)	99	489.5	Sphere	LCH_4	3.823	65.1	377.7	49.5	GN	603	(3)	5.247
Epstein and Anderson (1968)	Ref. 10	11220	Oblate Spheroid	LOX	201.2	1267.4	478	~46	He	325	(8)	1.375
Epstein and Anderson (1968)	Ref. 12	94996	Oblate Spheroid	LOX	2230 - 2256	14047 - 14227	360	36. - 37.5	GOX	510	(9)	1.325 - 1.500
Lacovic (1970)	12B	2596	Oblate Spheroid	LOX	57.7	363.5	47	34	He	520		2.432
Lacovic (1970)	13A	2596	Oblate Spheroid	LOX	57.7	363.5	120	34	He	527		2.605
Lacovic (1970)	10	2596	Oblate Spheroid	LOX	57.7	363.5	415	34	He	255		1.304
Lacovic (1970)	14A	2596	Oblate Spheroid	LOX	57.7	363.5	242	40	He	525		1.961
Nein and Head (1962)	?	59892	Multi-Cylinder	LOX	3767 - 3769	23740	114.5	60 - 80	GOX/GN	840 - 600	(4), (5), (6)	~1.700
Nein and Head (1962)	?	10098	Cylindrical	LOX	1261	7943	70	68 - 76	GOX/GN	602 - 641	(5), (6)	~1.650
Nein and Head (1962)	?	16.5	Cylindrical	LN	0.924	8.21	120	50	GN	530	(5)	~2.110
Shelburn (1990)	74	5000	Cylindrical	LN	30. - 525.	267. - 4729.	38	335. - 359.	GN	506 - 447		2.35 - 1.39
Shelburn (1990)	74	900	Sphere	LOX	10.2	61.5	26	8200 - 8300	GN	548 - 544	(7)	4.1 - 1.57

Notes:

(1) Assumed near constant ullage gas temperature and no GN in ullage for expulsion

(2) Tank pre-pressurized with helium prior to expulsion with steam as pressurant gas

(3) Data shows 69.3% of added GN pressurant gas dissolved into upper layer of LCH_4 propellant

(4) Multiple tanks with 4-each 70-inch diameter tanks connected to one-each central 105-inch diameter tank

(5) Collapse factors approximated using energy allocations for ullage gas; insufficient data for more exact computations

(6) Tank pre-pressurized with GN prior to using GOX for propellant expulsion

(7) Only last 26-seconds of 38-second run has reliable data

(8) Propellant explusion flowrate based on assumed 10% initial ullage and complete emptying of propellant from tank

(9) Tank pressure and LOX expulsion rate obtained from Cowart (1968) using average summations of LOX flow rate to 5-each J-2 engines on S-II stage

Table 2.2 Selected Empirical Collapse Factor Data for Hydrogen Propellant Tanks (Page 1 of 2)

					Propellant Expulsion				Pressurant Gas			
Reference Citation	Test Run #	Tank Volume (gallons)	Tank Shape	Prop.	Mass Flow Rate (lb/sec)	Vol. Flow Rate (gpm)	Time (sec)	Tank Press. (psia)	Species	Inlet Temp. (deg R)	Notes	Empirical Collapse Factor
Lockheed Report ER-5238 (1961)	B-1	12	Cylindrical	LH	Not Given	Not Given	62.4	39.25	GH/He	330	(1)	3.42
Lockheed Report ER-5238 (1961)	B-2	12	Cylindrical	LH	Not Given	Not Given	62.4	39.25	GH/He	265	(1)	2.16
Lockheed Report ER-5238 (1961)	B-1	12	Cylindrical	LH	No Expulsion	N/A	N/A	14.7 - 44.25	GH	505		4.45
Lockheed Report ER-5238 (1961)	B-1	12	Cylindrical	LH	No Expulsion	N/A	N/A	14.7 - 61.75	GH	295		3.26
Lockheed Report ER-5238 (1961)	2	500	Cylindrical	LH	2.561	259.4	100	45.5	GH	320	(2), (3)	2.23
Lockheed Report ER-5238 (1961)	5	500	Cylindrical	LH	2.031	205.7	99	45.5	He	300	(2), (3)	1.72
Lockheed Report ER-5238 (1961)	7	500	Cylindrical	LH	2.031	205.7	105	49.3	GH	300	(2), (4)	1.74
Lockheed Report ER-5238 (1961)	10	500	Cylindrical	LH	1.833	185.7	111	45	GH	300	(2)	1.74
Bourgarel, et al. (1968)	3	~370	Cylindrical	LH	0.939	95.1	197	44.1	He	450	(5)	0.878; 0.997
Bourgarel, et al. (1968)	6	~370	Cylindrical	LH	0.47	47.6	351	44.1	He	450	(5)	0.908; 1.033
Bourgarel, et al. (1968)	9	~370	Cylindrical	LH	0.624	63.3	352	29.4	He	450	(5)	1.043; 1.187
Bourgarel, et al. (1968)	10	~370	Cylindrical	LH	0.939	95.1	211	44.1	He	180	(5)	0.48; 0.527
Bourgarel, et al. (1968)	11	~370	Cylindrical	LH	0.939	95.1	214	44.1	GH	180	(5)	1.267; 1.277
Coxe and Tatum (1962)	1 of Ref. 3	500	Cylindrical	LH	2.995	303.4	89	45.5	GH	300	(3)	1.56
Coxe and Tatum (1962)	2 of Ref. 3	500	Cylindrical	LH	2.388	262.1	103	47.6	GH	520	(3)	2.23
Coxe and Tatum (1962)	3 of Ref. 3	500	Cylindrical	LH	2.22	224.8	120	46.5	GH	300	(3)	1.8
Coxe and Tatum (1962)	5 of Ref. 3	500	Cylindrical	LH	2.694	272.90	99	45.5	He	300	(3)	1.72
Epstein and Anderson (1968)	Ref. 11	49,472	Sphere	LH	60.84	6140.5	296	91.7	GH	530		1.64
Epstein and Anderson (1968)	Ref. 12	246,840	Multi-Cylinder	LH	391.4 - 394.1	39696 - 39970	360	28.5 - 30.0	GH	200	(6)	1.15 - 1.25
Hardy and Whalen (1991)	?	461.5	Sphere	SLH	1.478	131	190	50	GH	520	(7)	2.568
Hardy and Whalen (1991)	?	461.5	Sphere	SLH	0.552	48.9	510	25	GH	620	(7)	10.34
Hardy and Whalen (1991)	?	461.5	Sphere	SLH	0.668	59.2	420	50	GH	620	(7)	5.973
Mandell and Roubebush (1965)	2 of Ref. 2	210	Cylindrical	LH	1.062	106.6	93	161	GH	210		2.12
Mandell and Roubebush (1965)	3 of Ref. 2	210	Cylindrical	LH	0.346	35	284	57	GH	170		3.88
Mandell and Roubebush (1965)	8 of Ref. 2	210	Cylindrical	LH	1.161	116.6	90	159	He	161		2.14
Mandell and Roubebush (1965)	10 of Ref. 2	210	Cylindrical	LH	0.311	31.6	309	40	He	148		5.1
Moore, et al. (1960)	4 - 11	600	Horizontal Cyl	LH	0.56	57	420	27.5	GH	480 - 549	(8)	1.2 - 1.25
Moore, et al. (1960)	3	600	Horizontal Cyl	LH	0.31	31	1220	35	GH	480 - 549	(8)	4.32
Moore, et al. (1960)	7	600	Horizontal Cyl	LH	1.56	157	340	115	GH	480 - 549	(8)	1.67
Moore, et al. (1960)	9	600	Horizontal Cyl	LH	2.48	250	560	115	GH	480 - 549	(8)	2.20
Moore, et al. (1960)	5	600	Horizontal Cyl	LH	2.53	256	450	65	GH	480 - 549	(8)	2.52
Moore, et al. (1960)	6	600	Horizontal Cyl	LH	0.84	85	410	65	GH	480 - 549	(8)	1.80
Stochl and DeWitt (1969)		489	Sphere	LH	2	202	130	50	GH	500		~2.38
Stochl and DeWitt (1969)		489	Sphere	LH	0.5	50.6	522	50	GH	500		~3.33
Stochl and DeWitt (1969)		8604	Sphere	LH	10.3	1043	446	50	GH	500		~2.29
Stochl and DeWitt (1969)		8604	Sphere	LH	4.33	438	1060	50	GH	500		~2.86
Stochl and DeWitt (1969)		489	Sphere	LH	1.89	191	138	50	GH	540		~2.76
Stochl and DeWitt (1969)		8604	Sphere	LH	10	1012	459	50	GH	600		~2.33
Stochl, et al. (1970, TN-D-5621)	7	489	Sphere	LH	0.65	65.9	453.4	50	GH	481 - 517	(9)	~2.86
Stochl, et al. (1970, TN-D-5621)	10	489	Sphere	LH	1.86	187.9	193.2	50	GH	481 - 517	(9)	~2.53
Stochl, et al. (1970, TN-D-5621)	12	489	Sphere	LH	0.77	77.5	393.2	50	GH	481 - 517	(9)	~3.03
Stochl, et al. (1970, TN-D-5621)	14	489	Sphere	LH	0.92	92.9	337	50	GH	481 - 517	(9)	~2.94

Table 2.2 Selected Empirical Collapse Factor Data for Hydrogen Propellant Tanks (Page 2 of 2)

					Propellant Expulsion				Pressurant Gas			
Reference Citation	Test Run #	Tank Volume (gallons)	Tank Shape	Prop.	Mass Flow Rate (lb/sec)	Vol. Flow Rate (gpm)	Time (sec)	Tank Press. (psia)	Species	Inlet Temp. (deg R)	Notes	Empirical Collapse Factor
Stochl, et al. (1970, TN-D-5621)	84	489	Sphere	LH	0.98	98.8	307.6	50	GH	481 - 517	(9)	~2.73
Stochl, et al. (1970, TN-D-5621)	85	489	Sphere	LH	1.91	193	174.4	50	GH	481 - 517	(9)	~2.58
Stochl, et al, (1970, TN-D-7019)	4	8604	Sphere	LH	9.60	972	531.6	50	GH	302	(9)	1.85
Stochl, et al, (1970, TN-D-7019)	7	8604	Sphere	LH	4.28	433	1119.3	50	GH	302	(9)	2.07
Stochl, et al, (1970, TN-D-7019)	8	8604	Sphere	LH	4.66	472	1037.2	50	GH	303	(8), (9)	2.07
Stochl, et al, (1970, TN-D-7019)	15	8604	Sphere	LH	10.07	1019	509.3	50	GH	540	(9)	2.60
Stochl, et al. (1991)	5	1291	Oblate Spheroid	LH	0.60-0.65	66.3	2160	54.6	GH	491	(10), (14)	5.222
Stochl, et al. (1991)	5 R	1291	Oblate Spheroid	LH	0.38-0.40	66.3	1680	54.7	GH	491	(11), (14)	5.333
Stochl, et al. (1991)	6	1291	Oblate Spheroid	LH	0.60-0.65	40.8	2280	54.9	GH	491	(12), (14)	5.0
Stochl, et al. (1991)	9	1291	Oblate Spheroid	LH	0.60-0.65	66.3	1620	55.0	GH	594	(13), (14)	4.933
Van Dresar & Stochl (1993)	506	1291	Oblate Spheroid	LH	~0.83	83.6	760	33.9	GH	529		2.46
Van Dresar & Stochl (1993)	507	1291	Oblate Spheroid	LH	~0.58	58.5	1086	44.3	GH	531		2.568
Van Dresar & Stochl (1993)	508	1291	Oblate Spheroid	LH	~0.32	32.2	1974	44	GH	533		2.58
Van Dresar & Stochl (1993)	509	1291	Oblate Spheroid	LH	~0.84	84.7	741	54.3	GH	535		2.85
Van Dresar & Stochl (1993)	510	1291	Oblate Spheroid	LH	~0.58	58.3	1089	54.9	GH	531		2.74
Van Dresar & Stochl (1993)	511	1291	Oblate Spheroid	LH	~0.32	32.1	1978	55.1	GH	526		2.86
Whalen and Hardy (1992)	?	489	Sphere	SLH	~0.55	52.3	505	35	GHe	540		3.788
Whalen and Hardy (1992)	?	489	Sphere	SLH	~1.26	120.0	220	35	GHe	540	(7)	3.178
Whalen and Hardy (1992)	?	489	Sphere	SLH	~0.54	51.8	510	35	GHe	250	(7)	2.100
Whalen and Hardy (1992)	?	489	Sphere	SLH	~1.38	132.0	200	35	GHe	250	(7)	1.591
Whalen and Hardy (1992)	?	489	Sphere	SLH	~0.58	55.0	480	35	GHe/GH	540	(1), (7)	6.655
Whalen and Hardy (1992)	?	489	Sphere	SLH	~1.32	125.7	210	35	GHe/GH	540	(1), (7)	3.727

Notes:

(1) Pre-pressurized with helium followed by expulsion with hydrogen pressurant gas

(2) Propellant expulsion flow rates approximated by scaling of tank geometry drawings, given initial ullage height, liquid level change in tank with associated time span; Collapse Factor data also reported in Mandell & Roudebush (1965)

(3) Horizontal sloshing in tank at 0.5-Hz and 0.5-inch amplitude throughout expulsion

(4) Horizontal sloshing in tank at 0.5-Hz and 0.5-inch amplitude for last 85-seconds of expulsion

(5) Two collapse factors; first based on constant ullage gas temperature and pressure throughout expulsion; second based on saturated GH vapor in ullage at one atmosphere before tank pressurization

(6) Propellant mass flow rate data obtained from average LH propellant consumption of 5-each J-2 rocket engines on Saturn launch vehicle S-II stage from Cowart (1968); tank pressure also obtained from this reference

(7) SLH is slush hydrogen, mixute of solid and liquid hydrogen

(8) Pressurant gas inlet temp. not reported; est. based on description of test apparatus and procedures

(9) Initial 30 to 56 sec. of the total time is tank pressurization and hold prior to propellant expulsion

(10) Submerged injection of pressurant gas, 21 min. tank pressurization, 15 min. CLH expulsion

(11) Submerged injection of pressurant gas, 13 min. tank pressurization, 15 min. CLH expulsion

(12) Submerged injection of pressurant gas, 13 min. tank pressurization, 25 min. CLH expulsion

(13) Submerged injection of pressurant gas, 12 min. tank pressurization, 15 min. CLH expulsion

(14) Initial 12- to 21-minutes of the total time is tank pressurization and hold prior to propellant expulsion

Bourgarel, et al. (1968), DeWitt and McIntire (1974), Hardy and Whalen (1991), Lacovic (1970), Shelburne (1990), and Whalen and Hardy (1992). For these references, the ideal pressurant gas requirements are analytically computed in order to compute collapse factors.

Discussion of Empirical Collapse Factor Data

Tables 2.1 and 2.2 present a very wide range of collapse factors. In addition to the very wide range of collapse factor values shown in Tables 2.1 and 2.2, there are a number of interesting observations presented by the cited references.

Perhaps the most important and significant observation is the paucity of empirical data for supercritical and high subcritical tank pressure conditions. Only one case, Shelburne (1990), test number 74 for LOX propellant in Table 2.1, is a condition where tank pressures are above the critical pressures of the LOX propellant. The data from Barber (1966); Mandell and Roudebush (1965); and Moore, et al. (1960) have cases where high subcritical tank pressure conditions existed during tests. Another case from Shelburne (1990) also had a high subcritical pressure tank pressure condition for an LN tank expulsion.

In Bourgarel, et al. (1968), an unusually low collapse factor of 0.489 or 0.527 is determined, meaning that the actual pressurant gas requirement is about half of the requirement under ideal conditions. However, the validity of this and other data from Bourgarel, et al. (1968) is not certain because a number of important and critical details about initial ullage gas conditions and how the tank was conditioned and pressurized prior to LH expulsion are not clearly stated.

A number of the citations included in Tables 2.1 and 2.2 indicate that decreasing the time of tank pressurization and propellant expulsion has the net effect of decreasing the collapse factors. The results from Epstein (1965), Hardy and Whalen (1991), Lacovic (1970), Mandell and Roudebush (1965), Moore, et al. (1960), Stochl and DeWitt (1969), Stochl, et al. (1970, NASA TN-D-7019), Van Dresar and Stochl (1993), and Whalen and Hardy (1992) confirm this general trend. In a number of these references, decreased tank pressurization and propellant expulsion times result in less heat transfer time and, thus, less total heat transfer from ullage gas to propellant and tank walls.

For LH propellant expulsions, the use of helium pressurant gas yielded similar collapse factors to those when gaseous hydrogen (GH) was used as the pressurant. Comparison of data from Stochl and DeWitt (1969) to data from Stochl, et al. (1970, NASA TN-D-7019) for an 8605-gallon LH tank supports this finding. Data from Epstein (1965) also supports this finding. When horizontal LH sloshing occurs in the tank, data from Lockheed Report ER-5238 (1961) indicate that helium pressurant gas yields lower collapse factors when compared with GH pressurant. For all cases, the total mass required for GH pressurant is less than that of helium due to the much lower density of GH.

Ullage Gas Region Properties Distribution

One of the most important and influential attributes of a cryogenic propellant tank system with respect to collapse factors during tank pressurization and pressurized propellant expulsion processes is the variation and distribution of fluid properties within the ullage gas region. The variation of ullage gas properties is mainly due to temperature

gradients in the ullage gas region as pressures vary very little because of low ullage gas densities, short vertical tank (and maximum ullage gas region) heights, and ullage gas elevation head pressures being small in comparison to absolute tank pressures. For selected cases where propellant and pressurant gas are different species and where significant levels of mass transfer of propellant species into and within the ullage gas region are occurring, the distribution of propellant species mass fraction within the ullage gas region can also have an effect on the distribution of fluid properties in the ullage gas region. However, the ullage gas temperature distribution is likely the dominant effect on the distribution of fluid properties within this region for most cases. The dominant effect of temperature on the distribution of ullage gas properties is primarily due to the relatively short time durations of typical tank pressurization and propellant expulsion processes as well as the natural stability of the fluid regions inside the tank where fluid temperatures decrease and fluid densities increase when traversing from the top to the bottom in the tank.

Regarding the literature, there are a number of empirical tests where temperatures are measured at many discrete locations in the ullage gas region of cryogenic propellant tanks. These measurements have been recorded at discrete times through tank pressurization and pressurized propellant expulsion processes. Unfortunately, there are no ullage gas region temperature distribution data for supercritical tank pressure conditions and no practicable methods exist to obtain these data at the high supercritical pressures. Previous attempts to utilize insitu instruments inside cryogenic propellant tanks at supercritical pressures, necessary to obtain accurate temperature measurements

of fluids inside the tank, have resulted in unreliable data from, severe damage to, or destruction of these types of instruments.

Ullage Gas Region Vertical Temperature Gradients

Table 2.3 presents selected vertical ullage gas temperature distribution data obtained from direct temperature measurements within the ullage gas region during tank pressurization and pressurized propellant expulsion processes. Citations of corresponding studies are also included for data provided on Table 2.3.

In a small portion of the cases presented in Table 2.3, propellant expulsions from the tank were not performed and tank pressurizations were accomplished by closing all valves connected to the tank and using the naturally occurring heat transfer into the tank or externally supplied heat to vaporize cryogenic liquid propellant and heat all fluids inside the tank.

Virtually all of the cases presented in Table 2.3 indicate very large vertical temperature gradients in the ullage gas region. The differences between maximum and minimum temperatures in this region range from 150 R to 475 R.

In the majority of cases, the vertical temperature profiles in the ullage gas regions are more linear at the end of propellant expulsion than during initial tank pressurization and the start of propellant expulsion.

In Kendle (1969) and Stochl and DeWitt (1969), the geometry of the pressurant gas inlet injector (or diffuser) has a significant effect on the resulting vertical ullage gas temperature distribution which in turn effects the resulting collapse factors significantly.

Table 2.3 Selected Empirical Ullage Gas Region Vertical Temperature Distribution/Gradient Data (Page 1 of 2)

Reference Citation	Test Number	Prop.	Press. Gas	Press. Gas Inlet Temp. (deg R)	Prop. Expul. Time (sec)	Min. Ullage Gas Height (ft)	Max. Ullage Gas Height (ft)	Max. Ullage Gas Temp. (deg R)	Ullage Gas Region Vertical Temperature Gradient (deg R) Minimum	Ullage Gas Region Vertical Temperature Gradient (deg R) Maximum	Non-Linearity of Cert. Temp. Gradient (H,M,L)**	Notes
Lockheed Report ER-5238 (1961)	3	LH	GH	300	120	1.08	7.33	255	?	218.5	M	
Lockheed Report ER-5238 (1961)	5	LH	He	300	99	1.08	7.33	260	?	223.5	M	
Lockheed Report ER-5238 (1961)	7	LH	GH	300	111	1.08	6.67	292	?	255.5	M	
Arnett and Voth (1972)	B-2	LH	N/A	N/A	N/A	14.8	14.8	164.7	80.1	126	L to LM	(1)
Baral (1988)	(Fig. 4)	LOX	GOX	540	100	~6.56	29.53	495	288	333	H, L	
Bouregal (1968)	1	LH	He	450	217	~0.51	~9.20	441	342	405	LM	
Bouregal (1968)	3	LH	He	450	197	~0.72	~9.20	450	351	405	L	
Bouregal (1968)	7	LH	He	450	375	~1.37	~9.20	450	405	405	LM	
Bouregal (1968)	11	LH	GH	180	214	~0.63	~9.20	201.6	149.4	193	H	
Bowersock, et al. (1960)	RT-3	LN	GN	~520	175	1.41	2.50	380	140	195	H, L	
Cady, et al. (1990)	2.0-6	TPLH	GH	540	~980	1.00	2.50	279	193	238	H	(2)
Cady, et al. (1990)	2.0-8	TPLH	He/GH	144 and 540	~870	1.00	2.50	243	180	211	H, M	(2), (3)
Clark (1965)	130-15 in Ref. 2	LOX	He	500 - 605	120	2.80	31.0	595	380	405	L	
Coxe and Tatum (1962)	1 (Fig. 5)	LH	GH	300	89	0.70	8.17	~285	~223.5	~248.5	M, MH	
DeWitt and McIntire (1974)	8	LCH_4	GCH_4	400	231	~0.85	4.15	409	?	174.6	M	
DeWitt and McIntire (1974)	6	LCH_4	GCH_4	400	633	~0.85	4.15	410.4	?	176.4	M	
DeWitt and McIntire (1974)	11	LCH_4	GCH_4	600	234	~0,85	4.15	603	?	369	LM	
DeWitt and McIntire (1974)	37	LCH_4	He	400	223	~0.85	4.15	414	?	211	MH	
DeWitt and McIntire (1974)	42	LCH_4	He	600	224	~0.85	4.15	583	?	380	H	
DeWitt and McIntire (1974)	63	LCH_4	GH	400	219	~0.85	4.15	396	?	193	LM	
DeWitt and McIntire (1974)	68	LCH_4	GH	600	222	~0.85	4.15	601	?	398	H	
Hasan, et al. (1991)	?	LH	N/A	N/A	14400	1.42	1.42	90	5.4	49.5	L (5)	(1), (4), (5)
Hasan, et al. (1991)	?	LH	N/A	N/A	14400	1.42	1.42	84.6	4.5	48.6	L (5)	(1), (4), (5)
Kendle (1970)	?	LH	GH	~525	130	~0.35	6.75	535	?	~475	L (9)	(6), (9)
Kendle (1970)	?	LH	GH	~525	130	~0.35	6.75	495	?	~435	L (9)	(7), (9)
Kendle (1970)	?	LH	GH	~525	130	~0.35	6.75	305	?	~245	L (10)	(8), (10)
Nein and Thompson (1965)	130-6	LOX	GOX	540	150	~1.9	~34.0	535	302	372	M, L	
Nein and Thompson (1965)	130.9	LOX	GOX	370	150	~1.9	34.00	370	147	207	H	
Roudebush (1965)	Ex. 1	LH	GH	488-525	90	~0.8	2.0	488	?	428	L	
Roudebush (1965)	Ex. 1	LH	GH	488-525	178	~0.8	3.50	488	?	428	L	
Roudebush (1965)	Ex. 1	LH	GH	488-525	320	~0.8	5.91	488	?	428	L	
Roudebush (1965)	Ex. 2	LH	GH	480-515	93	?	5.91	507	?	436	M-L	(12)
Roudebush (1965)	Ex. 3	LH	GH	375-520	284	?	5.91	505	?	450	ML	

Table 2.3 Selected Empirical Ullage Gas Region Vertical Temperature Distribution/Gradient Data (Page 2 of 2)

Reference Citation	Test Number	Prop.	Press. Gas	Press. Gas Inlet Temp. (deg R)	Prop. Expul. Time (sec)	Min. Ullage Gas Height (ft)	Max. Ullage Gas Height (ft)	Max. Ullage Gas Temp. (deg R)	Ullage Gas Region Vertical Temperature Gradient (deg R) Minimum	Maximum	Non-Linearity of Cert. Temp. Gradient (H,M,L)**	Notes
Roudebush (1965)	Ex. 4	LH	GH	450-580	101	?	6.08	510	?	455	L	
Roudebush (1965)	Ex. 5	LH	GH	395-273	95	?	6.17	270	?	205	M-L	(12)
Roudebush (1965)	Ex. 6	LH	GH	380-630	88	?	5.91	630	?	575	L	
Roudebush (1965)	Ex. 7	LH	He	525-535	355	?	6.25	539	?	475	L	(13)
Roudebush (1965)	Ex. 8	LH	He	525-530	90	?	6.50	525	?	475	M-L	(12)
Roudebush (1965)	Ex. 9	LH	He	325-215	100	?	6.33	~215	?	165	M-L	(12)
Roudebush (1965)	Ex. 10	LH	He	350-610	309	?	5.83	~630	?	597	M	
Stochl, et al (1970) NASA TN-D-5621	88	LH	GH	331	396	0.5	4.5	300	?	250	LM	
Stochl, et al (1970) NASA TN-D-5621	85	LH	GH	488	137	0.5	4.5	500	?	445	L	
Stochl, et al (1970) NASA TN-D-5621	97	LH	GH	603	134	0.5	4.5	700	?	650	L	
Stochl, et al (1970) NASA TN-D-7019	4	LH	GH	306	478	~1.5	~11.5	297	?	247	M	
Stochl and DeWitt (1969)	?	LH	GH	520	278	0.4	4	525	?	~460	L	(4)
Stochl and DeWitt (1969)	?	LH	GH	520	278	0.4	4	370	?	~305	L	(8), (11)
Swalley (1966)	AS-203 (Saturn IB Launch 7/66)	LH	N/A	N/A	22,498	~30.4	~30.4	240	7	195	L-LM	(1), (14)
Van Dressar and Stochl (1993)	509	LH	GH	531	1110	~0.4	6.23	463	245	423	M-MH	
Van Dressar and Stochl (1993)	510	LH	GH	529	741	0.4	5.91	445	?	405	M	
Van Dressar and Stochl (1993)	511	LH	GH	526	1978	~0.35	5.91	432	?	392	M	

Notes:

(1) N/A for press. gas means no propellant expulsion and no press. gas entry

(2) TPLH is Triple Point Liquid Hydrogen

(3) Pre-pressurized with He; GH press. gas during propellant expulsion

(4) No propellant expulsion, 3.5 w/m^2 heat flux through tank walls

(5) Data shown for only lower half of ullage gas region height

(6) Multiple screen (hemisphere shaped) press. gas diffuser used in tank

(7) Radial ((cylindrical) press. gas diffuser used in tank

(8) Straight pipe (downward) injection diffuser used in tank

(9) Linear in lower 2.0 ft of ullage gas region

(10) Linear in lower 0.426 ft of ullage gas region; near constant temp. in remaining ullage gas region height

(11) Linear in lower 1.3 ft of ullage gas region; near constant temp. in remaining ullage gas region height

(12) Lower 0.75 ft to 1.25 ft medium non-linearity, remainder very close to linear temp. profile

(13) Two somewhat linear slopes; 375°R change for upper 3 ft; 195°R change for lower 3.25 ft.

(14) AS-203 flight of Saturn 1B, launched 7/5/66; 4th Earth orbit, micro-gravity environment

The straight pipe injector, which was designed to direct pressurant gas inlet velocity vectors vertically downward toward the cryogenic liquid propellant surface, produces near uniform temperatures, with 20 R or lower temperature differences, through the upper part of the ullage gas region while a steep 300 R to 400 R temperature variation occurred in the lower 0.58-foot to 2.40-foot height of the ullage gas region. On the other hand; the multi-screen hemisphere and conical injectors (diffusers), which direct pressurant gas inlet velocity vectors both horizontally and vertically (both horizontal and vertical velocity vector components), produce closely or moderately linear vertical temperature profiles throughout the full ullage gas region with a very large, 430 R to 490 R, temperature differences from top to bottom of this region. For all cases, the ullage gas temperature is highest at or near the upper part of the tank and near the elevation(s) where pressurant gas enters the ullage gas region. The lowest temperatures always exist at the interface between cryogenic propellant and ullage gas regions where this temperature is equal to or slightly higher than the temperature of the propellant immediately below this interface.

For cases where cryogenic propellant tanks were horizontally accelerated by oscillatory motions to induce liquid propellant sloshing, a steep vertical temperature gradient occurs in the lowest 0.3-foot to 3.0-foot height of the ullage gas region. The height of this steep-temperature-gradient section generally increases as the area of the liquid propellant surface increases.

A number of references cited on Table 2.3 also state that the non-uniformity of ullage gas temperatures can and often does have significant effects on the mean ullage gas temperatures and the resulting collapse factors. Some of the cited references in Table

2.3 state that the assumption of uniform ullage gas region temperatures in collapse factor analysis models, without reliable correction or influence factors to adjust or account for non-uniform temperature distribution in the ullage gas region, can lead to significant errors in collapse factor results. A number of the references in Table 2.3 cite this as a major weakness or contributor to errors regarding predictions and computations of collapse factors.

Horizontal Temperature Gradients in Ullage Gas Region

Although the data are extensive with regards to vertical temperature profiles and gradients in cryogenic propellant tank ullage gas regions, data are limited with regards to horizontal (or radial) temperature gradients.

Table 2.4 contains selected data and includes the literature citations. For the majority of cases, tank wall temperatures are measured at the outside surfaces of the tank wall. While the data in Table 2.4 do show large temperature differences between the tank vertical centerline and the corresponding tank wall surface at or near the same elevation, there are no data showing the full horizontal temperature distribution from tank vertical centerline to tank wall. Also, for nearly all cases the large horizontal temperature gradients from tank vertical centerline to tank wall are confined to the upper sections of the ullage gas region near the elevations where pressurant gas enters the tank ullage.

Although not supported with data, many of the horizontal temperature gradients are likely to exist in a very thin boundary-layer region near the inner tank wall surface with little or no temperature variations outside this boundary layer. Also, for 20 of the 29 cases cited in Table 2.4, a moderate-to-significant portion of the horizontal temperature

Table 2.4 Selected Empirical Ullage Gas and Adjacent Tank Wall Temperature Data for Approximations of Ullage Gas Region Horizontal Temperature Gradients

						Ullage Gas Height (ft.)			Horizontal Temperature Gradient, Tank Vertical Centerline to Tank Wall (deg R)		Ullage Gas Temperature at Tank Vertical Centerline (deg R)		
Reference Citation	Test Number	Prop.	Press. Gas	Press. Gas Inlet Temp. (deg R)	Expul. Time (sec)	Minimum	Maximum	Tank Wall Temp. Probe Locations	Minimum	Maximum	Minimum	Maximum	Notes
Lockheed Report ER-5238 (1961)	3	LH	GH	300	120	1.08	7.33	Internal	0	~63	37	282	(1)
Lockheed Report ER-5238 (1961)	4	LH	GH	300	87	1.58	8.25	Internal	4.5	~72	45	277	(1)
Lockheed Report ER-5238 (1961)	5	LH	He	300	99	1.08	7.33	Internal	0.5	51	43	~290	(1)
Lockheed Report ER-5238 (1961)	6	LH	He	300	95	1.46	7.33	Internal	26	95	40	~300	(1)
Lockheed Report ER-5238 (1961)	7	LH	GH	300	111	1.08	6.67	Internal	9	71	44	~297	
Bourgarel, et al. (1968)	4	LH	He	450	205	~0.69	~9.20	External	9	107	~39	450	
Bourgarel, et al. (1968)	7	LH	He	450	375	~1.37	~9.20	External	0	130	~39	450	
Bourgarel, et al. (1968)	9	LH	He	450	352	~0.68	~9.20	External	~5	126	~39	450	
Bourgarel, et al. (1968)	11	LH	He	180	214	~0.63	~9.20	External	0	59	~39	201.6	
Bowersock, et al. (1960)	19	LN	GN	?	N/A	?	?	External	0	107	?	?	(3), (5)
Coxe and Tatom (1962)	1	LH	GH	300	89	0.54	8.13	Internal	0	99	~37	286	
DeWitt and McIntire (1974)	8	LCH_4	GCH_4	400	231	~0.85	4.15	External	0	117	230	409	(2)
DeWitt and McIntire (1974)	6	LCH_4	GCH_4	400	633	~0.85	4.15	External	0	80	230	410.4	(2)
DeWitt and McIntire (1974)	11	LCH_4	GCH_4	600	234	~0.85	4.15	External	0	281	230	603	(2)
DeWitt and McIntire (1974)	37	LCH_4	He	400	223	~0.85	4.15	External	0	97	200	414	(2)
DeWitt and McIntire (1974)	42	LCH_4	He	600	224	~0.85	4.15	External	0	180	203	583	(2)
DeWitt and McIntire (1974)	63	LCH_4	GH	400	219	~0.85	4.15	External	2	99	202	396	(2)
DeWitt and McIntire (1974)	68	LCH_4	GH	600	222	~0.85	4.15	External	0	225	202	601	(2)
Hasan, et al. (1991)	?	LH	N/A	N/A	N/A	1.41	1.41	External	1	29	37	91.8	(3), (4)
Roudebush (1965)	Ex. 1	LH	GH	488 - 520	350	0.525	6.00	External	15	220	58	540	
Roudebush (1965)	Ex. 4	LH	GH	450 - 580	101	0.375	6.25	External	0	300	47	523	(2)
Roudebush (1965)	Ex. 6	LH	GH	385 - 630	88	0.483	6.00	External	0	415	45	630	(2)
Roudebush (1965)	Ex. 8	LH	He	524 - 530	90	0.675	6.41	External	~20	270	55	530	(2)
Stochl, et al. (1970), NASA TN-D-7019	4	LH	He	306	478	0.434	11.50	External	2	55	50	297	(2)
Stochl, et al (1970) NASA TN-D-5621	88	LH	He	331	396	0.134	4.25	External	2	100	50	312	(2)
Stochl, et al (1970) NASA TN-D-5621	85	LH	He	488	137	0.167	4.25	External	19	282	50	488	(2)
Stochl, et al (1970) NASA TN-D-5621	87	LH	He	603	134	0.167	4.20	External	0	540	50	675	(2)

Notes:

(1) Horizontal tank oscillations @ 0.5 Hz frequency and 0.5-inch amplitude to induce LH sloshing

(2) Data available only from end of propellant expulsion process

(3) Closed tank; no propellant expulsion and no pressurant gas supplied to tank

(4) Maximum temperature gradient at 14-hours hold time

(5) Maximum temperature differential @ 60 seconds after start of pressurization; tank wall and ullage gas initially @ -285F

gradients could also be through the thickness of the tank walls since the tank wall temperatures are measured on the external wall surfaces. Although tank walls are thin, less than ½-inch thick, for cases shown on Table 2.4, expulsion times are also relatively short, on the order of 90 seconds to 400 seconds. These short exposure times of colder tank walls to the warmer ullage gas could result in large temperature gradients through the tank wall.

One study not cited in Table 2.4, Van Dresar and Stochl (1993), presents horizontal temperature uniformity data for various cryogenic propellant tank pressurization and propellant expulsion processes. For seven of the 14 tests in this study where the LH tank is pressurized with no propellant expulsion, predefined criteria for horizontal ullage gas temperature uniformity are satisfied. These criteria are also satisfied for four of the six LH propellant expulsion tests. For the remaining two LH expulsion tests and for one LH tank pressurization test without propellant expulsion, "approximate" horizontal ullage gas temperature uniformity is observed. High non-uniformity of ullage gas temperatures at the top and bottom horizontal temperature probe rakes inside the ullage is observed in two of the fourteen LH tank pressurization tests. However, for both of these tests high mass flow rates of pressurant gas into the LH tank ullage are required and the tank is equipped with a conical pressurant gas inlet injector (diffuser) where high vertical downward velocity components for incoming pressurant gas exist.

Other references that contain discussion about horizontal ullage gas temperature distributions include Baral (1988), Clark (1965), Kendle (1970), Nein and Head (1962), Roudebush (1965), Stochl and DeWitt (1969), Stochl, et al. (1970, NASA TN-D-5621),

and Stochl, et al. (1970, NASA TN-D-7019). In Baral (1988) and Kendle (1970), general statements that temperatures were found to have small variations in radial directions from the tank vertical axis are made, but no further data or information is presented. In Nein and Head (1962), Roudebush (1965), Stochl, et al. (1970, NASA TN-D-5621), Stochl, et al. (1970, NASA TN-D-7019), and Stochl and DeWitt (1969), the tests include the use of horizontal temperature probe rakes at multiple, discrete elevations inside the test tanks.

Multiple Species in Ullage Gas Region

Although temperature distribution within the ullage gas region of a cryogenic propellant tank nearly always has the dominant effect on the distribution of ullage gas regional properties distribution that ultimately affects pressurant gas requirements, the mass fraction of constituent gases in a multi-component gas mixture within the ullage region can also have significant effects on the fluid property distribution in this region. Mixtures of two or more constituent gas species occur whenever pressurant gases are not the same species as the cryogenic propellant and when one or both of the following conditions exist:

1.) The cryogenic propellant tank is not completely filled with liquid cryogen, such that an ullage gas region exists, prior to the initial pressurization of the tank with externally supplied pressurant gas,

2.) Mass transfer of propellant species from the propellant region to the ullage gas region occurs at any time during initial tank pressurization or pressurized propellant expulsion processes.

For virtually all cases, only one or two pressurant gas species are used for cryogenic propellant tank pressurization and pressurized propellant expulsion processes. When two pressurant gas species are used, one of the two species is generally the same species as the cryogenic propellant. Therefore, for nearly all cases and for purposes of this study, the ullage gas region is occupied by either a single gas species or a two-component (binary) gas mixture.

Experimental data or the reduction/conversion of this data from Beduz, et al. (1984), Bowersock and Reid (1961), DeWitt and McIntire (1974), Gluck and Kline (1962), Nein and Thompson (1966); Stochl, et al. (1970, NASA TN-D-5621),and Stochl, et al. (1970, NASA TN-D-7019) confirm that mass transfer of propellant species into the ullage gas region does often occur during cryogenic propellant tank pressurization and pressurized propellant expulsion processes.

Findings for Ullage Gas Region Properties Distribution

All empirical data substantiate the existence of vertical temperature gradients within the ullage gas region of cryogenic propellant tanks during pressurization and propellant expulsion processes. Regarding the horizontal temperature gradients from tank vertical axial centerlines to tank walls, the empirical data are much less extensive and the results are not conclusive. However, where horizontal temperature distribution data have been obtained and presented, a large portion of the results provide indications that temperature variations with respect to horizontal position are small, zero to 25 R maximum. While other data provide evidence of very large differences between ullage gas temperatures at or near tank vertical tank axial centerline and the corresponding inner

or outer tank wall temperatures, this could be attributed to most or nearly all of the horizontal temperature gradient being contained within a thin thermal fluid boundary layer near the tank inner wall surface.

Where more than one fluid species occupies the ullage gas region due to a pressurant gas being a different species than the cryogenic propellant, the propellant species does transfer across the propellant-to-ullage-gas interface. However, the empirical data results all indicate that most of the propellant species is confined to a small lower horizontal segment of the ullage gas region. When the pressurant gas species has a lower molecular weight than that of the propellant species or helium pressurant gas is used, this segment is generally 3-inches to 2-feet in height, depending on tank size and ullage gas height. This phenomenon is observed during initial tank pressurization and the subsequent pressurized propellant expulsion. All data indicates that mass transfer rates from the lower portion of the ullage gas region to the remainder of this region is very small having minor or negligible effects on the ullage gas properties distribution.

Propellant Region Properties Distribution

Although not as significant as ullage gas region property distributions, pressurant gas requirements can be affected by the distribution of properties within the cryogenic propellant region of a pressurized tank. In contrast to ullage gas property gradients and distribution, which are likely to have direct and significant effects on collapse factors, the propellant property gradients and distribution are likely to have indirect and less significant effects. In this region, as with the ullage gas region, fluid temperature distribution has the predominant effect on property distributions.

In the propellant region, fluid densities are generally greater, on the order of three times to one thousand times greater depending upon tank pressure and cryogenic propellant species, which means that vertical pressure gradients are much larger than those in the ullage gas region. However, the other fluid properties (including density, thermal conductivity, specific heat, and viscosity) which affect heat and mass transfer processes (and which ultimately affect pressurant gas requirements), are not significantly affected by the spatial pressure distribution within the propellant region. Examination of data from Lemmon, et al. (2007) over a wide range of tank pressures and cryogenic propellant temperatures was performed as part of this study. The results of this examination substantiate the minor effects of pressure variations on fluid properties in the ullage gas and propellant regions. Pressures in these regions vary by less than 50-psia for nitrogen and oxygen and less than 0.2-psia for hydrogen with the typical sizes and geometries of cryogenic tanks.

However, the possible variations in temperature within the cryogenic propellant region does have a much more significant effect on the critical fluid properties affecting heat and mass transfer within and across the boundaries of the cryogenic propellant region.

Propellant Region Vertical Temperature Distribution

Table 2.5 provides a summary of selected empirical data that includes vertical temperature gradients within cryogenic propellant regions inside various tanks. A review of the data in this table indicates that the vertical temperature gradients within the cryogenic propellant region are much smaller than those within the ullage gas region.

Table 2.5 Empirical Propellant Vertical Temperature Gradient/Profile Data (Page 1 of 2)

Reference Citation	Test Number	Prop.	Press. Gas	Propellant Height (ft.)		Press. Hold or Expul. Time (sec.)	Tank Press. (psia)	Bulk Propellant Region				Stratified Propellant Region				Notes
								Temperature (deg. R)		Height (ft.)		Temperature (deg. R)		Height (ft.)		
				Minimum	Maximum			Minimum	Maximum	Minimum	Maximum	Minimum	Maximum	Minimum	Maximum	
Lockheed Report - ER-5238 (1981)	3	LH	GH	1	7.25	120	46.5	36.52	36.72	?	>4.16	36.72	44.79	?	~0.94	(1)
Lockheed Report - ER-5238 (1981)	4	LH	GH	0.08	6.75	87	46.6	36.71	37.00	?	>4.37	37.00	44.81	?	~1.38	(1)
Al-Najem, et al. (1993)	3L/min	Water	Note (2)	1.31	3.11	840	~14.7	531.30	531.30	0.00	2.16	531.30	617.70	0.96	~1.31	(2)
Al-Najem, et al. (1993)	15L/min	Water	Note (2)	1.31	3.11	180	~14.7	531.30	534.90	0.00	2.16	534.90	617.70	0.82	~1.31	(2)
Barnett (1967)	2	LN	N/A	3.17	3.17	60	39.7	162.4	162.9	2.83	2.83	162.9	164.7	0.34	0.34	(4)
Barnett (1967)	2	LN	N/A	3.17	3.17	360	29.7	163.8	164.7	2.75	2.75	162.9	164.6	0.42	0.42	(4)
Barnett (1967)	3	LN	N/A	3.17	3/17	60	29.7	162.4	162.9	2.75	2.75	162.9	164.6	0.42	0.42	(4)
Barnett (1967)	3	LN	N/A	3.17	3.17	360	29.7	163.8	164.7	2.75	2.75	164.7	167.3	0.42	0.42	(4)
Barnett, et al. (1964)	4	LH	He	13.17	13.17	119	18.7-32.7	36.8	37.1	11.67	11.67	37.1	38.6	1.50	1.50	(10)
Barnett, et al. (1964)	4	LH	He	13.17	13.17	119	18.7-32.7	36.8	37.1	11.67	11.67	37.1	38.6	1.50	1.50	(10)
Barnett, et al. (1964)	Fig. 8	LH	GH	4.75	4.75	100	?	36.15	36.7	2.92	2.92	36.7	37.9	1.83	1.83	(3), (10)
Barnett, et al. (1964)	Fig.8	LH	GH	4.75	4.75	600	?	39.25	39.7	3.91	3.91	39.7	40.3	0.84	0.84	(3), (10)
Coxe and Tatom (1962)	2	LH	GH	<0.50	7.46	103	47.6	~36.6	~37.1	0.00	6.23	~37.1	45.0	0.00	1.23	(1)
Coxe and Tatom (1962)	5	LH	He	<0.50	7.51	99	45.5	~36.6	~36.5	0.00	7.17	~36.5	44.6	0.00	0.34	(1)
Coxe and Tatom (1962)	6	LH	GH/He	<0.50	7.63	95	47.0	~36.9	~37.2	0.00	5.70	~37.2	44.9	0.00	1.93	(1)
Coxe and Tatom (1962)	7	LH	GH	<0.50	7.33	111	45.0	~36.7	~36.8	0.00	6.01	36.8	44.5	0.00	1.32	(1)
Coxe and Tatom (1962)	10	LH	GH	<0.50	7.39	105	45.5	~36.7	~37.0	0.00	5.63	~37.0	44.6	0.00	1.76	(1)
DeWitt and McIntire (1974)	9	LCH_4	GCH_4	~0.85	~4.15	638	48.6	202.9	203.3	0.00	3.57	203.3	~231.0	0.00	0.58	
DeWitt and McIntire (1974)	10	LCH_4	GCH_4	~0.85	~4.15	410	48.9	202.4	202.7	0.00	3.67	202.7	~231.5	0.00	0.48	
DeWitt and McIntire (1974)	11	LCH_4	GCH_4	~0.85	~4.15	234	49.2	202.9	203.1	0.00	4.00	203.1	~231.5	0.00	0.15	
DeWitt and McIntire (1974)	97	LCH_4	GN	~0.85	~4.15	568	49.5	202.3	202.3	0.00	0.00	202.3	210.2	0.85	4.15	
DeWitt and McIntire (1974)	98	LCH_4	GN	~0.85	~4.15	232	49.5	202.3	202.3	0.00	0.00	202.3	207.6	0.85	4.15	
Fan, et al (1969)	13	LN	GN	1.98	1.98	7200	450	162.0	165.4	1.33	1.33	165.4	~200.5	0.65	0.65	
Ghaddar, et al. (1989)	6.5L/min	Water	Note (2)	5.25	6.56	1500	~14.7	593.9	593.9	3.54	4.59	593.9	669.0	<1.97	1.97	(2)
Ghaddar, et al. (1989)	9L/min	Water	Note (2)	5.25	6.56	1500	~14.7	561.8	561.8	3.48	4.99	561.8	644.7	1.57	1.94	(2)
Gursu, et al. (1993)	B-2	LH	N/A	6.02	6.02	40	16.5 - 17.4	~37.1	37.1	5.53	5.53	37.1	37.6	0.49	0.49	(4)
Gursu, et al. (1993)	B-2	LH	N/A	6.02	6.02	152	16.5 - 19.5	~37.1	37.1	4.40	4.40	37.1	38.3	1.62	1.62	(4)
Hasan, et al. (1991)	?	LH	N/A	4.59	4.59	14,400	14.7 - 18.4	37.3	37.4	4.43	4.43	37.4	37.9	<0.16	0.16	(4)
Hasan, et al. (1991)	?	LH	N/A	4.59	4.59	43,200	14.7 - 27.0	38.3	38.7	4.43	4.43	38.7	40.5	<0.16	0.16	(4)
Kharin, et al. (1991)	?	LH	N/A	3.75	8.52	20,700	19.15	31.3	31.3	2.62	7.39	31.3	38.2	0.65	1.13	(4)
Liebenburg and Edeskuty (1965)	?	LH	N/A	18.47	18.47	136,800	18.7 - 39.1	36.5	36.5	17.26	17.26	36.5	43.4	1.21	1.21	(4)

Table 2.5 Empirical Propellant Vertical Temperature Gradient/Profile Data (Page 2 of 2)

Reference Citation	Test Number	Prop.	Press. Gas	Propellant Height (ft.)		Press. Hold or Expul. Time (sec.)	Tank Press. (psia)	Bulk Propellant Region				Stratified Propellant Region				Notes
								Temperature (deg. R)		Height (ft.)		Temperature (deg. R)		Height (ft.)		
				Minimum	Maximum			Minimum	Maximum	Minimum	Maximum	Minimum	Maximum	Minimum	Maximum	
Neff and Chiang (1967)	17	LH	N/A	3.91	3.91	120	~27	~36.75	~37.55	0.83	0.83	~37.55	~40.5	3.08	3.08	(4), (5)
Neff and Chiang (1967)	19	LH	N/A	1.38	1.38	400	~31.2	~37.0	~37.5	0.33	0.33	~37.55	~40.5	1.05	1.05	(4), (6)
Neff and Chiang (1967)	40	LN	N/A	3.97	3.97	160	~18.0	~139.4	~139.9	1.33	1.33	~139.9	~142.4	2.64	2.64	(4), (7)
Neff and Chiang (1967)	38	LN	N/A	1.27	1.27	700	~18.9	~139.9	~140.4	0.08	0.08	~140.4	~142.9	1.19	1.19	(4), (8)
Olsen (1966)	1	LH	GH	2.5	2.5	600	54.7	36.3	38.5	~2.5	~2.5	38.5	46.1	0.04	0.09	
Olsen (1966)	3	LH	GH	2.5	2.5	720	22.7	36.3	37.0	~2.5	~2.5	37.0	46.2	0.08	0.15	
Ordin, et al. (1960)	?	LH	GH	?	~2	600	14.7 - 55	43.8	44.3	1.5	2.0	44.0	47.0	?	0.33	(9), (10)
Schmidt, et al. (1960)	A-3	LH	GH	4.19	4.19	900	125 - 160	36.0	36.4	4.18	4.19	36.9	56.0	0	0.01	(9), (10)
Schmidt, et al. (1960)	B-1	LH	GH	3.98	3.98	104,400	15.5 - 24.7	35.8	37.8	3.17	3.98	36.0	45.0	0	0.82	(9), (10)
Segel (1965)	?	LH	N/A	2.36	2.36	600	14.7 - 73.5	36.7	37.6	2.13	?	36.7	48.9	?	0.23	(4), (11)
Segel (1965)	?	LH	N/A	2.21	2.21	600	14.7 - 73.5	37.3	39.1	2.03	?	37.3	48.9	?	0.18	(4), (12)
Segel (1965)	?	LH	N/A	2.30	2.30	600	14.7 - 73.5	37.1	40.3	2.10	?	37.1	48.9	?	0.20	(4) (13)
Segel (1965)	?	LH	N/A	2.14	2.14	600	14.7 - 73.5	37.4	43.0	1.89	?	37.4	48.9	?	0.25	(4), (14)
Tanyun, et al. (1996)	?	LH	N/A	6.50	6.50	120	?	36.5	37.0	5.28	6.50	36.5	40.2	0	1.21	(4), (15)
Tanyun, et al. (1996)	?	LH	N/A	6.50	6.50	300	?	36.7	37.4	4.92	6.50	36.7	42.0	0	1.57	(4), (15)

Notes:

(1) Stratified propellant region height is approximated from propellant temp. vs. time plots at tank bottom discharge and known volumetric rate of propellant expulsion

(2) Thermoclines in water storage tanks w/warmer water folowing into top and cooler water flowing out investigated

(3) 40 in. diameter vertical cylindrical tank to simulate Saturn S-IV

(4) N/A in press. gas column means no propellant expulsion and no press. gas entry; constant heat flux through tank walls maintained in selected cases for experimental data collection and studies.

(5) 0.115 BTU/ft^2 sec heat flux into side walls, 0.017 BTU/ft^2 sec heat flux through false bottom

(6) 0.119 BTU/ft^2 sec heat flux into side walls, 0.017 BTU/ft^2 sec heat flux through false bottom

(7) 0.139 BTU/ft^2 sec heat flux into side walls, 0.020 BTU/ft^2 sec heat flux through false bottom

(8) 0.134 BTU/ft^2 sec heat flux into side walls, 0.019 BTU/ft^2 sec heat flux through false bottom

(9) GH press. gas used only as needed to keep initial tank pressure or higher pressure, gas vented from ullage as needed to prevent overpressure

(10) Pressurization and no expulsion

(11) 8 x 10^{-3} kCal/m^2 heat flux into tank side walls

(12) 19 x 10^{-3} kCal/m^2 heat flux into tank side walls

(13) 28 x 10^{-3} k/Cal/m^2 heat flux into tank side walls

(14) 60 x 10^{-3} kCal/m^2 heat flux into tank side walls

(15) 262.6 W/m^2 heat flux into tank side wall

Cryogenic propellant region vertical temperature gradients are generally on the order of 5 R to 30 R. Also, the majority of data from Table 2.5 show that the major portion of the vertical temperature gradient has a vertical height that does not exceed 2% to 20% of the total propellant region height at the start of propellant expulsion from the tank or when the tank is 80% to 90% full of liquid propellant. For larger tanks, this major portion of the vertical temperature gradient extends from three inches to three feet below the interface between propellant and ullage gas; while for smaller tanks this depth below this interface is nominally 6-inches or less. Below these depths, where the major temperature gradient exists, the cryogenic propellant temperature is nearly uniform within 1 R.

Barnett, et al. (1964), Coxe and Tatom (1962), and Neff and Chiang (1967) present cases where larger vertical temperature gradients occur through more than 20% of the maximum or initial height of the propellant region. However, for the cases where this phenomenon was observed, high heat fluxes were applied by enhanced heating of tank walls or liquid propellant sloshing was induced by horizontal tank oscillatory motions. However, even for these cases, vertical temperature gradients through the entire cryogenic propellant region are usually less than 5 R and never exceed 10 R.

Approximately half of the cases presented in Table 2.5 are those where a tank is partially filled with cryogenic liquid propellant and no propellant expulsion from the tank is occurring. In most of these cases, tank pressurization is provided by heating and boil-off of liquid propellant through normal heat leak or enhanced heat input into the tank. A few cases involve the use of externally supplied pressurant gas for initial tank pressurization.

In addition to Table 2.5 data, a number of studies present or discuss similar results with liquid and cold supercritical cryogenic fluids in tanks. These studies include Atkinson, et al. (1984), Beduz, et al. (1984), Clark, et al. (1960), Segel (1965), Tuttle, et al. (1994), and Zenner (1960) where experiments were conducted with LH, LN, LOX, and liquid helium tanks.

Propellant Region Horizontal Temperature Distribution

Empirical data from a number of the cited references in Table 2.4 indicate zero or extremely small horizontal temperature gradients in the cryogenic propellant region. A large number of graphical plots in these references illustrate both the tank wall and ullage gas temperatures approaching the temperature of the bulk cryogenic propellant, within 0 R to 20 R, when traversing from the top of the tank down to the interface between ullage gas and cryogenic propellant.

For cases where the horizontal temperature gradient in the propellant region can have temperature variations as high as 10 R to 40 R, there are data from studies that indicate that virtually all of this gradient exists in a very thin thermal boundary layer adjacent to the tank walls.

Multiple Species in Propellant Region

For the cases where the pressurant gas is not the same species as the cryogenic propellant, the pressurant gas species can dissolve or condense into the cryogenic propellant region. This phenomenon has the net effect of making a portion of the fluid in the propellant region a mixture of pressurant gas and propellant species where both can

be liquids, supercritical fluids, or solution of vapor dissolved within the liquid propellant. When this condition occurs, there is also a variation of fluid properties within the cryogenic propellant region caused by mass fraction variations of the constituent fluid species. Mass fraction of pressurant gas species is likely to be highest at the ullage-gas-to-propellant interface, and the mass fraction generally decreases as the vertical depth below this interface increases.

Although actual empirical data are very limited, a number of studies do report findings where pressurant gas species is present within the cryogenic propellant where the cryogenic propellant and pressurant gas are different species. These studies include Lockheed Report ER-5238 (1961), Lockheed Report ER-5296 (1961), Bowersock, et al. (1960), DeWitt and McIntire (1974), Greenfield (1958), Nein and Thompson (1966), Stochl, et al. (1970, NASA TN-D-5621), and Stochl, et al. (1970, NASA TN-D-7019).

Findings for Propellant Region Properties Distribution

Data from studies substantiate the existence of vertical temperature gradients in the cryogenic propellant region, but the temperature differences in these gradients are much less than those in the ullage gas region. Temperature differences in the propellant region nominally range from 5 R to 40 R as opposed to the 150 R to 475 R or higher ranges observed in the ullage gas region. Furthermore, nearly all of the vertical temperature gradient exists in the upper 2% to 20% of the initial or maximum propellant region height where this is normally the top one-foot to three-foot thick top layer of the propellant region in larger tanks or the one-inch to six-inch thick top layer of this region in the smaller tanks. Exceptions generally occur when liquid propellant sloshing or other

means of forced mixing between ullage gas and cryogenic propellant occur or when very high external heat fluxes are applied at tank bottom or sidewalls. Even with these exceptions the total vertical temperature gradient through the full height of the propellant region rarely exceeds 5 R to 10 R.

Data from prior studies indicates horizontal temperature gradients in the cryogenic propellant region are usually near zero or negligibly small. For cases where larger horizontal temperature variations of 10 R to 40 R are observed, all presented data indicate that virtually all of these variations exist within a 0.20-inch or thinner thermal boundary-layer adjacent to the tank wall.

As with the ullage gas region for cases where the pressurant gas is a different species than the cryogenic propellant, the propellant region can also contain a mixture of two or more fluid species as a result of mass transfer across the interface between propellant and ullage gas regions. The mixture of multiple species in the cryogenic propellant region most likely occupies only a very thin upper layer of the propellant region rather than a large portion or all of the entire region. The nominal thickness of this layer is generally one-inch or less under the following conditions and provisions:

1.) No mechanisms exist or sufficient counter-measures do exist to prevent disturbance of the horizontal interface between the ullage gas and propellant regions; this includes a properly designed pressurant gas inlet diffuser in the tank ullage region or anti-slosh baffles when needed,

2.) Pressurant gas species has a higher normal boiling point than the propellant species,

3.) With the exception of helium pressurant gas over liquid, slush, or cryogenic hydrogen propellant, the pressurant gas species has a lower molecular weight than the propellant species,

4.) Pressure rise rates during initial tank pressurization and possibly during pressurized cryogenic propellant expulsion are low enough to ensure conformance with item 1.).

As with the ullage gas region, the vertical temperature distribution in the propellant region has the dominant effect on the distribution of fluid properties within this region although the reasons differ when comparing the propellant region with the ullage gas region.

Tank Wall Temperature Distribution

The distributions of temperatures through the tank walls have not been directly measured for cryogenic tanks. A number of studies include measurement of tank wall temperatures at discrete locations on the outer or inner wall surface in addition to discrete temperature measurements within the propellant and ullage gas regions (usually near the tank's vertical axis centerline). Table 2.4, presented earlier in this chapter, cites most of the studies where this was done. Epstein, et al. (1965) as well as Nein and Thompson (1966) also include empirical tank wall temperature data.

The predominant simplifying assumption with regards to analytical modeling of heat and mass transfer processes in cryogenic propellant tanks is that of a negligibly small temperature gradient through the tank wall thickness normal to the inner wall local tangent plane. Virtually all of the data from prior studies indicate that either this is a

valid assumption or that the resultant errors in determining pressurant gas requirements are negligible or acceptably small. These studies include Bourgarel, et al. (1968), DeWitt and McIntire (1974), Hasan, et al. (1991), Nein and Thompson (1966), Roudebush (1965), Stochl, et al. (1970, NASA TN-D-5621), and Stochl, et al. (1970, NASA TN-D-7019).

The above studies also compare analytically predicted tank wall temperatures with experimentally measured tank wall temperatures. Bourgarel, et al. (1968), DeWitt and McIntire (1974), and Stochl, et al. (1970, NASA TN-D-5621) provide experimental outer wall temperature data where measured temperatures are generally 5 R to 20 R colder than analytically computed temperatures, except for a few cases in Bourgarel, et al. (1968) where experimentally measured temperatures were 45 R colder. Nein and Thompson (1966) and Stochl, et al. (1970, NASA TN-D-7019) report experimentally measured tank outer wall temperatures to be 0 R to 10 R warmer than analytically computed temperatures. With the exception of a few isolated cases, data from all studies indicate that temperature gradients through the tank wall thickness have temperature differences of less than 20 R between inner and outer surfaces of the tank walls. This holds true even in Hasan, et al. (1991) where external heat fluxes were applied to the outer tank wall surface for one to 14 hour durations.

In addition to the temperature distributions through the tank wall normal to the plane tangent to each local inner wall surface (through thickness of the wall), the temperature distribution parallel to the tank wall inner and outer surfaces needs to be considered. Many of the studies cited in Table 2.4 also present data confirming that the outer and inner tank wall surface temperature varies significantly with respect to vertical

position from the top of a tank downward to the interface between ullage gas and cryogenic propellant. The general trends show the wall surface temperature decreasing in either a near-linear or highly non-linear fashion when traversing from top of tank downward to the vertical position of the ullage-gas-to-propellant interface. These data indicate that the tank wall surfaces have a much colder temperature than the ullage gas at the same corresponding vertical position where the range of typical temperature differences are shown in Table 2.4. For all of the cited references in Table 2.4 where vertical ullage gas and tank wall temperature profile are shown, the general trend shows that the difference between ullage gas temperature and tank wall surface temperature decreases when traversing from the top of the tank or from the elevation(s) where pressurant gas enters the tank ullage downward to the aforementioned interface. When approaching this interface from above the ullage gas temperature and tank wall temperature both converge to nearly the same temperature that is nearly equal to, within 10 R and usually within 1 R to 2 R of, the bulk cryogenic propellant temperature.

Regarding tank wall temperature profiles in the vicinity of the interface between ullage gas and cryogenic propellant regions, the empirical data all indicate that heat conduction through the tank wall parallel to the inner tank wall surface tends to "smooth out" or eliminate the occurrence of any abrupt temperature changes through the tank wall.

The phenomena described in the above two paragraphs are supported or confirmed with data presented in Bourgarel, et al. (1968), Clark, et al. (1960), DeWitt and McIntire (1974), Hasan, et al. (1991), Nein and Thompson (1966), Roudebush (1965), Stochl, et al. (1970, NASA TN-D-5621) and Stochl, et al. (1970, NASA TN-D-7019).

Clark, et al. (1960) and Hasan, et al. (1991) show that these phenomena exist also when tank outer wall surfaces are heated with a constant heat flux.

No empirical tank wall temperature data were found in the research of studies for cases where tank pressures where near critical or supercritical nor for cases with heavy walled cryogenic propellant tanks with wall thicknesses above ½-inch.

Effects of Mass Transfer on Pressurant Gas Requirements

Most of the studies cited in the "Multiple Species in Ullage Gas Region" and "Multiple Species in Propellant Region" subsections of this chapter acknowledge the potential for mass transfer processes between ullage gas and cryogenic propellant regions to have significant effects on required mass transfer of pressurant gas into the tank ullage. A number of the studies also conclude that this mass transfer can have effects that either increase or decrease the requirements depending on a number of parameters and operating conditions. However, there are also a number of prior studies that report very accurate predictions of requirements from analytical models when treating mass transfer between ullage gas and cryogenic propellant as negligible. The data from Roudebush (1965) is one example. On the other hand, studies where enhanced mass transfer between ullage gas and cryogenic propellant is known to have occurred (usually due to induced propellant sloshing) state significant increases in collapse factors over those where no propellant sloshing occurred. The data of DeWitt and McIntire (1974) are examples indicating this occurrence. For other selected studies, the results are mixed where enhanced mass transfer due to propellant sloshing increases collapse factors significantly

in some cases and has minor or negligible effects in other cases. The data of Lockheed Report ER-5238 (1961) as reported by Mandell and Roudebush (1965) are examples where mixed results occurred.

Perhaps the studies that most clearly demonstrate the significance of mass transfer effects on collapse factors are DeWitt and McIntire (1974) and Lacovic (1970). In Lacovic (1970), the second test series has empirical collapse factors that are nominally two to three times lower than collapse factors from similar and corresponding tests from the first test series. The cause of this very significant collapse factor reduction is greatly enhanced vaporization of the LOX propellant and mass transfer of this vaporized propellant into the tank ullage gas region when helium gas is bubbled up through this propellant. On the other hand, DeWitt and McIntire (1974) report very high collapse factors due to significant mass transfer of GN pressurant into LCH_4 propellant where 60 to 75% of the pressurant gas supplied to the tanks is dissolved into the propellant. Further analyses and tests presented in this study indicate the density of LCH_4 with dissolved GN increases as the concentration of GN increases which enhanced the buoyancy driven mixing of GN into a large portion of the propellant region. The use of GN pressurant gas was subsequently rejected as a cost savings option to replace helium.

The net result from the data in prior studies is that there is no consistent trend regarding the magnitude and direction of mass transfer across the interface between ullage gas and cryogenic propellant regions. The same is likely to be true for mass transfer of propellant species within the ullage gas region when pressurant gas and cryogenic propellant are different species, but there is insufficient empirical data to

substantiate this. There is also no consistent trend or level of influence with regards to how this mass transfer ultimately affects collapse factors.

With respect to cryogenic propellant tanks operating at supercritical and high subcritical pressures, no empirical data for mass transfer across the ullage-gas-to-propellant interface have been found. From the studies researched for the literature review, the effects of this mass transfer on collapse factors have not been evaluated in depth for the higher tank operating pressure conditions.

Pressurant Gas Entry Effects

The controlling-parameter that generally has one of the strongest influences on pressurant gas requirements and associated collapse factors in cryogenic propellant tanks is fluid flow conditions within and across volume boundaries in the tank. These conditions are predominantly influenced by pressurant gas flow velocity vectors at the point(s) of entry into the tank ullage gas region. Extensive empirical data indicate that these velocity vectors can yield two to six fold increases in convection heat transfer between the ullage gas and tank walls as well as between the ullage gas and cryogenic propellant. Additionally, these velocity vectors can provide forced mixing within the ullage gas region to create more uniform temperatures within most, or all, of the upper ullage gas region which can have either a beneficial effect in reducing ullage collapse or a detrimental effect by increasing this collapse. Pressurant gas inlet velocity vectors directed downward into the tank ullage and along tank walls can cause moderate to high levels of forced mixing between the ullage gas and cryogenic propellant.

Bailey, et al. (1990), Bailey and Arif (1992), Blatt (1968), Coxe and Tatum (1962), Denisov, et al. (1981), Humphrey (1961), Kamat and Abraham (1968), Rotenburg (1986), Stochl, et al. (1991), Van Dresar, Lin, and Hasan (1992), and Van Dresar and Haberbusch (1994) provide data, observed cases, or indications where enhanced mixing between ullage gas and propellant increases pressurant gas mass transfer requirements and associated collapse factors, often by factors of two or three.

A number of other studies support the concept of reducing ullage collapse by prevention of forced mixing between ullage gas and cryogenic propellant, but they report or conclude that enhanced mixing within the ullage gas region, rather than keeping this region stratified, also serves to reduce collapse factors. These studies include Denisov, et al. (1981), Olsen (1966), Smith (1961), and Stochl and DeWitt (1969). Denisov et al. (1981) and Stochl and DeWitt (1969) present quantitative data.

In addition to the studies described above for cryogenic tank pressurization followed by pressurized propellant expulsion processes, there are a number of studies where methods to intentionally increase ullage gas collapse are employed to reduce or eliminate the need to vent (and lose) ullage gas from a cryogenic fluid tank during long term storage. The main end-use applications for these studies are onboard spacecraft cryogenic liquid tank systems to reduce quantities of lost and wasted fluids as much as possible. All of these studies provide strong indications that enhanced heat and mass transfer between ullage gas and cryogenic liquid propellant does cause significant collapsing (with associated pressure reduction) of the ullage gas. The following studies provide empirical data showing ullage gas collapse through this enhanced heat and mass transfer: Aydelott (1983), Bentz, et al. (1992), Bentz (1993), Bentz, et al. (1993), Chato

(1991), Chato (1993), Meserole, Jones, and Fortini (1987), Moran, et al. (1991), Reaser, et al. (1965), Schmidt, et al. (1991), and Vaughan, et al. (1991).

In summary, the effects of pressurant gas entry velocities and conditions into cryogenic propellant tanks on collapse factors are not always consistent. While some data indicates that enhanced mixing within the ullage gas region to attain more uniform properties within this region reduces collapse factors, other data indicates that maintaining a thermally stratified ullage gas region lowers collapse factors.

With the exception of cases where helium pressurant gas is bubbled up through LOX and LCH_4 propellant at low (50-psia nominal) subcritical pressures, enhanced mixing between ullage gases and cryogenic propellants results in increased pressurant gas requirements and associated collapse factors. The requirements tend to increase when the effects of ullage gas temperature reduction dominate over the effects of mass addition to the ullage gas region when vaporized propellant transfers to this region. This dominant effect appears to be the case most of the time. The exceptions appear to be cases where the effects of added propellant mass dominate.

A consistent trend supported by all studies cited in this section where ullage-gas-to-tank-wall heat transfer is evaluated indicates the reduction of this heat transfer is a primary method to reduce ullage collapse and the resulting pressurant gas requirements.

Another consistent trend observed in all studies is the reduction of mass transfer across the ullage-gas-to-cryogenic-propellant interface to very low or negligible levels when this interface is not disturbed with enhanced mixing of fluids across this interface and when the molecular weight of the pressurant gas species is less than that of the propellant species or helium pressurant gas is used.

As with much of the empirical data discussed in this chapter, there are no data regarding pressurant gas entry effects on its mass transfer and flow rate requirements for cryogenic propellant tanks operating at supercritical and high subcritical pressures.

Pressurant Gas Mass Transfer Modeling and Computational Techniques

A wide variety of analytical models and computational techniques have been devised to predict or to provide reliable and practical methods in determining mass and mass flow rate requirements of cryogenic propellant tank pressurant gases. Initial work, starting in the late 1950's, has been focused on analytical methods that would consistently and reliably predict pressurant gas requirements that were sufficiently higher than actual requirements such that a conservative safety margin was always provided for design of pressurant gas subsystems. Through the 1960's as launch vehicle liquid propulsion systems were being developed for the space program and their cryogenic propellant tanks grew in size, the prediction of pressurant gas requirements with reduced margins of conservatism and errors grew in importance. For the larger flight vehicles weight reductions including those of the cryogenic liquid propellant tank pressurant gases and their supply subsystems, was of premium importance. This resulted in the development of elaborate computer based programs or empirically based computation methods to determine collapse factors.

In the early 1970's, new types of ground testing facilities were being constructed for developmental and flight certification testing of liquid propellant rocket engine components and subassemblies. These facilities employed the use of relatively large high

flow rate cryogenic propellant run systems operating at high subcritical or supercritical pressures. Central to each of these run systems, as shown in simplified form by Figure 1.3, is a cryogenic propellant (run) tank where externally-supplied pressurant gas is used to initially pressurize the tank from near atmospheric to elevated pressures and then maintain required tank pressures as cryogenic propellant is expelled from the tank. Since the basic principles of operation of these higher pressure run systems are virtually the same as those of the lower subcritical pressure systems, similar issues of pressurant gas requirements predictions are present. However, the work to understand and predict requirements for the high subcritical and supercritical pressure tanks in these run systems is very limited. Since reduction and control of system and pressurant gas commodity weights has not been deemed to be a critical design objective for the design of ground testing facilities, general design approaches have been to set and use assumptions of very high collapse factors, usually 4.0 or higher, as a design basis when sizing and designing pressurant gas subsystems for high-pressure cryogenic propellant run tanks.

In the late 1980's and early 1990's analytical work was performed to predict collapse factors more accurately for supercritical tank pressure applications. The work of Hodge and Koenig (1992) as well as Ludwig and Houghton (1989), with the reduction of empirical data from Shelburne (1990), are the major efforts in this area. From these efforts, predicted collapse factors ranged nominally from 1.05 to 1.40 and empirically obtained collapse factors ranged from 1.42 to 4.10 with the higher values occurring at the start of propellant expulsion reducing to cumulative collapse factors between 1.05 and 1.60 at the end of this expulsion process.

In this study, the work is limited to cases where cryogenic propellant tanks are on the Earth's surface and where the model can be readily adapted to tanks on accelerating flight vehicles. However, selected studies performed for micro-gravity conditions are generally discussed where they provide selected characteristics and insights that are beneficial to this study.

"Saturation Rule"

For the earlier pressurized cryogenic liquid tank expulsion and transfer studies performed in the late 1950's and early 1960's, analytical techniques using the "Saturation Rule" have been employed to predict or provide a conservative estimate of pressurant gas requirements. The "Saturation Rule" is based on the assumption that the ullage gas is always at a density corresponding to the saturation temperature of the cryogenic propellant and the tank pressure. If the ullage gas is the same species as the propellant, then the ullage gas is assumed to be a saturated vapor. The initial and final ullage gas volumes and densities are then used to compute the net addition of mass to the ullage region.

Use of the "Saturation Rule" is presented in Bowersock, et al. (1960), Humphrey (1961), and Vance and Duke (1962) for LN and LOX expulsions with nitrogen and oxygen pressurant gases. When comparing the saturation rule results with test data, the analysis results had errors ranging from 16.3% under-predicted to 10.0% over-predicted in Bowersock, et al.

In Humphrey (1961) use of the "Saturation Rule" is combined with evaluation of ullage gas condensation along cylindrical tank walls where the tank was immersed in a

bath of LN at near atmospheric pressure (LN bath temperature near –320 F ≅ 140 R). When comparisons of empirical data to analytically predicted data are made in Humphrey, the predicted pressurant gas requirements are consistently higher than those from empirical data with errors within 11% for most of the time duration of each liquid cryogen expulsion process. However, the predicted pressurant gas mass flow rate data near the start of cryogenic liquid expulsions are nearly two times higher than data from experimental tests.

Modifications and Enhancements to the "Saturation Rule"

Subsequent studies reported by Bowersock and Reid (1961) and Moore, et al. (1960) found that analytical results using the "Saturation Rule" were excessively conservative (predicted pressurant gas requirements were four to ten times higher than those from actual tests) or resulted in physically impossible conditions for LH expulsions using hydrogen pressurant gas. Moore, et al. (1960) presents a revised technique using the "Worst Case Rule" which is based on the following assumptions:

1.) The tank is completely full of liquid cryogen at the start of expulsion (0% initial ullage gas volume),

2.) The pressurant gas exits the supply source and enters the tank at constant inlet enthalpy,

3.) The tank is at constant and uniform internal pressure,

4.) All pressurant gas that enters the tank displaces all of the liquid cryogen initially in the tank,

5.) All pressurant gas in the tank at the end of liquid cryogen expulsion is in the saturated vapor state.

Bowersock and Reid (1961) present an alternative analytical method to the methods using the "Saturation Rule," although this method involves more steps and increased complexity as compared to that of Moore, et al. (1960). The method in Bowersock and Reid (1961) is called the "Equivalent Mass Model."

Results obtained from use of the "Equivalent Mass Model" in Bowersock and Reid (1961) show 10.0% under-prediction to 12.8% over-prediction of pressurant gas required as compared to data.

The "Equivalent Mass Model" presented in Bowersock and Reid (1961) proved to yield more accurate pressurant gas requirement results than both the "Saturation Rule" and "Worst Case Rule" analytical methods, but the computation processes are more complex and involved. Additionally the "Equivalent Mass Model" provides good comparisons with empirical data for a wide range of cryogenic liquid tank geometries and sizes from 3 to 28,000 gallons.

Semi-Empirical Curve-fit Models

After the development of the "Equivalent Mass Model," semi-empirical models were developed, tested, and used for ground-based tank systems. These models were utilized for a large variety of tank sizes, diameter-to-height ratios, and combinations of liquid cryogen propellant and pressurant gases. Efforts were made to derive a single equation or a series of simple equations, that included a set of empirically-derived constants, where collapse factors and the associated pressurant gas requirements were

computed explicitly. The equations all used various ullage gas, incoming pressurant gas, and tank wall material properties, tank geometric data, and either known heat transfer rates or thermal boundary-layer film temperature gradients with user input or computed convection heat transfer coefficients. The main purpose for development of the semi-empirical curve-fit models was to provide methods that enabled sufficiently accurate, with error less than 10% to 15%, computation of collapse factors and pressurant gas requirements without having to rely on the large and expensive mainframe computers that were needed in the 1960's for running the high fidelity and more complex computer program analysis tools used to predict collapse factors at that time.

One of the early precursors to the semi-empirical curve-fit models is reported in Barrere, et al. (1960) for applications where air, nitrogen, or helium are used to expel generic fuel and oxidizer propellants from tanks into rocket engine combustion chambers.

Another semi-empirical computation method is presented in Lockheed Report ER-5296 Volume III (1961) in which six simultaneous equations are solved numerically by an iterative procedure. The net result is a computed final mean ullage gas temperature used to determine final mean ullage gas density and total mass. The collapse factors can then be computed. Errors of predictions for final mean ullage gas region temperatures are as large as 52 %.

Epstein (1965) as well as Epstein and Anderson (1968) present a single semi-empirical correlation to directly compute cumulative collapse factors and required total mass of pressurant gas at the end of a propellant expulsion processes. Errors of collapse factors predicted by the correlation when compared to those obtained empirically are all less than 12% with most falling between 5% and 6%. Also, the majority of results show

that the correlation errs on the conservative side; i.e., the correlation predicts collapse factors higher than actual collapse factors from tests for most cases.

Later work presented in Van Dresar (1995) provides enhancements to the collapse factor correlation described above. These enhancements include:

1.) Addition of new correlations to adjust parameters for cases where initial ullage gas volume is less than 20% of total tank volume,

2.) Addition of correlations to adjust parameters for cases where a large residual propellant volume remains in the tank at the end of propellant expulsion,

3.) Addition of a new correlation to compute an improved equivalent tank wall thickness and specific heat capacity for cases when the tank has highly non-uniform wall thicknesses including heavy walled nozzles and flange connections as well as accessory hardware inside the tank volume;

4.) Improved correlation to compute equivalent tank diameter, based on vertical cylindrical tanks geometries, for spherical and ellipsoidal tanks,

5.) Addition of revised and improved empirical constants for LH propellant expulsions.

Additionally, the study presented in Van Dresar (1995) investigated the effects of mass transfer between cryogenic liquid propellant and ullage gas. The study concluded that evaporated propellant into the ullage gas region must be less than 26% of the total mass of pressurant gas supplied to the tank for the collapse factor correlation to be valid. The author also concludes that no more than 19% of the pressurant gas supplied to the tank ullage can condense into the propellant region to maintain validity of the collapse factor correlation.

An alternate and more comprehensive correlation is presented in Nein and Thompson (1965) where final mean ullage gas temperature, at the end of cryogenic propellant expulsion, is computed by use of 19 fluid property, tank wall property, tank geometry, and pressurant gas inlet properties, and pressurant gas inlet flow condition variables. Thirteen empirically developed constants, ten of which are exponents, are also used in the correlation. From determination of the final mean ullage gas temperature and the tank internal pressure (assumed to be near uniform), the final mass of ullage gas can be computed which can then be used to compute the final cumulative collapse factor.

In addition to variables used in the correlation of Epstein (1965), the correlation of Nein and Thompson (1965) utilizes total cross-sectional flow area of the pressurant gas inlet diffuser, ambient external air temperature, an input convection heat transfer coefficient (instead of an input external heat flux), pressurant gas thermal conductivity and viscosity properties at point(s) of entry in tank ullage, cryogenic liquid propellant temperature, and initial ullage gas volume.

The information presented in Thompson and Nein (1965) is nearly identical to that of Nein and Thompson (1965), but the former study contains added discussion about the computation of equivalent tank radius for non-cylindrical tanks.

No comparisons between analytically computed and empirically obtained data are presented in Nein and Thompson (1965) or Thompson and Nein (1965).

Upper and Lower Bound Analyses

More recent work performed in the middle 1980's through the early 1990's include upper and lower bound analyses in order to predict more realistic maximum and

minimum possible mass requirements for pressurant gas in the expulsion of cryogenic propellants from tanks. A major focus of the upper and lower bound analyses is the ability to evaluate pressurant gas requirements for tanks operating at supercritical pressures.

The study presented in Moore, et al. (1960) can be classified as the original early version of an upper and lower bound analysis method. Subsequent work presented in Riemer and Scarlotti (1984), Van Dresar and Stochl (1991), Van Dresar and Haberbusch (1994), and Wapato, et al. (1971) also provide analytical methods for determining upper and lower bounds of pressurant gas requirements.

The upper- and lower-bound analytical techniques have been shown to be consistently reliable in providing the possible ranges of cumulative collapse factors. However, the ranges are quite wide and the actual collapse factors and associated pressurant gas requirements are often well below upper-bound values even though the more recent studies have brought the upper bounds to more realistic and less conservative values.

Lumped Mass Fluid Region Models

In parallel to development and use of the modeling methods described in the previous subsections of this chapter, models using numerical techniques to model intra-tank heat and mass transfer processes and requiring iterative computation methods have also been developed. When developed and utilized in the 1960's these models were in the form of computer programs. These computer programs involve the solution to two or more complex simultaneous equations where each contains and utilizes a number of

dependent variables and where numerical techniques and multiple iteration routines are needed to arrive at converged solutions. The dependent variables mainly include selected thermal and transport properties of ullage gas and incoming pressurant gas, a limited number of cryogenic (liquid) propellant properties, selected tank wall geometric parameters, and selected tank wall material properties.

Table 2.6 provides a summation of data and selected details for the Lumped-Mass Fluid Region (LMFR) models researched for this study. Included in this table are general descriptions of the heat and mass transfer computation methods used at regional boundaries and the comparison of analytical model results with empirical results where the actual test conditions and parameters correspond to those modeled analytically.

With the exception of Hodge and Koenig (1992) and Ludwig and Houghton (1989), the tank wall is assumed to have a negligible temperature gradient through the thickness of the tank wall.

To account for non-uniform temperatures through thick tank walls, Ludwig and Houghton (1989) model the inner 70% of the tank wall thickness to be uniformly heated by ullage gas while the remaining 30% of wall thickness is thermally isolated from the heated wall.

The model presented in Hodge and Koenig (1992) utilizes an explicit finite-difference technique from Incropera and DeWitt (1990) to map the tank wall temperature distribution through the tank wall thickness at discrete time steps. The explicit finite-difference method is used in Hodge and Koenig (1992) because the thermal properties of cryogenic tank wall materials vary very widely and in a highly non-linear fashion with respect to temperature in the cryogenic temperature regimes. To address stability

Table 2.6 Summary Data for Lumped Mass Fluid Region (LMFR) Models (Page 1 of 2)

Reference Citation	Heat Transfer				Mass Transfer	Model Errors Compared to Empirical Data
	Ullage Gas to Wall	Propellant to Wall	Ullage Gas to Propellant	External Tank Wall	Ullage Gas to Propellant	
Lockheed Report ER-5296 (1961)	Notes 1 and 3	Note 2	Note 4	Note 1	Note 1	Range: -9.3 to 13.1%; Mean: 2.75%; Std. Dev. 5.74%; 11 Tests Compared
Anderson, et al. (1967)	NLC, NC	NLC, NC	Not Discussed	Not Discussed	Not Discussed	~10 to 12% estimated from UG Press. & Temp. data
Coxe and Tatum (1962)	NLC, Correlation for Conv. H.T. Coeff. not provided	Based on H.T. from wall boiling liquid propellant	Not Discussed	NLC, Correlation for Conv. H.T. Coeff. not shown	Not Discussed	Range: -9.6 to 7.8%; Mean: 1.11%; Std. Dev. 5.0%; 10 Tests Compared
Gluck and Kline (1962)	NLC, NC, Note 9	Assumed Negligible	Not Modeled	Modeled as Adiabatic	Determined from Empirical Data	Range: -9.0 to 8.4%; Mean: 0.34%; Std. Dev. 4.57%; 12 Tests Compared
Hodge and Koenig (1992)	NLC, NC, VP & HP [Incorpera & DeWitt (1990) correlations]	NLC, NC, VP & HP [Incorpera & DeWitt (1990) correlations]	NLC, NC, HPCSU [Incropera & DeWitt (1990) correlations]	Modeled as Adiabatic	Assumed Negligible	Pressurant gas supply bottle press. And temp. show < 1 K and <0.5 Mpa error for part of Test 74 on E-8 Test Stand
Ludwig and Houghton (1989)	NLC, NC & FC, Notes 3 and 5 [Nein & Thompson (1966) correlations]	Assumed Negligible	NLC, NC & FC, Notes 3 and 6 [Nein & Thompson (1966) correlations]	Modeled as Adiabatic, Note 5	None, equivalent mass transfer modeled by added H.T., Note 6	No comparisons presented; model predicts Collapse Factor of 1.20 to 1.24
Majumdar and Steadman (1998)	NLC, NC, HPCSD	EC	NLC, NC, HPCSU	Not Discussed	Not Discussed	~18 to 30% based on comparison with model data in Epstein and Anderson (1968)
Mandell and Roudebush (1965)	NLC, NC, Note 7	Assumed Negligible	Assumed Negligible	Not Discussed	Assumed No Mass Transfer	Range: -10.4 to 18.5%; Mean: 0.65%; Std. Dev. 7.74%; 18 Tests Compared

Table 2.6 Summary Data for Lumped Mass Fluid Region (LMFR) Models (Page 2 of 2)

Reference Citation	Heat Transfer				Mass Transfer	Model Errors Compared to Empirical Data
	Ullage Gas to Wall	Propellant to Wall	Ullage Gas to Propellant	External Tank Wall	Ullage Gas to Propellant	
Momenthy (1964)	NLC, NC, Note 7	Assumed Negligible	NLC, NC, HPCSU [from Ring (1964)]	Not Discussed	(1) and (2)	-14.1, 4.7, -1.8, 0% for GH over LH; -2.5, -8.7, 6.7, -2.5% for GHe over LH
Ring (1964)	NLC,NC, VP & HP	NLC,NC, VP & HP	NLC,NC, HPCSU	NLC, FC & Radiation	(1), (6), and Note 8	No Comparisons Presented

Key:

NLC = Newton's Law of Cooling

NC = Natural (Free) Convection; Table 2.8 shows correlation coefficient and exponent; Same reference citation unless noted otherwise

FC = Forced Convection

HP = Horizontal Plate (Natural Convection Correlations)

HPCSD = Horizontal Plate (Natural Convection Correlations), Cold Side Down

HPCSU = Horizontal Plate (Natural Convection Correlations), Cold Side Up

VP = Vertical Plate (Natural Convection Correlations)

EC = Equivalent Conduction; thermal conductivity and slope of temperature gradient across finite segment/element at boundary

(1) = First Mass Transfer Computation Technique, from "Mass Transfer Correlations" section of Chapter II

(2) = Second Mass Transfer Computation Technique, from "Mass Transfer Correlations" section of Chapter II

(6) = Sixth Mass Transfer Computation Technique, from "Mass Transfer Correlations" section of Chapter II

Notes:

1. An energy balance equation using propellant, mean ullage gas, entering pressurant gas, and tank wall temperatures; temperature differentials; and empirically determined coefficients is used to calculate rate of change of ullage gas temperature at discrete time steps.
2. A condensation or evaporation energy balance equation, whichever has highest magnitude, using propellant, mean ullage gas, and tank wall temperatures; temperature differentials; and empirically determined coefficients is used to calculate rate of change of liquid propellant temperature at discrete time steps.
3. Ullage gas is divided into two regions; the lower region contains only the initial mass of ullage gas prior to entry of pressurant gas and the upper region contains only pressurant gas supplied from external source.
4. External tank heating is assumed to heat and evaporate liquid propellant only. Evaporation rate of propellant is calculated from heat transfer equation using tank wall and liquid propellant temperatures, heat transfer areas, latent heat of vaporization, and empirically determined coefficients.
5. To simulate effects of transient and non-uniform temperatures through thick tank walls, the wall is modeled as having uniform temperature through 70% of the actual wall thickness where heat is transferred from the ullage gas; 30% of the wall thickness is modeled as thermally isolated from remaining wall.
6. 740 BTU/hr-ft2-R for GH over LH and 520 BTU/hr-ft2-R for GN over LOX added to calculated convective heat transfer coefficient from Nein and Thompson (1966) correlations to simulate effects of mixing between ullage gas and cryogenic propellant; these resulted in approximate 10% increase in required pressurant gas.
7. Ullage gas modeled as having linear vertical temperature profile with temperature at top of region equal to entering pressurant gas temperature and temperature at bottom of region equal to saturation temperature of propellant; Mean ullage gas temperature used to calculate heat transfer at ullage gas boundaries with tank wall is average of temperatures at top and bottom of ullage gas region.
8. During rapid change in tank pressure, mass transfer across ullage-gas-to-cryogenic-propellant interface is product of ullage volume and ullage gas density change based on net difference between new tank pressure and propellant saturation pressure.
9. Natural convection correlation used with time of pressurant gas entry, thermal properties of ullage gas and tank wall, tank wall thickness and inside diameter to compute ratio of actual to maximum total heat in tank wall; Maximum total heat in tank wall is when all of tank wall is at temperature of the incoming pressurant gas; Coefficients and exponents in the correlation to compute ratio of actual to maximum total heat in tank wall are derived from curvefits of empirical data.

concerns with use of the explicit finite-difference method, the model subdivides global time-steps into smaller discrete (local) time-steps to model the transient tank wall temperature distributions.

Another unique attribute of the Hodge and Koenig (1992) model is the use of the fourth-order Runge-Kutta numerical integration method to determine mass and internal energy of fluids in cryogenic propellant and ullage gas regions at subsequent time steps.

Regarding vertical tank wall temperature distributions or the vertical component of the tank wall temperature profile parallel to the tank wall inner surface, the analytical models presented in references cited in Table 2.6 each employ one of two methods. The simpler method treats the entire section of tank wall in contact with ullage gas at each discrete time step as a lumped mass having a uniform temperature, or in the case of Hodge and Koenig (1992) a uniform temperature profile through the tank wall thickness.

Lockheed Report ER-5296, Volume 4 (1961), Mandell and Roudebush (1965), and Momenthy (1964) employ a more complex method for modeling the temperature of the tank wall section in contact with ullage gas. For the models presented in these studies, the tank wall is modeled as finite discrete segments vertically stacked from the top to the bottom of the tank. Those tank segments in contact with liquid propellant are set at temperatures equal to that of the liquid propellant. The tank segments in contact with the ullage gas are each modeled as nodes with each having uniform temperature and thermal properties.

Review of the information in Table 2.6 indicates good-to-excellent predictions provided by the LMFR models in comparison to empirical data. There are occasional occurrences where model prediction errors exceeded 10% with an error of approximately

30% in one case. However, all models presented by reference citations in Table 2.6 were used for subcritical tank pressure conditions with the exception of Hodge and Koenig (1992) and Ludwig and Houghton (1989).

Multiple Discrete Fluid Segment Models

In contrast, and as an intended enhancement to the LMFR computer models, other models have been developed and used where one or more intra-tank fluid regions are subdivided into discrete horizontal segments in order to provide a more accurate representation of temperature gradients in the intra-tank fluid regions. Each segment is treated as a small bulk mass of fluid having uniform properties throughout.

Table 2.7 presents a listing of studies where subdivision of the ullage gas region, cryogenic (liquid) propellant region, or both regions into discrete finite segments was employed in computer programs used to predict pressurant gas requirements or pressure rise rates in cryogenic propellant tanks for pressurization or pressurized propellant expulsion processes. With the exception of Lin and Hasan (1992), all of the Multiple Discrete Fluid Segment (MDFS) Models cited in Table 2.7 subdivide the ullage gas region into vertically stacked discrete finite horizontal segments. Each segment is modeled as having uniform properties where a portion of the pressurant gas entering the ullage uniformly mixes with gas already in this segment. This was done in order to provide a more accurate representation of the vertical temperature gradients known from empirical data to exist in the cryogenic tank ullage gas regions and adjacent tank walls, as shown on Table 2.3 and as illustrated in references cited in Table 2.4 of this chapter.

Table 2.7 Summary Data for Multiple Discrete Fluid Segment (MDFS) Models

Reference Citation	Heat Transfer						Mass Transfer		Model Errors Compared to Empirical Data
	Ullage Gas to Wall	Propellant to Wall	Ullage Gas to Propellant	Intra-Ullage-Gas Segment-to-Segment	Intra-Propellant Segment-to-Segment	External Tank Wall	Ullage Gas to Propellant	Intra-Ullage-Gas Segment-to-Segment	
Rocketdyne Report R-3936-1 (1963)	NLC, NC & FC	NLC, NC	NLC, NC & FC	EC	EC	NLC, NC & Radiation, Note 1	(1) and (6)	(6)	Comparisons not presented; ~10% Max. Cumulative Error; ~20% Max. Instantaneous Error from Nein and Thompson (1966)
Baral (1988)	NLC, NC, & FC	NLC, NC	EC	EC	EC	NLC, NC, Note 2	(1)	(6)	<5%
Epstein, et al. (1965)	NLC, NC & FC	NLC, NC	NLC, NC & FC	EC	EC	Unknown	(1)	Unknown	~10% for Test 130-9; ~10 to 12% for Test 130-6; ~5% for Test 6E
Lin and Hasan (1992)	No Heat Transfer Assumed	EC	EC (liquid side only)	N/A	EC	Input Heat Flux	(1)	N/A; Ullage Gas at Uniform Temp.	No Comparisons Presented
Masters (1974)	NLC, NC & FC	No Heat Transfer Assumed	NLC, NC [Same correlation as Momenthy (1964)]	EC	N/A, Uniform Propellant Region Modeled	Input Heat Flux	Not Discussed	No Mass Transfer other than Pressurant Gas Entry	0.5 to 16.0% Error for Tank Pressurization; 7.0 to 12.4% Error for Propellant Expulsion
Nein and Thompson (1966)	NLC, NC & FC	NLC, NC	NLC, NC & FC	EC	EC	NLC, NC & Radiation, Note 1	(6)	(6)	Range: Approx. -30 to 12%; Mean: 0.1 to 2.3%; Std. Dev.: 10.9 to 8.5%; 11 Tests Compared
Roudebush (1965)	NLC, NC	N/A, No Heat Transfer Assumed	NLC, NC	N/A, No Heat Transfer Assumed	N/A, Uniform Propellant Region Modeled	Input Heat Flux	N/A, Assumed to be Zero	No Mass Transfer other than Pressurant Gas Entry	Range: -8.23 to 12.04%; Mean: 2.22%; Std. Dev.: 6.05%; 10 Tests Compared
Stochl, et al. (1970, NASA TN-D-5621) and Stochl, et al. (1970, NASA TN-D-5621)	NLC, NC	N/A, No Heat Transfer Assumed	NLC, NC [Same correlation as Momenthy (1964)]	EC	N/A, Uniform Propellant Region Modeled	Adiabatic Outer Wall Modeled	(1)	No Mass Transfer other than Pressurant Gas Entry	Range: -2.73 to 19.48%; Mean: 5.29%; Std. Dev.: 5.56%; 19 Tests Compared

Key:

NLC = Newton's Law of Cooling

NC = Natural (Free) Convection; Table 2.8 shows correlation coefficient and exponent; Nein and Thompson (1966) reference citation unless noted otherwise

FC = Forced Convection; correlation presented in "Combined Natural and Forced Convection Correlations" section in Chapter II

EC = Equivalent Conduction; thermal conductivity and slope of temperature gradient across finite segment/element at boundary

(1) = First Mass Transfer Computation Technique, from "Mass Transfer Correlations" section of Chapter II

(6) = Sixth Mass Transfer Computation Technique, from "Mass Transfer Correlations" section of Chapter II

Notes:

1. Equivalent conductance based on natural convection and radiation heat transfer is used; this parameter is calculated from equation using empirically derived constants, bottle wall temperature and ambient air temperature, and these temperatures raised to the fourth power
2. Equivalent conductance based on natural convection only; correlation not presented

Although the MDFS models involve a higher level of computer program complexity, significantly increased numbers of repetitive and iterative calculations, increased computing time, and increases in computer memory requirements, the developers of these models deemed that this was necessary to provide consistently accurate model results for a wide variety of cryogenic tank sizes and geometries as well as for a wide variety of operating conditions.

The majority of MDFS computer models in Table 2.7 treat the cryogenic (liquid) propellant region as a single lumped mass having uniform properties throughout the region. Most of these models also apply the assumption of negligible heat transfer between propellant region and adjacent tank walls due to a negligible temperature difference between propellant region and tank walls adjacent to this region.

With regards to the modeling of transient heat conduction in the tank walls, all models presented by the cited references on Table 2.7 apply the assumption of near zero temperature gradient through the thickness of the tank wall.

For all of the models referenced in Table 2.7, except Lin and Hasan (1992), the tank wall is subdivided into vertically-stacked finite segments. For all of these models, the heat transfer between any two adjacent wall segments is assumed to be negligible.

Results obtained with the MDFS computer program models referenced in Table 2.7 provide good to excellent predictions of pressurant gas requirements and associated collapse factors when compared to corresponding empirical data. For all models, predicted pressurant gas flow rates or collapse factors are generally within 14% of corresponding empirical data.

When initially comparing Tables 2.6 and 2.7, the MDFS models (cited in Table 2.7) appear to provide little or no improvements over the LMFR models (cited in table 2.6). However, the former models are evaluated for accuracy for a much wider range of tank geometries and sizes ranging from 17.7-gallons to thousands and tens of thousands of gallons while the latter models were only evaluated for vertical cylinder tanks of 500-gallon and smaller capacities, except for the one 2400-gallon spherical LH tank expulsion test in Hodge and Koenig (1992). Also, each of the studies cited in Table 2.6 where error ranges are more favorable, employed correlations with coefficients and exponents determined to provide best results for a single tank configuration and a limited range of test conditions. Therefore, the MDFS collapse factor analysis computer programs generally provide a much better assurance that "good" to "excellent" collapse factor predictions will result. Because of this, the added model complexities, increased computer run time, increased computer memory requirements, and additional attention to details on the part of the program user appear to be fully justified at least for the moderate to low subcritical tank pressure applications. For high subcritical and supercritical tank pressures, the MDFS collapse factor analysis computer programs have not been used in prior work, so their accuracy and reliability is not known or proven from prior studies.

Two-Dimensional Finite Segment Numerical
Finite Difference Analysis Programs

The literature survey performed for this study identified three computer program models employing grid generation to subdivide fluid contents in cryogenic tanks into two-dimensional segments (or finite elements) for tank pressurization and cryogenic

propellant expulsion processes. These models are presented and described in Greer (1995), Hsu (1994), Hsu and Witt (1994), Sasmal, et al. (1991), and Sasmal, et al. (1993).

Although no comparisons with empirical data are made or presented in Sasmal et al. (1993), two very interesting and useful results occur. One result provides evidence of more rapid pressurization rates (decreased pressurization times) or higher mass flow rates of incoming pressurant gas yielding much lower total mass requirements for the pressurant gas. Another result indicates downward pressurant gas inlet velocity vectors nominally at 1.4 ft/sec and lower results in very small horizontal temperature gradients from the vertical axial centerline of the tank to the tank walls for all or most of the ullage gas region. This lends further support to the general findings stated earlier in this chapter in the subsection entitled "Horizontal Temperature Gradients in Ullage Gas Region."

Although two-dimensional finite segment numerical finite difference computer programs have been used to model cryogenic liquid propellant tank pressurization and propellant expulsion processes, output results from these programs have not been compared with empirical data with the exception of one test presented in Sasmal et al. (1991). Due to the very small time step intervals required for computational stability, the large number of grids, and the large number of repetitive calculations in algorithm and iteration routines, memory requirements often reached or exceeded limits for computers in use in the early 1990's. Computation times for a single program run could take days or weeks.

Internal Tank Heat Transfer Correlations

Many of the models described in this chapter involve the computation and use of heat transfer rates across fluid regional boundaries. The majority of these models utilize correlations that determine heat transfer rates at the ullage-gas-to-tank-wall boundaries while considering heat transfer at the interface between ullage gas and cryogenic (liquid) propellant to be negligibly small. A smaller select group of models employ correlations for heat transfer across this interface. An even smaller select group of models evaluate and account for heat transfer rates across boundaries between cryogenic propellant and tank walls, but the vast majority of models are either based on the assumption of negligible heat transfer at cryogenic-propellant-to-tank-wall boundaries where temperatures of propellant and adjacent tank walls or wall segments are considered to be virtually equal. Tables 2.6 and 2.7 provide further details about applied assumptions regarding heat transfer across ullage gas and cryogenic propellant regional boundaries.

Natural Convection Correlations

For the majority of LMFR and MDFS computer models, natural or free convection heat transfer is treated as being the only mode of heat transfer at ullage gas and cryogenic propellant region boundaries. The general natural convection correlation for propellant Nusselt number used in these models for computing natural convection heat transfer is given as

$$Nu_L = \frac{h_L L}{k} = c_1 \left(Ra\right)^{c_4} = c_1 \left[\left(Gr_L\right)\left(\mathrm{Pr}\right)\right]^{c_4} = c_1 \left[\left(\frac{g_c c_7 \beta \left|T_{fl} - T_w\right| L^3}{\nu^2}\right)\left(\frac{\mu c_P}{k}\right)\right]^{c_4} \quad (2\text{-}1)$$

The values of c_1 and c_4 used in Equation (2-1) and obtained from studies of natural convection processes or used in selected numerical finite difference collapse factor analysis modeling programs are provided on Table 2.8. Table 2.8 also references the studies where the general natural convection correlation was developed or used. The table also states how this correlation was used with regard to collapse factor modeling. Many of the referenced studies cited in Table 2.8 are also cited in Table 2.6 or Table 2.7, so that Table 2.8 essentially provides further details about heat transfer correlations used for the LMFR and MDFS computer models.

The characteristic length, "L," used in Equation (2-1) is generally the total length along a vertical or inclined wall parallel to the buoyant upward or downward motion of fluid along the wall surface or interface with another fluid region. For fluids in spherical enclosures, above or below the concave side of a hemispherical or ellipsoid dome, and for fluids along horizontal flat surfaces the characteristic length, "L," is equated to the vertically projected area of the dome or flat surface divided by the horizontal perimeter of the widest section of the dome or the flat surface.

In addition to the general natural convection Nusselt number correlation of Equation (2-1), a number of other Nusselt number correlations of different forms have been developed and presented in prior literature. These correlations are presented in Chen and Anderson (1972), Ede (1967), Gebhart (1973), Hodge and Koenig (1992), Neff and Chiang (1967), Ostrach (1972), Polyakov (1991), Raithby and Hollands (1975), Stochl, et al. (1970, NASA TN-D-5621), and Stochl, et al. (1970, NASA TN-D-7019). Hodge and Koenig (1992) references Mills (1992) which is based on correlations of

Table 2.8 General Natural Convection Nusselt Number Correlation Coefficient and Exponent Values (Page 1 of 2)

Reference Citation	C_1	C_4	Applicable Cases	How Used in Collapse Factor Model
Anderson, et al. (1967)	0.13	0.333	Vertical Wall Heat Transfer	Ullage-Gas-to-Tank-Wall, Propellant-toTank-Wall, and Ullage-Gas-to-Propellant Heat Transfer
Barber (1966)	0.5	0.25	Vertical Wall and Domed Closure over Gas Heat Transfer	Ullage-Gas-to-Tank-Wall Heat Transfer
Beekman and Martin (1991)	0.27	0.25	Horizontal Flat Plate Heat Trans., Cold Side Up; $10^5<=Ra_L<=10^{10}$	Not Used
Blackmon (1974)	0.55	0.24	Vertical Wall Heat Transfer	Not Used
Blackmon (1974)	0.08	0.333	Domed Tank Closure over Gas	Not Used
Clark (1968)	0.59	0.25	Vertical Flat Plate Heat Transfer; $10_4<=Ra_L<=10^9$ (Laminar)	Not Used
Clark (1968)	0.13	0.333	Vertical Flat Plate Heat Transfer; $10^9<=Ra_L<=10^{12}$ (Turbulant)	Not Used
Clark (1968)	0.54	0.25	Horizontal Square Flat Plate Heat Transfer, Hot Side Up; $10^5<=Ra_L<=2x10'$ (Laminar)	Not Used
Clark (1968)	0.14	0.333	Horizontal Square Flat Plate Heat Transer, Hot Side Up; $2x10^7<=Ra_L<=3x10^{10}$ (Turbulent)	Not Used
Clark (1968)	0.27	0.25	Horizontal Square Flat Plate Heat Transfer, Cold Side Up	Not Used
Ede (1967)	0.548	0.25	Heat Transfer for Flat Plat in Any Orientation w/Major Simplifying Assumptions	Not Used
Estey, et al. (1983)	0.725 L/k	0.25	Horizontal Tube O.D. Condensation (Corr. For "h", not Nu)	Ullage-Gas-to-Liquid Propellant Heat Transfer w/condensation
Estey, et al. (1983)	0.14	0.333	Vertical Wall Heat Transfer	Ullage-Gas-to-Vertical-Tank-Wall Heat Transfer
Estey, et al. (1983)	0.098	0.345	Fluid Inside a Sphere Heat Transfer	Not Used
Gluck and Kline (1962)	0.13	0.333	Vertical Wall Heat Transfer	Ullage-Gas-to-Vertical-Tank-Wall Heat Transfer
Hoogendoorn (1986)	0.62	0.25	Enclosures Including Cryogenic Tank; $10^{10}\leq Ra\leq 10^{12}$	Suggested for Cryogenic Vessels, Not Used
Hochstein, et al. (1990)	0.0605	0.333	Heat Transfer for Liquid in Cylindrical Tank w/Ellipsodial Heads	Not Used (Used in Other Analysis for Overall H.T. from Tank Wall to LH in tanks)
Incropera and DeWitt (1990) & Incropera and DeWitt (1996)	0.54	0.25	Horizontal Flat Plate Heat Transfer, Cold Side Down; $10^4<=Ra_L<=10^7$	Upper Tank Closure to Fluid Heat Transfer, used in Hodge and Koenig (1992)
Incropera and DeWitt (1990)	0.14	0.333	Horizontal Flat Plate Heat Transfer, Cold Side Down; $10^7<=Ra_L<=10^{11}$	Upper Tank Closure to Fluid Heat Transfer, used in Hodge and Koenig (1992)
Incropera and DeWitt (1996)	0.15	0.333	Horizontal Flat Plate Heat Transfer, Cold Side Down; $10^7<=Ra_L<=10^{11}$	Not Used, update from Incropera and DeWitt (1990)
Incropera and DeWitt (1990) & Incropera and DeWitt (1996)	0.27	0.25	Horizontal Flat Plate Heat Transfer, Cold Side Down; $10^5<=Ra_L<=10^{10}$	Lower Tank Closure to Fluid Heat Transfer, used in Hodge and Koenig (1992)
Ludwig and Houghton (1989)	0.13	0.333	Vertical and Horizontal Wall Heat Transfer	Ullage-Gas-to-Tank-Wall and Ullage-Gas-to-Propellant Heat Transfer
Majumdar and Steadman (1998)	0.54	0.25	Horizontal Wall Heat Transfer, Cold Side Down	Ullage-Gas-to-Tank-Wall Heat Transfer
Majumdar and Steadman (1998)	0.27	0.25	Horizontal Wall Heat Tranfer, Cold Side Up	Ullage-Gas-to-Tank-Wall Heat Transfer
McAdams (1954)	0.13	0.333	Vertical and Horizontal Plates	Used for Ullage-Gas -to-Tank-Wall and Ullage-Gas-to-Propellant in Other References
Momenthy (1964)	0.14	0.333	Vertical and Horizontal Plates	Ullage-Gas-to-Tank-Wall
Nein and Thompson (1965)	0.13	0.333	Vertical Wall Heat Transfer	Ullage-Gas-to-Tank-Wall Heat Transfer and Ullage-Gas-to-Propellant Heat Transfer
Pasley (1972) and Pasley (1970)	0.098	0.345	Heat Transfer for Fluids in Spherical Tank	Not Used [Used for Blowdown Propellant Feed System Modeling (1972); Used for Heat Transfer in Press. Gas Supply Bottles (1970)]

Table 2.8 General Natural Convection Nusselt Number Correlation Coefficient and Exponent Values (Page 2 of 2)

Reference Citation	C_1	C_4	Applicable Cases	How Used in Collapse Factor Model
Ring (1964)	0.59	0.25	Vertical Wall $10^4 \leq Ra < 10^9$	Ullage Gas and Propellant-to-Wall Heat Transfer
Ring (1964)	0.13	0.333	Vertical Wall $10^9 \leq Ra < 10^{12}$	Ullage Gas and Propellant-to-Wall Heat Transfer
Ring (1964)	0.54	0.25	Horizontal Wall, Cold Side Down $10^4 \leq Ra < 2x10^7$	Ullage Gas-to-Wall Heat Transfer
Ring (1964)	0.14	0.333	Horizontal Wall, Cold Side Down $2x10^7 \leq Ra < 3x10^{10}$	Ullage Gas and Propellant-to-Wall Heat Transfer
Ring (1964)	0.27	0.25	Horizontal Wall, Cold Side Up $3x10^5 \leq Ra < 3x10^{10}$	Ullage Gas-to-Propellant and Propellant-to-Wall Heat Transfer
Rolfes and Visser (1991)	0.10	0.33	Vertical Cylinders with Thermal B.L. Thickness << Cylinder Diameter, $10^9 < Ra < 10^{13}$	Not used (Used for Heat Leak Analysis of Horizontal Cryo Vessels)
Rolfes and Visser (1991)	0.25 and 0.27	0.25	Horizontal Surface, Cold Side Down	Not used (Used for Heat Leak Analysis of Horizontal Cryo Vessels) Top Surfaces
Rolfes and Visser (1991)	0.15	0.25	Horizontal Surface, Cold Side Up	Not used (Used for Heat Leak Analysis of Horizontal Cryo Vessels, Bottom Surfaces)
Schuster, et al. (1990)	0.6	0.25 or 0.20	Liquid Cryogen in Vertical Cylinder or Spherical Tank, Laminar Buoyancy Driven Flow	Not Used (Used for Analysis of On-Orbit Spacecraft Tank)
Stochl, et al. (1970, NASA TN-D-5621) and Stochl (1970, NASA TN-D-7019)	0.14 0,13	0.333 0.333	Vertical Planes and Cylinders Horizontal Plates	Ullage Gas-to-Tank Wall Heat Transfer Ullage-Gas-to-Propellant Heat Transfer
Taylor, et al. (1991)	0.555	0.25	Horizontal Cylinder Vessel Wall to Ullage Gas Heat Transfer, $Ra < 10^9$	Not Used (Used for Evaluation of On-Orbit Spacecraft Tank)
Taylor, et al. (1991)	0.021	0.40	Horizontal Cylinder Vessel Wall to Ullage Gas Heat Transfer, $Ra \geq 10^9$	Not Used (Used for Evaluation of On-Orbit Spacecraft Tank)
Vliet (1969)	0.6	0.2	Laminar Flow on Inclined Vert. Flat Plate, 30 - 85 deg. From Horizontal (Modified Grashof No., Gr *, equal to Grashof No. Times Sine of Incline Angle of Wall	Not Used
Vliet (1969)	0.30	0.24	Inclinded Plate with Slope of 0.22 to 0.25	Not Used
Vliet (1969)	0.14	0.333	Heated Horizontal Surfaces Facing Up, $2x10^7 < Ra < 3x10^{10}$	Not Used
Vliet (1969)	0.23	0.25	Heated Horizontal Surfaces Inclined, $2x10^9 < Ra < 3x10^{13}$ (Uses Modified Grashof of No. Gr *, Equal to Grashof No. Times Sine of Incline Angle of Wall	Not Used
Wulff and Schipma (1967)	0.555	0.25	Spherical Tank w/Internal Bladder $Ra \leq 10^8$	Used for Determining P. G. Requirements for Non-Cryogenic Liquid Propellant Expulsion from Spherical Tanks w/Bladder
Wulff and Schipma (1967)	0.129	0.333	Spherical Tank w/Internal Bladder $Ra > 10^8$	Used for Determining P. G. Requirements for Non-Cryogenic Liquid Propellant Expulsion from Spherical Tanks w/Bladder
Wulff and Schipma (1967)	0.54	0.25	Tank Wall Surfaces Cooled From Above or Heated From Below, $Ra < 2x10^7$	Used for Determining P. G. Requirements for Non-Cryogenic Liquid Propellant Expulsion from Spherical Tanks w/Bladder
Wulff and Schipma (1967)	0.14	0.33	Tank Wall Surfaces Cooled From Above or Heated From Below, $Ra > 2x10^7$	Used for Determining P. G. Requirements for Non-Cryogenic Liquid Propellant Expulsion from Spherical Tanks w/Bladder
Wulff and Schipma (1967)	0.27	0.29	Tank Wall Surfaces Cooled From Below or Heated From Above, $Ra < 2x10^7$	Used for Determining P. G. Requirements for Non-Cryogenic Liquid Propellant Expulsion from Spherical Tanks w/Bladder
Wulff and Schipma (1967)	0.07	0.33	Tank Wall Surfaces Cooled From Below or Heated From Above, $Ra > 2x10^7$	Used for Determining P. G. Requirements for Non-Cryogenic Liquid Propellant Expulsion from Spherical Tanks w/Bladder

Churchill and Chu (1975). The Nusselt number correlations generally use fluid properties and characteristic dimensions.

Combined Natural and Forced Convection Correlations

The majority of numerical finite difference computer models presented by studies cited in Tables 2.6 and 2.7 are based on all natural convection heat transfer at all or selected fluid regional boundaries. The reference citations in Table 2.7 that indicate natural and forced convection ("NC" and "FC") for ullage-gas-to-wall heat transfer combine the effects of natural and forced convection at boundaries of the discrete horizontal segments in the ullage gas region as indicated by this table. For these models, the total equivalent convective heat transfer coefficients (or Nusselt numbers) at ullage-gas-to-tank-wall and at ullage-gas-to-cryogenic-propellant boundaries are equated as the sum of forced and natural convection components.

In contrast, Ring (1964) and Wulff and Schipma (1969) recommend using the higher of the natural and forced convective heat transfer coefficients to determine rate of heat transfer at ullage-gas-to-wall and ullage-gas-to-propellant boundaries. For combined forced and natural convection heat transfer processes, Incropera and DeWitt (1990) recommend the correlation

$$Nu_T = \left[\left(Nu_L \right)^n + \left(Nu_F \right)^n \right]^{1/n} \tag{2-2}$$

In Incropera and DeWitt (1990), the exponent "n" is generally taken to have a value of three (for non-transverse flows) while selected studies in Table 2.7, where "NC & FC" are column entries, essentially set "n" to unity. For cases where the forced convection

effects oppose the natural convection effects (forced convection alone would cause fluid to flow in direction opposite to flow direction if natural convection was acting alone), the plus sign in Equation (2-2) would change to a minus sign.

In the references in Table 2.7, the following expression is used to compute the forced convection heat transfer coefficient for heat transfer between ullage gas and tank walls where applicable

$$Nu_{F,W} = \left(\frac{h_o r}{k}\right) = b_1 \left[\frac{r \cdot \dot{m}_{PG}}{A_d \mu}\right]^{b_2} (\mathrm{Pr})^{b_3} \, e^{-\beta_W z_W} \tag{2-3}$$

For the forced convection component of heat transfer on the ullage gas side of the boundary between ullage gas and cryogenic (liquid) propellant, the following correlation is used where applicable

$$Nu_{F,O} = \left(\frac{h_{so} r}{k}\right) = d_1 \left[\frac{r_i \dot{m}_{PG}}{A_d \mu}\right]^{d_2} (\mathrm{Pr})^{d_3} \, e^{-\beta_S z_i} \tag{2-4}$$

In Rocketdyne Report R-3936-1 (1963) and in Nein and Thompson (1966) the variables "b_1," "b_2," and "b_3" are given values of 0.06, 0.8, and 0.333 respectively. In Nein and Thompson (1966), the variables "β_S" and "β_W" are developed from a wide range of empirical data results and are expressed by

$$\beta_S = 0.00117 r_i^2 \tag{2-5}$$

$$\beta_W = 0.00117 r_z^2 \tag{2-6}$$

Internal Tank Heat Transfer Correlations Summary

In summary, convection heat transfer Nusselt number correlations have mainly been used for the LMFR and MDFS computer models. The majority of these models are based on the application of natural convection heat transfer only at ullage gas regional boundaries. Most of the procedures in this category also treat heat transfer across the ullage-gas-to-propellant interface as negligible, but a substantial number also model heat transfer at this interface. MDFS models presented by five of the studies cited in Table 2.7 use the sum of forced and natural convection Nusselt numbers as the equivalent total convection Nusselt number. These models also treat heat transfer between cryogenic propellant and adjacent tank walls as being all natural convection heat transfer.

External Tank Wall Heat Transfer Correlations

The majority of analytical methods and models either apply the condition of an adiabatic outer tank wall surface (negligible heat transfer at this surface) or utilize a user specified and input heat flux into the outer wall of the tank. Tables 2.6 and 2.7 include general descriptions of how heat transfer at the outer tank wall is determined or computed for the LMFR and MDFS models. However, a number of the other analysis techniques described previously in this chapter also model heat transfer or apply preset or previously approximated heat transfer data for the external tank wall surfaces. Table 2.9 provides a summary of external tank wall heat transfer analysis methods used for computer models previously presented and described in this chapter. A few selected computer programs that model heat and mass transfer processes in cryogenic tanks, not associated with

Table 2.9 Description for Heat Transfer to External Tank Wall Surfaces for Various Computer Models (Page 1 of 2)

Reference Citation	Analytical Model Type	External Tank Wall Heat Transfer Modeling
Rocketdyne Report R-3936-1 (1963)	Multiple Discrete Fluid Sement Model	Case 1, Insulated Tank uses Transient Lumped Mass Heat Accumulation in Tank Wall Segments with Conduction Heat Transfer Through External Insulation and Fixed Temperature at Insulation External Surface. Case 2, Non-Insulated Tank uses Overall Equivalent Conductance Correlation Based on Difference Between Tank Wall and Ambient Environment Temperature Raised to First and Fourth Powers to Model Forced Convection and Radiation heat Transfer in Parallel, Correlation Coefficient Input from User
Lockheed Report ER-5296 Vol. IV (1961)	Lumped Mass Fluid Region Model	Forced Convection in Parallel with Radiation Heat Transfer, Forced Convection Uses Newton's Law of Cooling w/Forced Convection Heat Transfer Coeffcient Correlation Based on Reynold's Number of Free Air Stream Adjacent to Tank External Wall
Anderson, Scott, and Brady (1967)	Lumped Mass Fluid Region Model	Combined Forced Convection in Parallel with Radiation Heat Transfer, Forced Convection Based on Newton's Law of Cooling with User Specificed and Input Convection Heat Transfer Coefficient
Barber (1966)	Lumped Mass Fluid Region Model	Newton's Law of Cooling with Forced Convection Heat Transfer Coefficient Based on Colburn "j" Equation for a Flat Plate
Baral (1966)	Multiple Discrete Fluid Sement Model	[Same as Rocketyne Report R-3936-1 (1963)]
Barrere, et al. (1960)	Semi-Empirical	Not Considered
Bowersock, et al. (1960)	Saturation Rule	No Heat Transfer to and from Any Tank Wall Surfaces is Assumed
Bowersock and Reid (1961)	Equivalent Mass Model	Assumed Adiabatic (Vacuum Jacketing Around Tank)
Clark (1965)	(Propellant Heating Model; not a Collapse Factor Analysis Model)	User Speficied and Input Side Wall Heat Flux (Vertical Cylinder Tank)
Clark , et al. (1960)	(Propellant-to-Ullage-Gas mass Transfer and Temperature Profile Moel; Not a Collapse Factor Analysis Model)	Newton's Law of Cooling w/User Set Natural Convection Heat Transfer Coefficient of 2 BTU/(ft^2-^oR-hr)
Coxe and Tatom (1962)	Lumped Mass Fluid Region Model	Equivalent Conduction Heat Transfer Based on User Input Equivalent Composite Conductance, Free Stream Ambient Environment Temperature, and Uniform Tank Wall Temperature
DeWitt and McIntire (1974)	Multiple Discrete Fluid Sement Model	Assumed Adiabatic (Vacuum Jacketing Around Tank)
Epstein and Anderson (1968)	Semi-Empirical	User Specified and Input Constant and Uniform Heat Flux (Sample Solution Performed for One Test Shows No Heat Transfer at External Tank Wall)
Epstein (1965)	Semi-Empirical	User Specified and Input Constant and Uniform Heat Flux (Sample Solution Performed for One Test Shows No Heat Transfer at External Tank Wall)
Epstein, et al. (1965)	Multiple Discrete Fluid Sement Model	[Same as Rocketdyne Report R-3936 (1963)]
Gluck and Kline (1962)	Lumped Mass Fluid Region Model	Assumed Adiabatic (Vacuum Jacketing Around Tank)
Greer (1995)	2-Dimensional Numerical Finite Difference	User Input Heat Flux; can be Input as a Function of Circumferential Position Around Tank's Circular Cross-Section (Tank must be Horizontal Cylinder for this Model)
Hodge and Koenig (1992)	Lumped Mass Fluid Region Model	Assumed Adiabatic (Vacuum Jacketing Around Tank)
Hsu ((1994)	2-Dimensional Numerical Finite Difference	Not Applicable; Tank Wall is Not Modeled w/Any Heat Transfer
Humphrey (1961)	Saturation Rule w/Ullage Gas Side Wall Condensaiton	Tank Wall set to Uniform Temperature of LN Bath Around the Tank
Lin and Hasan (1992)	Multiple Discrete Fluid Sement Model	User Specified and Input Constant and Uniform Heat Flux
Ludwig and Houghton (1989)	Lumped Mass Fluid Region Model	Assumed Adiabatic (Vacuum Jacketing Around Tank)

Table 2.9 Description for Heat Transfer to External Tank Wall Surfaces for Various Computer Models (Page 2 of 2)

Reference Citation	Analytical Model Type	External Tank Wall Heat Transfer Modeling
Majumdar and Steadman (1998)	Lumped Mass Fluid Region Model	Not Stated; Appears to Assume Adiabatic Outer Tank Wall Surface
Mandell and Roudebush (1965)	Multiple Discrete Fluid Sement Model	Assumed Adiabatic (Vacuum Jacketing Around Tank)
Masters (1974)	Multiple Discrete Fluid Sement Model	User Specified and Input Constant and Uniform Heat Flux
Momenthy (1964)	Lumped Mass Fluid Region Model	Newton's Law of Cooling w/User Specified and Input Convection Heat Transfer Coefficient and External Free Stream Air Temperature Values as Functions of Time
Moore, et al. (1960)	Upper and Lower Bound with "Worst Case Rule" for Upper Bound	No Heat Transfer to and from Any Tank Wall Surfaces is Assumed
Nein and Thompson (1965)	Semi-Empirical	Newton's Law of Cooling w/User Specified and Input Convection Heat Transfer Coefficient and External Free Stream Air Temperature
Nein and Thompson (1965)	Multiple Discrete Fluid Sement Model	[Refers to Rocketdyne Report R-3936-1 (1963)]
Nevrovskii (1994)	[Model to Determine Time of Specified Pressure Rise in Closed Off Tank in Micro-Gravity Environment; Not a Collapse factor Analysis Model]	User Specified and Input Constant and Uniform Heat Flux
Riemer and Scarlotti (1983)	Upper and Lower Bound Analysis	No Heat Transfer to and from Any Tank Wall Surfaces is Assumed
Riemer (1986)	Upper and Lower Bound Analysis w/Addition of Heat Flux into Tank; Simplified to Determine Pressure Rise in Closed Off Tank	User Specified and Input Constant and Uniform Heat Flux
Ring (1964)	Lumped Mass Fluid Region Model	Newton's Law of Cooling w/Forced Convection Heat Transfer Coefficient Correlation Using Reynold's Number of Air Flow Stream Along Tank Walls and External Air Properties
Roudebush (1965)	Multiple Discrete Fluid Sement Model	Assumed Adiabatic (Vacuum Jacketing Around Tank) or User Specified and Input External Heating Rate as a Function of Time
Sasmal, Hochstein, and Hardy (1993)	2-Dimensional Numerical Fiinite Difference [Tank Pressurization without Propellant Expulsion Only]	Set to Constant 0.00884 BTU(ft^2-sec) Heat Flux Into Tank External Walls
Sasmal, et al. (1991)	2-Dimensional Numerical Fiinite Difference (Tank Pressurization without Propellant Expulsion Only)	Not Stated; Appears to Assume Adiabatic Outer Tank Wall Surface
Stochl, et al. (1970), NASA TN-D-7019	Multiple Discrete Fluid Sement Model	Assumed Adiabatic (Vacuum Jacketing Around Tank)
Stochl, et al. (1970), NASA TN-D-5621	Multiple Discrete Fluid Sement Model	Assumed Adiabatic (Vacuum Jacketing Around Tank)
Thompson and Nein (1965)	Semi-Empirical	Newton's Law of Cooling w/User Specified and Input Convection Heat Transfer Coefficient and External Free Stream Air Temperature
Van Dresar and Stochl (1991)	Upper and Lower Bound Analysis	No Heat Transfer to and from Any Tank Wall Surfaces is Assumed
Van Dresar, Lin, and Hasan (1992)	Upper Bound Analysis Based on Fully Mixed Uniform Fluid Properties Throughout Tank [No Entering Pressurant, No Propellant Expulsion]	User Specified and Input Constant and Uniform Heat Flux
Van Dresar and Haberbusch (1994)	Upper and Lower Bound Analysis	No Heat Transfer to and from Any Tank Wall Surfaces is Assumed
Van Dresar (1995)	Semi-Empirical	No Heat Transfer to and from Any Tank Wall Surfaces is Assumed
Wapato, et al. (1971)	Upper Bound Analysis Based on Fully Mixed Uniform Fluid Properties Throughout Tank [No Entering Pressurant, No Propellant Expulsion]	No Heat Transfer to and from Any Tank Wall Surfaces is Assumed

typical tank pressurization and cryogenic propellant expulsion processes, are also cited in Table 2.9 for comparative purposes.

A number of the collapse factor models and techniques use Newton's law of cooling with forced convection heat transfer correlations based on ambient air properties and flow conditions, ambient air temperature, local or uniform tank wall temperature, and surface area of the external tank wall. Most of the models in this category are used for flight vehicle propellant tanks where aerodynamic and forced convection heating cause high heat fluxes into the external tank wall. In some cases, radiation heat transfer from the ambient surroundings to the outer tank wall is modeled as transferring heat in parallel with the convection heat transfer.

The majority of the analytical tools described in studies cited by Table 2.9 treat the external tank wall as an adiabatic surface where no heat transfer occurs. This is done because cryogenic propellant tanks generally used for flight vehicles or ground test facility run systems are very well insulated or enclosed inside a vacuum annulus with radiation shielding. The resulting heat transfer rates from surrounding environment into cryogenic propellant tanks are, therefore, very small, especially with the relatively short time durations of typical tank pressurization and propellant expulsion processes when compared to these rates of heat transfer. For purposes of this study, which is mainly focused on supercritical tank pressure applications that are essentially only used in ground testing facilities where cryogenic propellant tanks are almost always vacuum jacketed to minimize heat leakage into the tanks, the external tank wall surfaces are considered to be adiabatic.

Mass Transfer Correlations

There have been a number of studies performed in which mass transfer across the interface between cryogenic liquids and ullage gas inside tanks have been modeled and evaluated. However, the mass transfer of evaporated or supercritical propellant species through an ullage gas region containing pressurant gas that is a different species than the propellant has not been extensively studied. Virtually all studies to date, where intra-tank mass transfer processes have been modeled and evaluated, are applied to low subcritical tank pressure applications.

At the subcritical tank pressure conditions, a distinct boundary or interface exists between the cryogenic propellant in the liquid phase and the ullage gas in the vapor phase and the temperature at this interface is generally equal to the propellant species saturation temperature. Additionally, a phase change has to occur to enable transfer of mass across this interface when cryogenic propellant and pressurant gas are the same species. When not the same species, the propellant species cannot transfer across this interface without changing phase and the pressurant gas species would have to readily dissolve as a gas into the cryogenic liquid propellant. Empirical data indicate that properly selected pressurant gases will not dissolve into the liquid propellant of a different species if proper design measures are utilized.

Regarding the mass transfer across the interface between ullage gas and cryogenic liquid propellant at subcritical pressures, six predominant analytical methods are used to model this mass transfer.

For the first mass transfer computation method, mass transfer rates at the ullage-gas-to-propellant interface are equated as the quotient of the net rate of heat transfer to

and from this interface divided by the propellant latent heat of vaporization at tank pressure. For one study, Anderson, Scott, and Brady (1967), the net difference between bulk ullage gas and cryogenic liquid propellant enthalpies is substituted for latent heat of vaporization of the propellant. The prior studies utilizing this mass transfer computation method are summarized in Table 2.10.

The second analytical method to model mass transfer at the ullage-gas-to-propellant interface is based on condensation of ullage gas along adjacent tank walls or segments thereof. Humphrey (1961), Momenthy (1964), and Ring (1964) are three studies where this method is employed. In all cases, this mode of mass transfer results in condensation of ullage gas or propellant species within the ullage gas along all or segments of tank walls in contact with the ullage gas.

For the third analytical mass transfer computation method, heat flux from the external environment into the cryogenic liquid propellant via the tank walls adjacent to this propellant is used to determine mass transfer rate across the ullage-gas-to-propellant interface. However, this method is only applicable to cases where significant and relatively high levels of external heat flux into the tank exist. This condition generally occurs on flight vehicles with un-insulated propellant tanks where aerodynamic heating is a major source of heat influx. In these cases, the liquid propellant is very near or at saturation temperature with virtually uniform temperatures throughout the entire propellant region. Prior studies where this method is applied include Lockheed Report ER-5296, Vol. IV (1961), Rocketdyne Report R-3936-1 (1963), Anderson, Scott, and Brady (1967), Arnett and Voth (1972), Clark (1965), Clark et al. (1960), Coxe and Tatom (1962), Epstein and Anderson (1968), and others listed in Table 2.9.

Table 2.10 Information Summary for Analytical Methods and Models that Compute Mass Transfer Rates at Ullage-Gas-to-Propellant Interface from Net Heat Transfer Above and Below This Interface Divided by Propellant Latent Heat of Vaporization

Reference Citation	Above Interface; Ullage Gas Region to Interface Heat Transfer	Below Interface; Interface to Propellant Region Heat Transfer
Rocketdyne Report R-3936-1 (1963)	Summation of Forced and Natural Convection Using Newton's Law of Cooling; Ref. Eqn. (2-2) and Nein and Thompson (1966) Values on Table 2.8 for Natural Convection Component, Ref. Eqn. (2-4) for Forced Convection Component	Conduction using Numerical Finite Difference Model with Vertical Horizontal propellant Segment Temperatures Near Interface to Determine Temperature Gradient at Interface; Product of Temperature Gradient at Interface and Thermal Conductivity of Propellant at Top Propellant Segment is Heat Transfer Rate
Akyuzlu (1993)	Natural Convection Using Newton's Law of Cooling with Nusselt Number Correlation Based on Grashof and Prandti Numbers Raised to Exponential Powers, but Exponent and Constant Values Not Given for Correlations	Natural Convection Using Newton's Law of Cooling with Nusselt Number Correlation Based on Grashof and Prandtl Numbers Raised to Exponential Powers, but Exponent and Constant Values Not Given for Correlations
Anderson, Scott, and Brady (1967)	Natural Convection Using Newton's Law of Cooling with Nusselt Number Correlation from Eqn. (2-2) and Table 2I8	Natural Convection Using Newton's Law of Cooling with Nusselt Number Correlation from Eqn. (2-2) and Table 2.8
Beekman and Martin (1991)	Natural Convection Using Newton's Law of Cooling with Nusselt Number Correlation from Eqn. (2-2) and Table 2.8	Natural Convection Using Newton's Law of Cooling with Nusselt Number Correlation from Eqn. (2-2) and Table 2.8
Clark and Barakat (1965)	Conduction Only; Numerical Finite Difference Modeling w/Discrete Horizontal Ullage Gas Segments Used to Determine Vertical Temperature Gradient at Interface; Product of This Temperature Gradient and Thermal Conductivity of Ullage Gas at Interface is Heat Transfer Rate	Conduction Only; Numerical Finite Difference Modeling w/Discrete Horizontal Liquid Propellant Segments Used to Determine Vertical Temperature Gradient at Interface; Product of This Temperature Gradient and Thermal Conductivity of Liquid Propellant at Interface is Heat Transfer Rate
Clark, et al. (1960)	Considered Negligible in Comparison to Heat Transfer Below Interface	Conduction Only; with Vertical Temperature Profile Determined from Similarity (Transient Heat Conduction w/Error Function) Solution Treating Liquid Propellant as Semi-Infinite Solid Slab Bounded on Top Surface w/Interface Temperature Equal to Propellant Saturation Temperature
Hasan and Lin (1991)	Considered Negligible in Comparison to Heat Transfer Below Interface	Convection Correlation Based on Newton's Law of Cooling w/Nusselt Number Correlation Based on Upflow Jet Conditions Where Liquid Jet is Used to Enhance Ullage Gas Condensation at Interface
O'Loughlin and Glenn (1966)	Conduction Only; Numerical Finite Difference Modeling w/Discrete Horizontal Ullage Gas Segments Used to Determine Vertical Temperature Gradient at Interface; Product of This Temperature Gradient and Thermal Conductivity of Ullage Gas at Interface is Heat Transfer Rate	Conduction Only; Numerical Finite Difference Modeling w/Discrete Horizontal Liquid Propellant Segments Used to Determine Vertical Temperature Gradient at Interface; Product of This Temperature Gradient and Thermal Conductivity of Liquid Propellant at Interface is Heat Transfer Rate
Olsen (1966)	Conduction Only w/Vertical Temperature Gradient Set Equal on Both Sides of (Above and Below) Interface; Product of This Vertical Temperature Gradient and the Difference in Thermal Conductivities in Ullage Gas and Liquid Propellant Essentially Determine Net Heat Transfer Rate at Interface	Conduction Only w/Vertical Temperature Gradient Set Equal on Both Sides of (Above and Below) Interface; Product of This Vertical Temperature Gradient and the Difference in Thermal Conductivities in Ullage Gas and Liquid Propellant Essentially Determine Net Heat Transfer Rate at Interface
Ring (1964)	Natural Convection Using Newton's Law of Cooling with Nusselt Number Correlation from Eqn. (2-2) and Table 2.8	Natural Convection Using Newton's Law of Cooling with Nusselt Number Correlation from Eqn. (2-2) and Table 2.8
Segel (1965)	Considered Negligible in Comparison to Heat Transfer Below Interface	Conduction Only; with Vertical Temperature Profile Determined from Similarity (Transient Heat Conduction w/Error Function) Solution Treating Liquid Propellant as Semi-Infinite Solid Slab Bounded on Top Surface w/Interface Temperature Equal to Propellant Saturation Temperature
Schmidt, et al. (1960)	Considered Negligible in Comparison to Heat Transfer Below Interface	Conduction Only; with Vertical Temperature Profile Determined from Similarity (Transient Heat Conduction w/Error Function) Solution Treating Liquid Propellant as Semi-Infinite Solid Slab Bounded on Top Surface w/Interface Temperature Equal to Propellant Saturation Temperature
Vaughan and Schmidt (1990)	Natural Convection Using Newton's Law of Cooling with Nusselt Number Correlation from Eqn. (2-2), but Coefficient and Exponent Values Not Given	Natural Convection Using Newton's Law of Cooling with Nusselt Number Correlation from Eqn. (2-2), but Coefficient and Exponent Values Not Given

The fourth mass transfer computation method uses a similarity variable computed from time and liquid propellant properties (generally thermal diffusivity and density) to model the velocity of the interface between the ullage gas and the liquid propellant. This method treats the liquid propellant and ullage gas regions as two semi-infinite volumes of fluid with a common plane interface, and it is analogous to the methods used to model freezing and melting fronts between interfacing semi-infinite liquid and solid substances presented in Gebhart (1993). Prior studies employing the fourth method include Clark (1965), Knuth (1959), and O'Loughlin (1966).

The fifth method for determining mass transfer across the interface between ullage gas and propellant is based on excess liquid propellant superheating or ullage gas subcooling where rapid pressure changes inside a tank cause a net evaporation of liquid propellant or a net condensation of ullage gas. The prior studies employing this method include Arnett and Voth (1972), O'Loughlin and Glenn (1966), and Ring (1964).

The sixth (and final) method used to determine rates and quantities of mass transferred across the ullage-gas-to-propellant interface is restricted to cases where the ullage gas is a mixture of two gas species due to the pressurant gas being a different species than the cryogenic propellant. The method is also the only method where mass transfer within the ullage gas region is also modeled since the mixture ratio of heated or evaporated propellant species to pressurant gas species is generally not uniform within the ullage gas region. The studies in which the sixth analytical methods of mass transfer are utilized include Rocketdyne Report R-3936-1 (1963), Epstein, Georgius, and Anderson (1965), Nein and Thompson (1966), and Ring (1964).

No studies were found where analytical methods have been used to model the mass transfer of pressurant gas into the cryogenic propellant region where the pressurant gas and propellant are different species.

Transient Properties of Pressurant Gas Entering Tank Ullage

In general most of the models presented for cryogenic propellant tank pressurization and expulsion processes use either a constant ullage gas pressure and pressurant gas inlet temperature or predetermined profiles of these properties with respect to time. For these studies, the pressurant gas supplied to the cryogenic propellant tank ullage generally flows through a heat exchanger with an active outlet temperature and flow control system to maintain required tank pressure set points and pressurant gas inlet temperature set points.

However, there are selected collapse factor models described in the literature where pressurant gas can also be modeled as being supplied from a (fixed volume) reservoir of one or more pressurized gas bottles. In these models the gas pressure in these bottles decreases with time during the cryogenic tank pressurization and propellant expulsion processes since mass is continually being transferred from the gas bottle to the cryogenic tank ullage. The pressurant gas within the bottles also undergoes thermodynamic property changes as bottle pressure decreases. These property changes are determined by the mass transferred out of the bottles and heat transfer from ambient environment and gas bottle wall materials into the gas contained within the bottle.

Hodge and Koenig (1992) and Ludwig and Houghton (1989) also present cryogenic propellant tank collapse factor analysis computer program models that are able

to model the transient thermodynamic properties of pressurant gas supplied from a fixed volume reservoir [gas bottle(s)]. However, both of these studies make the case and conclude that heat transfer from pressurant gas supply bottle walls to the pressurant gas inside these bottles has a negligible effect on the properties of the pressurant gas. Both Hodge and Koenig (1992) and Ludwig and Houghton (1989) present the argument that heat transfer to pressurant gas inside the pressurant gas supply bottle(s) is all natural convection with very low Nusselt number values, relatively poor thermal conductivity of the pressurant gas, and large mass of pressurant gas inside the bottle(s) that result in very small increases in gas temperature due to heat transfer from bottle walls to this gas.

Hodge and Koenig (1992) also cite an example from Saad (1993) where a blow-down (rapid pressure decay inside a gas bottle due to the gas being vented from the bottle) process from an air bottle was studied. Saad (1993) provides plots where the blow-down process is bounded by an isentropic (reversible and adiabatic) process, where heat transfer from gas bottle walls to internal gas is zero, and an isothermal process. The initial part of the blow-down process very closely follows the isentropic process. Deviations from the isentropic process occur only during the latter part of the blow-down process as reservoir gas pressures and temperatures become much lower than initial gas pressures and temperatures.

Rocketdyne Report R-3936-1 (1963) provides computation methods and correlations to model incremental changes in pressurant gas and supply bottle wall temperatures across finite time intervals. The correlations are derived from explicit numerical finite-difference methods and are based on the bottle wall having a spatially uniform temperature. The correlations also model the effects of heat transfer from the

ambient atmosphere to bottle walls and from these walls to pressurant gas inside the bottle(s). Heat transfer from the ambient atmosphere to the bottle walls is modeled with a correlation based on combined radiation and natural convection where an equivalent conductance is computed and used to account for the combined modes of heat transfer. Heat transfer from the bottle walls to the internal pressurant gas is modeled as natural convection.

In summary, only a few of the collapse factor models have the capability to model transient pressurant gas thermodynamic property conditions associated with the blow-down mass decrease and pressure decay in pressurant gas supply bottle(s) which are often used for supplying gas to cryogenic propellant run tanks. One study provides correlations for modeling heat transfer processes that may occur from ambient environment and gas bottle wall materials to the pressurant gas inside the bottle as the gas temperature decreases below the ambient environmental temperature. However, this study does not provide numerical values or methods to determine numerical values for selected parameters needed to calculate rates of heat transfer or the effects of this heat transfer on pressurant gas temperature inside the supply bottle(s).

Literature Review Summary

All of the information found in the review of literature and presented in this chapter provides interesting and valuable insights that are beneficial to this study. A substantial portion of the work or end results of studies presented in this chapter are also directly or indirectly applied to the development of the new analysis program presented and evaluated in this study.

CHAPTER III

PROGRAM ALGORITHM DEVELOPMENT

The computer program developed under this study employs a number of algorithms that compute and use fluid properties, tank wall material properties, rates of heat and mass transfer across boundaries, accumulated mass and heat in fluid and tank-wall segments and regions, and geometric parameters that define boundaries and effect all of the processes being analyzed. An overall description of algorithms and their development is presented in this chapter.

General Layout of the Tank and Internal Fluids System

Figure 3.1 shows a simplified layout of the tank with the internal ullage gas and cryogenic propellant regions. When the internal tank pressure is less than the critical pressure of the propellant, the propellant is in the liquid phase and there is a distinct horizontal boundary between the propellant and the ullage gas. For the computer model this boundary is treated as a horizontal plane as illustrated in this figure.

The computer model is designed such that the initial pressure (at the very first time step) at the main tank bottom discharge nozzle has to be less than half of the critical pressure of the cryogenic propellant species. It is also designed to limit the incremental

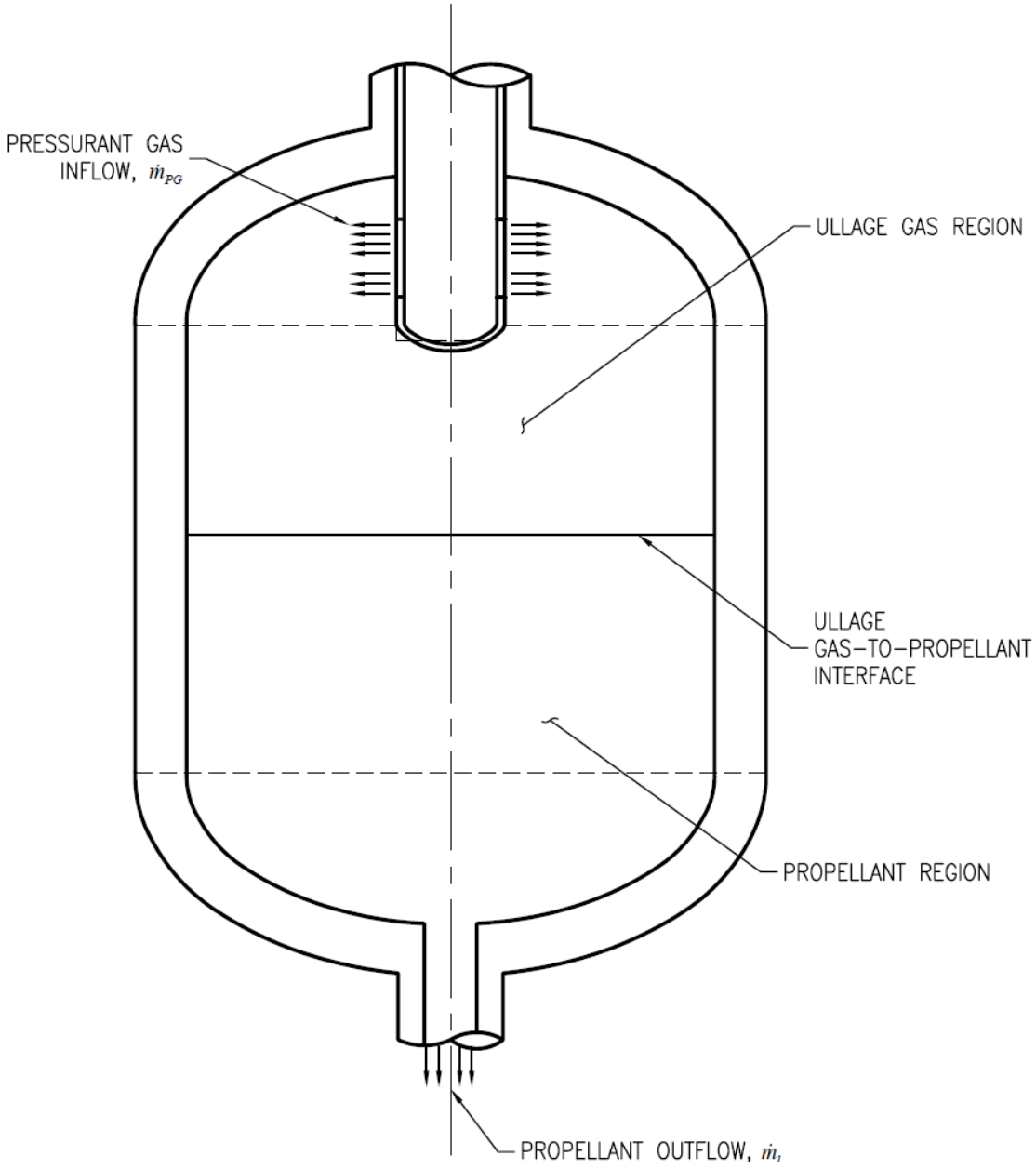

Figure 3.1 General Layout of Tank System

increase in pressure at this nozzle across sequential time steps, such that the tank pressure is subcritical for the first five or more time steps.

When the tank pressure is increased to supercritical pressures, there is no longer a distinction between liquid and gas phases. However, the computer model continues to treat the boundary, or interface, between propellant and ullage gas as a horizontal plane dividing the two fluid regions with different properties. The computer model is also based on the assumption of no mass transfer across this interface.

Figure 3.1 also shows propellant being discharged out of the tank through the bottom discharge nozzle at a mass flow rate assigned to the variable $\dot{m}_l$. This variable value and the pressure at the bottom main discharge nozzle are program user input values at each time step. The mass flow rate out of the main bottom discharge nozzle can be set to zero at any time step when the tank is being pressurized or depressurized with no propellant being expelled from the tank. However, the model does limit incremental changes in this mass flow rate, so that excessively large changes in mass flow are not allowed across small time steps. Also the model does not allow negative values of $\dot{m}_l$ which would represent propellant mass entering the tank.

Figure 3.2 illustrates the same tank and fluid system as Figure 3.1, but with added details indicating subdivision of the propellant and ullage gas regions into discrete segments in order for vertical temperature gradients in each of these regions to be modeled. Key variables that set values for tank geometric features and that set and track boundaries of each fluid segment are also presented in the figure.

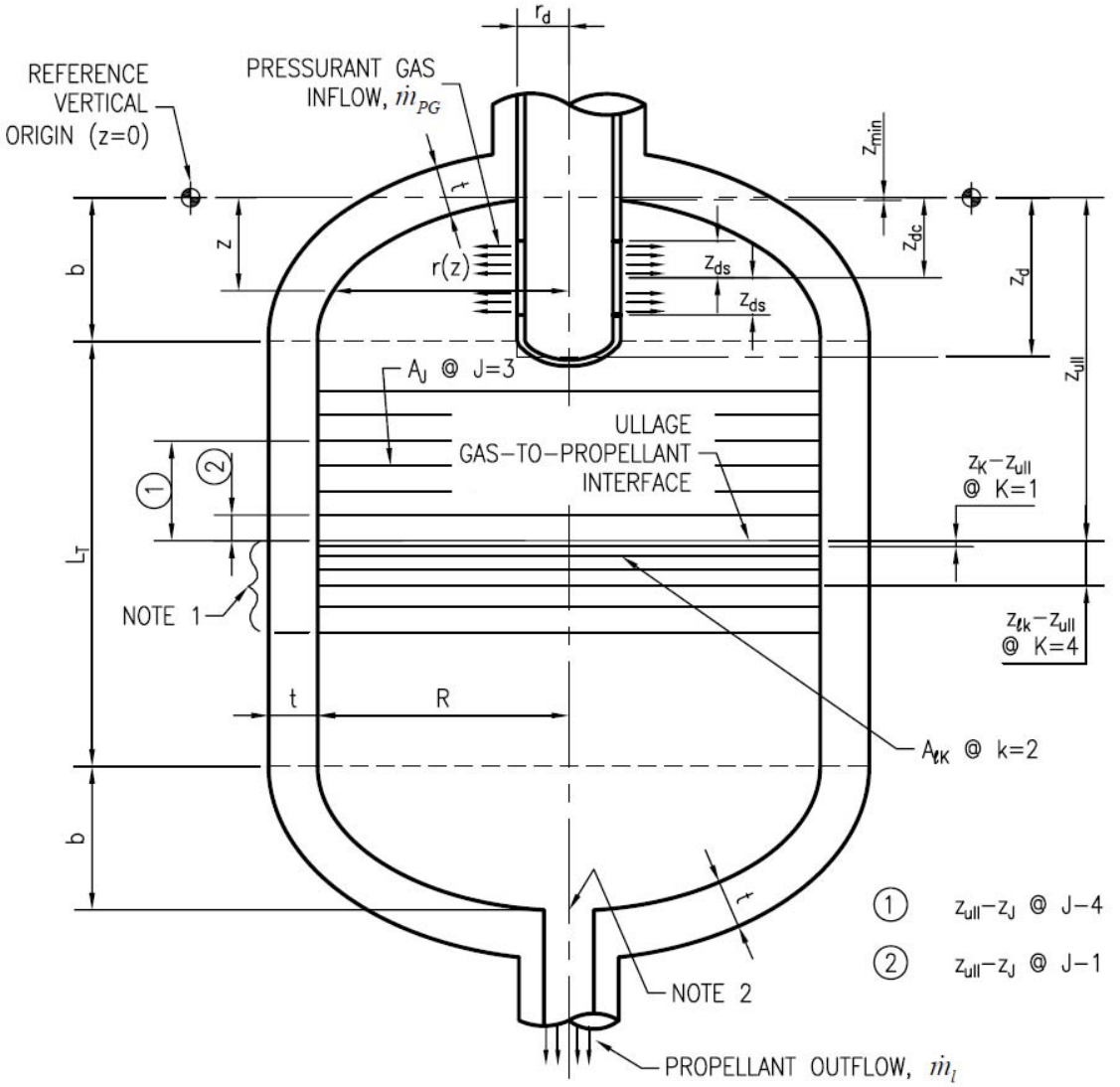

NOTES:

1. SLL=STRATIFIED LIQUID LAYER; REMAINING BULK LIQUID AT UNIFORM TEMP.

2. VORTEX BREAKER LOCATION, ASSUME NEGLIGIBLE VOLUME OF VORTEX BREAKER, ASSUME NEGLIGIBLE HEAT CAPACITANCE OF VORTEX BREAKER

OBLATE SPHEROID TANK IS SPECIAL CASE WITH $L_T = \emptyset$ AND R>b

SPHERICAL TANK IS SPECIAL CASE WITH R=b AND $L_T = \emptyset$

Figure 3.2 General Layout of Tank System with Fluid Segment, Boundary, and Dimensional Details

The variable $\dot{m}_{PG}$, indicated in both Figures 3.1 and 3.2, is the mass flow rate of pressurant gas into the tank ullage. The rate of mass transfer of pressurant gas into each of the ullage gas segments is the product of $\dot{m}_{PG}$ and the ratio of the volume of the respective segment to the total ullage gas region volume. The program computes the total pressurant gas mass flow into the tank ullage region for each time step for three cases. The first case has no heat transfer at any cryogenic and ullage gas segment boundaries. The second case considers heat transfer only at fluid boundaries in contact with the tank wall. The third case accounts for heat transfer across all of the fluid segment boundaries.

Ullage Gas Segment Conservation of Mass

Referring to Figure 3.3 and specifying that the mass of pressurant gas added to all ullage gas segments is uniformly distributed through the entire ullage gas volume, the rate of change in mass in each ullage gas segment J is given by

$$\frac{dm_J}{d\tau} = \dot{m}_{PG,J} = \dot{m}_{PG}\left(\frac{V_J}{V_{Ull}}\right) \tag{3-1}$$

Integrating all terms in Equation (3-1) with respect to time and rearranging the resulting equation to solve for the mass of ullage gas at time $\tau + \Delta\tau$ yields

$$m_J{}^{\langle\tau+\Delta\tau\rangle} = m_J{}^{\langle\tau\rangle} + \left(m_{PG,J}{}^{\langle\tau+\Delta\tau\rangle} - m_{PG,J}{}^{\langle\tau\rangle}\right) \tag{3-2}$$

where:

$$m_{PG,J}{}^{\langle\tau+\Delta\tau\rangle} = m_{PG}{}^{\langle\tau+\Delta\tau\rangle}\left(\frac{V_J}{V_{Ull}}\right)^{\langle\tau+\Delta\tau\rangle} \tag{3-3}$$

$$m_{PG,J}^{\langle\tau\rangle} = m_{PG}^{\langle\tau\rangle}\left(\frac{V_J}{V_{Ull}}\right)^{\langle\tau\rangle} \tag{3-4}$$

Equation (3-2) is utilized in the model to calculate mass in each ullage gas segment at the end of a given time step from previously computed results at the start of the same time step and latest iteration values of ullage gas segment volumes and total mass of pressurant gas added to tank ullage.

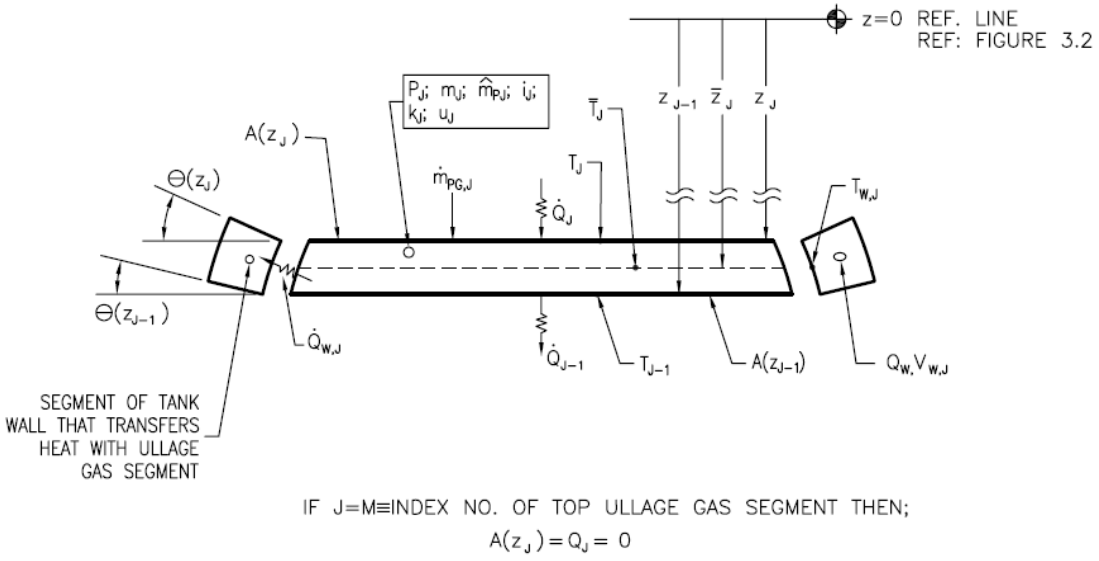

Figure 3.3 Ullage Gas Segment

Ullage Gas Segment Conservation of Energy

Referring to Figure 3.3, the rate of change of total internal energy in each ullage gas segment J is given by

$$\frac{d}{d\tau}(u_J m_J) = \dot{Q}_J - \dot{Q}_{J-1} - \dot{Q}_{w,J} + \dot{m}_{PG,J} i_{PG} - P_J\left[\frac{d}{d\tau}\left(\frac{m_J}{\rho_J}\right)\right] \tag{3-5}$$

The first three terms on the right hand side of Equation (3-5) are respectively the rates of heat transfer at upper, lower, and tank wall boundaries as shown in Figure 3.3. The fourth term represents the rate of total enthalpy added by the addition of pressurant gas to the ullage gas segment. The last term represents the net work done by the volumetric expansion of the ullage gas segment.

The total internal energy in each ullage gas segment J at the end of a given time step is determined from the total internal energy of the same segment at the start of the time step and integral of Equation (3-5) with respect to time as follows

$$u_J^{\langle\tau+\Delta\tau\rangle} m_J^{\langle\tau+\Delta\tau\rangle} = u_J^{\langle\tau\rangle} m_J^{\langle\tau\rangle} + \int_{\tau}^{\tau+\Delta\tau} \frac{d}{d\tau}(u_J m_J) d\tau \tag{3-6}$$

If $\dot{Q}_J$, $\dot{Q}_{J-1}$, $\dot{Q}_{w,J}$, i_{PG}, P_J, and ullage gas segment volume, m_J/ρ_J, vary linearly with respect to time from time τ to time $\tau+\Delta\tau$, substitution of Equation (3-5) as the integrand in Equation (3-6) and evaluating the integral yields

$$\begin{aligned} u_J^{\langle\tau+\Delta\tau\rangle} m_J^{\langle\tau+\Delta\tau\rangle} = u_J^{\langle\tau\rangle} m_J^{\langle\tau\rangle} + \left[\bar{\dot{Q}}_J - \bar{\dot{Q}}_{J-1} - \bar{\dot{Q}}_{w,J}\right](\Delta\tau) + \left[m_{PG,J}^{\langle\tau+\Delta\tau\rangle} - m_{PG,J}^{\langle\tau\rangle}\right]\bar{i}_{PG} \\ -\bar{P}_J\left[\left(\frac{m_J}{\rho_J}\right)^{\langle\tau+\Delta\tau\rangle} - \left(\frac{m_J}{\rho_J}\right)^{\langle\tau\rangle}\right] \end{aligned} \tag{3-7}$$

In Equation (3-7), $\bar{\dot{Q}}_J$, $\bar{\dot{Q}}_{J-1}$, and $\bar{\dot{Q}}_{w,J}$ are respectively $\dot{Q}_J$, $\dot{Q}_{J-1}$, and $\dot{Q}_{w,J}$ evaluated at time $\tau+\Delta\tau/2$. The mean enthalpy of pressurant gas and the mean pressure of the ullage gas fluid segment are computed by the following averages

$$\bar{i}_{PG} = \left(\tfrac{1}{2}\right)\left(i_{PG}^{\langle\tau+\Delta\tau\rangle} + i_{PG}^{\langle\tau\rangle}\right) \tag{3-8}$$

$$\bar{P}_J = \left(\tfrac{1}{2}\right)\left(P_J^{\langle\tau+\Delta\tau\rangle} + P_J^{\langle\tau\rangle}\right) \tag{3-9}$$

Dividing both sides of Equation (3-7) by $m_J^{\langle \tau+\Delta\tau \rangle}$, total mass of fluid in ullage gas segment J, yields the internal energy of the fluid

$$u_J^{\langle \tau+\Delta\tau \rangle} = u_J^{\langle \tau \rangle}\left(\frac{m_J^{\langle \tau \rangle}}{m_J^{\langle \tau+\Delta\tau \rangle}}\right)+\left[\bar{\dot{Q}}_J-\bar{\dot{Q}}_{J-1}-\bar{\dot{Q}}_{w,J}\right]\left(\frac{\Delta\tau}{m_J^{\langle \tau+\Delta\tau \rangle}}\right) \qquad (3\text{-}10)$$
$$+\bar{i}_{PG}\left[\frac{m_{PG,J}^{\langle \tau+\Delta\tau \rangle}-m_{PG,J}^{\langle \tau \rangle}}{m_J^{\langle \tau+\Delta\tau \rangle}}\right]-\left(\frac{\bar{P}_J}{m_J^{\langle \tau+\Delta\tau \rangle}}\right)\left[\left(\frac{m_J}{\rho_J}\right)^{\langle \tau+\Delta\tau \rangle}-\left(\frac{m_J}{\rho_J}\right)^{\langle \tau \rangle}\right]$$

Equation (3-10) is utilized in the model to calculate the specific internal energy of fluid in each ullage gas segment at the end of a given time step from previously computed properties of the same segment at the start of the same time step and latest iteration values of ullage gas segment properties, rates of heat transfer, total mass and mean enthalpy of pressurant gas added to the respective ullage gas segment.

Cryogenic Propellant Segment Conservation of Mass

Referring to Figures 3.4 and 3.5, the rate of change of mass in each cryogenic propellant segment is given by

$$\frac{dm_{lK}}{d\tau}=\begin{cases}0 & \text{if } K<K_{max}\\ -\dot{m}_l & \text{if } K=K_{max}\end{cases} \qquad (3\text{-}11)$$

In Equation (3-11), K_{max} is the total number of propellant segments (and the index number for the lowermost, bulk, propellant segment) and K is the index number of the propellant segment being evaluated as illustrated in Figure 3.2.

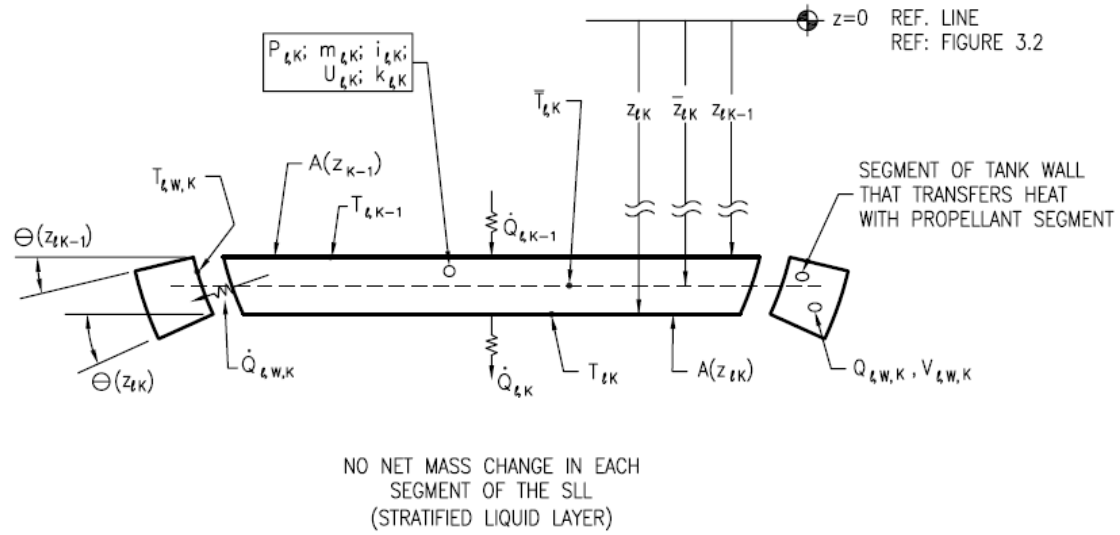

Figure 3.4 Cryogenic Propellant Stratified Liquid Layer Segment

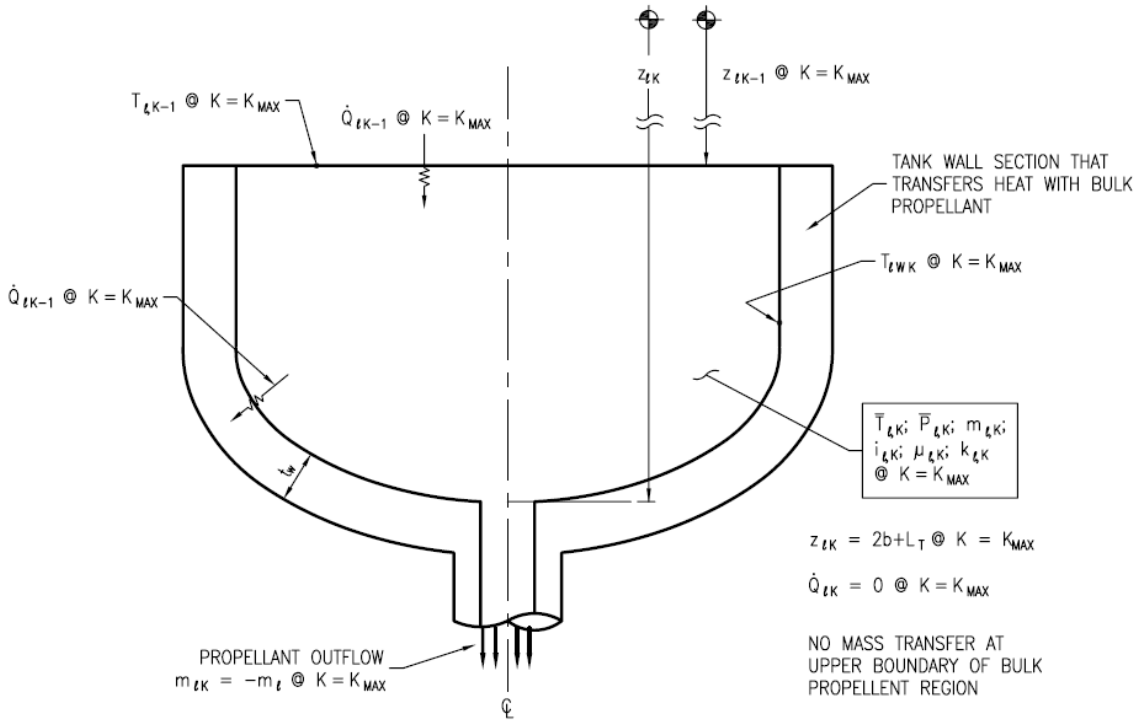

Figure 3.5 Bulk Cryogenic Propellant Segment

If $\dot{m}_l$ varies linearly with respect to time, integration of both sides of Equation (3-11) and rearranging to solve for mass of propellant in segment K at time $\tau + \Delta\tau$ yields

$$m_{lK}{}^{\langle \tau+\Delta\tau \rangle} = \begin{cases} m_{lK}{}^{\langle \tau \rangle} & \text{if K<K}_{\max} \\ m_{lK}{}^{\langle \tau \rangle} - \left(\frac{\Delta\tau}{2}\right)\left(\dot{m}_l{}^{\langle \tau+\Delta\tau \rangle} + \dot{m}_l{}^{\langle \tau \rangle}\right) & \text{if K=K}_{\max} \end{cases} \tag{3-12}$$

Equation (3-12) is utilized in the model to calculate the mass in each propellant segment at the end of a given time step from previously computed propellant mass. When the resulting value of $\dot{m}_{lK}{}^{\langle \tau+\Delta\tau \rangle}$ at K=K$_{\max}$ is less than zero, the program terminates as all of the bulk propellant has been expelled out of the tank.

Cryogenic Propellant Segment Conservation of Energy

Referring to Figures 3.4 and 3.5, the rate of change of total internal energy of each cryogenic propellant segment is given by

$$\frac{d}{d\tau}\left(u_{lK} m_{lK}\right) = \dot{Q}_{lK-1} - \dot{Q}_{lK} - \dot{Q}_{l,w,K} - \dot{m}_l i_{lK} - P_{lK}\left[\frac{d}{d\tau}\left(\frac{m_{lK}}{\rho_{lK}}\right)\right] \tag{3-13}$$

The first three terms on the right hand side of Equation (3-13) are respectively the rates of heat transfer at upper, lower, and tank wall boundaries as shown in Figure 3.4 or 3.5, whichever applies. The fourth term represents the rate of total enthalpy removed by the loss of propellant mass from propellant segment K. The last term represents the net work done by the volumetric expansion of propellant segment K. If the segment is compressed, then work is done to the segment and will have the effect of adding to the total internal energy of fluid in this segment.

The total internal energy in each propellant segment K at the end of a given time step is as follows

$$u_{lK}{}^{\langle \tau+\Delta\tau \rangle} m_{lK}{}^{\langle \tau+\Delta\tau \rangle} = u_{lK}{}^{\langle \tau \rangle} m_{lK}{}^{\langle \tau \rangle} + \int_{\tau}^{\tau+\Delta\tau} \frac{d}{d\tau}\left(u_{lK} m_{lK}\right) d\tau \tag{3-14}$$

If $\dot{Q}_{lK-1}$, $\dot{Q}_{lK}$, $\dot{Q}_{l,w,K}$, i_{lK}, P_{lK}, and propellant segment volume, m_{lK}/ρ_{lK}, vary linearly with respect to time from time τ to time $\tau+\Delta\tau$, substitution of Equation (3-13) into Equation (3-14), evaluating the integral, and rearranging to solve for internal energy at time $\tau+\Delta\tau$ yields

$$\begin{aligned} u_{lK}{}^{\langle \tau+\Delta\tau \rangle} = u_{lK}{}^{\langle \tau \rangle} &+ \left[\bar{\dot{Q}}_{lK-1} - \bar{\dot{Q}}_{lK} - \bar{\dot{Q}}_{l,w,K}\right]\left(\frac{\Delta\tau}{\bar{m}_{lK}}\right) \\ &+ \left[\frac{\rho_{lK}{}^{\langle \tau+\Delta\tau \rangle} - \rho_{lK}{}^{\langle \tau \rangle}}{2\bar{m}_{lK}}\right]\left[\left(\frac{P_{lK}}{\rho_{lK}}\right)^{\langle \tau+\Delta\tau \rangle}\left(\frac{m_{lK}}{\rho_{lK}}\right)^{\langle \tau \rangle} + \left(\frac{P_{lK}}{\rho_{lK}}\right)^{\langle \tau \rangle}\left(\frac{m_{lK}}{\rho_{lK}}\right)^{\langle \tau+\Delta\tau \rangle}\right] \end{aligned} \tag{3-15}$$

In Equation (3-15), $\bar{\dot{Q}}_{lK-1}$, $\bar{\dot{Q}}_{lK}$, and $\bar{\dot{Q}}_{l,w,K}$ are respectively $\dot{Q}_{lK-1}$, $\dot{Q}_{lK}$, and $\dot{Q}_{l,w,K}$ evaluated at time $\tau+\Delta\tau/2$. The average mass of propellant in the segment between time τ and time $\tau+\Delta\tau$ is

$$\bar{m}_{lK} = \left(\tfrac{1}{2}\right)\left(m_{lK}{}^{\langle \tau+\Delta\tau \rangle} + m_{lK}{}^{\langle \tau \rangle}\right) \tag{3-16}$$

For the case where K<K_{max}, $\dot{m}_l = 0$ and Equation (3-15) reduces to

$$u_{lK}{}^{\langle \tau+\Delta\tau \rangle} = u_{lK}{}^{\langle \tau \rangle} + \left[\bar{\dot{Q}}_{lK-1} - \bar{\dot{Q}}_{lK} - \bar{\dot{Q}}_{l,w,K}\right]\left(\frac{\Delta\tau}{m_{lK}{}^{\langle \tau \rangle}}\right) - \bar{P}_{lK}\left[\left(\frac{1}{\rho_{lK}{}^{\langle \tau+\Delta\tau \rangle}}\right) - \left(\frac{1}{\rho_{lK}{}^{\langle \tau \rangle}}\right)\right] \tag{3-17}$$

where:

$$\bar{P}_{lK} = \left(\tfrac{1}{2}\right)\left(P_{lK}{}^{\langle \tau+\Delta\tau \rangle} + P_{lK}{}^{\langle \tau \rangle}\right) \tag{3-18}$$

Fluid and Tank Wall Properties

Many computations in the model compute and utilize thermodynamic and transport properties of fluids for the ullage gas and the cryogenic propellant. Additionally, the tank wall heat transfer and capacity properties are treated as temperature dependent in the model.

The REFPROP 23 fluid properties database, Lemmon, et al. (2007), is a FORTRAN based suite of programs that computes fluid properties for a large number of pure (single species) fluids and a number of fluids comprised of a predefined mixture of multiple species (air and a large number of refrigerants). This program suite is able to compute properties of para-hydrogen, normal-hydrogen, nitrogen, oxygen, methane and many other gases and propellants typically used in propellant run tanks covered under this study. It has also been verified to provide accurate properties data for all of the thermodynamic and transport properties used by the model developed under this study and for all pressure and temperature regimes that would occur in the run tanks being analyzed.

The set of REFPROP 23 programs are compiled into a FORTRAN library workspace that is used interactively by the model throughout its execution. In general, each call of the fluid properties library by the model includes the entry/transfer of two known (or latest iteration values of) properties entered as inputs followed by the routine returning other properties needed and used by the model. In virtually all library calls, the input properties are pressure and either (specific) enthalpy or internal energy.

For the tank-wall material, the specific heat and thermal conductivity are treated as temperature dependent. The material density is set to a constant value for the material.

Thermal diffusivity is calculated as needed by the model. To determine the specific heat and thermal conductivity for each tank-wall material as a function of temperature, a metallic materials properties subroutine with a series of polynomial curve-fit equations was developed for the program. Data from Touloukan, et al. (1970) and Touloukan & Buyco (1970) were utilized to generate the curve-fits. For each tank wall material, plots of specific heat and thermal conductivity versus temperature were evaluated to assure that the curve-fit equations produced continuous and smooth curves with no sudden or abrupt property changes with respect to temperature and less than 0.2% error.

Properties of Binary Gas Mixtures for Ullage Gas Segments

For cases when the initial ullage volume in the tank is not zero, the program sets the initial ullage gas species to be that of the propellant. The lowermost ullage gas segment (J=1) is taken to be a saturated vapor at a pressure equal to the initial propellant pressure at the bottom main discharge nozzle of the tank minus the hydrostatic pressure of the propellant, initially a liquid where the top propellant segment is saturated liquid. For these cases and when the pressurant gas is a different species from that of the cryogenic propellant, such as normal-hydrogen pressurant gas with liquid (or cold supercritical) para-hydrogen propellant or nitrogen pressurant gas with liquid oxygen propellant, the ullage gas segments will be a mixture of two different gas species. For higher pressures, well above critical pressures of the propellant, the mass fraction of the propellant species will be small and could be considered negligible in most cases. However, the model requires that the initial tank pressure be less than half of the critical pressure of the propellant species. The model is also designed to limit the incremental

increase in tank pressure between subsequent time steps, such that the tank pressures could be subcritical for a significant length of time. Additionally, the model is designed to simulate run tank expulsions at subcritical pressures through all time steps.

The fluid property effects of propellant species mixed with the pressurant gas species in each ullage gas segment must be taken into account.

The expression used to determine density of a gas mixture in ullage gas segment J is as follows

$$\rho_J = \left[\frac{\hat{m}_{J,a}}{\rho_{J,a}} + \frac{\hat{m}_{J,b}}{\rho_{J,b}} \right]^{-1} \tag{3-19}$$

where:

$$\hat{m}_{J,a} = \frac{m_{J,a}}{m_{J,a} + m_{J,b}} \tag{3-20}$$

$$\hat{m}_{J,b} = \frac{m_{J,b}}{m_{J,a} + m_{J,b}} \tag{3-21}$$

Subscripts J,a and J,b in Equations (3-19) through (3-21) represent gas species a and b respectively in ullage gas segment J (generally, variable 'a' represents the propellant and variable 'b' represents the pressurant gas).

Since $\hat{m}_{J,b} = 1 - \hat{m}_{J,a}$, ρ_J then becomes

$$\rho_J = \left[\frac{\hat{m}_{J,a}}{\rho_{J,a}} + \frac{\left(1 - \hat{m}_{J,a}\right)}{\rho_{J,b}} \right]^{-1} \tag{3-22}$$

The expressions for specific heats, internal energy, enthalpy, viscosity, and thermal conductivity are given in Equations (3-23) through (3-28) below.

$$c_{v_J} = \hat{m}_{J,a} c_{v_{J,a}} + \left(1 - \hat{m}_{J,a}\right) c_{v_{J,b}} \tag{3-23}$$

$$c_{p_J} = \hat{m}_{J,a} c_{p_{J,a}} + \left(1 - \hat{m}_{J,a}\right) c_{p_{J,b}} \tag{3-24}$$

$$u_J = \hat{m}_{J,a} u_{J,a} + \left(1 - \hat{m}_{J,a}\right) u_{J,b} \tag{3-25}$$

$$i_J = \hat{m}_{J,a} i_{J,a} + \left(1 - \hat{m}_{J,a}\right) i_{J,b} \tag{3-26}$$

$$\mu_J = \left[\frac{\hat{m}_{J,a} \mu_{J,a}}{\rho_{J,a}} + \frac{\left(1 - \hat{m}_{J,a}\right) \mu_{J,b}}{\rho_{J,b}} \right] \rho_J \tag{3-27}$$

$$k_J = \left[\frac{\hat{m}_{J,a} k_{J,a}}{\rho_{J,a}} + \frac{\left(1 - \hat{m}_{J,a}\right) k_{J,b}}{\rho_{J,b}} \right] \rho_J \tag{3-28}$$

Ullage-Gas-to-Tank-Wall Heat Transfer

Referring to Figure 3.3, the rate of heat transfer from the fluid to the inner tank wall surface for each ullage gas segment J is calculated as

$$\dot{Q}_{w,J} = h_{w,J} A_{w,J} \left(\overline{T}_J - T_{w,J} \right) \tag{3-29}$$

The overall convective heat transfer coefficient is calculated using a correlation based on the one provided in Nein and Thompson (1966) where the convective heat transfer coefficient is the sum of the free convective heat transfer coefficient and the product of the maximum possible forced convective heat transfer coefficient and an exponential decay parameter. This correlation is

$$h_{w,J} = h_{c,J} + h_{o,J} e^{-\beta_w z_w} \tag{3-30}$$

The natural (free) convective heat transfer coefficient is computed using correlations depending on the incline angle of the tank wall at the top-, middle-, and bottom-elevation location of ullage gas segment J

$$h_{c,J} = \begin{cases} \left(Nu_{L_{4,Top}} + 4Nu_{L_{4,Mid}} + Nu_{L_{4,Btm}} \right) \left(\dfrac{k_J}{L_{4,Top} + 4L_{4,Mid} + L_{4,Btm}} \right) & \text{if } \theta_J < 60^o \\ c_1 k_J \left(\overline{Ra_{L_4}}^* \right) \left(\bar{L}_4 \right)^{3c_4 - 1} & \text{if } \theta_J \geq 60^o \end{cases} \quad (3\text{-}31)$$

For cases where an ullage gas segment spans across a boundary where the incline angle is 60^o, the overall free convective coefficient is based on a weighted average of both correlations in Equation (3-31) where each is weighted by the heat transfer wall area above or below this boundary, whichever applies.

Where θ_J, the incline angle of the tank wall, is less than 60^o from vertical (where $\theta_J = 0^o$ is a vertical wall), the expression in Equation (3-31) employs a principle applied in Simpson's rule for numerical integration, Wylie and Barrett (1982), where the midpoint between upper and lower limits is given a heavier weighting than the end-points. Each Nusselt number used in Equation (3-31) for an evaluated ullage gas segment, or portion of the evaluated segment, where the wall incline angle is less than 60^o, is computed using the following correlations based on those from Churchill and Chu (1975) as reported by Mills (1992) and Hodge and Koenig (1992)

$$Nu_{L_4} = \begin{cases} 0.68 + 0.67 \left(Ra_{L_4} \psi \right)^{1/4} & \text{if } \mathrm{Ra}_{L_4} < 9 \times 10^8 \\ 0.68 + \left[0.67 \left(Ra_{L_4} \psi \right)^{1/4} \right] \left[1 + \left(1.6 \times 10^{-8} \right) Ra_{L_4} \psi \right] & \\ & \text{if } 9 \times 10^8 \leq Ra_{L_4} \leq 10^{12} \end{cases} \quad (3\text{-}32)$$

where:

$$Ra_{L_4} = \frac{c_{7a} c_{p_J} g_c \rho_J^{\,2} \left| \overline{T}_J - T_{w,J} \right| L_4^{\,3}}{\overline{T}_J \mu_J k_J} \tag{3-33}$$

$$\psi = \left[1 + \left(\frac{0.492}{\mathrm{Pr}_J} \right)^{9/16} \right]^{16/9} \tag{3-34}$$

$$c_{7a} = \cos\left(\theta_J\right) \tag{3-35}$$

The correlation presented in Equation (3-31) for the case where the incline angle of the tank-wall is equal to or greater than 60^o from vertical is based on natural convection heat transfer correlations for fluids in contact with horizontal flat plats in Incropera and DeWitt (1996). The modified Rayleigh number used in Equation (3-31) is computed using

$$\overline{Ra_{L_4}^{\,*}} = \left(1/6\right)\left(Ra_{L_{4,Top}} + 4 Ra_{L_{4,Mid}} + Ra_{L_{4,Btm}} \right) \tag{3-36}$$

where:

$$Ra_{L_4}^{\,*} = \frac{c_{7b} c_{p_J} g_c \rho_J^{\,2} \left| \overline{T}_J - T_{w,J} \right|}{\overline{T}_J \mu_J k_J} \tag{3-37}$$

$$c_{7b} = \sin\left(\theta_J\right) \tag{3-38}$$

In Equation (3-31) the characteristic length is defined as

$$\overline{L}_4 = \frac{r_{60}}{2} \tag{3-39}$$

In Equation (3-31), the values of variables 'c_1' and 'c_4' are based on horizontal flat plat natural convection correlations in Incropera and DeWitt (1996) and are set as presented in Equations (3-40) and (3-41).

$$c_1 = \begin{cases} 0.54 \text{ upper closure in tank with } \left(\mathrm{Ra}_{L_4}^{*}\right)\left(\bar{L}_4\right)^3 < 1.084\times10^7 \\ 0.14 \text{ upper closure in tank with } \left(\mathrm{Ra}_{L_4}^{*}\right)\left(\bar{L}_4\right)^3 \geq 1.084\times10^7 \\ 0.13 \text{ lower closure in tank with } \left(\mathrm{Ra}_{L_4}^{*}\right)\left(\bar{L}_4\right)^3 < 6442 \\ 0.27 \text{ lower closure in tank with } \left(\mathrm{Ra}_{L_4}^{*}\right)\left(\bar{L}_4\right)^3 \geq 6442 \end{cases} \tag{3-40}$$

$$c_4 = \begin{cases} 0.25 \text{ upper closure in tank with } \left(\mathrm{Ra}_{L_4}^{*}\right)\left(\bar{L}_4\right)^3 < 1.084\times10^7 \\ 0.33 \text{ upper closure in tank with } \left(\mathrm{Ra}_{L_4}^{*}\right)\left(\bar{L}_4\right)^3 \geq 1.084\times10^7 \\ 0.33 \text{ lower closure in tank with } \left(\mathrm{Ra}_{L_4}^{*}\right)\left(\bar{L}_4\right)^3 < 6442 \\ 0.25 \text{ lower closure in tank with } \left(\mathrm{Ra}_{L_4}^{*}\right)\left(\bar{L}_4\right)^3 \geq 6442 \end{cases} \tag{3-41}$$

In Equations (3-40) and (3-41) the threshold values of 1.084×10^7 and 6442 for $\left(\mathrm{Ra}_{L_4}^{*}\right)\left(\bar{L}_4\right)^3$ are to provide continuity in Equation (3-31) across the range of modified Rayleigh numbers.

The forced convective heat transfer coefficient used in Equation (3-30) is from Nein and Thompson (1966) and is calculated using

$$h_{o,J} = \left(\frac{b_1 k_J}{r_z}\right)\left(\frac{r_z \dot{m}_{PG}}{A_d \mu_J}\right)^{b_2} \left(\mathrm{Pr}_J\right)^{b_3} \tag{3-42}$$

where: b_1= 0.54 increased from 0.06 in Nein & Thompson (1966)

b_2=0.8

b_3=0.33

The rationale for increasing the value of variable b_1 from 0.06 to 0.54 in Equation (3-42) is described in Chapter V. In this equation, the parameter, r_z, is the horizontal radial distance from the tank centerline to the tank wall at the mid-elevation of ullage gas

segment J if above the tank mid-elevation or equator. Otherwise, this parameter is equal to the maximum inside radius of the tank.

The forced convective heat transfer exponential decay parameter, β_w, in Equation (3-30) is defined from the following:

$$\beta_w = \min\left(\beta_{w,a}, \beta_{w,\max}\right) \tag{3-43}$$

where:

$$\beta_{w,a} = \left(0.0137 + 0.00808 z_w\right)\left(r_z - r_a\right)^2 \tag{3-44}$$

$$\beta_{w,\max} = 0.00117\left(r_z - r_a\right)^2 - \left(\frac{1}{z_w}\right)\ln\left|\frac{0.06}{4b_1}\right| \tag{3-45}$$

$z_w \equiv$ Vertical distance from tank wall location being evaluated to closest point of pressurant gas entry into ullage

$r_a \equiv$ Radius of standard pressurant gas inlet diffuser

For reasons presented in Chapter V, the correlations in Equations (3-43) through (3-45) to compute β_w replace the following correlation from Nein and Thompson (1966)

$$\beta_w = 0.00117 r_z^{\,2} \tag{3-46}$$

Ullage-Gas-to-Cryogenic-Propellant Interface Heat Transfer

Referring to Figure 3.3, the rate of heat transfer at the bottom of the lowermost ullage gas segment boundary is assigned the variable $\dot{Q}_{J-1}$ at J=1 and this rate of heat transfer is computed as

$$\dot{Q}_{Je0} = h_s A_s \left(\overline{T}_J - T_{Je0}\right) \tag{3-47}$$

The total convective heat transfer coefficient h_s in Equation (3-47), obtained from Nein and Thompson (1966), is defined as

$$h_s = h_{sc} + h_{so} e^{-\beta_s z_i} \tag{3-48}$$

The natural (free) convective heat transfer coefficient h_{sc} in Equation (3-48), also obtained from Nein and Thompson (1966), is calculated as

$$h_{sc} = c_1 k_J \left[\frac{g_c c_7 c_{p_J} \rho_J{}^2 \left| \bar{T}_J - T_{Je0} \right|}{\bar{T}_J \mu_J k_J} \right]^{c_4} \tag{3-49}$$

where: $c_1 = 0.13$

$c_4 = 0.33$

$c_7 = 1.00$

From the same reference, the forced convective heat transfer coefficient in Equation (3-48) is given by

$$h_{so} = \left(\frac{d_1 k_J}{r_i} \right) \left(\frac{r_i \dot{m}_{PG}}{A_d \mu_J} \right)^{d_2} \left(\mathrm{Pr}_J \right)^{d_3} \tag{3-50}$$

where: $d_1 = 0.06$

$d_2 = 0.8$

$d_3 = 0.33$

In Equation (3-50), the variable r_i is the horizontal radial distance from the tank centerline to the tank wall adjacent to the interface if this interface is above the tank mid-elevation or equator. If this interface is below the tank mid-elevation or equator, r_i is the maximum inside radius of the tank.

The forced convective heat transfer exponential decay parameter, β_s, in Equation (3-48) is defined as

$$\beta_s = \min\left(\beta_{s,a}, \beta_{s,\max}\right) \tag{3-51}$$

where:

$$\beta_{s,a} = \left(0.00117 + 0.0921034 z_i\right) r_i^2 \tag{3-52}$$

$$\beta_{s,\max} = 0.00117 r_i^2 - \left(\frac{1}{z_i}\right) \ln\left|\frac{0.06}{10 b_1}\right| \tag{3-53}$$

In Equations (3-48) and (3-52), the parameter z_i is the vertical distance from the propellant-to-ullage-gas interface to the closest point of pressurant gas entry into the tank ullage.

The above correlations in Equations (3-51) through (3-53) to compute β_s replace the correlation from Nein & Thompson (1966), which is the same as that given by Equation (3-46) except that the variable r_i replaces the variable r_z. The rationale for replacing the correlation from Nein and Thompson (1966) is presented in Chapter V.

Computation of T_{Je0}, temperature at the cryogenic-propellant-to-ullage-gas interface, used in Equations (3-49) and (3-51), is computed from

$$T_{Je0} = \begin{cases} T_{l,Sat} \quad \text{if } P_J \le P_{Crit} \quad @\ \text{J=1} \\ \dfrac{h_s T_J + h_{la} T_{lK}}{h_s + h_{la}} \quad @\ \text{J=1, K=1, if } P_J > P_{Crit} \text{ and } \mathrm{K_{max}} > 1 \\ \max\left(T_{Crit}, \overline{T}_{lK}\right) \quad \text{if } P_J > P_{Crit} \text{ and } \mathrm{K_{max}} = 1 \end{cases} \tag{3-54}$$

The variable $T_{l,Sat}$ in Equation (3-54) is the saturation temperature of the propellant at pressure P_J.

Cryogenic-Propellant-to-Tank-Wall Heat Transfer

Referring to Figures 3.4 and 3.5, the rate of heat transfer from the cryogenic propellant to the tank wall is determined from

$$\dot{Q}_{l,w,K} = h_{l,w,K} A_{l,w,K} \left(\overline{T}_{lK} - T_{l,w,K} \right) \tag{3-55}$$

In Equation (3-55) the convective heat transfer coefficient is based on all free convection between the propellant and the tank wall. This coefficient is computed with the following correlation:

$$h_{l,w,K} = \begin{cases} \left(Nu_{L_{Top}} + 4Nu_{L_{Mid}} + Nu_{L_{Btm}} \right) \left(\dfrac{k_{lK}}{L_{Top} + 4L_{Mid} + L_{Btm}} \right) & \text{if } \theta_{lK} < 60^o \\ c_1 k_{lK} \left(\overline{Ra_L^*} \right) \left(\overline{L} \right)^{3c_4 - 1} & \text{if } \theta_{lK} \geq 60^o \end{cases} \tag{3-56}$$

The restrictions applied to Equation (3-31) also apply to Equation (3-56) for cases where the propellant segment spans across a boundary where the wall incline angle equals 60^o.

For the case where the wall incline angle is less than 60^o from vertical, $\theta_{lK} < 60^o$, the following correlation for each Nusselt number, that is used in Equation (3-56), applies

$$Nu_L = \begin{cases} 0.68 + 0.67 \left(Ra_L \psi \right)^{1/4} & \text{if } \mathrm{Ra}_L < 9 \times 10^8 \\ 0.68 + \left[0.67 \left(Ra_L \psi \right)^{1/4} \right] \left[1 + \left(1.6 \times 10^{-8} \right) Ra_L \psi \right] & \\ \qquad \text{if } 1.1 \times 10^9 \leq Ra_L \leq 10^{12} & \\ Nu_{L,a} + \left(Nu_{L,b} - Nu_{L,a} \right) \left(\dfrac{Ra_L - 9 \times 10^8}{2 \times 10^8} \right) & \\ \qquad \text{if } 9 \times 10^8 \leq Ra_L \leq 1.1 \times 10^9 & \end{cases} \tag{3-57}$$

where:

$$Ra_L = \frac{c_{7a}\beta_{lK}c_{p_{lK}}g_c\rho_{lK}{}^2\left|\overline{T}_{lK} - T_{l,w,K}\right|L^3}{\mu_{lK}k_{lK}} \tag{3-58}$$

$\beta_{lK} \equiv$ Compression bulk modulus of propellant in segment K

$$\psi = \left[1+\left(\frac{0.492}{\mathrm{Pr}_{lK}}\right)^{9/16}\right]^{16/9} \tag{3-59}$$

$$c_{7a} = \cos\left(\theta_{lK}\right) \tag{3-60}$$

The correlation in Equation (3-57) for the case where the Rayleigh number, Ra_L, is between 9×10^8 and 1.1×10^9 is included to provide a continuous function.

For the case when the wall incline angle is greater than 60^o from vertical, the mean modified Rayleigh number used in Equation (3-56) is defined as

$$\overline{Ra_L{}^*} = \left(1/6\right)\left(Ra_{L_{Top}}{}^* + 4Ra_{L_{Mid}}{}^* + Ra_{L_{Btm}}{}^*\right) \tag{3-61}$$

The first, second, and third modified Rayleigh number terms on the right hand side of Equation (3-61) represent, respectively, the modified Rayleigh numbers for the top, middle, and bottom elevations of the propellant segment being evaluated. For each elevation, the modified Rayleigh number is determined from

$$Ra_L{}^* = \frac{c_{7b}\beta_{lK}c_{p_{lK}}g_c\rho_{lK}{}^2\left|\overline{T}_{lK} - T_{l,w,K}\right|}{\mu_{lK}k_{lK}} \tag{3-62}$$

where:

$$c_{7b} = \sin\left(\theta_{lK}\right) \tag{3-63}$$

Variables $\bar{L}$, c_1, and c_4 used in Equation (3-56) are set to values from Equations (3-39) through (3-41).

Ullage Gas Segment-to-Segment Heat Transfer

Referring to Figure 3.3, the rate of heat transfer at the upper and lower boundaries of each ullage gas segment adjacent to another fluid segment is computed by the following two expressions respectively

$$\dot{Q}_J = \left[\left(\frac{k^*}{\Delta z}\right)_{J,J+1}\right] A_J \left(\bar{T}_{J+1} - \bar{T}_J\right) \tag{3-64}$$

$$\dot{Q}_{J-1} = \begin{cases} \left[\left(\frac{k^*}{\Delta z}\right)_{J-1,J}\right] A_{J-1}\left(\bar{T}_J - \bar{T}_{J-1}\right) & \text{if } J > 1 \\ \dot{Q}_{Je0} \quad \text{from Equation (3-44) if } J = 1 \end{cases} \tag{3-65}$$

For the upper and lower boundaries of each ullage gas segment, the total equivalent heat transfer coefficients used in Equation (3-70) and (3-71) above are computed from the following two expressions acquired from Rocketdyne Report R-3936-1 (1963):

$$\left(\frac{k^*}{\Delta z}\right)_{J,J+1} = \frac{2\left(\bar{z}_{J-1} - \bar{z}_J\right)k_J + 2\left(\bar{z}_J - \bar{z}_{J+1}\right)k_{J+1}}{\left(\bar{z}_{J-1} - \bar{z}_{J+1}\right)^2} + EK_{gJ} \tag{3-66}$$

$$\left(\frac{k^*}{\Delta z}\right)_{J-1,J} = \frac{2\left(\bar{z}_{J-2} - \bar{z}_{J-1}\right)k_{J-1} + 2\left(\bar{z}_{J-1} - \bar{z}_J\right)k_J}{\left(\bar{z}_{J-2} - \bar{z}_J\right)^2} + EK_{gJ-1} \tag{3-67}$$

The last terms on the right-hand sides of Equations (3-66) and (3-67) represent an equivalent forced convective heat transfer coefficient between ullage gas segments. These are computed using

$$EK_{gJ} = h_{so,J} e^{-\beta_{s,J} z_J} \tag{3-68}$$

$$EK_{gJ-1} = h_{so,J-1} e^{-\beta_{s,J-1} z_{J-1}} \tag{3-69}$$

In Nein and Thompson (1966) and in Rocketdyne Report R-3936-1 (1963), EK_{gJ} and EK_{gJ-1} are zero.

Parameters $h_{so,J}$ and $h_{so,J-1}$ in Equations (3-68) and (3-69) are calculated using Equation (3-50) with r_{z_J} substituted for r_i when computing $h_{so,J}$ and $r_{z_{J-1}}$ substituted for r_i when computing $h_{so,J-1}$. Parameter r_{z_J} is the horizontal radial distance from the tank centerline to the tank wall adjacent to the mid-elevation of ullage gas segment J if this location is above the tank mid-elevation or equator. Otherwise, this parameter is the maximum inside radius of the tank. Similarly, $r_{z_{J-1}}$ is the horizontal radial distance from the tank centerline to the tank wall adjacent to the mid-elevation of ullage gas segment J-1 if this location is above the tank mid-elevation or equator. Otherwise, this parameter is the maximum inside radius of the tank.

Parameters $\beta_{s,J}$ and $\beta_{s,J-1}$, the exponential decay coefficients, in Equations (3-68) and (3-69) are computed using Equations (3-51) through (3-53), but r_{z_J} and z_J are substituted for r_i and z_i, respectively, when computing $\beta_{s,J}$ and $r_{z_{J-1}}$ and z_{J-1} are

substituted for r_i and z_i, respectively, when computing $\beta_{s,J-1}$. Parameters z_J and z_{J-1} are defined in Figure 3.3.

Cryogenic Propellant Segment-to-Segment Heat Transfer

Referring to Figures 3.4 and 3.5, the rate of heat transfer at the upper and lower boundaries of each cryogenic propellant segment that is adjacent to another fluid segment is computed by the following two equations respectively

$$\dot{Q}_{lK-1} = \begin{cases} \left[\left(\frac{k^*}{\Delta z}\right)_{K-1,K}\right] A_{K-1}\left(\overline{T}_{lK-1} - \overline{T}_{lK}\right) & \text{if } K > 1 \\ \dot{Q}_{Je0} \text{ from Equation (3-48)} & \text{if } K = 1 \end{cases} \tag{3-70}$$

$$\dot{Q}_{lK} = \left[\left(\frac{k^*}{\Delta z}\right)_{K,K+1}\right] A_K\left(\overline{T}_{lK} - \overline{T}_{lK+1}\right) \tag{3-71}$$

For the upper boundary of each propellant segment, the total equivalent heat transfer coefficient used in Equation (3-70) is computed from the following expression

$$\left(\frac{k^*}{\Delta z}\right)_{K-1,K} = \begin{cases} \dfrac{h_s h_{la}}{h_s + h_{la}} & \text{if } K = 1 \text{ and } P_{lK} \geq P_{Crit} \\ \dfrac{k_{l,Sat} + k_{lK}}{2\left(\overline{z}_{lK} - z_{Je0}\right)} & \text{if } K = 1 \text{ and } P_{lK} < P_{Crit} \\ \dfrac{2\left(\overline{z}_{lK-1} - \overline{z}_{lK-2}\right)k_{lK-1} + 2\left(\overline{z}_{lK} - \overline{z}_{lK-1}\right)k_{lK}}{\left(\overline{z}_{lK} - \overline{z}_{lK-2}\right)^2} & \text{if } K > 1 \end{cases} \tag{3-72}$$

In Equation (3-72), the parameter h_s is the convection heat transfer coefficient used in Equation (3-47) and computed using Equation (3-48). Parameter h_{la} is computed from the following equation

$$h_{la} = \frac{k_{lK}}{\overline{z}_{lK} - z_{Je0}} \quad @ \text{ K=1} \tag{3-73}$$

For the lower boundary of each propellant segment that is adjacent to another propellant segment, the total equivalent heat transfer coefficient used in Equation (3-71) is computed from the following expression

$$\left(\frac{k^*}{\Delta z}\right)_{K,K+1} = \frac{2\left(\overline{z}_{lK} - \overline{z}_{lK-1}\right)k_{lK} + 2\left(\overline{z}_{lK+1} - \overline{z}_{lK}\right)k_{lK+1}}{\left(\overline{z}_{lK+1} - \overline{z}_{lK-1}\right)^2} \tag{3-74}$$

Equation (3-74) and the applied case of K greater than one in Equation (3-72) are obtained from Rocketdyne Report R-3936-1 (1963).

Mass Transfer Across Ullage-Gas-to-Cryogenic-Propellant Interface

Information in Chapter II provides data that supports the findings that mass transfer across the ullage-gas-to-cryogenic-propellant interface can be neglected for cases where tank diffuser designs and operating conditions prevent disturbances and forced mixing of fluids across this interface. When operating conditions could result in some level of forced mixing between ullage gas and propellant, the modified forced convection heat transfer correlations presented in this chapter and further explained and justified in Chapter V provide sufficient modeling of the effects of this mass transfer.

Also when considering cases of cryogenic propellant tanks at supercritical or high subcritical pressures, the free diffusion component of mass transfer of propellant species into and within the ullage gas region containing a different pressurant gas species is expected to be significantly less than cases for low subcritical pressures. An approximate correlation from Handbook of Compressed Gases, 3rd Ed. (1990) shows that the mass diffusion coefficient, 'D,' is inversely proportional to pressure. This correlation is as follows:

$$D = D_0 \left(\frac{T}{T_0} \right)^{1.5} \left(\frac{P_0}{P} \right) \tag{3-75}$$

The reference temperature, P_0, is typically 14.7 psia while the reference temperature is typically in the range of 525 R to 540 R (Approximately 65 F to 80 F). With supercritical and high subcritical tank pressures ranging from 400 to 8500-psia and with ullage gas temperatures near or below reference temperatures, the mass diffusion coefficient will have much smaller values than at low subcritical pressures. The rate of mass diffusion of one gas species within a two-component (binary) gas mixture is roughly proportional to this mass diffusion coefficient.

Given the above, neglecting mass transfer from the propellant to ullage gas region and vice-versa does not significantly degrade accuracy of analytically-computed pressurant gas requirements and associated collapse factor results at the higher tank pressures.

Mass Transfer Within Ullage Gas Region

For mass transfer of propellant species within the ullage gas region, the model is based on a uniform distribution of this species throughout the region. The total mass of propellant species in this region remains unchanged and is equal to the initial mass of ullage gas prior to entry of pressurant gas. For supercritical and high subcritical tank pressures the mass fraction of propellant becomes very small and could be considered negligible.

Transient Tank Wall Heat Conduction

While the data from prior studies strongly support the validity of the assumption that there are negligible or at least relatively small temperature gradients through the tank wall thicknesses, the test tanks used in these studies all have wall thicknesses less than ½-inch thick, and often ¼-inch to 1/8-inch thick. Therefore, this assumption may be invalid for high subcritical and supercritical tank pressure conditions where the tank wall thicknesses can range from 2-inches to 15.5-inches. While application of the assumption of uniform temperature through the tank wall would almost certainly result in errors on the conservative side (where predicted pressurant gas requirements are higher than actual requirements) this may not be beneficial as one of the major objectives of this study is to predict these requirements accurately without excessive conservatism.

The model therefore incorporates an explicit numerical finite-difference analytical method based on that presented in Incropera and DeWitt (1996) to simulate transient and spatially non-uniform temperatures through the thickness of the tank wall.

Figure 3.6 is a diagram showing the segments through the thickness of a section the tank wall and how the boundaries of these segments are defined. It also illustrates the conduction heat transfer across the boundaries at wall segment m, the heat transfer area at each boundary, and the total volume of this segment.

Figure 3.6 also shows increasing wall segment thickness when traversing from the inner to outer segment. This is done to allow for a reduced number of segments in order to decrease the computation time and the number of repeated computations in the model while providing thinner segments near the inner wall where the temperature gradients are much higher than those in the outer segments, especially during the initial times when a cold wall is being heated rapidly due to rapid increases in ullage gas temperature.

Wall Segment-to-Segment

For the case where a wall segment m is bounded on all sides by other wall segments, as is the case in Figure 3.6, the following energy balance applies

$$\rho_w V_{w,m} c_{w,m} \left(\frac{dT_{w,m}}{d\tau} \right) = k_{w,m} A_{w,m} \left(\frac{dT_{w,m}}{dr_m} \right) + k_{w,m} A_{w,m+1} \left(\frac{dT_{w,m+1}}{dr_{m+1}} \right) \tag{3-76}$$

Referring to Figure 3.6, the heat transfer area of the inner and outer boundaries of wall segment m are given, respectively, by Equations (3-77) and (3-78) for the case where the

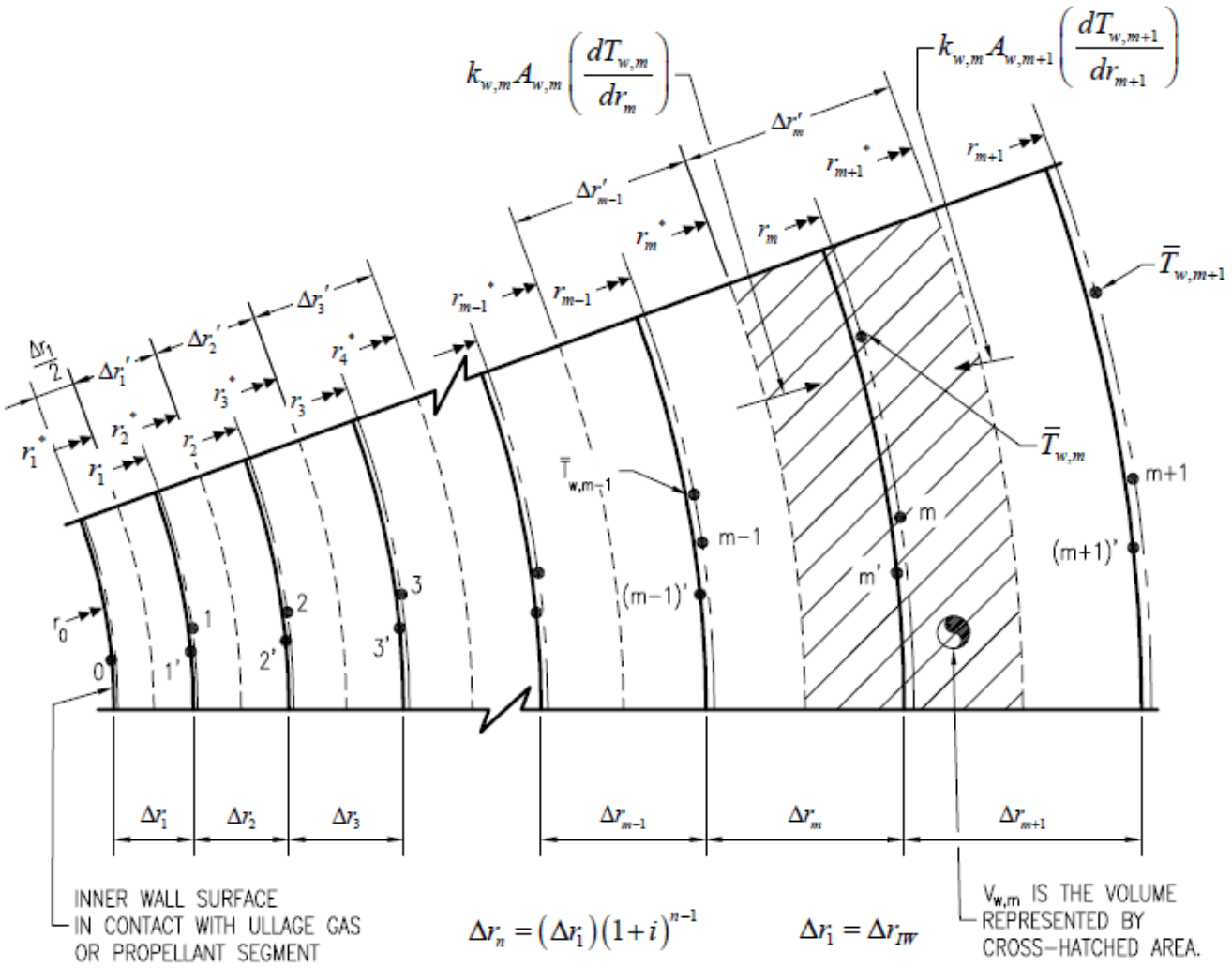

Figure 3.6 Schematic Diagram of Tank Wall Segments for Numerical Finite-Difference Modeling

inner wall of the innermost wall segment covers the full inside wall surface of a spherical tank or the full inside surface of a cylindrical vessel shell of length w.

$$A_{w,m} = \begin{cases} 2\pi\left(r_m^*\right)w & \text{for full cylindrical wall section} \\ 4\pi\left(r_m^*\right)^2 & \text{for full spherical wall section} \end{cases} \tag{3-77}$$

$$A_{w,m+1} = \begin{cases} 2\pi\left(r_{m+1}^*\right)w & \text{for full cylindrical wall section} \\ 4\pi\left(r_{m+1}^*\right)^2 & \text{for full spherical wall section} \end{cases} \tag{3-78}$$

The total volume of segment m for the case described above is given by

$$V_{w,m} = \begin{cases} \pi\left[\left(r_{m+1}^*\right)^2 - \left(r_m^*\right)^2\right]w & \text{for full cylindrical wall section} \\ \dfrac{4\pi}{3}\left[\left(r_{m+1}^*\right)^3 - \left(r_m^*\right)^3\right] & \text{for full spherical wall section} \end{cases} \tag{3-79}$$

Referring to Figure 3.6, the reference radial distance of the inner boundary of wall segment m is determined from

$$r_m^* = r_0 + \left(\Delta r_1\right)\left[\sum_{j=1}^{m}\left(1+i\right)^{j-1}\right] - \left(\frac{\Delta r_1}{2}\right)\left(1+i\right)^{m-1} \tag{3-80}$$

The reference radial distance of the mid-span distance between the inner and outer boundaries of wall segment m is determined from

$$r_m = r_0 + \left(\frac{\Delta r_1}{2}\right)\left\{1 + \left[\sum_{j=1}^{m}\left[\left(1+i\right)^{j-1} + \left(1+i\right)^{j}\right]\right] - \left(\frac{1}{2}\right)\left[\left(1+i\right)^{m-1} + \left(1+i\right)^{m}\right]\right\} \tag{3-81}$$

In Equations (3-80) and (3-81), the parameter i is the incremental percentage increase in thickness between adjacent wall segments divided by 100 when traversing from the inner to outer wall. This parameter is selected by the program user, but the model input module checks that this input provides proper wall segment thicknesses and number of segments through the total thickness of the tank wall.

The change in wall temperature with respect to radial distance through the tank wall thickness at the inner and outer boundaries of wall segment m are approximated by Equations (3-82) and (3-83) which are

$$\frac{dT_{w,m}}{dr_m} \cong \frac{\overline{T}_{w,m-1} - \overline{T}_{w,m}}{r_m - r_{m-1}} \tag{3-82}$$

$$\frac{dT_{w,m+1}}{dr_{m+1}} \cong \frac{\overline{T}_{w,m+1} - \overline{T}_{w,m}}{r_{m+1} - r_m} \tag{3-83}$$

The rate of increase in temperature in wall segment m is

$$\frac{dT_{w,m}}{d\tau} \cong \frac{T_{w,m}^{\langle \tau + \Delta\tau_n \rangle} - T_{w,m}^{\langle \tau \rangle}}{\Delta\tau_n} \tag{3-84}$$

In order to eliminate the need to track and carry the cylindrical length w in Equations (3-77) through (3-79) and to demonstrate that this term has no effect on computation results, the parameters A_m, A_{m+1}, and V_m can be expressed as the following area-to-volume ratios

$$\frac{A_{w,m}}{V_{w,m}} = \begin{cases} \dfrac{2\left(r_m^*\right)}{\left(r_{m+1}^*\right)^2 - \left(r_m^*\right)^2} & \text{for cylindrical wall section} \\ \dfrac{3\left(r_m^*\right)^2}{\left(r_{m+1}^*\right)^3 - \left(r_m^*\right)^3} & \text{for spherical wall section} \end{cases} \tag{3-85}$$

$$\frac{A_{w,m+1}}{V_{w,m}} = \begin{cases} \dfrac{2\left(r_{m+1}^*\right)}{\left(r_{m+1}^*\right)^2 - \left(r_m^*\right)^2} & \text{for cylindrical wall section} \\ \dfrac{3\left(r_{m+1}^*\right)^2}{\left(r_{m+1}^*\right)^3 - \left(r_m^*\right)^3} & \text{for spherical wall section} \end{cases} \tag{3-86}$$

Substitution of Equations (3-82), (3-83), and (3-84) into Equation (3-76) and rearranging the resulting expression to explicitly solve for $T_{w,m}^{\langle \tau+\Delta\tau_n \rangle}$

$$T_{w,m}^{\langle \tau+\Delta\tau_n \rangle} = T_{w,m}^{\langle \tau \rangle} + \left[\frac{\alpha_{w,m}(\Delta\tau_n)}{r_m - r_{m-1}}\right]\left(\frac{A_{w,m}}{V_{w,m}}\right)\left(\overline{T}_{w,m-1} - \overline{T}_{w,m}\right) + \left[\frac{\alpha_{w,m}(\Delta\tau_n)}{r_{m+1} - r_m}\right]\left(\frac{A_{w,m+1}}{V_{w,m}}\right)\left(\overline{T}_{w,m+1} - \overline{T}_{w,m}\right) \tag{3-87}$$

Applying the stability criterion for explicit finite-difference methods for transient one-dimensional heat conduction as prescribed in Incropera and DeWitt (1996), the following is derived:

$$T_{w,m}^{\langle \tau \rangle} > \left[\frac{\alpha_{w,m}(\Delta\tau_n)}{V_{w,m}}\right]\left(\frac{A_{w,m}}{r_m - r_{m-1}} + \frac{A_{w,m+1}}{r_{m+1} - r_m}\right)\overline{T}_{w,m} \tag{3-88}$$

Rearranging Equation (3-88) to solve for maximum allowed time step, $\Delta\tau_n$, yields

$$\Delta\tau_n < \left(\frac{T_{w,m}^{\langle \tau \rangle}}{\alpha_{w,m}\overline{T}_{w,m}}\right)\left[\left(\frac{A_{w,m}}{V_{w,m}}\right)\left(\frac{1}{r_m - r_{m-1}}\right) + \left(\frac{A_{w,m+1}}{V_{w,m}}\right)\left(\frac{1}{r_{m+1} - r_m}\right)\right]^{-1} \tag{3-89}$$

Since the internal fluid, ullage gas or propellant, will generally be warmer than any location within the tank wall and since $\overline{T}_{w,m}$ is iteratively determined after each time the stability criterion is applied, the following is required to assure computational stability at each iteration

$$\Delta\tau_n < \frac{\left(\frac{1}{\alpha_{w,m}}\right)\left[\min\left(1, \frac{T_{w,m}^{\langle \tau \rangle}}{\overline{T}_{fl}}\right)\right]}{\left[\left(\frac{A_{w,m}}{V_{w,m}}\right)\left(\frac{1}{r_m - r_{m-1}}\right) + \left(\frac{A_{w,m+1}}{V_{w,m}}\right)\left(\frac{1}{r_{m+1} - r_m}\right)\right]} \tag{3-90}$$

The parameter $\overline{T}_{fl}$ in Equation (3-90) is the temperature of the fluid in the ullage gas or propellant segment in contact with the tank wall segment being evaluated.

Inner Wall Boundary Conditions

Referring to Figure 3.6, convective heat transfer is occurring between inner surface of the innermost wall segment and the fluid in contact with this surface. Applying the energy balance to the innermost wall segment, where m equals zero and m+1 equals one, yields

$$\rho_w V_{w,0} c_{w,0} \left(\frac{dT_{w,0}}{d\tau} \right) = h_{fl} A_{w,0} \left(\overline{T}_{fl} - \overline{T}_{w,0} \right) + k_{w,1} A_{w,1} \left(\frac{dT_{w,1}}{dr} \right) \tag{3-91}$$

Setting m equal to zero in Equations (3-83) and (3-84), substituting the resulting equations into Equation (3-91), and rearranging to explicitly solve for $T_{w,0}^{\langle \tau + \Delta\tau_n \rangle}$ produces

$$\begin{aligned} T_{w,0}^{\langle \tau + \Delta\tau_n \rangle} = T_{w,0}^{\langle \tau \rangle} &+ \left[\frac{h_{fl} \left(\Delta\tau_n \right)}{\rho_w c_{w,0}} \right] \left(\frac{A_{w,0}}{V_{w,0}} \right) \left(\overline{T}_{fl} - \overline{T}_{w,0} \right) \\ &+ \left[\frac{k_{w,0} \left(\Delta\tau_n \right)}{\rho_w c_{w,0} \left(r_1 - r_0 \right)} \right] \left(\frac{A_{w,1}}{V_{w,0}} \right) \left(\overline{T}_{w,1} - \overline{T}_{w,0} \right) \end{aligned} \tag{3-92}$$

Applying the stability criterion for explicit finite-difference methods for transient one-dimensional heat conduction at the wall boundary where convective heat transfer is occurring, as presented in Incropera and DeWitt (1996), results in

$$T_{w,0}^{\langle \tau \rangle} > \left\{ \left[\frac{h_{fl} \left(\Delta\tau_n \right)}{\rho_w c_{w,0}} \right] \left(\frac{A_{w,0}}{V_{w,0}} \right) + \left[\frac{k_{w,0} \left(\Delta\tau_n \right)}{\rho_w c_{w,0} \left(r_1 - r_0 \right)} \right] \left(\frac{A_{w,1}}{V_{w,0}} \right) \right\} \overline{T}_{w,0} \tag{3-93}$$

Rearranging Equation (3-93) to solve for the maximum allowed time step and applying the conditions where the tank wall is generally always being warmed by the fluid in the tank, the maximum allowed time step to maintain computational stability is obtained

$$\Delta\tau_n < \left(\frac{r_1 - r_0}{\alpha_{w,0}}\right)\left(\frac{V_{w,0}}{A_{w,0}}\right)\left[\min\left(1, \frac{T_{w,0}^{\langle\tau\rangle}}{\overline{T}_{fl}}\right)\right]\left[\frac{h_{fl}\left(r_1 - r_0\right)}{k_{w,0}} + \left(\frac{A_{w,0}}{A_{w,1}}\right)\right]^{-1} \quad (3\text{-}94)$$

Outer Wall Boundary Conditions

For the computer model, the outer surface of the outermost wall segment is treated as adiabatic; no heat transfer occurs at this boundary. Referring to Figure 3.7, the techniques described in Incropera and DeWitt (1996) are applied where an imaginary mirror image wall segment, outside the evaluated wall segment and having a through-thickness temperature gradient of equal magnitude and opposite direction, is modeled. Referring to the heat transfer across real and imaginary boundaries shown in Figure 3.7 and the total volume within these boundaries, an energy balance is

$$\rho_w V_{w,m} c_{w,m}\left(\frac{dT_{w,m}}{d\tau}\right) = k_{w,m} A_{w,m}\left(\frac{dT_{w,m}}{dr_m}\right) + k_{w,m+1} A_{w,m+1}\left(\frac{dT_{w,m+1}}{dr_{m+1}}\right) \quad (3\text{-}95)$$

Substituting Equations (3-82), (3-83), and (3-84) into Equation (3-95), replacing r_m with r_{ow}, applying the condition of $\overline{T}_{w,m+1} = \overline{T}_{w,m-1}$ (by mirror image symmetry) as presented in Figure 3.7, and rearranging to solve for $T_{w,m}^{\langle\tau+\Delta\tau_n\rangle}$ explicitly yields

$$T_{w,m}^{\langle\tau+\Delta\tau_n\rangle} = T_{w,m}^{\langle\tau\rangle} + \left[\frac{2\alpha_{w,m}\left(\Delta\tau_n\right)}{r_{ow} - r_{m-1}}\right]\left(\frac{A_{w,m}}{V_{w,m}}\right)\left(\overline{T}_{w,m-1} - \overline{T}_{w,m}\right) \quad (3\text{-}96)$$

Applying the computation stability criterion as prescribed by Incropera and DeWitt (1996) and applying the conditions where the outer tank wall segment is always colder than the fluid adjacent to the innermost wall segment, the maximum allowed time step becomes

$$\Delta\tau_n < \left(\frac{r_{ow} - r_{m-1}}{2\alpha_{w,m}}\right)\left(\frac{V_{w,m}}{A_{w,m}}\right)\left[\min\left(1, \frac{T_{w,m}^{\langle\tau\rangle}}{\overline{T}_{fl}}\right)\right] \tag{3-97}$$

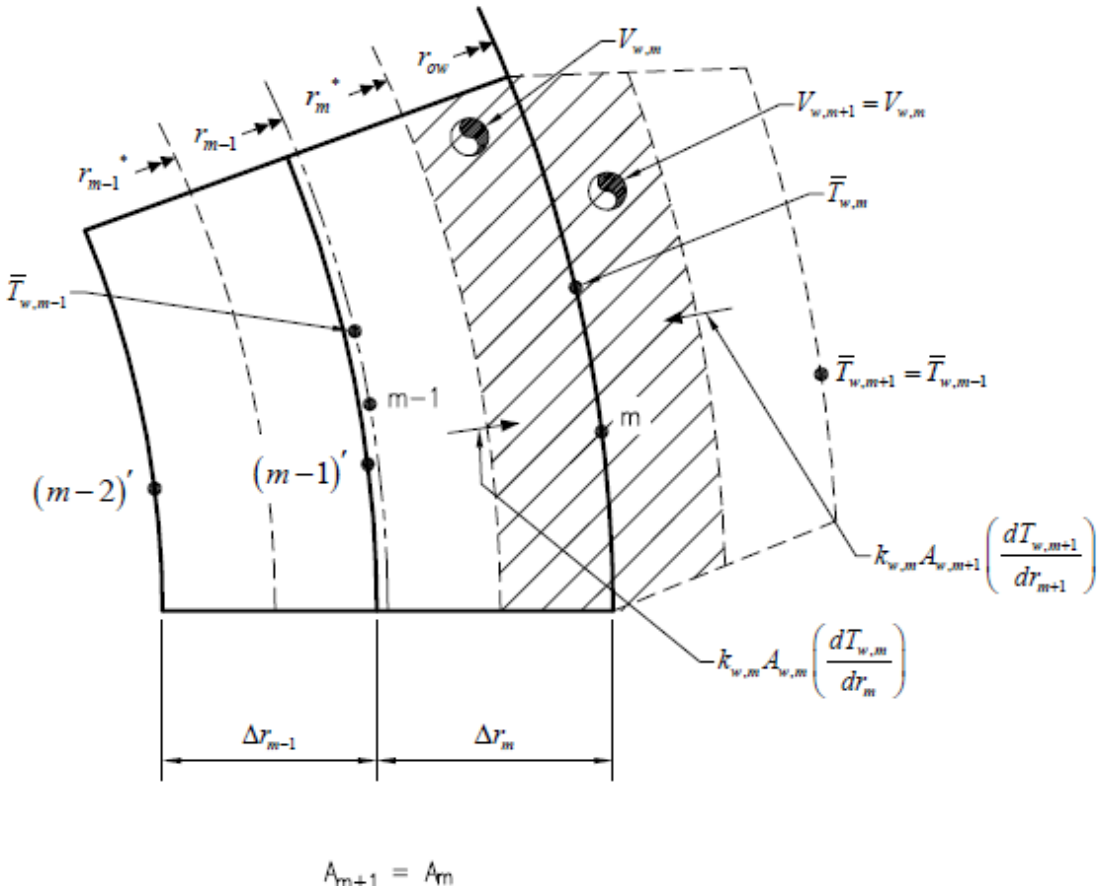

Figure 3.7 Schematic of Model to Simulate Adiabatic Outer Wall Using Numerical Finite-Difference Modeling

Tank Wall Segment Spatial-Temporal Transformation

Referring to Figures 3.2 through 3.5, the boundaries of each cryogenic propellant and ullage gas segment change with respect to time as propellant is expelled from the bottom of the vessel and pressurant gas enters the ullage region of the vessel. As a result, the wall section adjacent to each fluid segment at any given time step will have boundaries that differ from those of the wall section adjacent to the same fluid segment at the preceding or subsequent time step.

For clarity in describing the transformation methods, the terms "section," "wall section," or "tank wall section" refer to portions of the tank wall, extending from inner to outer wall surfaces, adjacent to a given ullage gas or propellant segment. Figures 3.3, 3.4, and 3.5 illustrate the tank wall sections. The "segment," "wall segment," or "tank wall segment" refers to each layer within a tank wall section as delineated in Figure 3.6. Whenever the transient tank wall heat conduction computations are executed, the initial temperature profile for (or through the thickness of) the wall section spatially at boundaries where it is adjacent to the fluid, ullage gas or propellant, segment being evaluated at the current time step needs to first be determined. However, the heat content of this same wall segment must reflect that associated with the prior time step in order to provide an (equivalent) initial temperature profile through the section thickness. Therefore a transformation process is needed to accomplish this.

To perform this transformation, the total heat content and how it relates to tank wall material temperature must be known. For each tank wall segment m within any given wall section, the total heat content of this segment is given by

$$Q_{w,m} = \rho_w \int_{T_{ref}}^{T_{w,m}} V_{w,m}\left[c_{w,m}(T)\right]dT \tag{3-98}$$

The temperature T_{ref} in Equation (3-98) is a reference temperature where the heat content is set to zero. At the start of program execution, the model numerically determines the heat content per unit volume at discrete temperatures, at one degree Rankin intervals, using Simpson's rule as presented in Wylie and Barrett (1982). An array of heat content per unit volume values with a corresponding array of material temperatures is created by the computer model. The discrete temperatures range from slightly below the propellant temperature at the initial time step to the maximum possible temperature of pressurant gas corresponding to its highest enthalpy over the full range of tank pressures. To determine tank wall material temperature from known or input heat content per unit volume and vice versa, linear interpolation is used.

The total heat content of wall segment m of the wall section adjacent to ullage gas segment J spatially at the current time $\tau + \Delta\tau$, but temporally at the prior time τ is

$$\begin{aligned}(Q_{w,m})_J^{\langle\tau\rangle} = &\left[\frac{1}{\left(V_{w,m}\right)_J^{\langle\tau+\Delta\tau\rangle}}\right]\left[\sum_{J_{OLD}=1}^{J_{O,\max}}\left(Q_{w,m}\right)_{J_{OLD}}\left(V_{w,m}\right)_{z_{1,J_{OLD}}}^{z_{2,J_{OLD}}}\right] \\ &+\left[\frac{1}{\left(V_{w,m}\right)_J^{\langle\tau+\Delta\tau\rangle}}\right]\left[\sum_{K_{OLD}=1}^{K_{O,\max}}\left(Q_{w,m}\right)_{K_{OLD}}\left(V_{w,m}\right)_{z_{1,K_{OLD}}}^{z_{2,K_{OLD}}}\right]\end{aligned} \tag{3-99}$$

The term $\left(V_{w,m}\right)_{z_{1,J_{OLD}}}^{z_{2,J_{OLD}}}$ at each value of J_{OLD} in Equation (3-99) is defined by the volume shown in Figure 3.8 corresponding to the case that applies. If none of the cases

apply for a given value of J_{OLD}, this term is set to zero. Similarly, the term $\left(V_{w,m}\right)_{z_{1,K_{OLD}}}^{z_{2,K_{OLD}}}$ at each value of K_{OLD} in Equation (3-99) is defined by the volume shown in Figure 3.8 corresponding to the case that applies. If none of the cases apply for a given value of K_{OLD}, this term is set to zero.

Similarly, for propellant segment K spatially at the current time $\tau+\Delta\tau$, but temporally at the prior time τ, the total heat content of wall segment m in the adjacent wall section is

$$\begin{aligned}\left(Q_{w,m}\right)_K^{\langle\tau\rangle} = &\left[\frac{1}{\left(V_{w,m}\right)_K^{\langle\tau+\Delta\tau\rangle}}\right]\left[\sum_{J_{OLD}=1}^{J_{O,\max}}\left(Q_{w,m}\right)_{J_{OLD}}\left(V_{w,m}\right)_{z_{1,J_{OLD}}}^{z_{2,J_{OLD}}}\right] \\ &+\left[\frac{1}{\left(V_{w,m}\right)_K^{\langle\tau+\Delta\tau\rangle}}\right]\left[\sum_{K_{OLD}=1}^{K_{O,\max}}\left(Q_{w,m}\right)_{K_{OLD}}\left(V_{w,m}\right)_{z_{1,K_{OLD}}}^{z_{2,K_{OLD}}}\right]\end{aligned} \tag{3-100}$$

For Equation (3-100), the terms $\left(V_{w,m}\right)_{z_{1,J_{OLD}}}^{z_{2,J_{OLD}}}$ and $\left(V_{w,m}\right)_{z_{1,K_{OLD}}}^{z_{2,K_{OLD}}}$ at each value of J_{OLD} and K_{OLD} is defined by the volume shown in Figure 3.9 corresponding to the case that applies.

From the computed heat content for each wall segment m of a given wall section as determined by Equation (3-99) or (3-100), the initial temperature of the respective wall segment is determined to generate an initial (beginning of time step) temperature profile for the respective wall section.

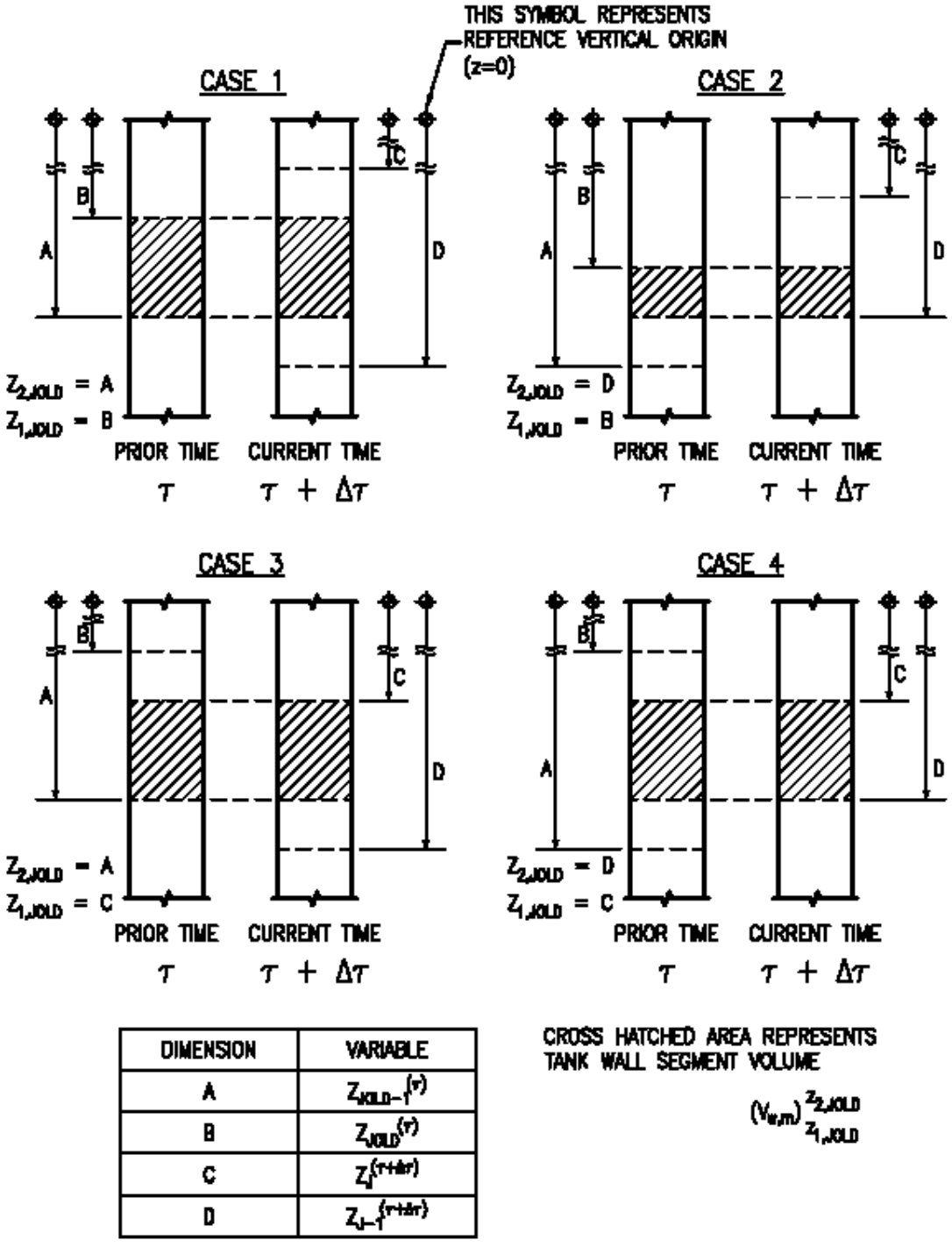

DIMENSION	VARIABLE
A	$Z_{JOLD-1}^{(\tau)}$
B	$Z_{JOLD}^{(\tau)}$
C	$Z_J^{(\tau+\Delta\tau)}$
D	$Z_{J-1}^{(\tau+\Delta\tau)}$

Figure 3.8 Cases for Wall Segment Spatial-Temporal Transformation Across Time Step, Inner Wall Segment Spatially in Contact with Ullage Gas Segment J at Current Time Step (Page 1 of 2)

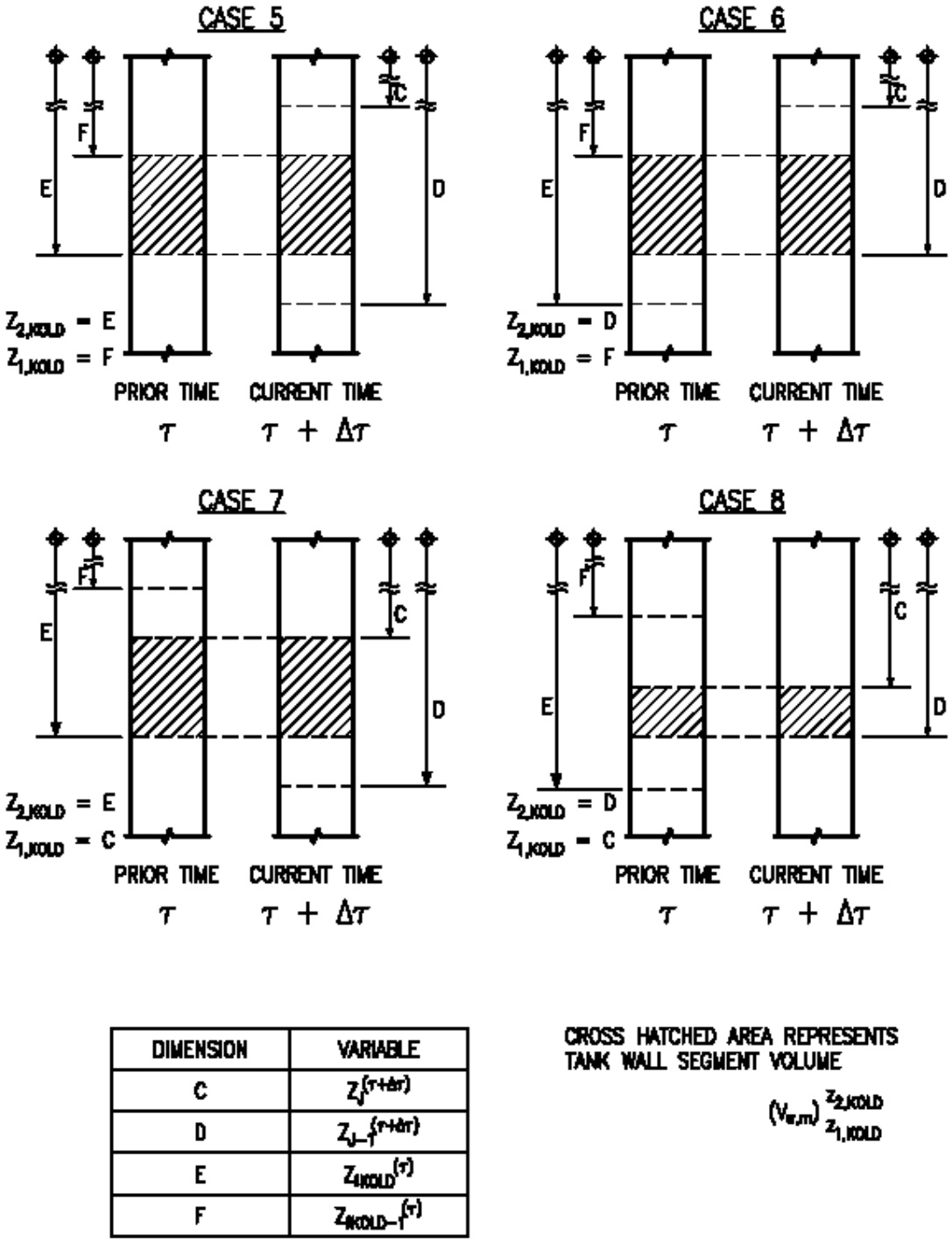

DIMENSION	VARIABLE
C	$Z_J^{(\tau+\Delta\tau)}$
D	$Z_{J-1}^{(\tau+\Delta\tau)}$
E	$Z_{KOLD}^{(\tau)}$
F	$Z_{KOLD-1}^{(\tau)}$

CROSS HATCHED AREA REPRESENTS TANK WALL SEGMENT VOLUME

$(V_{w,m})_{Z_{1,KOLD}}^{Z_{2,KOLD}}$

Figure 3.8 Cases for Wall Segment Spatial-Temporal Transformation Across Time Step, Inner Wall Segment Spatially in Contact with Ullage Gas Segment J at Current Time Step (Page 2 of 2)

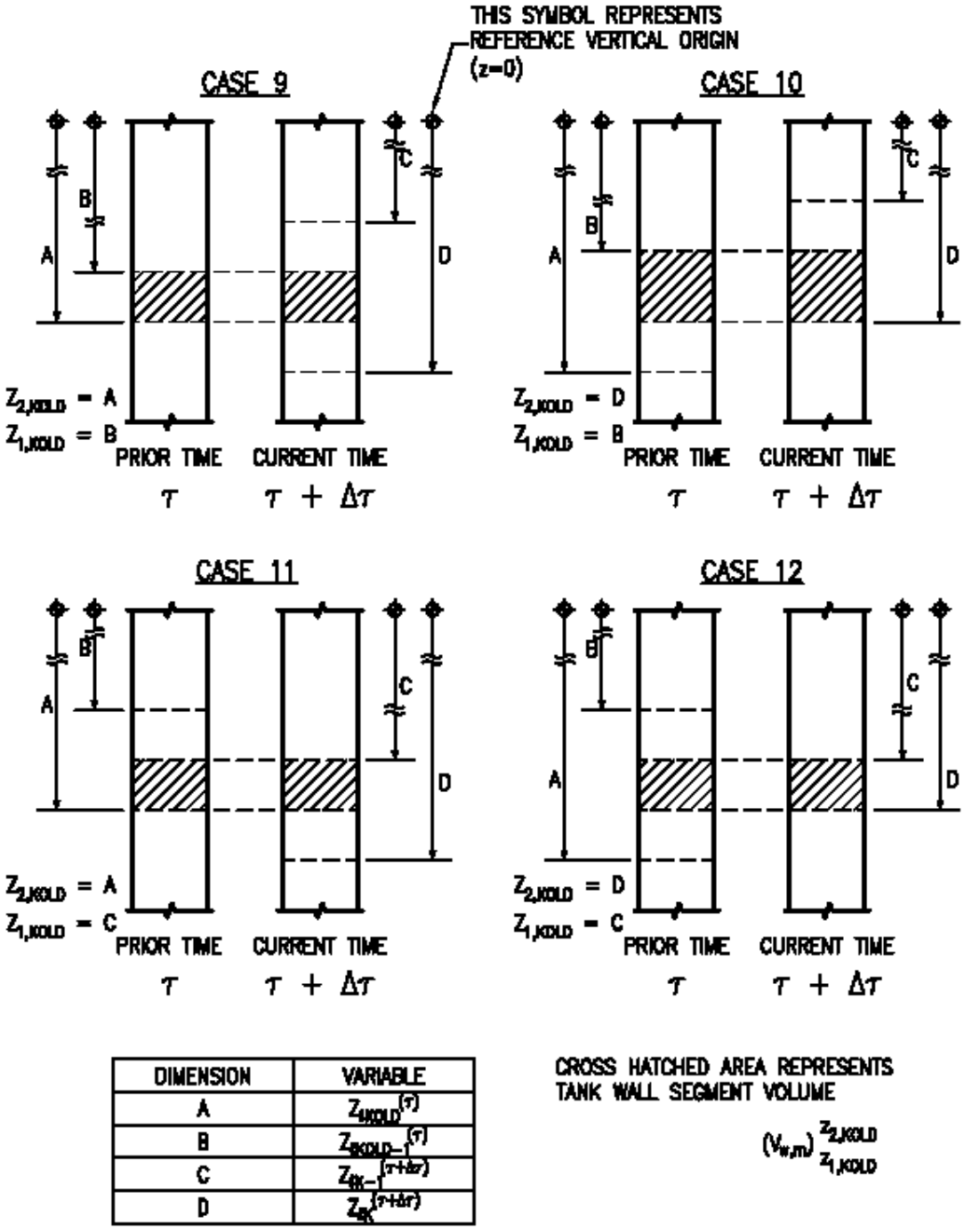

Figure 3.9 Cases for Wall Segment Spatial-Temporal Transformation Across Time Step, Inner Wall Segment Spatially in Contact with Cryogenic Propellant Segment K at Current Time Step (Page 1 of 2)

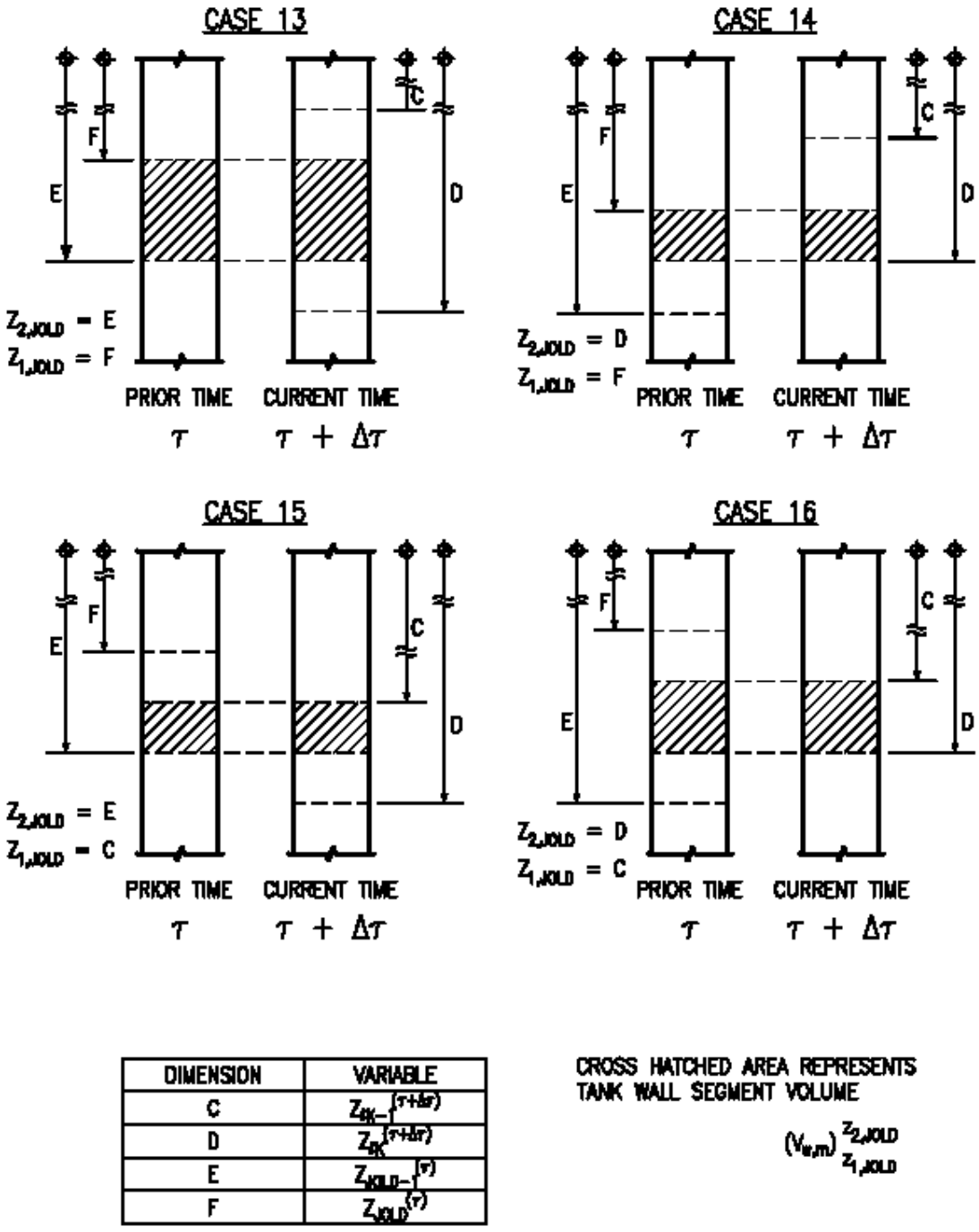

DIMENSION	VARIABLE
C	$Z_{SK-}^{(\tau+\Delta\tau)}$
D	$Z_{SK}^{(\tau+\Delta\tau)}$
E	$Z_{JOLD-}^{(\tau)}$
F	$Z_{JOLD}^{(\tau)}$

Figure 3.9 Cases for Wall Segment Spatial-Temporal Transformation Across Time Step, Inner Wall Segment Spatially in Contact with Cryogenic Propellant Segment K at Current Time Step (Page 2 of 2)

CHAPTER IV

PROGRAM DEVELOPMENT

The model developed for this study is a Visual FORTRAN ® based main program linked with subroutines and an interactive fluid properties library in a program workspace environment. Included in the program and subroutines are the algorithms presented in Chapter III.

This chapter presents flowcharts to provide an overall concept of the computation sequences, the iteration loops and procedures, and the supporting logic utilized in development and use of the computer model.

General Program

Figure 4.1 is a flowchart illustrating the overall sequence of major computation routines within the main program and calls to subroutines from the main program. Each block in the flowchart is numbered for reference.

Blocks 1 through 6 in the flowchart are essentially calls to modules and subroutines where the program user interactively enters or edits input parameters used by the program and where these parameters are printed to and saved in data files as reference information. The "Input Module" also creates new input parameter data files or opens

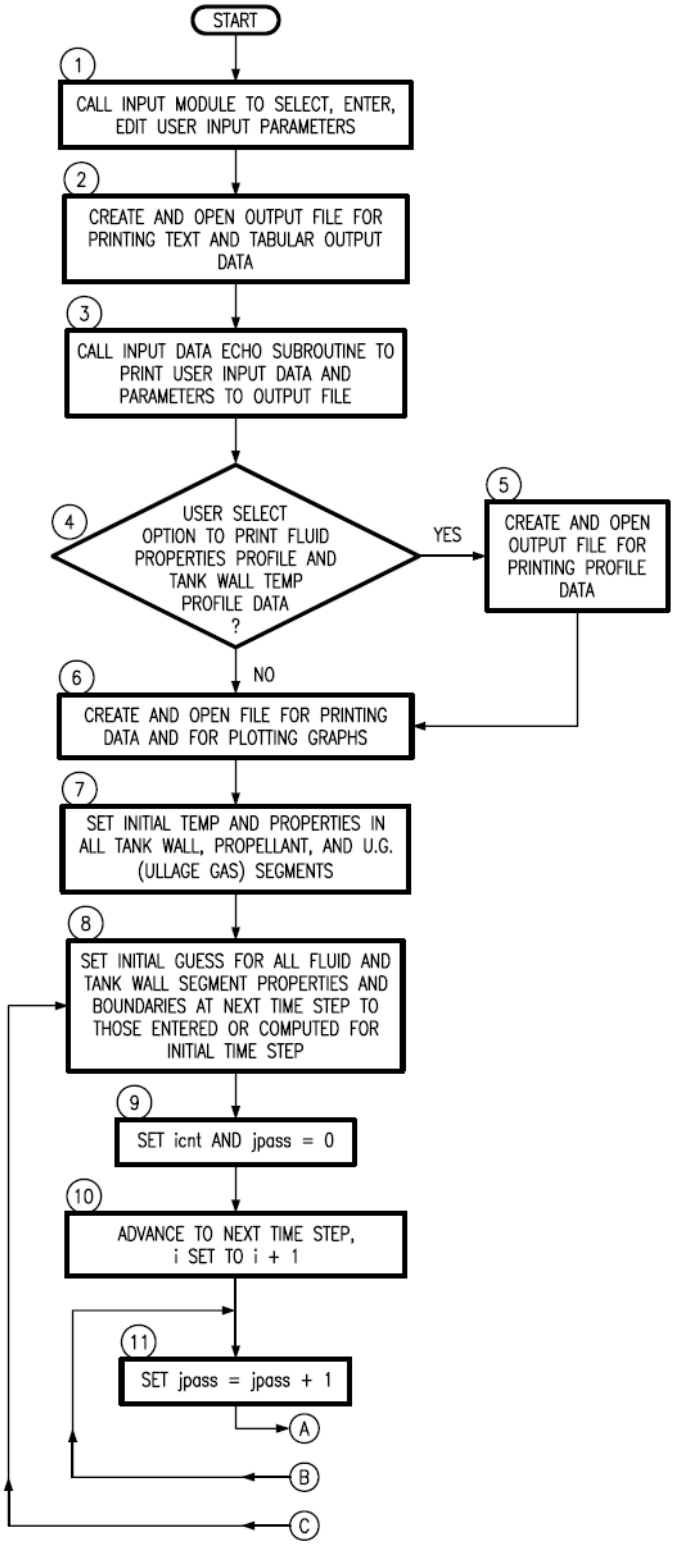

Figure 4.1 General Collapse Factor Program Flowchart (Page 1 of 2)

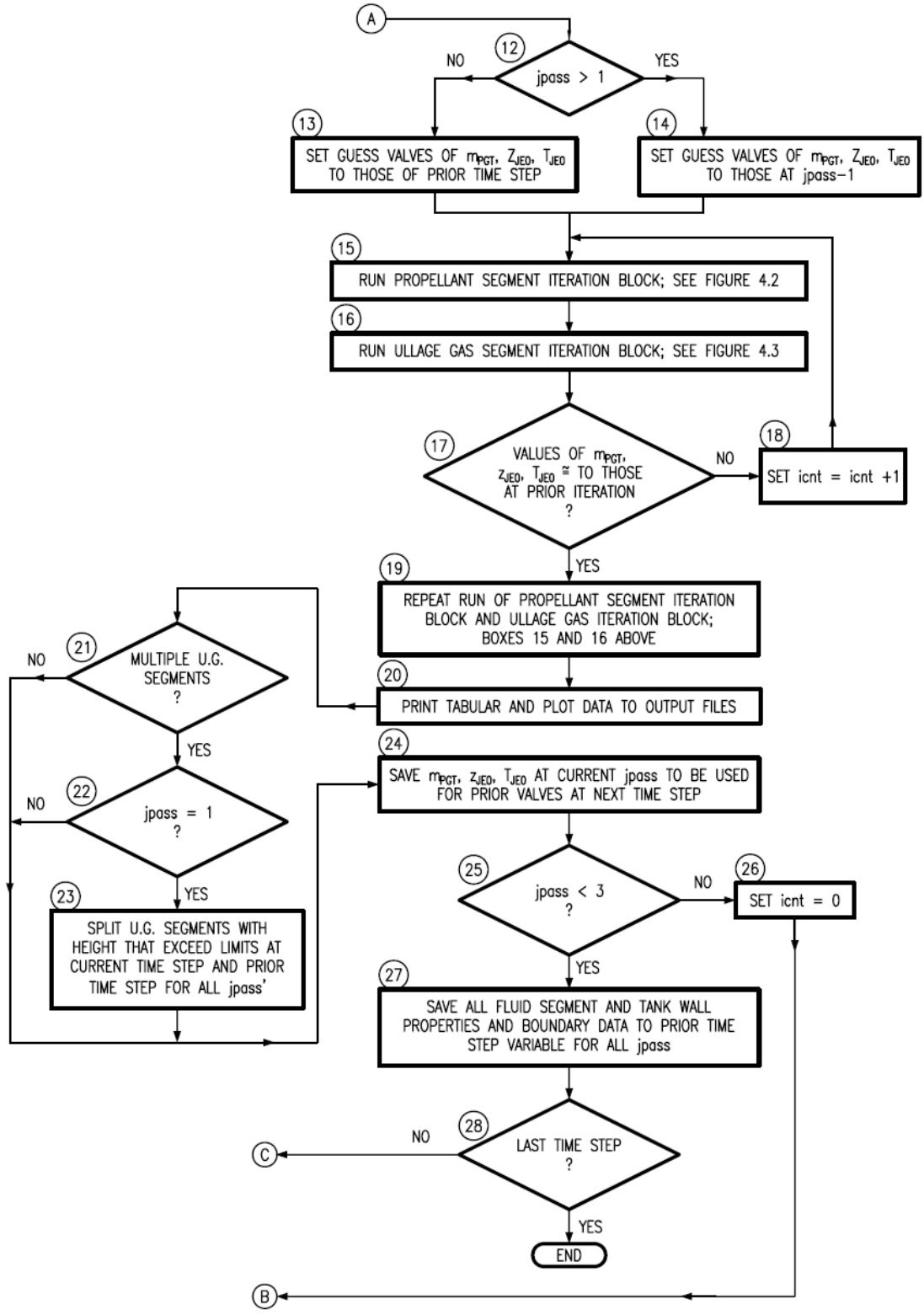

Figure 4.1 General Collapse Factor Program Flowchart (Page 2 of 2)

and edits previously created input parameter data files, depending on user selections, so that the user does not have to manually re-enter all input data each time the program is run.

In addition to the tank geometric parameters and initial conditions, the primary inputs are times with corresponding mass flow rate of propellant out of the main tank bottom discharge nozzle and the pressure at this location. For cases where the user selects the option of constant volume bottles supplying pressurant gas to the tank ullage, the user must also enter an auxiliary mass flow rate for each entered time. The auxiliary mass flow rate reflects the quantity of gas being diverted from the same bottles to interfaces other than the tank ullage. If no gases are diverted to other interfaces, zero values are entered for auxiliary mass flow rates.

Block 7 sets all initial conditions for all fluid, ullage gas and cryogenic propellant, segments and all tank wall sections adjacent to these fluid segments. The temperature of all wall sections and fluid segments are set to the saturation temperature of the propellant species at the initial ullage gas pressure previously assigned by the user. The initial ullage gas and propellant segment properties are respectively fixed to those at saturated vapor and saturated liquid states.

The main sequential loop in Figure 4.1, encompassing blocks 10 through 28, defines the program sequence from one time step to the next. The variable 'i' is the index associated with each time step. Within the main sequential loop is a smaller nested loop where the variable 'jpass' is assigned a value of 1, 2, or 3 at each pass through the loop. These values of 'jpass' correspond to the three cases that are evaluated for each time step.

The first case applies the condition of no heat transfer at any cryogenic and ullage gas segment boundaries. The second case models heat transfer only at fluid boundaries in contact with the tank wall. The third case accounts for heat transfer across all of the fluid segment boundaries.

Within the nested loop (for each time step and each value of 'jpass' within the time step), the convergence criteria indicated in Block 17 must be satisfied. After these criteria are satisfied for the case where 'jpass' equals 1 and where the model allows for more than one ullage gas segment, the program tests the height of each ullage gas segment. When the height of an ullage gas segment exceeds a prescribed limit based on user input, the segment is split into two segments of equal volume and, for 'jpass' equals 1, having the same properties.

Blocks 15 and 16 in Figure 4.1 represent the Cryogenic Propellant Iteration Module and the Ullage Gas Iteration Module, respectively. Flowcharts that provide further details about these modules are presented in Figures 4.2 and 4.3.

Cryogenic Propellant Iteration Module

Figure 4.2 presents the flowchart for the module of the main program that computes properties in each cryogenic propellant segment starting from the lowermost (or bulk) propellant segment to the uppermost propellant segment.

There are two primary iteration loops in this module. The inner (nested) loop determines the internal energy of each propellant segment based on latest iteration pressure, computed rates of heat transfer at the boundaries, and an energy balance

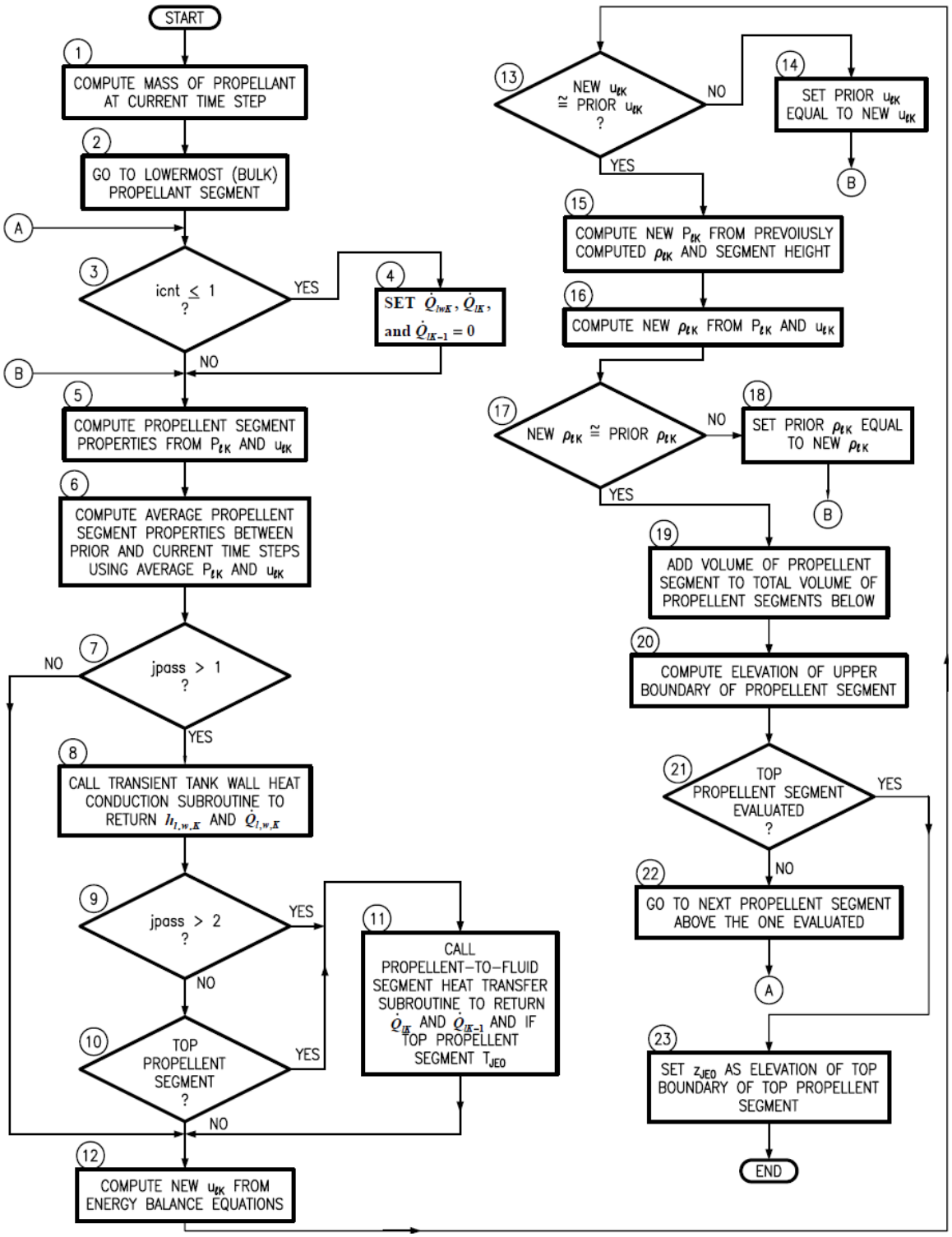

Figure 4.2 Propellant Segment Iteration Module Flowchart

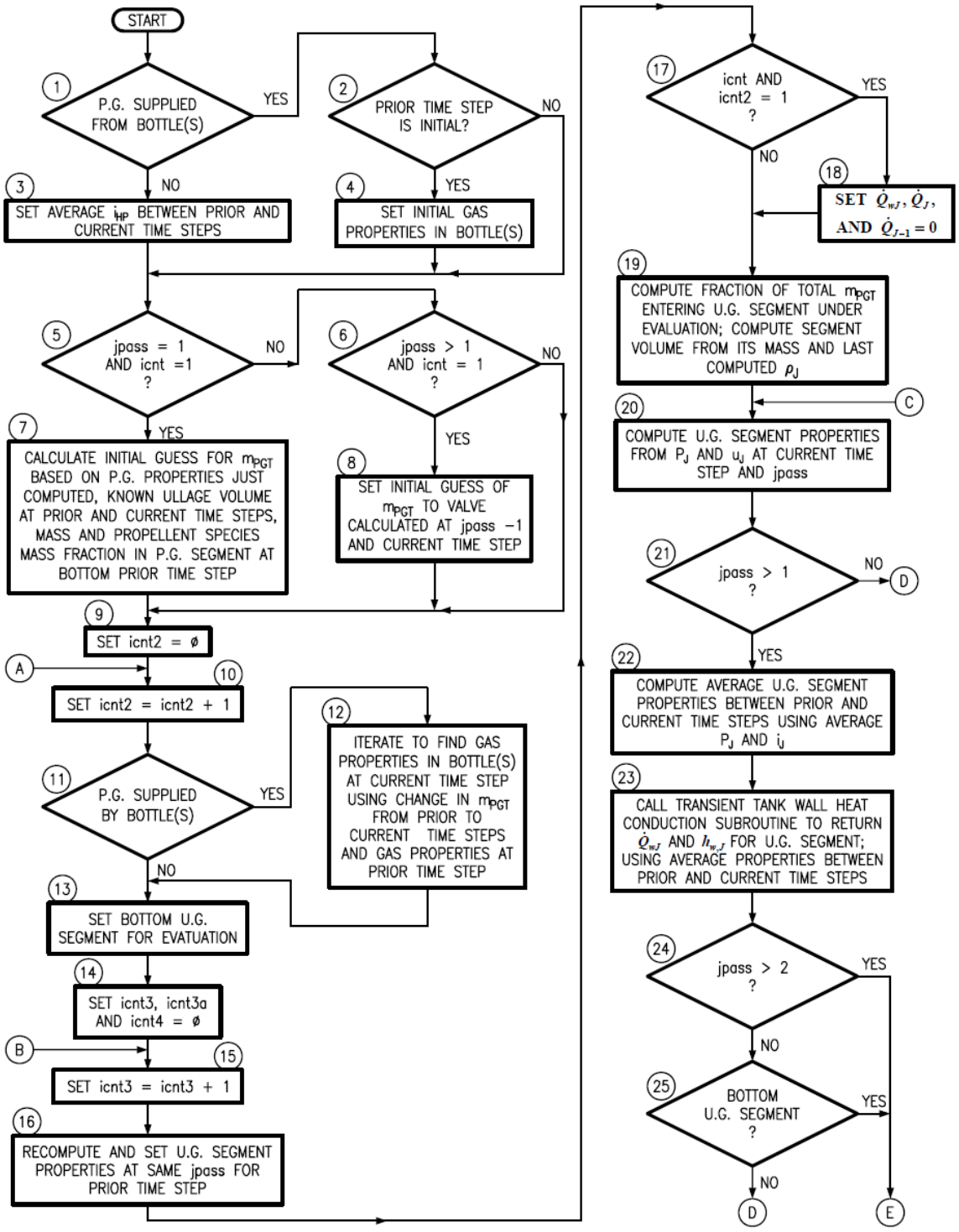

Figure 4.3 Ullage Gas Segment Iteration Module Flowchart (Page 1 of 2)

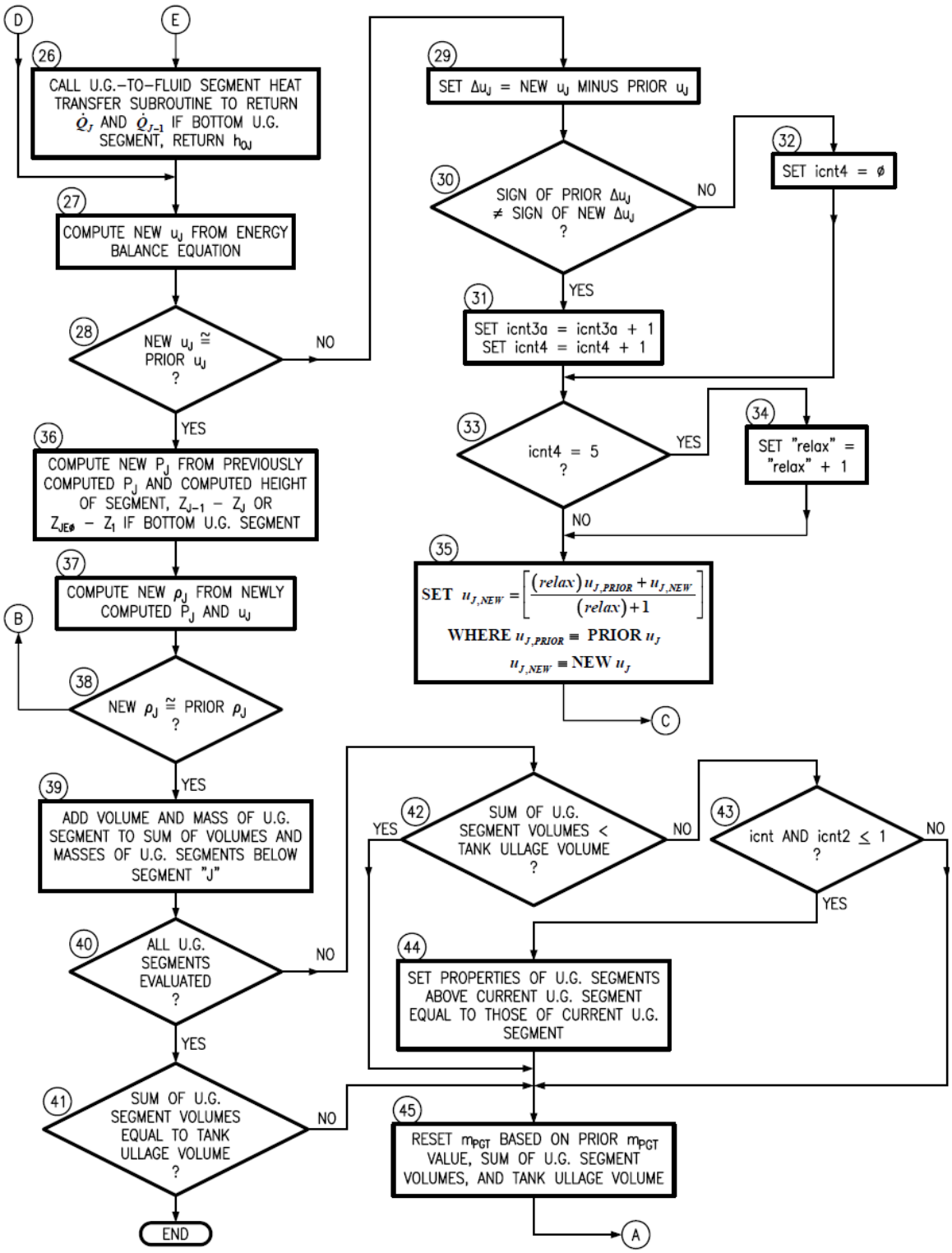

Figure 4.3 Ullage Gas Segment Iteration Module Flowchart (Page 2 of 2)

equation, Equation (3-15) or (3-17), in Chapter III. The rates of heat transfer at segment boundaries are computed using algorithms discussed in Chapter III. The outer loop determines the mean pressure of each propellant segment based on its mass, pressure at its lower boundary, mean density, and mid- and top- segment heights. The mean density and the mid-segment height define the hydrostatic pressure change from the bottom boundary to where the segment volume is bisected, which determines the mean pressure. Pressure at the upper segment boundary is computed from the segment height, the mean density, and the pressure at the lower segment boundary. Blocks 13 and 17 contain the convergence criteria before evaluating the adjacent propellant segment or exiting the module.

After the convergence criterion in Block 17 is satisfied for each propellant segment, the volume of the segment is added to the sum of propellant segment volumes below the segment. After all propellant segments have been evaluated, the total volume of cryogenic propellant in the tank is found, and the elevation of the ullage-gas-to-cryogenic-propellant interface is calculated in Block 23.

Block 8 represents the call to the transient tank wall heat conduction subroutine for the rate of heat transfer and the convective heat transfer coefficient at tank wall surfaces adjacent to a segment. Figure 4.4 is a flowchart of this subroutine.

Block 11 represents a call to the propellant-to-fluid heat transfer subroutine, which returns the rates of heat transfer at the upper and the lower boundaries of the propellant segment. This subroutine utilizes the cryogenic propellant segment-to-segment heat transfer algorithms developed in Chapter III. For the upper boundary of the uppermost propellant segment, the convective heat transfer coefficient computed from

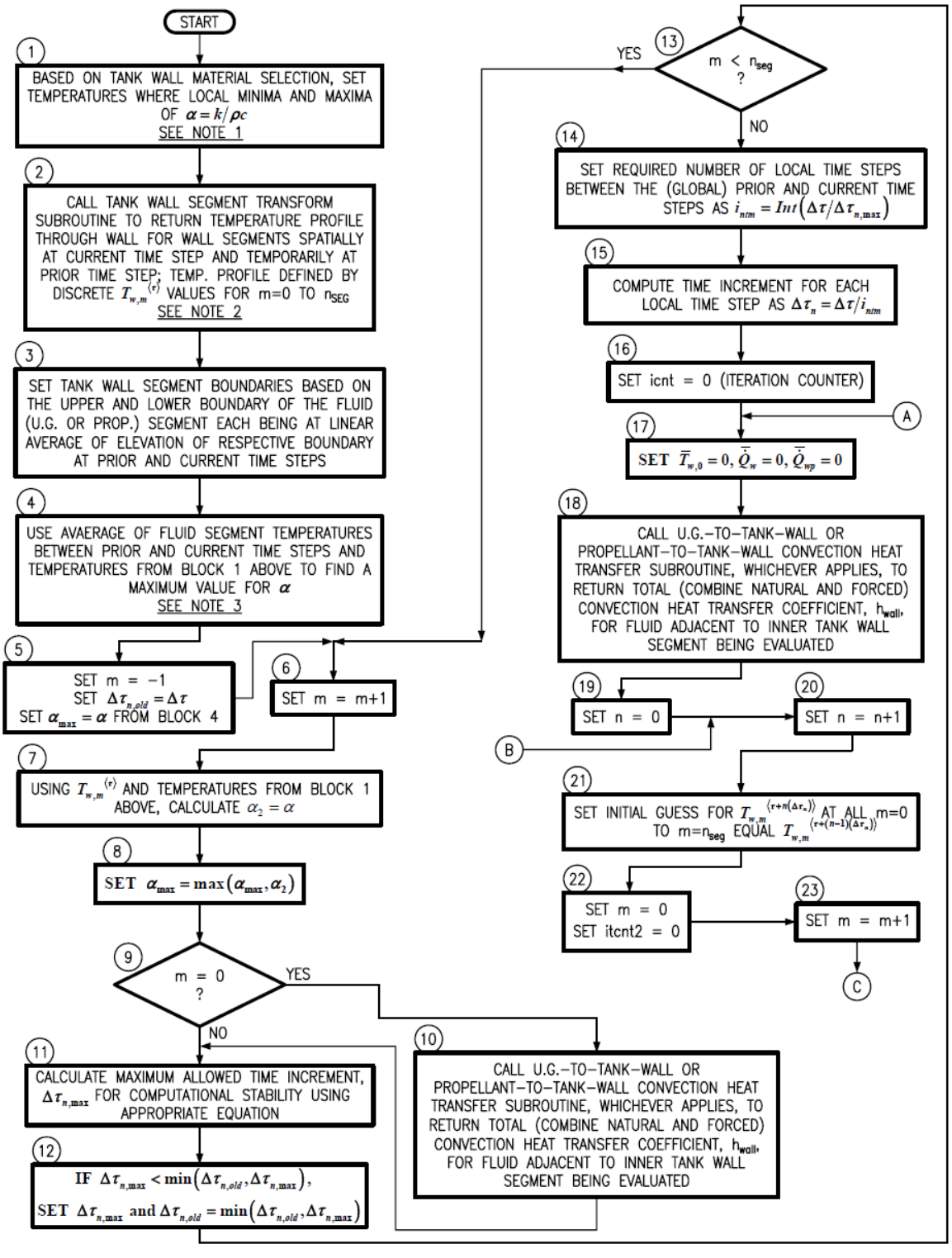

Figure 4.4 Transient Tank Wall Heat Conduction Subroutine Flowchart (Page 1 of 3)

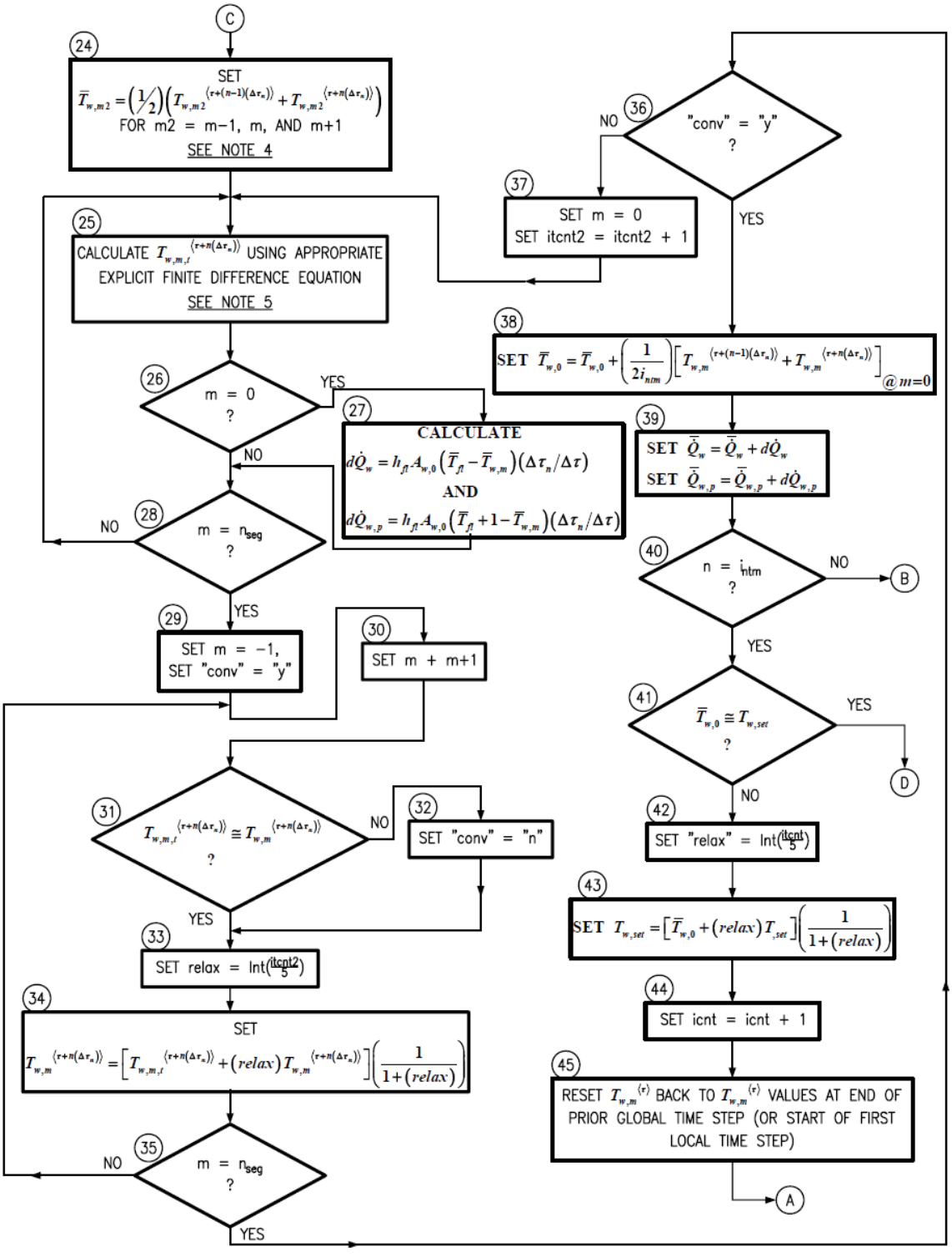

Figure 4.4 Transient Tank Wall Heat Conduction Subroutine Flowchart (Page 2 of 3)

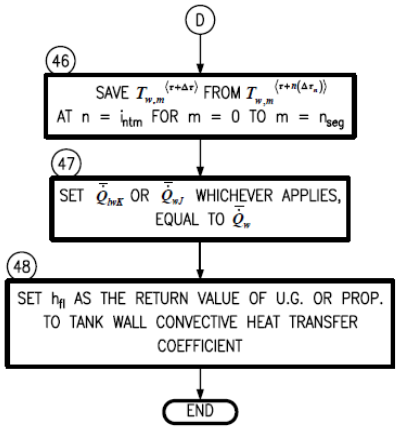

NOTES:

1. FOR EACH MATERIAL SELECTED FOR THE TANK, THERE ARE TEMPERATURES WHERE α IS AT A LOCAL MINIMUM OR MAXIMUM VALUE WHERE THESE TEMPERATURE ARE BETWEEN THOSE CALCULATED LATER IN BLOCKS 4 AND 7.
2. TRANSFORM SETS THE TEMPERATURE PROFILE FOR THE WALL SEGMENT ADJACENT TO THE FLUID SEGMENT AT THE CURRENT TIME STEP. n_{seg} IS THE NO. OF SEGMENTS THROUGH THICKNESS OF THE TANK WALL SECTION.
3. AVERAGE OF FLUID SEGMENT TEMPERATURES BETWEEN PRIOR AND CURRENT TIME STEPS IS ALWAYS THE MAXIMUM TEMPERATURE AS TANK WALLS WILL ALWAYS BE COLDER THAN THIS TEMPERATURE.
4. m−1 NOT EVALUATED IF m=0, m+1 NOT EVALUATED IF m=n_{seg}.
5. $T_{w,m,t}^{\langle \tau+n(\Delta\tau_s) \rangle}$ IS A TEMPORARY ITERATION VALUE OF $T_{w,m}^{\langle \tau+n(\Delta\tau_s) \rangle}$.

Figure 4.4 Transient Tank Wall Heat Conduction Subroutine Flowchart (Page 3 of 3)

the last iteration using computed ullage gas segment properties and the ullage-gas-to-cryogenic-propellant interface heat transfer algorithms presented in Chapter III, is used to find the rate of heat transfer across the upper boundary of the segment. An updated iteration value for temperature at the ullage-gas-to-cryogenic-propellant interface is also computed and returned from this subroutine.

Ullage Gas Iteration Module

Figure 4.3 presents the flowchart for the module of the main program that computes properties in each ullage gas segment starting from the lowermost ullage gas segment and proceeding to the uppermost segment.

Blocks 1 through 8 set the initial approximation (or guess) for the total mass of pressurant gas in the tank ullage at the end of the current time step. This process is only performed when this module is called for the first time after each time step and after the value of 'jpass' changes.

The primary iteration loop in the ullage gas iteration module encompasses blocks 10 through 45. Criteria in Blocks 40 and 41 must be satisfied to exit this iteration loop. If both criteria are not satisfied, Block 45 computes a revised value for total mass of pressurant gas in the tank ullage based on the most recently computed sum of ullage gas segment volumes and the tank ullage region volume, where the latter volume is determined from total tank volume and the most recent cryogenic propellant volume computed by the cryogenic propellant segment iteration module. After Block 45, computation steps starting at Block 10 are repeated.

The first part of the primary iteration loop, Blocks 10 through 13, determines the properties of pressurant gas if this fluid is supplied by constant volume bottles and sets an initial guess for properties of the lowermost ullage gas segment. The bottle supplied pressurant gas properties are based on initial pressurant gas properties in the bottle(s), the latest iteration value for the total mass of pressurant gas accumulated in the tank ullage, and the computed total amount of gas supplied from the bottle(s) to auxiliary interfaces. Specific entropy of the pressurant gas supplied from constant volume bottle(s) is taken to

be constant (the entropy at end of each time step is equal to the initial entropy determined by the input initial bottle conditions). When the variable 'jpass' equals 1, the initial guess for properties of the lowermost ullage gas segment is based on the specific enthalpy of the pressurant gas and the computed pressure at the ullage-gas-to-cryogenic-propellant segment interface. When 'jpass' is greater than 1, the initial properties of this segment are set to those determined at the prior 'jpass' value and the end of the current time step.

Following Block 13 in the primary iteration loop, there is a nested secondary iteration loop and a tertiary iteration loop. The secondary and tertiary loops are similar to the primary and secondary iteration loops previously described for the cryogenic propellant segment iteration module. The (nested) tertiary loop determines the internal energy of each ullage gas segment based on latest iteration pressure, computed rates of heat transfer at boundaries, and the energy balance equation, using Equation (3-10) in Chapter III. The rates of heat transfer at segment boundaries are computed using algorithms presented in Chapter III. The outer loop determines the mean pressure of each ullage gas segment based on its mass, pressure at its lower boundary, mean density, and mid- and top-segment heights. The mean pressure and the pressure at the upper boundary of each ullage gas segment are computed applying the same methods described in the "Cryogenic Propellant Iteration Module" section. Blocks 28 and 38 contain the convergence criteria before evaluating the adjacent ullage gas segment or proceeding to the criteria in Blocks 40 and 41.

Block 23 represents a call to the transient tank wall heat conduction subroutine to return the rate of heat transfer and convective heat transfer coefficient at the tank wall surface adjacent to this segment. This subroutine is the same one called by the Cryogenic

Propellant Iteration Module, and the flowchart for this subroutine is presented in Figure 4.4.

Block 26 represents a call of the ullage-gas-to-fluid heat transfer subroutine, which returns the rates of heat transfer at the upper and the lower boundaries of the ullage gas segment. This subroutine utilizes the ullage gas segment-to-segment heat transfer algorithms developed in Chapter III. For the lower boundary of the lowermost ullage gas segment, the convection heat transfer coefficient is computed from the ullage-gas-to-cryogenic-propellant interface heat transfer algorithms presented in Chapter III. The latest iteration value for this coefficient is also returned from the ullage-gas-to-fluid heat transfer subroutine, since it is used for subsequent computations and iterations within (and external) to the ullage gas segment iteration module. An updated iteration value for temperature at the ullage-gas-to-cryogenic-propellant interface is also found and returned from this subroutine.

Transient Tank Wall Heat Conduction Subroutine

The general outline and sequence of computations used for the transient tank wall heat conduction subroutine is provided in Figure 4.4. There are three main parts within this subroutine: (1.) set-up, (2.) local time step sizing, and (3.) through-wall temperature profile computations.

For this part of the chapter, the "global time step" is equivalent to "time step" used in the "General Program" part of this Chapter and referred to in Figure 4.1. The "local time step" is defined as an interval of time that is equal to or smaller than that of the global time step being evaluated when the subroutine is called. The maximum

allowed time interval for each local time step is determined by the computational stability criterion described in the "Transient Tank Wall Heat Conduction" part of Chapter III. In this subroutine there will usually be multiple local time steps spanning the global time step and there will always be at least one local time step for each global time step.

The "section," "wall section," or "tank wall section" refer to portions of the tank wall, extending from inner to outer wall surfaces, adjacent to a given ullage gas or propellant segment. Figures 3.3, 3.4, and 3.5 illustrate the tank wall sections. The "segment,", "wall segment," or "tank wall segment" refers to each layer within a tank wall section as delineated in Figure 3.6.

The first part of the subroutine, set-up, is represented by Blocks 1 through 4. In this part, the maximum values for thermal diffusivity and minimum possible values for thermal conductivity of the tank wall material are determined. These are used in the next part of the subroutine where computational stability criteria are applied to determine the size of local time steps. The minimum and maximum values of the thermal properties are based on known (or latest iteration values for) temperatures of the fluid adjacent to the wall section and initial discrete temperatures of all wall segments through the wall section. These wall segment temperatures were previously calculated at the end of the prior global time step (or start of the current global time step).

Another major component in the first part of the subroutine is represented by Block 2, where a transformation, as described in the "Tank Wall Segment Spatial-Temporal Transformation" part of Chapter III, is applied to determine the initial wall segment temperatures.

The second part of the transient tank wall heat conduction subroutine employs algorithms, Equations (3-89), (3-93), and (3-96), in Chapter III that are associated with computational stability. This part of the subroutine is comprised of Blocks 5 through 16. For a given wall section, all wall segments are evaluated and the maximum allowed time interval for the local time step is set to the minimum value of '$\Delta\tau_n$.' The time interval for the local time step is then set to the global time step divided by the smallest positive integer value where the minimum value of '$\Delta\tau_n$' is not exceeded.

The third part of the subroutine is comprised of the blocks that follow Block 16. In this part of the subroutine, the main loop encompasses Blocks 20 through 40, where the subroutine marches from the first to last local time step, computing discrete temperatures for the wall segments at the end of each local time step. Block 25 within this main loop represents the use of Equations (3-87), (3-92), or (3-96), depending on the wall segment, to compute discrete wall segment temperatures at the end of each local time step.

Since the material thermal properties for each wall segment are based on the average temperature across the local time step when Block 25 computations are executed, an iteration loop is built around this block. This iteration loop is needed because the average temperature across each local time step is dependent on the temperature at the end of the local time step, which is an unknown and is determined in Block 25. This iteration loop encompasses Blocks 23 through 37 and the criterion for convergence is the string variable 'conv' being equal to 'y,' meaning that all discrete wall segment temperatures are within the prescribed error tolerances between subsequent iterations.

The transient tank wall heat conduction subroutine is designed to return the mean rate of heat transfer, the inner wall surface temperature, and the fluid-to-inner-wall

convective heat transfer coefficient for the tank wall section and across the global time step being evaluated. Therefore, each of these parameters, which are evaluated across each local time step, needs to be converted to an average parameter value across the global time step. This is accomplished by steps represented by Blocks 27, 38, and 39.

Before completion of the transient tank wall heat conduction subroutine a final convergence criterion must be satisfied. This criterion is indicated in Block 41, where the global time step mean inside wall surface temperature between subsequent iterations must be approximately equal within a prescribed tolerance. This convergence test must be applied and its criterion must be satisfied because the fluid-to-tank wall convection heat transfer coefficient, which influences the discrete wall segment temperatures previously calculated at all local time steps, is dependent on the inner wall surface temperatures at all local time steps.

Of interest in Figure 4.4 are blocks 10 and 18, which represent the call of the "ullage-gas-to-tank-wall convection heat transfer" and the "cryogenic-propellant-to-tank-wall convective heat transfer subroutines. These subroutines return fluid-to-tank-wall convective heat transfer coefficients utilizing algorithms presented in Chapter III.

CHAPTER V

RESULTS

In order to validate the fidelity of the model developed in this study, the model has been run to perform simulations of the pressurization and propellant expulsion processes for high pressure liquid hydrogen and oxygen run tanks on the E-1 Test Stand at the NASA Stennis Space Center (NASA/SSC) in Hancock County, Mississippi. The simulation of the high pressure liquid hydrogen run tank on the Pratt and Whitney E-8 Test Stand in West Palm Beach, Florida is also presented. The run tanks on these test stands are utilized to supply cryogenic propellants at controlled pressures and mass flow rates to the interfaces of rocket engine combustion devices or turbopumps as they are being tested.

For the E-1 Test Stand, the first simulation is for the high pressure liquid hydrogen run tank supplying propellant to the fuel injector inlet of the preburner (PB) of a prototype RS-83 rocket engine. The second and third simulations are for the high pressure liquid oxygen run tank supplying propellant to the oxidizer injector inlet of the Integrated Propulsion Demonstrator (IPD) pre-burner combustion device which in turn supplies a mixture of high temperature gaseous oxygen and steam to drive the turbine of the oxidizer turbopump (OTP). The second and third simulations correspond to the IPD OTP operating at the 75 and 95 % power levels respectively.

The Pratt and Whitney E-8 Test Stand High Pressure Liquid Hydrogen Run Tank simulation is for a ground test of a development prototype Space Shuttle Main Engine High Pressure Oxidizer Turbopump (SSME HPOT). For this case, the run tank is supplying cryogenic hydrogen propellant, at 50 R to 80 R, to a mixer which in turn supplies gaseous hydrogen at 265 R to 285 R, to the fuel-injector inlet of an SSME HPOT Pre-Burner (SSME HPOTPB) combustion device. Further details of this simulation are presented in this Chapter.

Description of Tests

Tables 5.1 and 5.2 present parameters for the three run tank simulations used for this study. Figure 5.1 illustrates the time profile for the mass flow rate of propellant being expelled from the main tank bottom discharge nozzle. Figure 5.2 shows the time profile for the propellant pressure at this nozzle.

The negative time values on the x-axes of Figures 5.1 and 5.2 reflect tank pressurization processes that occur before the reference zero time (where $\tau = 0$). This reference time is preset by test operators at an arbitrarily selected event, generally the start of the main ramp up of mass flow of propellant from one or more run tanks or maximum attained power level for the test article.

For Test 004A of the RS-83 rocket engine PB (preburner), the reference zero time is when ramp up of propellant mass flow, almost a step increase, starts. Prior to this time, there is a very low mass flow rate of hydrogen being expelled from the tank, nominally two to five pounds mass per second (lb_m/sec), to bring the liquid level in the tank to be below the pressurant gas diffuser prior to the rapid increase in tank pressure, which starts

Table 5.1 Run Tank Geometric Parameters and Initial Conditions Data

Test Article:	RS-83 PB	IPD OTP	IPD OTP
Test No.:	004A	0027A	0029B
Run Tank Main Parametric Data:			
Propellant:	LH	LOX	LOX
Shape:	Sphere	Sphere	Sphere
Wall Thickness (in.):	15.5	13.4	13.4
Inside Diameter (in.):	130.2	104.72	104.72
Volume (gallons):	5002.5	2603.1	2603.1
Run Tank Diffuser:			
Outside Diameter (in.):	17.500	17.500	17.500
Volume (gallons):	25.155	13.382	13.382
Figure 3.2 Dim. Z_d (in.):	24.750	13.589	13.589
Figure 3.2 Dim. Z_{dc} (in.):	11.850	5.737	5.737
Figure 3.2 Dim. Z_{ds} (in.):	9.625	4.625	4.625
Wall Thickness (in.):	0.250	0.375	0.375
Hole Diameter (in.):	0.250	0.250	0.250
Number of Holes:	4736	2329	2329
Run Tank Initial Conditions:			
Ullage Pressure (psia):	31.19	42.38	40.00
Volume Percent Ullage:	5.00	15.00	12.50
Height of Liquid (in.):	111.94	78.71	81.11
Ht. of Liq. In Diffuser (in.):	6.49	N/A	N/A

Table 5.2 Pressurant Gas Bottle Volumes and Initial Conditions Data

Test Article:	RS-83 PB	IPD OTP	IPD OTP
Test No.:	004A	0027A	0029B
Pressurant Gas Bottle:			
Gas:	Hydrogen	Nitrogen	Nitrogen
Volume (act. cubic feet)	1875	1250	1250
Initial Press. (psia)	12670.4	12702.4	12762.8
Initial Temperature (R):	549.8	550.0	549.8

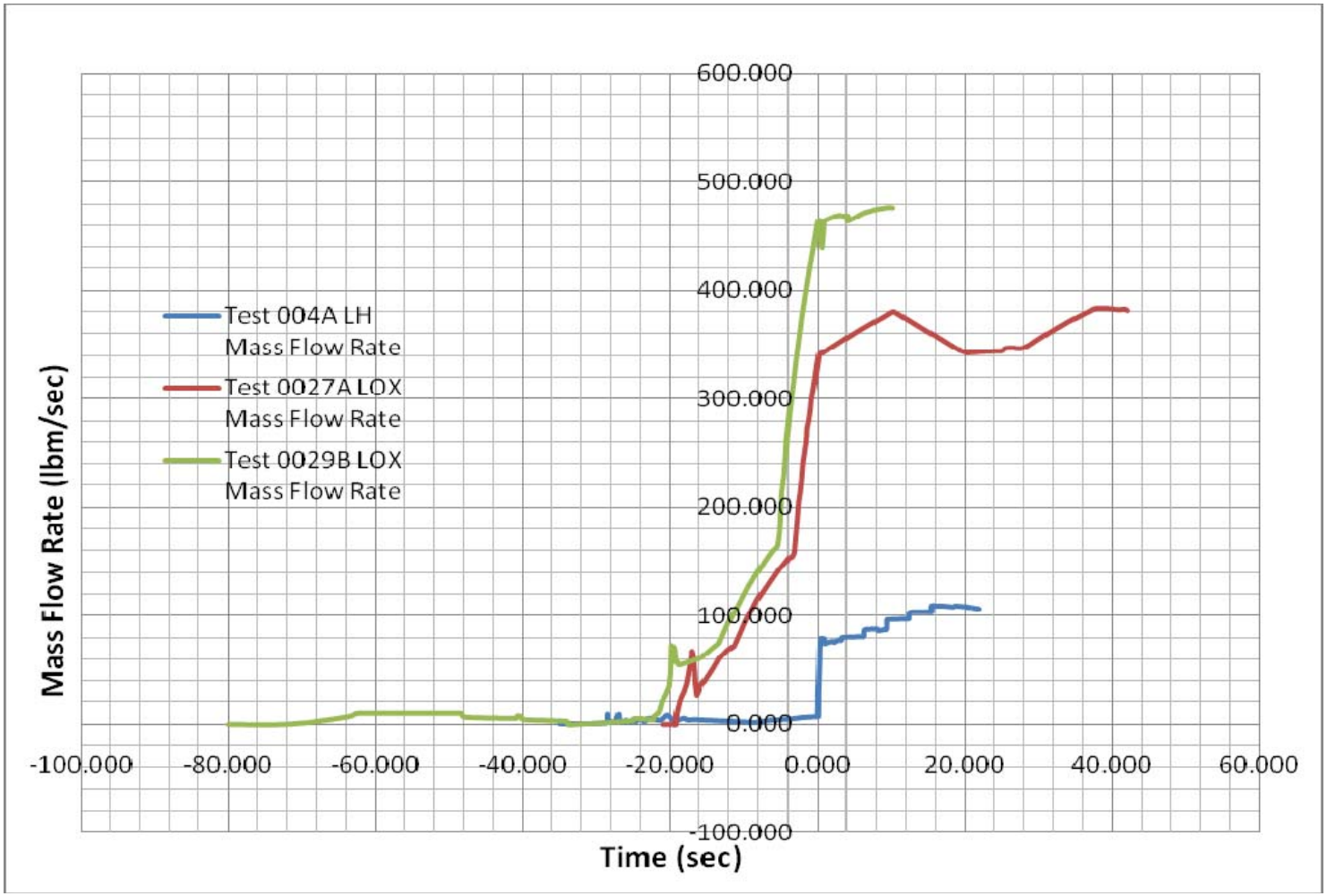

Figure 5.1 Run Tank Propellant Discharge Mass Flow Rate vs. Time Plots for Selected Rocket Engine Component Ground Tests

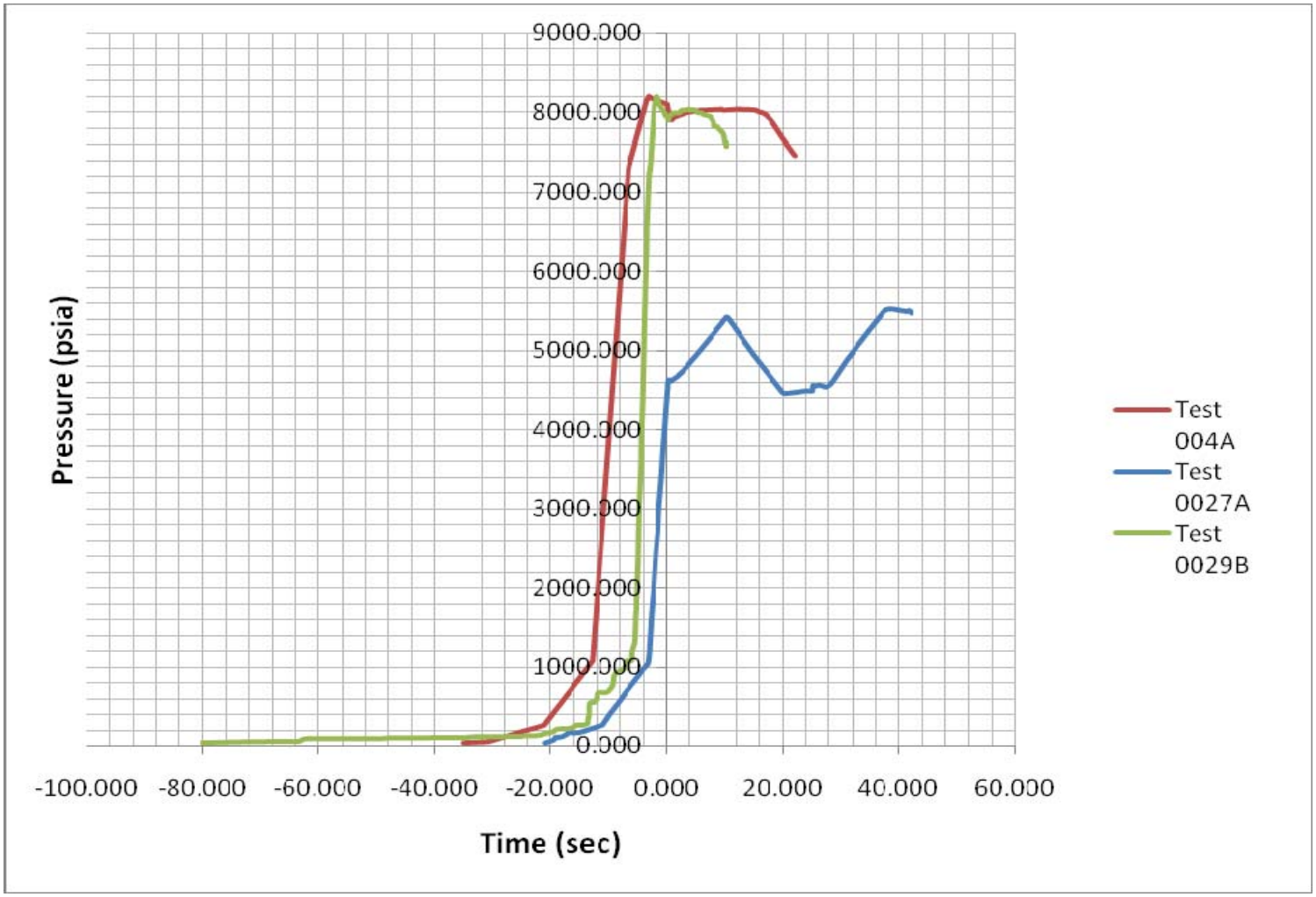

Figure 5.2 Run Tank Propellant Discharge Pressure vs. Time Plots for Selected Rocket Engine Component Ground Tests

at time equal to minus 12 seconds. This is done to prevent excessively high flow rates of pressurant gas into the tank ullage so that ullage gas collapse, due to intense mixing of the pressurant gas with liquid hydrogen propellant inside the diffuser, is prevented. From minus 12 seconds to minus 4 seconds, or 4 seconds before the reference zero time, the tank pressure is ramped up rapidly from approximately 1000 psia to 8200 psia. At the reference zero time, mass flow rate ramps up very rapidly from approximately 6.5 lbm/sec to over 78 lbm/sec in approximately 0.3 seconds. Following this ramp up, a series of much more gradual ramp ups and small step increases occur to attain mass flow rates as high as 110 lb_m/sec. Once the tank pressure reaches 8200 psia, tank pressures above or near 8000 psia are sustained for approximately 20 seconds as most of the aforementioned gradual ramp ups and small step increases in mass flow occur. After this time period, both mass flow rate and tank pressure decrease to approximately 105 lb_m/sec and 7450 psia, respectively.

Test 0027A of the IPD OTP starts at minus 21 seconds where a very gradual rate followed by a moderate rate of tank pressurization to approximately 1000 psia occurs until time of minus 3 seconds. During all but the first two seconds of this time period, the liquid oxygen expulsion mass flow rate has a general increase from zero to approximately 155 lb_m/sec with one short one-second span of decreasing mass flow. The main ramp up occurs from minus 3 seconds to reference zero time where the mass flow increases rapidly from 155 lbm/sec nominal to over 340 lbm/sec and the tank pressure increases from approximately 1000 to 4600 psia. A main stage time duration of nearly 38 seconds is maintained where a near linear ramp up, near linear ramp down, near steady, and another near linear ramp up in propellant mass flow and tank pressure sequentially occur.

Mass flow rates range between 340 and 380 lb_m/sec and run tank pressures range between 4500 and 5550 psia during the main stage time duration.

Test 0029B of the IPD OTP starts at minus 80 seconds, but zero or very low propellant mass flow rates and a very slow rate of pressure increase occurs from this time until 59-seconds later at minus 21 seconds. From minus 21 seconds to minus 5 seconds, the mass flow rate increases from approximately 20 to 160 lbm/sec and the tank pressure increases from under 200 to above 1100 psia. Following this time interval, the main ramp up occurs over a five-second span of time where propellant mass flow increases from approximately 160 to over 460 lb_m/sec. The tank pressure increases within this time span, but most of the increase occurs from minus 5 seconds to minus 2 seconds where a very rapid increase in pressure from 1100 to 8200 psia occurs. Following the zero reference time, the mass flow rate increases slightly to a little less than 480 lbm/sec and the tank pressure has a slight increase followed by a decrease to 7600 psia occurs.

RS-83 Test 004A Results

Figure 5.3 presents plots for the total mass of pressurant gas accumulated in the liquid hydrogen run tank ullage through the duration of Test No. 004A of the RS-83 PB. The plots demonstrate very good agreement between empirical and model results.

However, between time of minus 12 seconds and minus 2 seconds the model predicts slightly lower mass accumulation and rates of increase in accumulated mass than the empirical results. These deviations are substantially larger when the ullage-gas-to-tank-wall forced convective heat transfer coefficient b_1 used in Equation (3-42) of Chapter III is set to a value of 0.06 in accordance with the information in Nein and

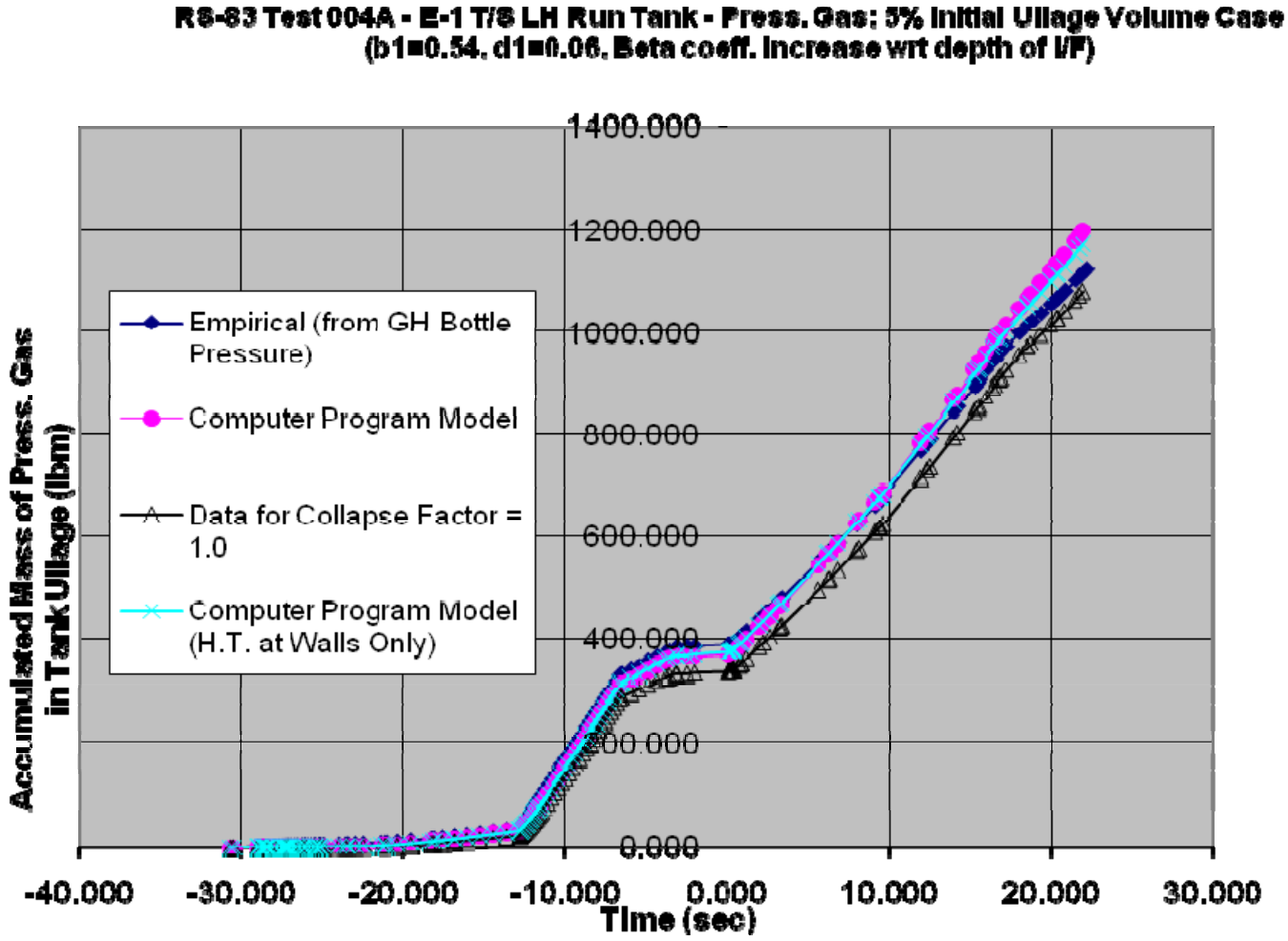

Figure 5.3 RS-83 Test 004A, Total Pressurant Gas Mass Transfer to High Pressure Liquid Hydrogen Run Tank Ullage

Thompson (1966). Increasing coefficient b_1 to 0.54 reduces the deviation to what is illustrated in Figure 5.3 between minus 12 and minus 2 seconds. Also, the trend shows the deviation between empirically derived and model results steadily increasing after 10 seconds with the empirically derived mass accumulation being less than that from the model. This deviation is much larger when the exponential decay coefficients for ullage-gas-to-tank-wall and ullage-gas-to-cryogenic-propellant-interface forced convective heat transfer, β_w and β_s reported by Nein and Thompson (1966) and given by Equation (3-46) from Chapter III, are used for the model. The use of Equations (3-43) to (3-45) and (3-51) to (3-53), from Chapter III, in the model is necessary to acquire model data results presented in Figure 5.3.

The modifications of the correlations from Nein and Thompson (1966) described above are necessary (and logical) because the cryogenic tank designs and operating conditions presented in this reference are substantially different from those of Test 004A and the other tests evaluated and presented in this study. In Nein and Thompson (1966), the propellant tanks are much larger in size and operated at low subcritical pressures for the cases where empirical and model data are compared. As a result, the distances from locations where the pressurant gas enters the ullage to the tank inner walls and to the surface of the liquid propellant are larger, especially during the initial tank pressurization process and the start of propellant expulsion from the tank. From Table 5.1, the liquid hydrogen propellant is actually filling part of the diffuser at the start of tank pressurization. For cases where empirical and model data are compared and presented in Nein and Thompson, the liquid surface is no less than two to five feet below the diffuser. Additionally, the effected inner tank-wall surfaces are between a few inches and two to

three feet away from the locations where pressurant gas enters the ullage during tank pressurization and the initial part of propellant expulsion for all tests listed on Tables 5.1 and 5.2. For cases in Nein and Thompson these distances are no less than five feet and often much greater than ten feet. Finally, the operating pressures of tanks listed on Table 5.1 are in the supercritical regime during most of the test duration, including initial tank pressurization, as indicated in Figure 5.2. This phenomenon results in significantly (two to three orders of magnitude) higher mass flow rates of pressurant gas into the tank ullage when compared to mass flow rates presented in Nein and Thompson.

The combined effects of conditions described above results in significantly higher rates of heat transfer at all ullage gas region boundaries during the initial portion of the tests evaluated in this study. Additionally, there is likely to be some level of forced mixing of cryogenic propellant with pressurant gas during the times where the propellant occupies part of the diffuser and when the interface between ullage gas and propellant is in close proximity, within one foot, of the diffuser.

As the ullage-gas-to-cryogenic-propellant interface translates downward (and away from the diffuser) during the course of a given test, the correlations presented in Nein and Thompson (1966) are likely to provide improved results. Therefore, the modifications to exponential decay coefficients for forced convective heat transfer, as presented in Chapter III, are necessary to offset the effects of increased parameter values used to model increased heat transfer and ullage gas collapse during initial tank pressurization and the initial part of propellant expulsion.

Figure 5.3 also provides plots for a collapse factor of one where the assumption of no heat transfer at ullage gas and cryogenic propellant region boundaries; except where

pressurant gas enters the ullage and propellant is expelled from the bottom of the tank. The plots of the empirically derived and model data both show total accumulated mass of pressurant gas mass in the tank to be higher than that when the collapse factor equals one, conforming to expectations and increasing level of confidence in both the empirical and model data.

Additionally, Figure 5.3 includes a plot of total pressurant gas accumulation data for the case where heat transfer is only modeled for fluid boundaries in contact with the tank walls and the assumption of no heat transfer at other (fluid-to-fluid) boundaries is applied. Interestingly, there are time spans where slightly higher accumulated mass of pressurant gas results occur as compared to the case where heat transfer is modeled at all fluid segment and regional boundaries. Further examination of model (tabular output file) data reveals that the increase in propellant temperature and specific volume, predominantly in the upper segments, dominated over the effects of decreased ullage gas segment temperatures and specific volumes during these spans of time.

Figure 5.4 is a plot of the empirically derived and model data with associated uncertainty data or upper and lower bounds derived from uncertainty analysis results. For the model data, error bars to reflect a conservatively low uncertainty of 5% are included for each data point. For the empirical data, upper and lower bounds are presented. The upper bound is based on the published repeatability error of 0.25% of full scale (20 ksig) for the transducer measuring pressurant gas supply bottle pressure and a repeatability error increasing from 0.10 to 0.40 % for the thermocouple measuring gas temperature in these bottles. These repeatability errors are based on and conservatively low compared to the published 0.5 to 1.0 % errors for the thermocouples in use. The

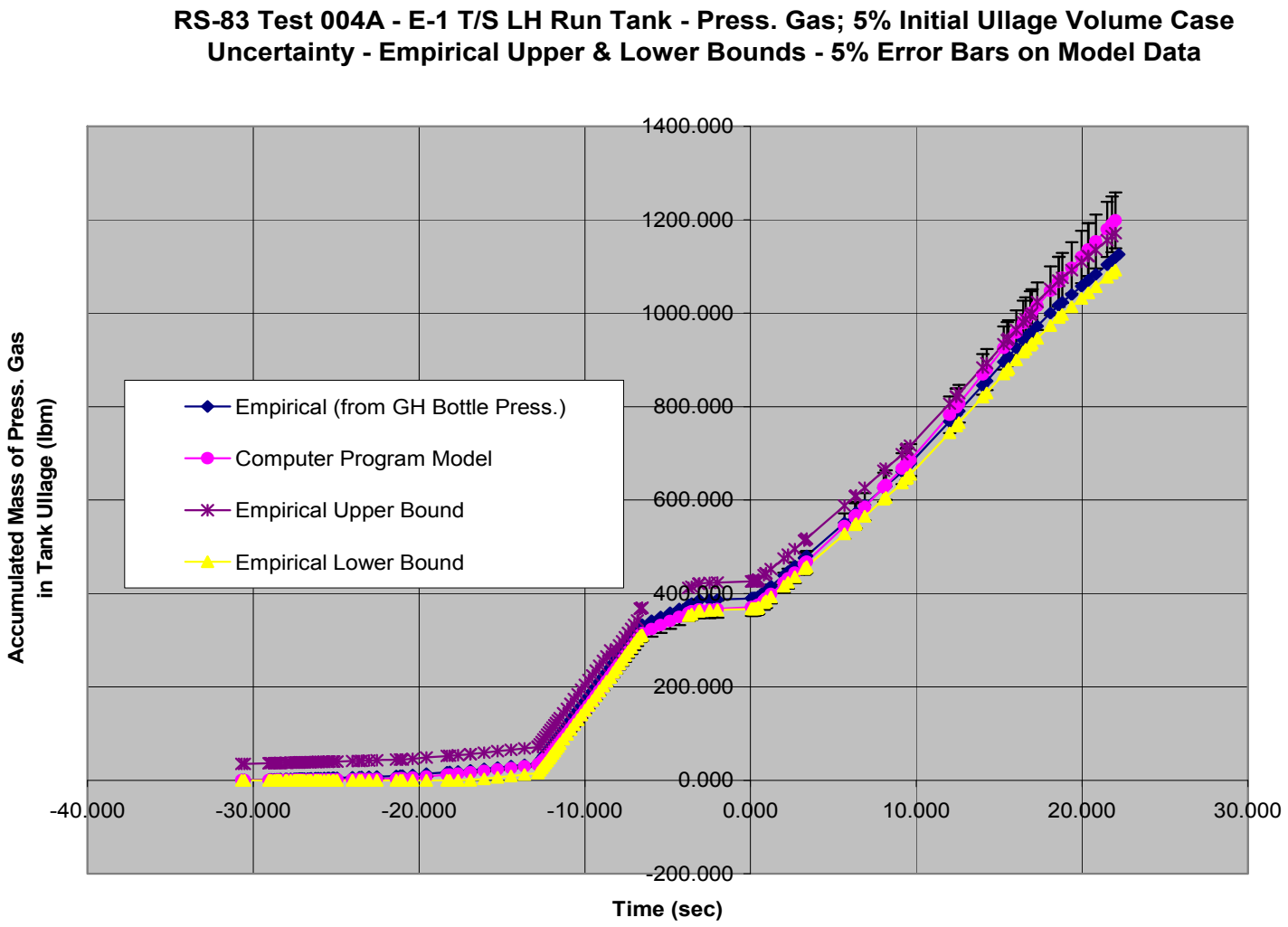

Figure 5.4 RS-83 Test 004A, Total Pressurant Gas Mass Transfer to High Pressure Liquid Hydrogen Run Tank Ullage with Uncertainty Data and Error Bounds

lower bound results are based on the aforementioned pressure transducer errors and an isentropic blowdown process in the pressurant gas supply bottles. The plots in Figure 5.4 show substantial overlap between error bounds of the model data the region between upper and lower bounds for the empirical data.

IPD Test 0027A Results

Figure 5.5 contains plots of the accumulated mass of nitrogen pressurant gas in the high pressure liquid oxygen run tank ullage through the duration of Test 0027A of the IPD OTP on the E-1 Test Stand. As with Figure 5.3, plots of empirically derived and model predicted accumulated mass of pressurant gas are presented together for comparison. However, for Test 0027A, the process in the bottles supplying nitrogen pressurant gas to the run tank deviates from an isentropic blowdown and this deviation is much greater than that of the bottles supplying hydrogen pressurant gas during Test 004A. The two blue plots in Figure 5.5 illustrate the extent of this deviation for Test 0027A. Additionally, after 20 seconds the mass of pressurant gas transferred into the tank ullage based on isentropic temperature decrease corresponding to the measured pressure in the pressurant gas supply bottles is less than that for the case corresponding to collapse factor equal to one. Therefore, the assumption of isentropic blowdown corresponding to the empirically measured bottle temperatures is a highly unlikely, if not impossible, scenario after approximately 20 seconds.

As is the case for Test 004A of the RS-83 PB, the modifications to correlations from Nein and Thompson (1966) described in the previous section of this chapter are necessary for the model data to closely match or be no less than the empirical data based

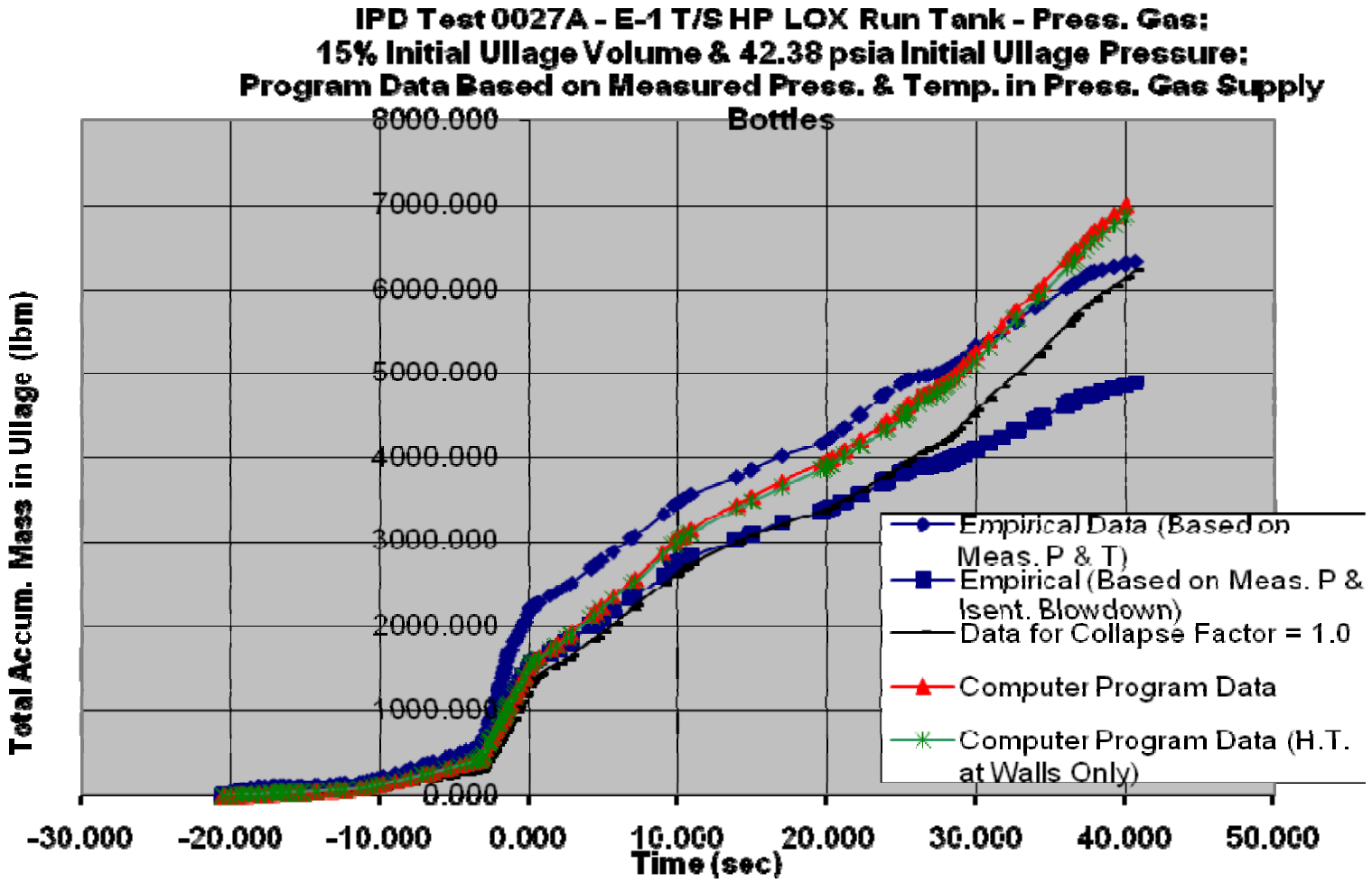

Figure 5.5 IPD Test 0027A, Total Pressurant Gas Mass Transfer to High Pressure Liquid Oxygen Run Tank Ullage

on measured pressure with isentropic temperature profile in the pressurant gas supply bottles at times that precede 3 seconds. Also, the modifications are needed to provide the reduced deviation between model data and empirical data based on measured pressure and temperature for times that follow 32 seconds.

Initial examination of Figure 5.5 indicates a very poor fit between the empirically derived and model data. However, when taking into account the uncertainties associated with the empirical and model data, the model data with a conservatively low 5% error bound, as reflected by the data point error bars, has a substantial overlap with the region between the upper and lower bounds that define the extents of uncertainty in the empirical data as illustrated in Figure 5.6.

Additionally, Figure 5.6 illustrates a very wide range between upper and lower bounds for empirical data. The upper bound is based on the published repeatability error of 0.25% of full scale (20 ksig) for the transducer measuring pressurant gas supply bottle pressure and a repeatability error increasing from 0.07 to 0.40 % for the thermocouple measuring gas temperature in these bottles. Also, an error of 1.25 R for times that follow the 38.5-second mark, to at least partially account for delayed response of the thermocouple, is applied for the upper bound results. The lower bound results are based on the aforementioned pressure transducer errors and temperatures corresponding to an isentropic blowdown process in the pressurant gas supply bottles. Where this lower bound results in an accumulated mass less than that for collapse factor of one, the lower bound is set to the latter mass.

A further explanation for the very wide range between upper and lower bounds for empirical data in Figure 5.6 and why it exists is presented later in this chapter.

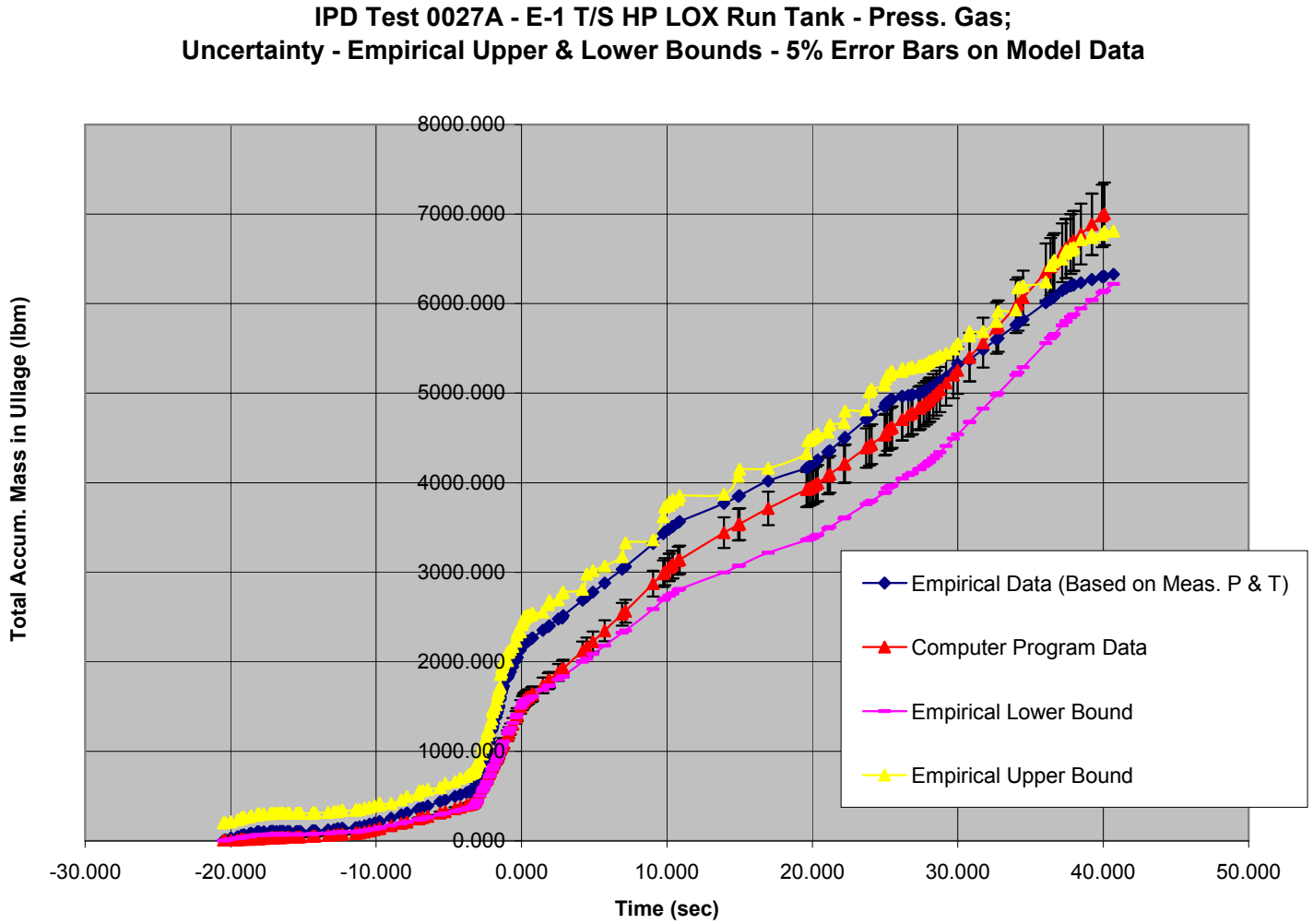

Figure 5.6 IPD Test 0027A, Total Pressurant Gas Mass Transfer to High Pressure Liquid Oxygen Run Tank Ullage with Uncertainty Data and Error Bounds

IPD Test 0029B Results

Figure 5.7 presents plots of data for accumulated mass of nitrogen pressurant gas in the high pressure liquid oxygen run tank ullage for Test 0029B of the IPD OTP. The deviations between the empirical data plots, one based on measured pressure and temperature in the pressurant gas supply bottles and the other based on the same measured pressure data with isentropic temperatures corresponding to these data, are similar in form to those for Test 0027A in Figure 5.5. Similarly, the data based on isentropic temperatures shows the highly unlikely or impossible condition of accumulated masses being less than those for collapse factor equal to one at times that follow the time span between minus 2.5 and minus 2.0 seconds.

The same modifications to correlations from Nein and Thompson (1966), described previously, have been incorporated into the model and are reflected in results for Test 0029B. Rationale for these modifications is the same as those for Tests 004A and 0027A, although the effected time spans relative to the τ equal zero reference time differ.

The comparison between empirical and model data for Test 0029B in Figure 5.7 appear to be better than that in Figure 5.5 for Test 0027A as the deviations are smaller. On closer inspection, however, the same trends exist and the phenomena behind these trends are the same.

Figure 5.8 provides the model data compared with the empirical data based on measured pressure and temperatures in pressurant gas supply bottles and with the upper and lower bounds associated with the empirical data. These bounds are set using the same methods and instrument errors described in the "IPD Test 0027A Results" section.

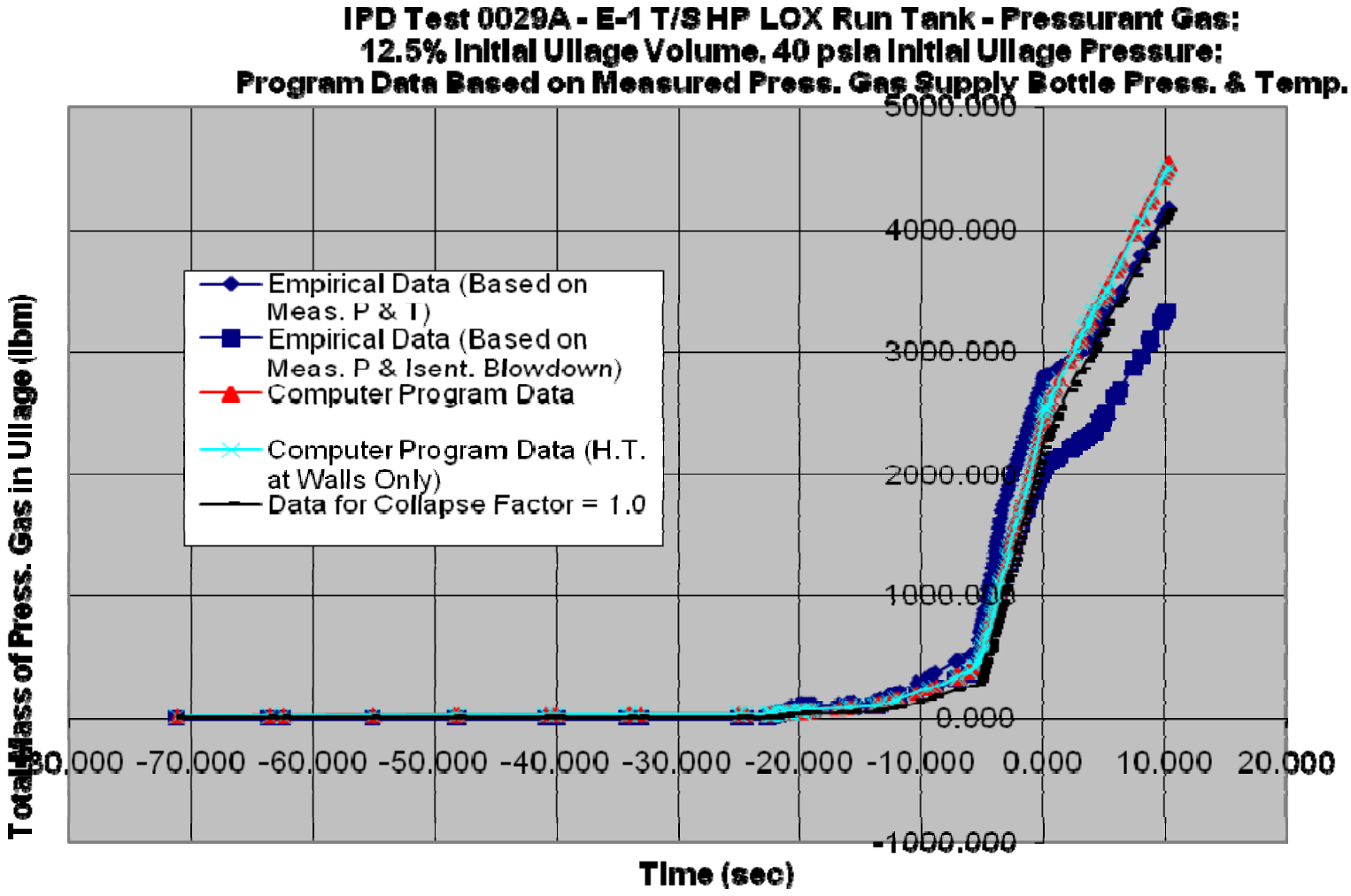

Figure 5.7 IPD Test 0029B, Total Pressurant Gas Mass Transfer to High Pressure Liquid Oxygen Run Tank Ullage

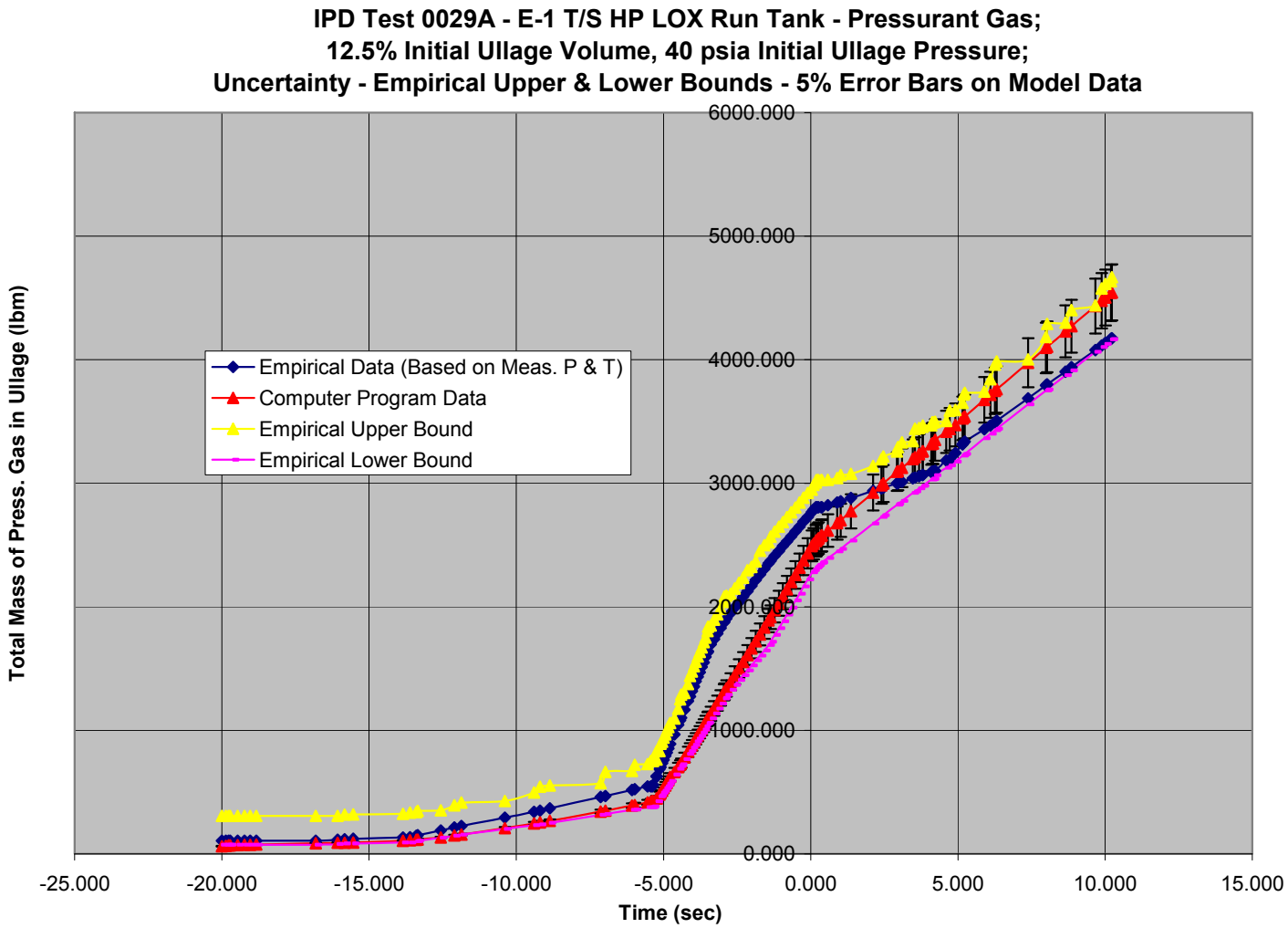

Figure 5.8 IPD Test 0029B, Total Pressurant Gas Mass Transfer to High Pressure Liquid Oxygen Run Tank Ullage with Uncertainty Data and Error Bounds

As with plots in Figures 5.4 and 5.6, Figure 5.8 shows that model data with an applied 5% upper and lower error band has a very substantial overlap with the region between the upper and lower bounds for empirical data.

Further Evaluation of Empirical Data of Tests 0027A and 0029B

Upon review of plots of pressurant gas supply bottle pressures and temperatures versus time for Tests 0027A and 0029B, an apparent time lag or delayed response of the thermocouple measuring bottle gas temperature is observed. Furthermore, an apparent hysteresis effect is observed where a rapid change in the thermocouple reading results in an error where the reading is 1.75 to 2.5 R below the actual temperature.

Figure 5.9 presents a plot of both gas bottle pressure and temperature versus time for Test 0029B. If the thermocouple was working properly, e.g. with minimal delays in response to decreasing temperatures, the form of the temperature plot should have the same shape as that of the pressure plot. The sudden change in slope for the pressure plot starting at minus 5 seconds and the downward slope and shape of the curve from this time to time zero should also be present for the temperature line. The sudden change in slope for the pressure plot starting at time τ equal to approximately 5 seconds and the continuation of this near linear slope to 10 seconds should also be reflected in the temperature plot. Further examination indicates that empirical data based on measured pressure and temperature in Figure 5.8 would more closely match the model data if the temperature plots in Figure 5.9 did follow the trends (times of sudden slope changes and general shape of the downward slopes at given time spans) seen in the pressure plots.

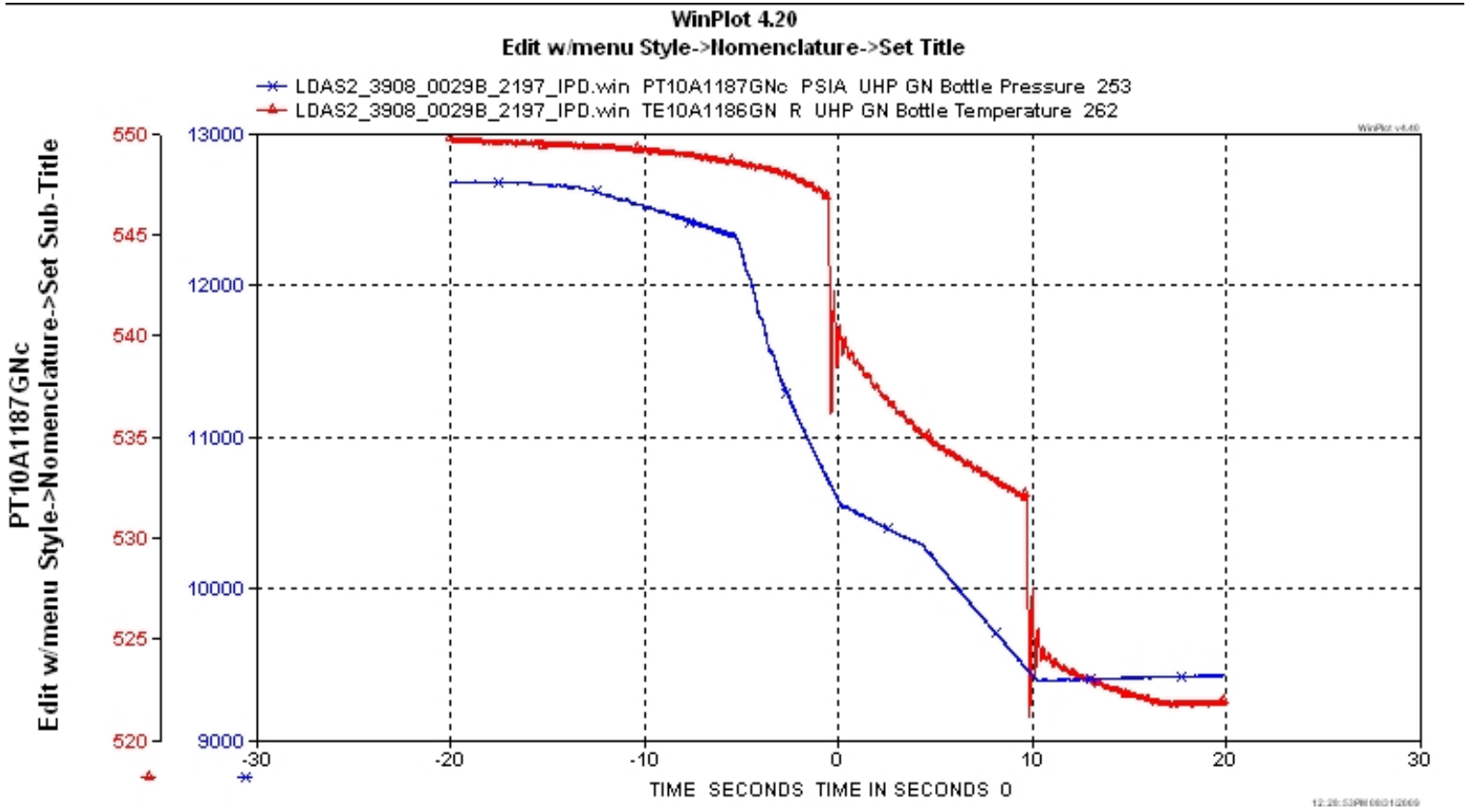

Blue plot and y-axis values indicate pressure in psia; Red plot and y-axis values indicate temperature in R

Figure 5.9 Pressure and Temperature vs. Time for Ultra-High Pressure Gaseous Nitrogen Bottles Supplying High Pressure Liquid Oxygen Run Tank for Test 0029B on E-1 Test Stand

There should also be no rapid or near step decrease in temperatures at times just prior to time zero and 10 seconds.

Similar findings exist when the pressurant gas supply bottle pressure and temperature data from Test 0027A are plotted as was done for Test 0029B in Figure 5.9. Two similar sudden, near step, temperature decreases exist for data from Test 0027A and the general form and shape of the temperature plot does not match those of the pressure plot.

Further evaluation indicates that the problems associated with the thermocouples providing pressurant gas bottle temperature data are due in large part to their locations in the system. Referring to Figure 1.3 in Chapter I, a thermocouple was placed in one end of one of the pressurant gas supply bottles. A better location would be inside the main discharge nozzle of one of the bottles, because flowing gas around the thermocouple improves its response to temperature transients. Since the plots in Figures 5.5 and 5.7 indicate that the blowdown process in the pressurant gas supply bottles is not isentropic (heat transfer from bottle walls to gas inside the bottles cannot be neglected), the importance of accurate thermocouple readings is enhanced.

Collapse Factor Data

Figures 5.10 and 5.11 provide instantaneous collapse factor data for Tests 004A and 0027A. For the empirical data plots on both figures, a very high fluctuation in instantaneous collapse factors is observed at times prior to the zero reference time. For the model data, these high fluctuations are apparent in Figure 5.11 for times prior to τ equal to minus 15-seconds. These high fluctuations are partially attributed to the very

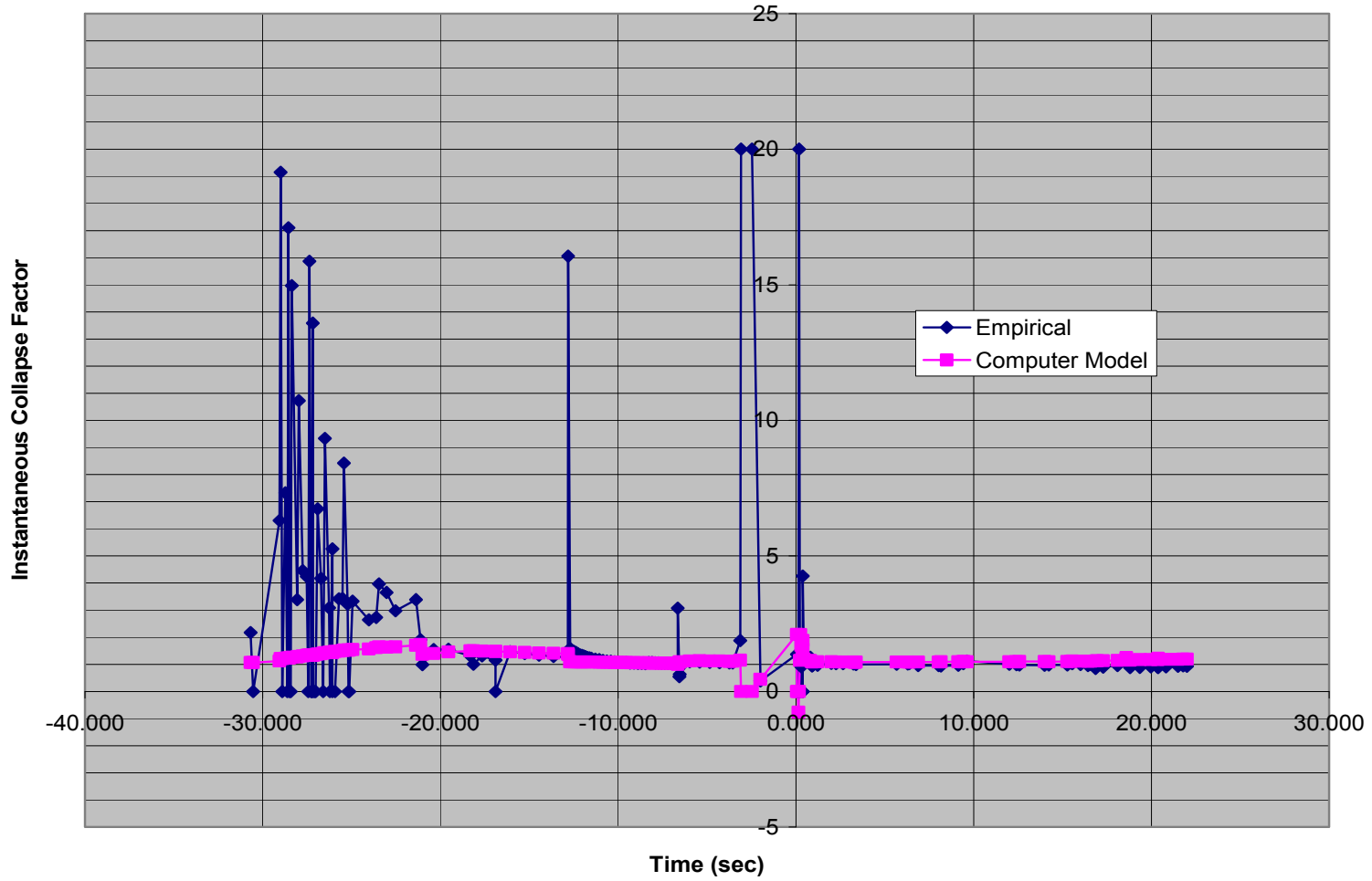

Figure 5.10 RS-83 Test 004A, Instantaneous Collapse Factor for High Pressure Liquid Hydrogen Run Tank

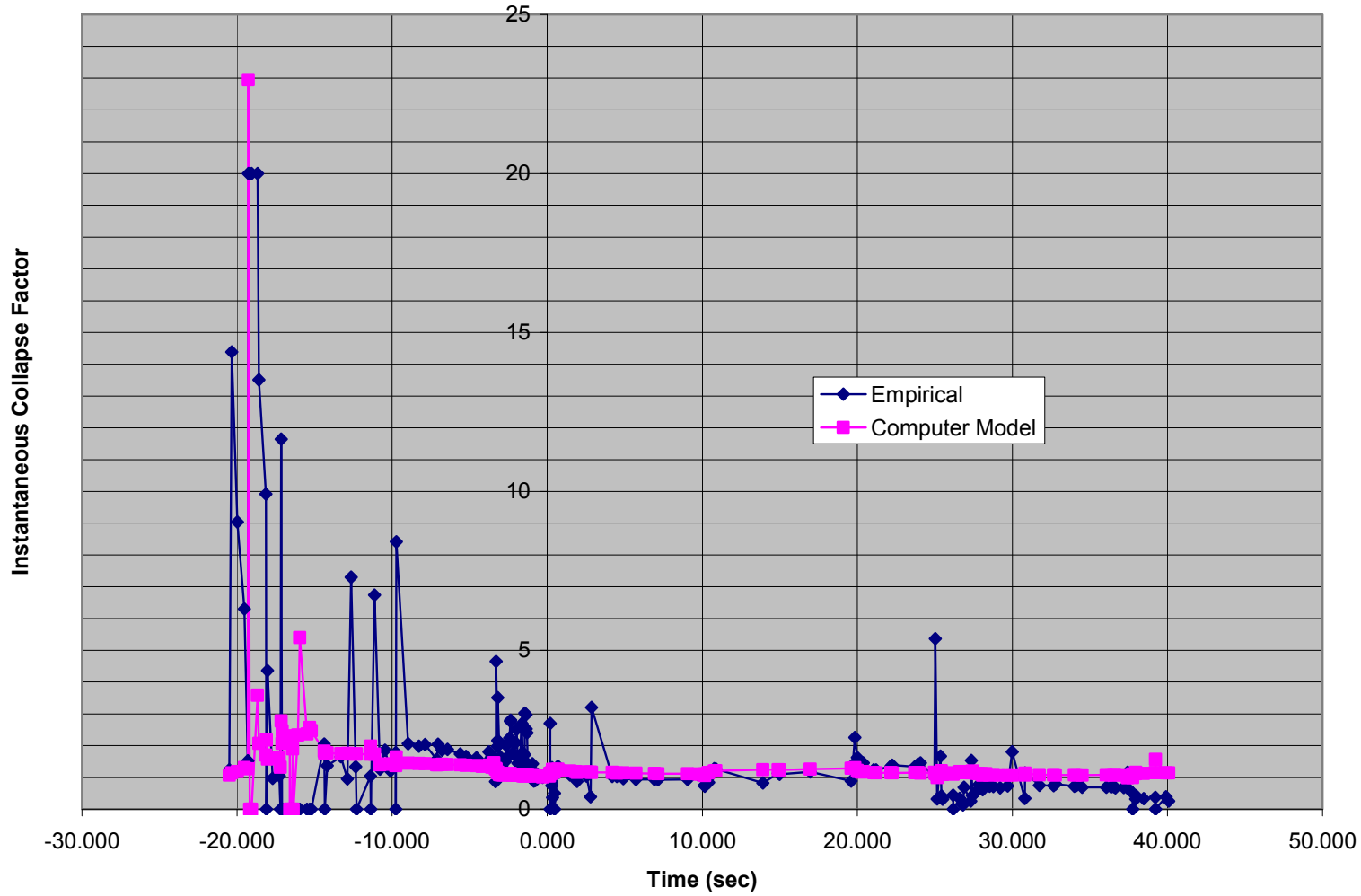

Figure 5.11 IPD Test 0027A, Instantaneous Collapse Factor for High Pressure Liquid Oxygen Run Tank

high sensitivity of computed mass flow rates to measured gas pressures and temperature in the pressurant gas supply bottles. During the first part of run tank pressurization, time less than minus 12 seconds for Test 004A and less than minus 3 seconds for Test 0027A, the mass flow rates of pressurant gas into the run tank ullage are very low in comparison to mass flow rates that occur later when the tank pressure or propellant expulsion mass flow rates are ramped up more rapidly. Also the total mass of pressurant gas in the bottles is significantly, two to three orders of magnitude, higher than the change in mass across incremental time steps during these times. As a result, small errors or variations in measured pressures and temperatures can be magnified by two or three orders of magnitude when computing changes in mass of pressurant gas across small time steps. These magnifying effects are deemed to be the major contributors to the observed fluctuations prior to the minus 12-second mark in Figure 5.10 and prior to the minus 3-second mark in Figure 5.11.

The other contributor to observed fluctuations in empirical instantaneous collapse factors is to actual system instabilities during the time spans when the tank ullage gas volume is small, less than 10- to 15-% of the tank volume, and tank pressure ramp rates are high. During these times, delays in feedback response of run tank pressure control valves are likely to be causing mass flow rate of pressurant gas into the tank ullage to overshoot and undershoot ideal demand flow rate requirements.

The high fluctuations observed in model data are limited to the first five seconds of Test 0027A in Figure 5.11. These are attributed to precision limits of program computations as the change in pressurant gas bottle mass is extremely small in comparison to the total mass of gas in the bottles during this time period. For the

remaining times, the fluctuations observed for the empirical data are not present in model data because the model is not affected by the instrument reading errors and variations nor the control feedback response delays described above.

For all plots in Figures 5.10 and 5.11, the trends show collapse factors as high as 2.0 to 2.5 for sustained time periods up to 3 seconds with some intermittent short duration spikes as high as 6.5 during the initial tank pressurization process, start of propellant expulsion, and main ramp ups in propellant expulsion flow rates and tank pressures. Following these processes, the instantaneous collapse factor decreases to and then maintains nominal values between 1.05 and 1.15 for the remaining test duration. In Figure 5.11, the cases where empirical collapse factor data have values less than 1.0 are attributed to the issues with pressurant gas bottle temperature readings described in the previous section of this chapter.

Fortunately, the increases in collapse factors above 2.0 to 2.5 occur during time spans when the ideal pressurant gas mass flow rates are much less than those during the main ramp ups in propellant expulsion mass flow rates and tank pressures. This serves to prevent the need to design and build excessively large and costly systems for supplying pressurant gas to the run tanks.

Special Case; SSME HPOT Test 74

As a special case to provide further support to the validity of model data produced for high pressure run tanks on the E-1 Test Stand at NASA/SSC, the model has been used to simulate tank pressurization and propellant expulsion processes in the high pressure

liquid hydrogen run tank at the Pratt and Whitney E-8 Test Stand in West Palm Beach, Florida.

For this case, the high pressure liquid hydrogen run tank is supplying propellant to a mixer where it is mixed with gaseous hydrogen. The same bottles supplying pressurant gas to the run tank are also supplying gas to the mixer. The purpose of the mixer is to mix the incoming propellant from the run tank and gas from the bottles to discharge a cold gas at a nominal temperature of 275 R. This cold gas supplies the fuel injector inlet of an SSME HPOTPB which in turn supplies a heated gas mixture of hydrogen and steam to drive the turbine of an SSME HPOT.

Data from Test 74 of a development prototype SSME HPOT were used for this study. Unfortunately, portions of these data from this test and other similar and useful tests are no longer available and could not be recovered from archives. These data include the time profile for the following: 1.) temperatures in pressurant gas supply bottles, 2.) mass flow rates of gaseous hydrogen entering the mixer, 3.) mixer inlet pressures, and 4.) mass flow rates and pressures at the SSME HPOTPB fuel injector inlet. Therefore, various assumptions had to be applied in order to model the high pressure liquid hydrogen run tank processes during this test. These include: 1.) deviation from isentropic temperatures in pressurant gas supply bottles that increases linearly from zero to 7 R from the zero reference time to 55.25 seconds, 2.) pressure drop from run tank discharge to SSME HPOTPB fuel injector inlet during start of flow and ramp up to main stage is a linear function of the mass flow rate at this interface, and 3.) hydrogen temperature at the SSME HPOTPB fuel injector inlet is maintained at 275 R for the full duration of the test. The first assumption is reasonable and realistic and there are

available data that support its validity, but the deviation following a linear profile is likely an inexact approximation and there is a 2.5 R uncertainty in the final 7 R deviation. The second assumption is probably not valid, but pressure has a second order effect on enthalpy in comparison to temperature. Therefore, the expected pressure errors should yield minor, or negligible, errors for the proportional mass flow rates of fluids into the mixer. The third assumption is valid during main stage and it is generally valid for most of the main ramp up of flow into the SSME HPOTPB fuel injector if the systems are operating as intended. However, there have been tests where the fuel injector inlet temperature has differed by more than 175 R from 275 R immediately following ignition in the SSME HPOTPB and during the initial parts of start transients for various reasons.

Figure 5.12 contains plots of the mass flow rate of propellant out of the run tank and the expected mass flow rate of gas from the pressurant gas supply bottles to the mixer upstream of the SSME HPOTPB fuel injector inlet. The propellant mass flow rate data are obtained from turbine flow-meter volumetric flow measurements and fluid densities computed from measured pressures and temperatures on the upstream side of this flow-meter. The mass flow rates of gas from the bottles to the mixer, called "Auxiliary GH Mass Flow Rate" in the figure, are determined from an energy balance where total enthalpy at the SSME HPOTPB fuel injector inlet equals total enthalpy of fluids entering the mixer.

Figure 5.13 includes plots of empirically derived and model data for the total mass of pressurant gas accumulated in the run tank ullage for Test 74 of the SSME HPOT on the Pratt and Whitney E-8 Test Stand. The comparison between empirically derived and model data is excellent given the assumptions described previously in this section. A

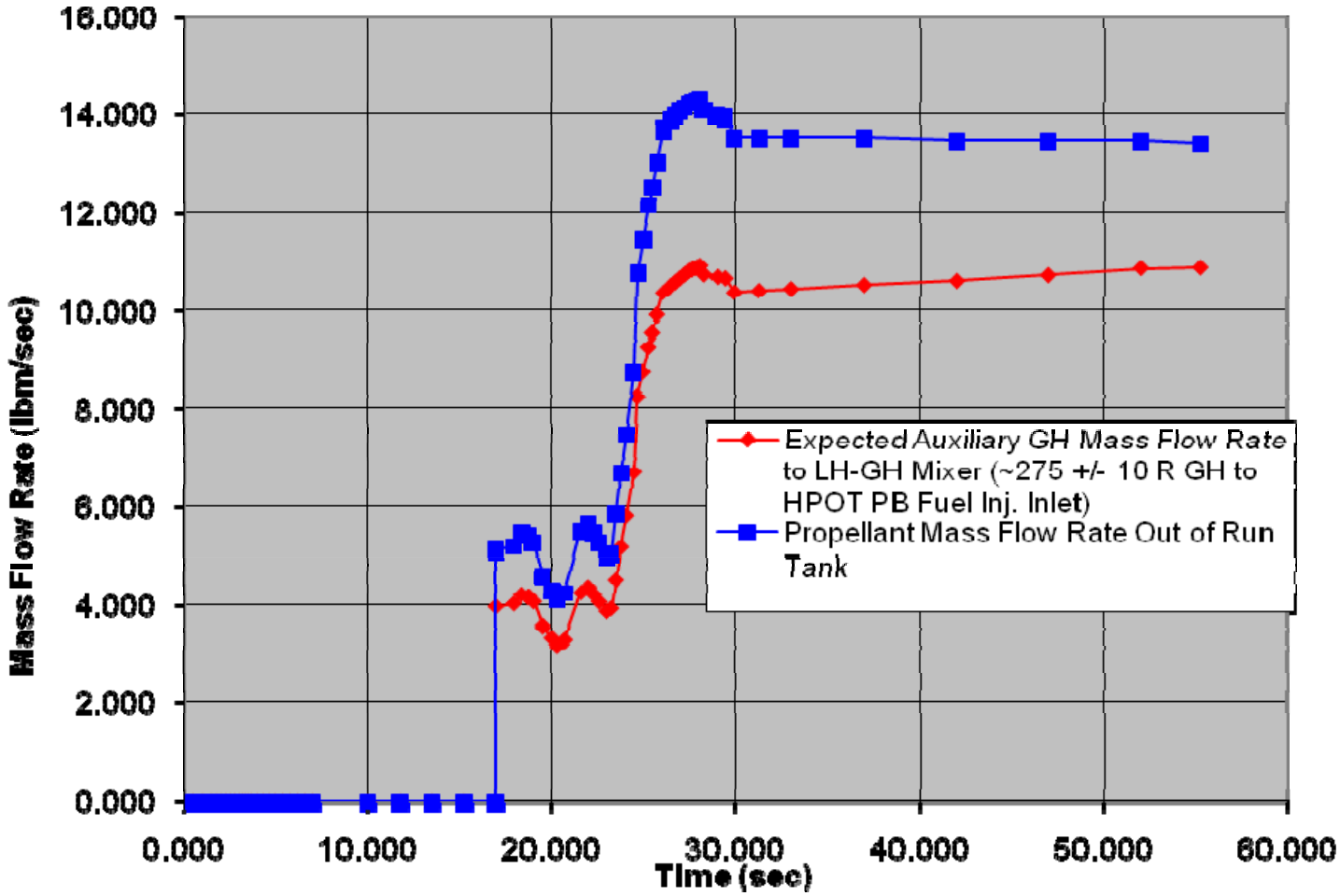

Figure 5.12 Special Case: Auxiliary Mass Flow from Pressurant Gas Supply Bottles and Input Mass Flow from High Pressure Liquid Hydrogen Run Tank; SSME HPOT on Pratt & Whitney E-8 Test Stand, Run Tank and Auxiliary GH Supplying Mixer that Supplies Pre-Burner Fuel Injector Inlet

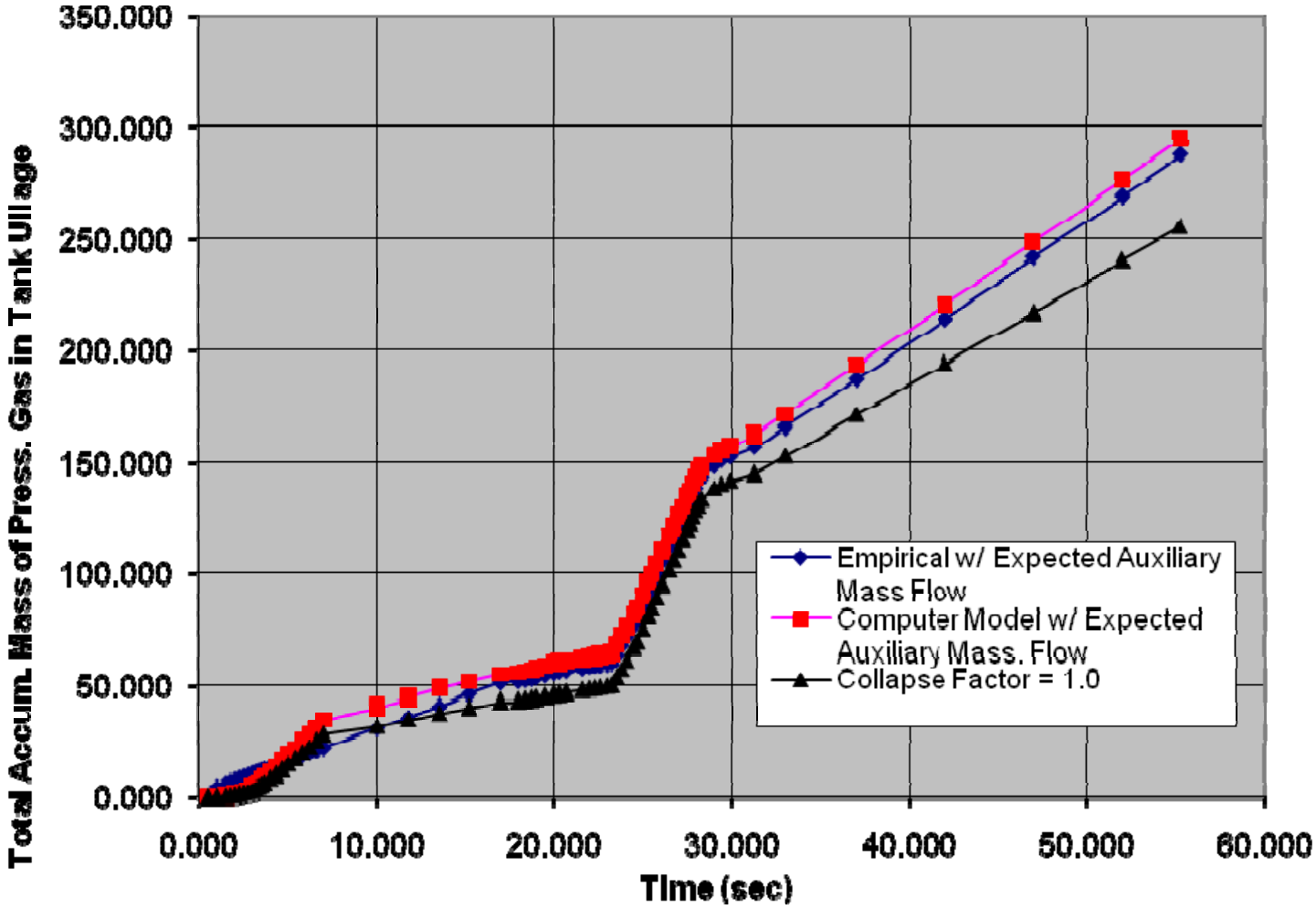

Figure 5.13 Special Case: Total Pressurant Gas Mass Transfer to Tank Ullage; SSME HPOT on Pratt & Whitney E-8 Test Stand; High Pressure Liquid Hydrogen Run Tank Supplying Mixer that Supplies Pre-Burner Fuel Injector Inlet

plot of the computed mass of pressurant gas mass transferred into the tank ullage under the conditions of no ullage gas collapse, collapse factor equal to one, is also included in Figure 5.13 for comparison. The plots for both the empirical and model data are above the plot for collapse factor equal to one with the exception of the time interval between six and 10 seconds for the empirical data. This serves to enhance the confidence in the empirical and model data.

CHAPTER VI

SUMMARY AND CONCLUSIONS

A model for predicting pressurant gas requirements in cryogenic propellant run tanks operating at high supercritical pressures has been developed, tested, and validated. A variety of different run tank sizes and operating conditions have been evaluated during model validation. Comparison of model results with empirical data shows good to excellent agreement when accounting for uncertainties in empirical data.

The model incorporates the use of heat transfer correlations based on the best of those used in previously developed models. A number of enhancements to these correlations, mainly to reflect increased convection heat transfer rates at ullage gas boundaries when ullage volumes are small, have been incorporated. These enhancements are based on sound physics and have yielded consistent improvements in results for all evaluated cases.

The model also incorporates methods to account for effects of non-uniform temperatures and properties in fluid regions and tank walls. The methods are based on those from previously developed models that have resulted in the best model predictions as compared to empirical data. Additionally, enhancements to previously developed explicit numerical finite-difference computation methods to simulate transient heat conduction in the tank wall are employed where the spacing of finite

element boundaries increase from inner to outer wall to provide high accuracy and improved computational efficiency (reduced number of repeated computations).

Future model development and validation is recommended to further substantiate results from this study and to improve the acquisition of empirical data used to validate the model. The improvements include locating instruments in system locations that provide the needed response to transient conditions and acquiring accurate measurements of initial cryogenic propellant liquid levels immediately before tank pressurization.

This study and its results have provided a significant advancement to the design and operation of rocket propulsion testing facilities expanding into the realm of cryogenic propellant run systems operating at supercritical pressures.

BIBLIOGRAPHY

"Main Propellant Tank Pressurization System Study and Test Program, Vol. I, Liquid Hydrogen and Liquid Oxygen," (1961). Lockheed Report ER-5238.

"Main Propellant Tank Pressurization System Study and Test Program, Vol. III, Design Handbook," (1961). Lockheed Report ER-5296, Vol. III.

"Main Propellant Tank Pressurization System Study and Test Program, Vol. IV, Computer Program," (1961). Lockheed Report ER-5296, Vol. IV.

"FORTRAN Program for the Analysis of a Single Propellant Tank Pressurization System," (1963). Rocketdyne Report R-3936-1. Also NASA-CR-53305.

_____ (1990). Handbook of Compressed Gases, 3rd Edition, Van Norstrand Reinhold, New York, pp. 34-36

Akyuzlu, K. M., (1993). "A Parametric Study of Boiloff Initiation and Continuous Boiling Inside a Cryogenic Tank Using A One-Dimensional Multi-Node Nonequilibrium Model," Heat Transfer Division Phase Change Heat Transfer Proceedings of the 1993 ASME Winter Meeting, Vol. 262, pp. 9-14

Al-Najem, N. M., Al-Marafie, A. M., & Ezuddin, K. Y. (1993). "Analytical and Experimental Investigation of Thermal Stratification in Storage Tanks," International Journal of Energy Research, Vol. 17, pp. 77-88.

Anderson, J. E., Scott, O. L., & Brady, H. F. (1967). "Advanced Pressurization Systems for Cryogenic Propellants," NASA-CR-54467.

Arnett, R. W. & Voth, R. O. (1972). "A Computer Program for the Calculation of Thermal Stratification and Self-Pressurization in a Liquid Hydrogen Tank," NASA-CR-2026.

Atkinson, M. C. M., Beduz, C., Rebiai, R., & Scurlock, R. G. (1984). "Heat and Evaporative Mass Transfer Correlation at the Liquid-Vapour Interface of Cryogenic Liquids," Proceedings of the 10th Cryogenic Engineering Conference, ed. Collan, et al., Butterworth Publishing Co., Northamptonshire, UK, pp. 95-97.

Aydelott, J. C. (1983). "Modeling of Space Vehicle Propellant Mixing," NASA-TP-2107.

Bailey, W. J., Weiner, S. P., Beckman, D. H., Dennis, M. F., & Martin, T. A. (1990). "Cryogenic On-Orbit Liquid Depot Storage, Acquisition and Transfer Satellite (COLD-SAT)," NASA-CR-185247.

Bailey, W. J. & Arif, H. (1992). "Cryogenic Fluid Management Investigations Using the CONE Flight Experiment," Cryogenics, Vol. 32, No. 2, pp. 220-229.

Baral, H. S. (1988). "Liquid Propellant Pressurization System," Journal of the Institution of Engineers, Mechanical Engineering Division, Calcutta, India, Vol. 68, No. 5, pp. 127-131.

Barber. H. E. (1966). "Advanced Pressurization Systems Technology Program Final Report," Technical Report AFRPL-TR-66-278, Edwards, CA.

Barnett, D. O., Winstead, J. W., & McReynolds, L. S. (1964). "An Investigation of Liquid-Hydrogen Stratification in a Large Cylindrical Tank of the Saturn Configuration," Advances in Cryogenic Engineering, Vol. 11, ed. Timmerhaus, K. D., Plenum Press, New York, NY, pp. 314-324.

Barnett, D. O. (1967). "Liquid Nitrogen Stratification Analysis and Experiments in a Partially Filled, Spherical Container," Advances in Cryogenic Engineering, Vol. 13, ed. Timmerhaus, K. D., Plenum Press, New York, NY, pp. 174-187.

Barrere, M., Jaumette, A., de Veubeke. B. F., & Vandenkerckhove, J. (1960). Rocket Propulsion, Elsevier Publishing Company, Amsterdam, London, New York, Princeton, pp. 474-480.

Beduz, C., Rebiai, R., & Scurlock, R. G. (1984). "Thermal Overfill, And The Surface Vaporisation of Cryogenic Liquids Under Storage Conditions," Advances in Cryogenic Engineering, Vol. 29, ed. Fast, R. W., pp. 793-803.

Beekman, D. H., & Martin, T. A. (1991). "Detailed Modeling of The No-Vent Fill Process," Advances in Cryogenic Engineering, Vol. 37 Part B, ed. Fast, R. W., Plenum Press, New York, NY, pp. 1237-1246.

Bentz, M. D., Meserole, J. S., & Knoll, R. H. (1990). "Tank Pressure Control Experiment – A Low-G Mixing Investigation," AIAA Paper 1990-2376.

Bentz, M. D., Meserole, J. S., & Knoll, R. H. (1992). "Jet Mixing in Low Gravity – Results of the Tank Pressure Control Experiment," AIAA Paper 1992-3060.

Bentz, M. D. (1993). "Tank Pressure Control in Low Gravity by Jet Mixing," NASA-CR-191012.

Blackmon, J. B. (1974). "Design, Fabrication, Assembly, and Test of a Liquid Hydrogen Acquisition Subsystem," NASA-CR-120447.

Blatt, M. H. (1968). "Empirical Correlations for Pressure Rise in Closed Cryogenic Containers," Journal of Spacecraft and Rockets, Vol. 5, No. 6, pp. 733-735.

Bourgarel, M., Clement, R., Segel, M. (1968). "A Cryogenic Propellant Tank Pressurization Analysis," Proceedings of the 2nd International Cryogenic Engineering Conference, Iliffe Science and Technology Publications, Guildford, UK, pp. 89-101.

Bowersock, D. C., Gardner, R. W., & Reid, R. C. (1960). "Pressurized Transfer of Cryogenic Liquids," Advances in Cryogenic Engineering, Vol. 4, ed. Timmerhaus, K. D., Plenum Press, New York, NY, pp. 342-356.

Bowersock, D. C., & Reid, R. C. (1961). "An Analytical Method for Estimating Gas Requirements in the Pressurization and Transfer of Cryogenic Fluids," Advances in Cryogenic Engineering, Vol. 6, ed. Timmerhaus, K. D., Plenum Press, New York, NY, pp. 261-271.

Cady, E. C., Flaska, T. L., & Worrell, P. K. (1990). "In-Tank Thermodynamics of Slush Hydrogen for the National Aerospace Plane," Advances in Cryogenic Engineering, Vol. 35, Part B, ed. Fast, R. W., Plenum Press, New York, NY, pp. 1755-1766.

Chato, D.J. (1991). "Ground Testing on the Nonvented Fill Method of Orbital Propellant Transfer: Results of Initial Test Series," AIAA Paper 1991-2326.

Chato, D. J. (1993). "Ground Testing for the No-Vent Fill of Cryogenic Tanks: Results of Tests for a 71 Cubic Foot Tank," AIAA Paper 1993-1967.

Chen, I. M. & Anderson, R. E. (1972). "A Thermal Stratification Model of a Cryogenic Tank at Supercritical Pressures," Advances in Cryogenic Engineering, Vol. 17, ed. Timmerhaus, K. D., Plenum Press, New York, NY, pp. 475-486.

Churchill, S. W. & Chu, H. H. S. (1975). "Correlating Equations for Laminar and Turbulent Free Convection from a Vertical Plate," International Journal of Heat and Mass Transfer, Vol. 18, Pergamon Press, Oxford, UK, pp. 1323-1329.

Clark, J. A., Van Wylen, G. J., & Fenster, S. K. (1960). "Transient Phenomena Associated with the Pressurized Discharge of a Cryogenic Liquid from a Closed Vessel," Advances in Cryogenic Engineering, Vol. 5, ed. Timmerhaus, K. D., Plenum Press, New York, NY, pp. 467-480.

Clark, J. A. (1965). "A Review of Pressurization, Stratification, and Interfacial Phenomena," International Advances in Cryogenic Engineering, Vol. 11, ed. Timmerhaus, K.D., Plenum Press, New York, NY, pp. 259-283.

Clark, J. A., & Barakat, H. Z. (1965). "Transient, Laminar, Free-Convection Heat and Mass Transfer in Closed, Partially Filled, Liquid Containers," Proceedings of the Conference on Propellant Tank Pressurization and Stratification, Vol. 1, NASA Marshall Space Flight Center, Huntsville, AL, pp. 119-189.

Clark, J. A. (1968). "Cryogenic Heat Transfer," Advances in Heat Transfer, Vol. 5, eds. Irvine, T. F., & Hartnett, J. P., Academic Press, New York, NY, pp. 375-400.

Cowart, E. G. (1968). "Saturn V S-II Final Propulsion System Performance Prediction Flight SA-503, Vol. II of III," dated July 15, 1968, Boeing Space Division Document No. D5-15530-3A.

Coxe, E. F., & Tatom, J.W. (1962). "Analysis of the Pressurizing Gas Requirements for an Evaporated Propellant Pressurization System," Advances in Cryogenic Engineering, Vol. 7, ed. Timmerhaus, K. D., Plenum Press, New York, NY, pp. 234-243.

Denisov, K. P., Lukovskij, A. P., Ledneva, L. P., Chuherov, A. I., Federov, V. I. (1981). "Experimental Study of the Effect of Gas Injection Velocity on Heat and Mass Transfer in the Gas Volume of a Tank," Aviatsionnaia Tekhnika, No. 1, 1981, pp. 84-86.

DeWitt, R. L., & McIntire, T. O. (1974). "Pressurant Requirements for Discharge of Liquid Methane from a 1.52-Meter- (5-ft-) Diameter Spherical Tank Under Both Static and Slosh Conditions," NASA-TN-D-7638.

Ede, A. J. (1967). "Advances in Free Convection," Advances in Heat Transfer, Vol. 4, eds. Irvine, T. F., & Hartnett, J. P., Academic Press, New York, NY, pp. 1-47.

Epstein, M., Georgius, H. K., & Anderson, R. E. (1965). "A Generalized Propellant Tank-Pressurization Analysis," International Advances in Cryogenic Engineering, Vol. 11, ed. Timmerhaus, K. D., Plenum Press, New York, NY, pp. 290-302.

Epstein, M. (1965). "Prediction of Liquid Hydrogen and Oxygen Pressurant Requirements," International Advances in Cryogenic Engineering, Vol. 11, ed. Timmerhaus, K. D., Plenum Press, New York, NY, pp. 303-307.

Epstein, M., & Anderson, R. E. (1968). "An Equation for the Prediction of Cryogenic Pressurant Requirements for Axisymmetric Propellant Tanks," Advances in Cryogenic Engineering, Vol. 13, ed. Timmerhaus, K. D., Plenum Press, New York, NY, pp. 207-214.

Estey, P. N., Lewis, D. H., & Connor, M. (1983). "Prediction of Propellant Tank Pressure History Using State Space Methods," Journal of Spacecraft and Rockets, Vol. 20, No. 1, Jan.-Feb. 1983, pp. 49-54.

Fan, B. C., Chu, J. C., & Scott, L. E. (1969) "Thermal Stratification in Closed Cryogenic Containers," Advances in Cryogenic Engineering, Vol. 14, ed. Timmerhaus, K. D., Plenum Press, New York, NY, pp. 249-257.

Gebhart, B. (1973). "Natural Convection Flows and Stability," Advances in Heat Transfer, Vol. 9, eds. Irvine, T. F., & Hartnett, J. P., Academic Press, New York, NY, pp. 273-297.

Gebhart, B. (1993). Heat Conduction and Mass Transfer, McGraw-Hill, New York, NY.

Ghaddar, N. K., Al-Marafie, A. M., & Al-Kandari, A. (1989). "Numerical Simulation of Stratification Behavior in Thermal Storage Tanks," Applied Energy, Vol. 32, No. 3, Applied Science Publishers, Barking, UK, pp. 225-239.

Gluck, D. F., & Kline, J. F. (1962). "Gas Requirements in Pressurized Transfer of Liquid Hydrogen," Advances in Cryogenic Engineering, Vol. 7, ed. Timmerhaus, K. D., Plenum Press, New York, NY, pp. 219-233.

Greenfield, S. (1958). "Dilution of Cryogenic Liquid Rocket Propellants During Pressurized Transfer," Proceedings of the 1957 Cryogenic Engineering Conference, ed. Timmerhaus, K. D., National Bureau of Standards, Boulder, CO, pp. 136-148.

Greer, D. S. (1995). "Numerical Modeling Of A Cryogenic Fluid Within A Fuel Tank," Progress in Aeronautics, Vol. 168, American Institute of Aeronautics and Astronautics, Washington, DC, pp. 3-21.

Gursu, S., Sherif, S. A., Veziroglu, T. N., & Sheffield, J. W. (1993). "Analysis and Optimization of Thermal Stratification and Self-Pressurization Effects in Liquid Hydrogen Storage Systems – Part 1: Model Development and Part 2: Model Results and Conclusions," Journal of Energy Resources Technology, Vol. 115, No. 3, Sept. 1993, pp. 221-231.

Hardy, T. L., & Whalen, M. V. (1991). "Slush Hydrogen Propellant Production, Transfer, and Expulsion Studies at the NASA K-Site Facility," AIAA Paper 1991-3550, Also NASA-TM-105191.

Hasan, M. M. & Lin, C. S. (1991). "A Numerical Study of the Direct Contact Condensation on a Horizontal Surface," AIAA Paper 1991-1307, Also NASA-TM-102437.

Hochstein, J. I., Hyun-Chul Ji, & Aydelott, J. C. (1990). "Prediction of Self-Pressurization Rate of Cryogenic Propellant Tankage," Journal of Propulsion and Power, Vol. 6, No. 1, Jan.-Feb. 1990, pp. 11-17.

Hodge, B. K., & Koenig, K. (1992). "A PC-Based Collapse Factor Analysis for High Pressure Cryogenic Systems," dated July 1992, NASA Stennis Space Center Contract NAS13-330 Order No. 30. (shorter version with same title is also presented in AIAA Paper 1992-3683)

Hoogendoorn, C. J. (1986). "Natural Convection in Enclosures," Heat Transfer 1986: Proceedings of the Eighth International Heat Transfer Conference, Vol. 1, eds. Tien, C. L., Carey, V. P., & Ferrell, J. K., pp. 111-120.

Hsu, M. W. (1994). "Development of a Numerical Algorithm for Space Based Cryogen Expulsion Operations," University of Wisconsin-Madison, Univ. Microfilms Order No. DA9419130.

Hsu, M., & Witt, R. J. (1994). "Simulations of Cryogen Expulsion from a Space Depot Under Zero Gravity," Cryogenics, Vol. 34, No. 5, pp. 415-419.

Humphrey, J. C. (1961). "Pressurized Transfer of Cryogenic Fluids from Tanks in Liquid Nitrogen Baths," Advances in Cryogenic Engineering, Vol. 6, ed. Timmerhaus, K. D., Plenum Press, New York, NY, pp. 281-292.

Incropera, F. P., & DeWitt, D. P. (1990). Introduction to Heat Transfer, 2nd Edition, John Wiley & Sons, New York, NY.

Incropera, F. P., & DeWitt, D. P. (1996). Fundamentals of Heat and Mass Transfer, 4th Edition, John Wiley & Sons, New York, NY.

Kamat, D. V., & Abraham, W. H. (1968). "Pressure Collapse in Oxygen Storage under Zero-g," Journal of Spacecraft and Rockets, Vol. 5, No. 2, February 1968, pp. 184-188.

Kendle, D. W. (1969). "Lecture 11: Tank Pressurization," Proceedings of Low-G Seminar, McDonnell Douglas Astronautics Company, Western Division, McDonnell Douglas Corporation Document DAC-63140, May 1969, pp. 119-134.

Kendle, D. W. (1970). "Ullage Mixing Effects on Tank Pressurization Performance," AIAA Paper 1970-681.

Kharin, V. M., Ryazhskikh, V. I., Zavadskikh, R. M. (1991). "Stratification of a Cryogenic Liquid in a Reservoir in the Case of Circulation Cooling," Journal of Engineering Physics, Vol. 60, No. 3, March 1991, Plenum Publishing Corporation, pp. 336-338.

Knuth, E. L. (1959). "Nonstationary Phase Changes Involving a Condensed Phase and a Saturated Vapor," The Physics of Fluids, Vol. 2, No. 1, Jan.-Feb. 1959, ed. Frenkiel, F. N., American Institute of Physics, Inc., pp. 84-86.

Lacovic, R. F. (1970). "Comparison of Experimental and Calculated Helium Requirements for Pressurization of a Centaur Liquid Oxygen Tank," NASA-TM-X-2013.

Lemmon, E. W., Huber, M. L., & Mc Linden, M. O. (2007). "Reference Fluid Thermodynamic and Transport Properties (REFPROP)," NIST Standard Reference Database 23, Version 8.0.

Liebenburg, D. H., & Edeskuty, F. J. (1965). "Pressurization Analysis of a Large-Scale Liquid Hydrogen Dewar," International Advances in Cryogenic Engineering, Vol. 11, ed. Timmerhaus, K. D., Plenum Press, New York, NY, pp. 284-289.

Lin, C. S., & Hasan, M. M. (1992). "Self-Pressurization of a Spherical Liquid Hydrogen Storage Tank in a Microgravity Environment," AIAA Paper 1992-0363, Also NASA-TM-105372.

Ludwig, K. A., & Houghton, P. A. (1989). "Collapse Factor Analysis Final Report," dated June 20, 1989, Air Products and Chemicals, Inc. Report to NASA Stennis Space Center for CTF Project.

Majumdar, A., & Steadman, T. (1998). "Numerical Modeling of Pressurization of a Propellant Tank," Draft Paper for the 37th AIAA Aerospace Sciences Meeting.

Mandell, D. A., & Roudebush, W. H. (1965). "Parametric Investigation of Liquid Hydrogen Tank Pressurization During Outflow," NASA-TN-D-2797.

Masters, P. A. (1974). "Computer Programs for Pressurization (Ramp) and Pressurized Expulsion from a Cryogenic Liquid Propellant Tank," NASA-TN-D-7504.

McAdams, W. H. (1954). Heat Transmission, 3rd Edition, McGraw-Hill, New York, NY.

Meserole, J. S., Jones, O. S., & Fortini, A. (1987). "Mixing-Induced Fluid Destratification and Ullage Condensation," NASA Lewis Research Center Microgravity Fluid Management Symposium Proceedings, published April 1, 1987, pp. 101-117.

Meserole, J. S., Jones, O. S., Brennan, S. M., & Fortini, A. (1987). "Mixing-Induced Condensation and Fluid Destratification," AIAA Paper 1987-2018.

Mills, A. F. (1992). Heat Transfer, Irwin, Boston, MA.

Momenthy, A. M. (1964). "Propellant Tank Pressurization-System Analysis," Advances in Cryogenic Engineering, Vol. 9, ed. Timmerhaus, K. D., Plenum Press, New York, NY, pp. 273-283.

Moore, R. W., Fowle, A. A., Bailey, B. M., Ruccia, F. E., & Reid, R. C. (1960). "Gas Pressurized Transfer of Liquid Hydrogen," Advances in Cryogenic Engineering, Vol. 5, ed. Timmerhaus, K. D., Plenum Press, New York, NY, pp. 450-459.

Moran, M. E., Nyland, T. W., & Driscoll, S. L. (1991). "Hydrogen No-Vent Fill Testing in a 34 Liter (1.2 Cubic Foot) Tank," Advances in Cryogenic Engineering, Vol. 37, Part B, ed. Fast, R. W., Plenum Press, New York, NY, pp. 1257-1264.

Neff, B. D., & Chiang, C. W. (1967). "Free Convection in a Container of Cryogenic Fluid," Advances in Cryogenic Engineering, Vol. 12, ed. Timmerhaus, K. D., Plenum Press, New York, NY, pp. 112-124.

Nein, M. E., & Head, R. R. (1962). "Experiences with Pressurized Discharge of Liquid Oxygen from Large Flight Vehicle Propellant Tanks," Advances in Cryogenic Engineering, Vol. 7, ed. Timmerhaus, K. D., Plenum Press, New York, NY, pp. 244-250.

Nein, M. E., & Thompson, J. F. (1965). "Experimental and Analytical Studies of Cryogenic Propellant Tank Pressurization," Proceedings of the Conference on Propellant Tank Pressurization and Stratification, Vol. 2, NASA Marshall Space Flight Center, Huntsville, AL, pp. 29-54.

Nein, M. E., & Thompson, J. F. (1966). "Experimental and Analytical Studies of Cryogenic Propellant Tank Pressurant Requirements," NASA-TN-D-3177.

Nevrovskii, V. A. (1994). "Estimation of the Time for Pressure Growth in a Tank with a Cryogenic Liquid in Zero Gravity," Journal of Engineering Physics and Thermophysics, Vol. 67, No. 1-2, Plenum Publishing Corporation, New York, NY, pp. 690-695.

O'Loughlin, J. R., and Glenn, H. (1966). "Bulk Liquid Interfacial Mass Transfer with Variable Ullage Pressure," Proceedings of the Conference on Propellant Tank Pressurization and Stratification, Vol. 1, 1966, NASA Marshall Space Flight Center, Huntsville, AL, pp. 125-142.

O'Loughlin, J. R. (1966). "Dimensionless Mass Transfer Alignment Chart for Suddenly Pressurized Liquid-Vapor Systems," Proceedings of the Conference on Propellant Tank Pressurization and Stratification, Vol. 1, 1966, NASA Marshall Space Flight Center, Huntsville, AL, pp. 143-155.

Olsen, W. A. (1966). "Experimental and Analytical Investigation of Interfacial Heat and Mass Transfer in a Pressurized Tank Containing Liquid Hydrogen," NASA-TN-D-3219.

Ordin, P. M., Weiss, S., & Christenson, H. (1960). "Pressure-Temperature Histories of Liquid Hydrogen Under Pressurization and Venting Conditions," Advances in Cryogenic Engineering, Vol. 5, ed. Timmerhaus, K. D., Plenum Press, New York, NY, pp. 481-486.

Ostrach, S. (1972). "Natural Convection in Enclosures," Advances in Heat Transfer, Vol. 8, eds. Hartnett, J. P. & Irvine, T. F., Academic Press, Inc., New York, NY, pp. 161-227.

Pasley, G. F. (1970). "Optimization of Stored Pressurant Supply for Liquid Propellant Systems," Journal of Spacecraft and Rockets, Vol. 7, No. 12, Dec. 1970, pp. 1478-1480.

Pasley, G. F. (1972). "Prediction of Tank Pressure History in a Blowdown Propellant Feed System," Journal of Spacecraft and Rockets, Vol. 9, No. 6, June 1972, pp. 473-475.

Polyakov, A. F. (1991). "Heat Transfer under Supercritical Pressures," Advances in Heat Transfer, Vol. 21, eds. Hartnett, J. P., Irvine, T. F., Cho, Y. I., Academic Press, New York, NY.

Raithby, G. D., & Hollands, K. G. T. (1975). "A General Method of Obtaining Approximate Solutions to Laminar and Turbulent Free Convection Problems," Advances in Heat Transfer, Vol. 11, eds. Irvine, T. F. & Hartnett, J. P., Academic Press, New York, NY, pp.265-315.

Reaser, W. W., Wilson, E. L., & Smith, D. A. (1965). "Design of Cryogenic Fluid Systems in the S-IV Stage Propulsion System," Annals of Reliability and Maintainability, Fourth Annual Reliability and Maintainability Conference, pp. 367-374.

Riemer, D. H., & Scarlotti, R. (1984). "Supercritical Hydrogen Expulsion Utilizing an External Pressurization System," Advances in Cryogenic Engineering, Vol. 29, ed. Fast, R. W., Plenum Press, New York, NY, pp. 741-747.

Riemer, D. H. (1986). " Cryogenic Tank Stratification, A Simpler Approach," Advances in Cryogenic Engineering, Vol. 31, ed. Fast, R. W., Plenum Press, New York, NY, pp. 957-962.

Ring, E. (1964). Rocket Propellant and Pressurization Systems, Prentice-Hall, Englewood Cliffs, NJ.

Rolfes, H., & Visser, J. A. (1991). "Use of 3-D Modelling Techniques to Generate a Single Algorithm that Predicts the Performance of Vacuum Insulated Cryogenic Tanks," Proceedings of the 7th International Conference on Numerical Methods in Thermal Problems, Pineridge Press, Swansea, Wales, UK, pp. 29-40.

Rotenburg, Y. (1986). "Numerical Simulation of Self Pressurization in a Small Cryogenic Tank," Advances in Cryogenic Engineering, Vol. 31, ed. Fast, R. W., Plenum Press, New York, NY, pp. 963-971.

Roudebush, W. H. (1965). "An Analysis of the Problem of Tank Pressurization During Outflow," NASA-TN-D-2585.

Saad, M. A. (1993). Compressible Fluid Flow, 2nd Edition, Prentice Hall, Englewood Cliffs, NJ.

Sasmal, G. P., Hochstein, J. I., Wendl, M. C., & Hardy, T. L. (1991). "Computational Modeling of the Pressurization Process in a NASP Vehicle Propellant Tank Experimental Simulation," AIAA Paper 1991-2407.

Sasmal, G. P., Hochstein, J. I., & Hardy, T. L. (1993). "Influence of Heat Transfer Rates on Pressurization of Liquid/Slush Hydrogen Propellant Tanks," AIAA Paper 1993-0278.

Schmidt, A. F., Purcell, J. R., Wilson, W. A., & Smith, R. V. (1960). "An Experimental Study Concerning the Pressurization and Stratification of Liquid Hydrogen," Advances in Cryogenic Engineering, Vol. 5, ed. Timmerhaus, K. D., Plenum Press, New York, NY, pp. 487-497.

Schmidt, G. R., Carrigan, R. W., Hahs, J. E., Vaughan, D. A., & Foust, D. C. (1991). "No-Vent Fill Pressurization Tests Using a Cryogen Simulant," NASA-TM-103561.

Schuster, J. R., Russ, E. J., & Wachter, J. P. (1990). "Cryogenic On-Orbit Liquid Depot Storage, Acquisition, and Transfer Satellite (COLD-SAT)", NASA-CR-185249.

Schuster, J. R., Wachter, J. P., Vento, D. M. (1990), "The COLD-SAT Experiment for Cryogenic Fluid Management Technology," JANNAF Propulsion Meeting, Anaheim, CA, (work performed under NASA Contract NAS3-25062).

Segel, M. F. (1965). "Experimental Study of the Phenomena of Stratification and Pressurization of Liquid Hydrogen," International Advances in Cryogenic Engineering, Vol. 11, ed. Timmerhaus, K. D., Plenum Press, New York, NY, pp. 308-313.

Shelburne, L. (1990). "E-8 Turbopump Testing" Facsimile Transmission dated June 4, 1990, Pratt and Whitney Advanced Launch System Space Transportation Engine Program Coordination Memo No. NSO-020-14.

Smith, I. E. (1961). "Cryogenic Rocket Propellants," Progress in Cryogenics, Vol. 3, ed. Mendelssohn, K., Academic Press, New York, NY.

Stochl, R. J., & DeWitt, R. L. (1969). "Pressurant Gas Requirements for the Pressurized Discharge of Liquid Hydrogen from Propellant Tanks," AIAA Paper 1969-526.

Stochl, R. J., Maloy, J. E., Masters, P. A., & DeWitt, R. L. (1970). "Gaseous-Helium Requirements for the Discharge of Liquid Hydrogen from a 1.52-Meter- (5-Ft-) Diameter Spherical Tank," NASA-TN-D-5621.

Stochl, R. J., Maloy, J. E., Masters, P. A., & DeWitt, R. L. (1970). "Gaseous-Helium Requirements for the Discharge of Liquid Hydrogen from a 3.96-Meter- (13-Ft-) Diameter Spherical Tank," NASA-TN-D-7019.

Stochl, R. J., Van Dresar, N. T., & Lacovic, R. F. (1991). "Autogenous Pressurization of Cryogenic Vessels Using Submerged Vapor Injection," Advances in Cryogenic Engineering, Vol. 37, Part B, ed. Fast, R. W., Plenum Press, New York, NY, pp. 1273-1280; Also NASA-TM-104516.

Sutton, G. P. (1992). Rocket Propulsion Elements; An Introduction to the Engineering of Rockets, 6th Edition, John Wiley & Sons, New York, NY.

Swalley, F. E., Ward, W. D., & Toole, L. E. (1966). "Low Gravity Fluid Behavior and Heat Transfer Results from the S-IVB-203 Flight," Proceedings of the Conference on Long Term Cryo-Propellant Storage in Space, Oct. 12-13, 1966, NASA Marshall Space Flight Center, Huntsville, AL, pp. 213-232.

Tanyun, Z., Zhongping, H., & Shimo Li (1996). "Numerical Simulation of Thermal Stratification in Liquid Hydrogen," Advances in Cryogenic Engineering, Vol. 41, Part A, ed. Kittel, P., Plenum Press, New York, NY, pp. 155-161.

Taylor, W. J., Honkonen, S. C., Liggett, M. W., Williams, G. E., & Tucker, S. (1991). "The Cryogenic On-Orbit Liquid Analytical Tool (COOLANT): A Computer Program For Evaluating The Thermodynamic Performance of Cryogenic Storage Facilities," AIAA Paper 1991-0487.

Thompson, J. F., & Nein, M. E. (1965). "Prediction of Propellant Tank Pressurization Requirements by Dimensional Analysis," NASA-TM-X-53218.

Touloukian, Y. S., Powell, R. W., Ho, C. Y., Klemens, P. G. (1970). Thermophysical Properties of Matter, The TPRC Data Series, Volume 1: Thermal Conductivity, Metallic Elements and Alloys, Plenum Press, New York, NY.

Touloukian, Y. S., & Buyco, E. H. (1970). Thermophysical Properties of Matter, The TPRC Data Series, Volume 4: Specific Heat, Metallic Elements and Alloys, Plenum Press, New York, NY.

Tuttle, J., DiPirro, M. J., & Shirron (1994). "Thermal stratification of liquid helium in the SHOOT Dewars," Cryogenics, Vol. 34, No. 5, Butterworth-Heinemann, Oxford, UK, pp. 369-374.

Van Dresar, N. T. & Stochl, R. J. (1991). "Pressurization and Expulsion of Cryogenic Liquids: Generic Requirements for a Low-Gravity Experiment," NASA-TM-104417.

Van Dresar, N. T., Lin, C. S., & Hasan, M. M. (1992). "Self-Pressurization of a Flightweight Liquid Hydrogen Tank: Effects of Fill Level at Low Wall Heat Flux," AIAA Paper 1992-0818, Also NASA-TM-105411.

Van Dresar, N. T. & Stochl, R. J. (1993). "Pressurization and Expulsion of a Flightweight Liquid Hydrogen Tank," AIAA Paper 1993-1966, Also NASA-TM-106427.

Van Dresar, N. T., & Haberbusch, M. S. (1994). "Thermodynamic Models for Bounding Pressurant Mass Requirements of Cryogenic Tanks," Advances in Cryogenic Engineering, Vol. 39, Part B, ed. Kittel, P., Plenum Press, New York, NY, pp. 1907-1914.

Van Dresar, N. T. (1995). "Prediction of Pressurant Mass Requirements for Axisymmetric Liquid Hydrogen Tanks," AIAA Paper 1995-2964, Also NASA-TM-106973.

Vance, R. W., & Duke, W. M. (1962). Applied Cryogenic Engineering, John Wiley & Sons, New York, NY.

Vaughan, D. A., & Schmidt, G. R. (1990). "Analytical Modeling of No-Vent Fill Process," AIAA Paper 1990-2377.

Vaughan, D. A., Foust, D. C., & Schmidt, G. R. (1991). "Enhancement of the No-Vent Fill Process," AIAA Paper 1991-1842.

Vliet, G. C. (1969). "Natural Convection Local Heat Transfer on Constant-Heat-Flux Inclined Surfaces," Journal of Heat Transfer, Vol. 91, Nov. 1969, American Society of Mechanical Engineers, New York, NY, pp. 511-516.

Wapato, P. G., Keeley, A. W., Jew, L. N., and Young, C. F. (1971). "Study of External Pressurization Systems for Cryogenic Storage Systems," NASA-CR-115205.

Whalen, M. V., & Hardy, T. L. (1992). "Slush Hydrogen Pressurized Expulsion Studies at the NASA K-Site Facility," AIAA Paper 1992-3385, Also NASA-TM-105597.

Wulff, W., & Schipma, P. (1967). "Design Guide for Pressurized Gas Systems; Task 7," ITT Research Institute Report No, ITTRI-C6070-20.

Wylie, C. R., & Barrett, L. C. (1982). Advanced Engineering Mathematics, 5th Edition, McGraw-Hill, New York, NY.

Yang, K. T. (1986). "Numerical Modeling of Natural Convection-Radiation Interactions in Enclosures," Heat Transfer 1986, Vol. 1, eds. Tien, C. L., Carey, V. P., & Ferrell, J. K., pp. 131-140.

Zenner, G. H. (1960). "The Storage and Handling of Cryogenic Liquids," Progress in Cryogenics, Vol. 2, ed. Mendelssohn, K., Academic Press, Inc., New York, NY.